Analytic calculations of MHD equilibria and of MHD stability boundaries in fusion plasmas

by
Antoine Julien Cerfon

B.S. Mathematics and Physics (2003), M.S. Nuclear Science and Engineering (2005)
Ecole Nationale Superieure des Mines de Paris

Submitted to the Department of Nuclear Science and Engineering
in partial fulfillment of the requirements for the degree of
Doctor of Philosophy in Applied Plasma Physics
at the

MASSACHUSETTS INSTITUTE OF TECHNOLOGY

September 2010

Author.....
Department of Nuclear Science and Engineering
August 24, 2010

Certified by.....
Jeffrey P. Freidberg
KEPCO Professor of Nuclear Science and Engineering Department
Thesis Supervisor

Certified by.....
Peter J. Catto
Senior Research Scientist, Plasma Science and Fusion Center
Thesis Reader

Accepted by.....
Mujid S. Kazimi
TEPCO Professor of Nuclear Science and Engineering Department
Chairman, Department Committee on Graduate Students

Analytic calculations of MHD equilibria and of MHD stability boundaries in fusion plasmas

by

Antoine Julien Cerfon

Submitted to the Department of Nuclear Science and Engineering
on August 25, 2010 in partial fulfillment of the requirements for the Degree of
Doctor of Philosophy in Applied Plasma Physics

Abstract

In this work, two separate aspects of ideal MHD theory are considered. In the first part, analytic solutions to the Grad-Shafranov equation (GSE) are presented, for two families of source functions: functions which are linear in the flux function Ψ, and functions which are quadratic in Ψ. The solutions are both simple and very versatile, since they describe equilibria in standard tokamaks, spherical tokamaks, spheromaks, and field reversed configurations. They allow arbitrary aspect ratio, elongation, and triangularity as well as a plasma surface that can be smooth or possess a double or single null divertor X-point. The solutions can also be used to evaluate the equilibrium beta limit in a tokamak and spherical tokamak in which a separatrix moves onto the inner surface of the plasma.

In the second part, the reliability of the ideal MHD energy principle in fusion grade plasmas is assessed. Six models are introduced, which are constructed to better describe plasma collisonality regimes for which the approximations of ideal MHD are not justified. General 3-D quadratic energy relations are derived for each of these six models, and compared with the ideal MHD energy principle. Stability comparison theorems are presented. The main conclusion can be summarized in two points. (1) In systems with ergodic magnetic field lines, ideal MHD accurately predicts marginal stability, even in fusion grade plasmas. (2) In closed field line geometries, however, the ideal MHD predictions must be modified. Indeed, it is found that in collisionless plasmas, the marginal stability condition for MHD modes is inherently incompressible for ion distribution functions that depend only on total energy. The absence of compressibility stabilization is then due to wave particle resonances. An illustration of the vanishing of plasma compressibility stabilization in closed line systems is given by studying the particular case of the hard-core Z-pinch.

Thesis Supervisor: Jeffrey P. Freidberg
Title: KEPCO Professor of Nuclear Science and Engineering Department

Acknowledgments

I have long known that no matter where you are, you always find someone who is smarter than you. I just never thought that at MIT, this would be true in each and every office, and each and every classroom. It is quite a luxury to be going to work every day knowing that one will be challenged, and looking forward to all the new things one will learn. I wish I could thank all the people I met in labs or classrooms during my time here.

My first thanks go to all the fantastic people I met and worked with at PSFC. To Jeffrey Freidberg, who gave me the opportunity to join the theory group, and who introduced me and guided me through really fun projects; my answer to the question " Are you happy or sad?" is unequivocal. To Peter Catto, with whom I never managed to go to an Irish music concert, but from whom I learned so much about transport, and who always had very interesting comments and suggestions to help improve this work. To Rick Temkin, for letting me join PSFC in the first place, and giving us so many useful tips about the art of scientific presentation (I still need practice, though...). To Felix and his encyclopedic knowledge. To Grisha, for teaching me the jumping relaxation techniques. To Matt, for being so thorough, and never letting any argument convince him too easily. To Arturo, and his always dangerous visits in the office. To Antonio, for our shared passion for soccer, err football. To Dave, for teaching me about hockey. To Haru, for coming so often to my concerts. To Abhay, Jay, John, Paul, Darin and Ted for the interesting conversations at lunch time.

More personally, Miranda, thank you so much for embarking with me on this beautifully crazy (and crazily beautiful) adventure, and for sharing my belief that we would make it.

Brice, Thom, Steve, j'espere que vous touchez vous aussi au but. Je me souviendrai pendant longtemps de ces conversations pendant lesquelles nous avons partage nos impressions de doctorants au telephone, autour d'une biere, ou en vacances. Je quitte le navire, certes, mais je n'ai pas oublie d'installer la passerelle! Je vous attends de pied ferme pour boire un coup au bar du port.

Edith, je te remercie du fond du coeur pour la curiosité que tu m'as génétiquement léguée, puis consciemment transmise.

Und Mameles, Sehsch, ich bin au mol Dockter Cerfon!

Contents

1. Introduction **11**

2. Static MHD equilibria and analytic solutions to the Grad-Shafranov equation **25**

2.1 Confined plasma equilibrium and Grad-Shafranov equation 27

2.1.1 Equilibrium equations in fusion plasmas 27

2.1.2 Equilibrium in toroidally axisymmetric plasmas: the Grad-Shafranov equation 32

2.2 Analytic solutions of the Grad-Shafranov equation with Solov'ev profiles 38

2.2.1 Analytic solutions of the Grad-Shafranov equation 38

2.2.2 The Grad-Shafranov equation with Solov'ev profiles 41

2.2.3 The boundary constraints 46

2.2.4 The plasma figures of merit 51

2.2.5 ITER 53

2.2.6 The spherical tokamak 54

2.2.7 The spheromak 60

2.2.8 The field reversed configuration 61

2.2.9 Up-down asymmetric formulation 65

2.3 Extension: Analytic solutions of the Grad-Shafranov equation with quadratic profiles 69

2.3.1 Solov'ev profiles and the discontinuity of the toroidal current density 69

2.3.2 Analytic solution of the Grad-Shafranov equation with quadratic profiles. 71

2.3.3 Up-down symmetric solutions 74
2.3.4 Up-down asymmetric solutions 76
2.4 Summary 79

3. Are fusion plasmas compressible? A new look at MHD comparison theorems 85

3.1 Ideal MHD linear stability and the ideal MHD energy principle 87
3.1.1 Ideal MHD linear stability 87
3.1.2 Ideal MHD variational formulation 91
3.1.3 Ideal MHD energy principle 96
3.2 Ideal MHD plasma compressibility 99
3.3 Collisionality regimes in plasmas of fusion interest and alternate MHD models 105
3.4 Five models, one general formulation 113
3.5 Two-Temperature MHD energy principle 115
3.5.1 Electron energy equation 116
3.5.2 Ion energy equation 121
3.5.3 Two-Temperature MHD static equilibrium 122
3.5.4 Two-Temperature MHD stability and energy principle 123
3.6 CGL – Fluid MHD energy principle 126
3.6.1 CGL – Fluid MHD closure 126
3.6.2 CGL – Fluid MHD static equilibrium 128
3.6.3 CGL – Fluid MHD stability and energy principle 129
3.7 Kinetic – Fluid MHD energy principle 133
3.7.1 Kinetic – Fluid MHD closure 133
3.7.2 Kinetic – Fluid MHD equilibrium 135
3.7.3 Kinetic – Fluid MHD energy principle 136
3.8 CGL energy principle 142

3.8.1 CGL closure 142
3.8.2 CGL static equilibrium 143
3.8.3 CGL stability and energy principle 144
3.9 Kinetic MHD energy principle 146
3.9.1 The Kinetic MHD closure 146
3.9.2 Kinetic MHD static equilibrium 148
3.9.3 Kinetic MHD energy principle 149
3.10 Energy relations for comparison theorems: Vlasov ions, fluid electrons 155
3.10.1 The electron model 157
3.10.2 The Vlasov-Fluid model 158
3.10.3 Vlasov-Fluid Equilibrium 159
3.10.4 Vlasov-Fluid Stability 161
3.11 Summary 164

4. The vanishing of MHD compressibility stabilization: illustration in the hard-core Z-pinch 173

4.1 LDX and the hard-core Z-pinch 175
4.1.1 The Levitated Dipole experiment (LDX) 175
4.1.2 The hard-core Z-pinch 181
4.2 Ideal MHD stability of the interchange mode in the hard-core Z-pinch 184
4.3 Vlasov-Fluid stability of the interchange mode in the hard-core Z-pinch 188
4.3.1 Previous kinetic studies of the interchange mode in Z-pinch and point dipole geometries 188
4.3.2 Vlasov-fluid stability analysis 192
4.3.3 The vanishing of MHD compressibility stabilization: a numerical example 203
4.3.4 Local approximation vs. global eigenvalue equation 210
4.4 Conclusion 215

5. Summary and Conclusions..... 221

Appendix A. Kinetic MHD Energy Relation..... 225

Appendix B. Kinetic MHD Ions, Fluid Electrons Energy Relation..... 240

Appendix C. Vlasov-Fluid Energy Relation..... 246

Chapter 1

Introduction

The ideal MHD model is perhaps the simplest description of neutral plasmas one can think of. It is defined by the following set of equations:

$$\begin{aligned}
&\frac{\partial \rho}{\partial t} + \nabla \cdot \left(\rho \mathbf{v}\right) = 0 \\
&\rho \frac{d\mathbf{v}}{dt} = \mathbf{J} \times \mathbf{B} - \nabla p \\
&\frac{d}{dt}\left(\frac{p}{\rho^{\gamma}}\right) = 0 \\
&\nabla \times \mathbf{B} = \mu_0 \mathbf{J} \\
&\frac{\partial \mathbf{B}}{\partial t} = \nabla \times \left(\mathbf{v} \times \mathbf{B}\right)
\end{aligned} \tag{1.1}$$

In eq. (1.1), ρ is the mass density of the plasma, $\mathbf{v}$ its velocity, and p its pressure. $\mathbf{J}$ is the current flowing in the plasma, and $\mathbf{B}$ the magnetic field. Because of its simplicity, and its somewhat surprising ability to accurately predict the macroscopic behavior of plasmas, ideal MHD is the model most commonly used in the early stages of the design of a magnetic fusion experiment. This early design phase is usually subdivided in the following two steps, which correspond to the two fundamental

missions of ideal MHD theory for magnetic fusion applications. First, one determines an equilibrium state consistent with the steady-state version of eq. (1.1). Then, one analyzes the perturbations around that equilibrium state, which are either stable waves or instabilities. Among other considerations, the desirable equilibria are those where the plasma is confined at a high pressure, and where major instabilities, potentially leading to the eventual loss of plasma confinement, cannot be excited.

In this thesis, we look separately at each of the two cornerstones of ideal MHD theory. In the first part, we calculate plasma equilibria in toroidally axisymmetric magnetic configurations with analytic solutions of the ideal MHD equilibrium equations. In the second part, we evaluate the validity of the set of equations (1.1) and the robustness of the ideal MHD linear stability predictions in fusion grade plasmas.

Part 1: Static MHD equilibria and analytic solutions to the Grad-Shafranov equation

The equilibria of most plasmas of fusion interest are well described by the steady-state, zero flow version of eq. (1.1):

$$\begin{aligned} \mathbf{J}\times\mathbf{B} &= \nabla p \\ \nabla\cdot\mathbf{B} &= 0 \\ \nabla\times\mathbf{B} &= \mu_0\mathbf{J} \end{aligned} \tag{1.2}$$

Now, with the notable exception of the stellarator, all the plasma confinement concepts which show promise as future fusion reactors have toroidal axisymmetry. For toroidally axisymmetric configuration, the set of seven equations for seven unknowns given in (1.2) reduces to a single two-dimensional, nonlinear, elliptic partial differential equation, whose solution contains all the information necessary to fully determine the nature of the equilibrium. This equation is usually known as the Grad-Shafranov equation (GS equation), and can be written as follows :

$$R\frac{\partial}{\partial R}\left(\frac{1}{R}\frac{\partial \Psi}{\partial R}\right)+\frac{\partial^2 \Psi}{\partial Z^2}=-\mu_0 R^2\frac{dp}{d\Psi}-F\frac{dF}{d\Psi} \tag{1.3}$$

In Eq. (1.3), (R,ϕ,Z) is the usual coordinate system associated with the toroidal symmetry, $2\pi\,\Psi(R,Z)$ is the poloidal flux, which is the unknown, $p\left(\Psi\right)$ is the plasma pressure, and $2\pi F\left(\Psi\right)=-I_p\left(\Psi\right)$ is the net poloidal current flowing in the plasma and the toroidal field coils.

In general, the GS equation has to be solved numerically. Several excellent accurate and fast numerical Grad-Shafranov solvers are available nowadays. Nevertheless, analytic solutions are always desirable from a theoretical point of view. They usually give more insights into the properties of a given equilibrium than numerical solvers do, for instance when used to derive scalings with the different

geometric parameters (aspect ratio, elongation, triangularity). They can also be the basis of analytic stability and transport calculations. Finally, they can be used to test the numerical solvers.

In several confinement concepts of fusion interest, such as the tokamak and the stellarator for instance, the inverse aspect ratio is a small number which can be used as an expansion parameter in eq. (1.3). Analytic solutions are obtained by expanding (1.3) order by order, as one usually does in asymptotic calculations. This method has led to a wealth of results, and a very deep analytic understanding of static equilibrium in tokamaks.

The problem, of course, is that asymptotic expansions break down in other confinement concepts of fusion interest, such as spherical tokamaks (STs), spheromaks, or Field Reverse Configurations (FRCs), in which the inverse aspect ratio is close to 1. For these configurations, one can therefore ask ourselves the following questions: are there specific forms for the forcing terms $-\mu_0 R^2 \frac{dp}{d\Psi}$ and $F\frac{dF}{d\Psi}$ such that analytic solutions of eq. (1.3) can only be found?

In Part I of this thesis, corresponding to Chapter 2, we show that the answer to this question is yes, and we propose new, improved analytic solutions to the GS equation for two families of specially chosen pressure and current profiles. The first profiles of interest are usually known as the Solov'ev profiles, and have the following general form:

$$\frac{dp}{d\Psi} = K_1 \quad \text{and} \quad F\frac{dF}{d\Psi} = K_2, \qquad K_1,\, K_2 \text{ constants} \tag{1.4}$$

With these profiles, the GS equation takes a particularly simple form, and the solutions are polynomials (or polynomial-like, with logarithms). We construct a solution with more degrees of freedom than any of the solutions previously proposed by Solov'ev and others, and associate to this solution new boundary constraints on the plasma surface, to determine all the free coefficients in our generic polynomial solution. With our choice of boundary constraints, the same solution can be used for the calculation of tokamak, ST, spheromak, and FRC equilibria, with or without up-down symmetry, with or without X-points, for arbitrary plasma β, inverse aspect ratio ε, elongation κ, and triangularity δ. Furthermore, the calculation of any equilibrium only involves the numerical solution of a linear algebraic system of a very limited number of equations (7 equations for up-down symmetric equilibria, 12 otherwise). This is a trivial numerical problem.

Unfortunately, the Solov'ev profiles (1.4) correspond to a somewhat unrealistic situation from an experimental point of view, since the toroidal current density has a jump at the plasma edge. For this reason, we demonstrate in the remainder of Chapter 2 that the procedure we developed for the Solov'ev profiles can be applied as successfully for more realistic profiles, given by:

$$p(\psi) = p_0\psi^2 \quad \text{and} \quad F^2 = R_0^{\,2}B_0^{\,2}\left(1 - \alpha\psi^2\right) \tag{1.5}$$

In (1.5), B_0 is the vacuum magnetic field, α represents the plasma diamagnetism ($\alpha > 0$) or paramagnetism ($\alpha < 0$), and p_0 is defined such that the pressure at the magnetic axis is $p_{axis} = p_0 \psi^2_{axis}$.

The solution of the GS equation which we find for the profiles (1.5) is more complicated than in the Solov'ev case. Instead of a polynomial expansion, we now have an expansion in Whittaker functions. Most importantly, some of the undetermined constants now appear nonlinearly in the solution, namely in the argument of Whittaker functions. However, the procedure to determine the free constants which we presented in the Solov'ev case can be applied in exactly the same way. The only difference is that the system of algebraic equations for the boundary constraints is now nonlinear. Solving this system is a less trivial numerical problem than in the previous case, and convergence issues may be encountered if the chosen geometric and plasma parameters are too extreme. Nevertheless, in most cases the system can readily be solved by calling a built-in nonlinear solver in any scientific computing program. We have been able to compute very plausible tokamak and ST equilibria with this procedure, for a wide range of parameters, and with or without up-down symmetry.

Part 2: MHD comparison theorems, and the vanishing of plasma compressibility

One of the most important criteria in the design of a magnetic fusion experiment is the stability of the plasma to the fast macroscopic modes known as MHD modes. These modes are known experimentally to considerably degrade the plasma properties, and can actually cause the termination of the plasma discharge.

MHD instabilities are usually studied using the ideal MHD model, because of the relative simplicity of this model, and of its particular mathematical properties. In ideal MHD, the problem of linear stability in any 3D configuration can be cast in a very convenient form known as the ideal MHD energy principle. It can be stated as follows:

A static ideal MHD equilibrium is stable if and only if

$$\delta W_{MHD}\left(\boldsymbol{\xi}^*, \boldsymbol{\xi}\right) \geq 0 \tag{1.6}$$

for all allowable displacements $\boldsymbol{\xi}$.

In eq. (1.6), $\boldsymbol{\xi}$ is the plasma displacement, and $\delta W\left(\boldsymbol{\xi}^*, \boldsymbol{\xi}\right)$ is the potential energy associated with the displacement $\boldsymbol{\xi}$. The energy principle (1.6) can be refined, and a more specific form can be given for the different families of magnetic configurations:

- *In ergodic systems (tokamaks, stellarators, STs, etc.), or closed field line systems with modes which do not conserve the closed-line symmetry, a static ideal MHD equilibrium is linearly stable if and only if*

$$\delta W_{\perp}\left(\boldsymbol{\xi}^{*},\boldsymbol{\xi}\right) \geq 0 \tag{1.7}$$

for all allowable displacements $\boldsymbol{\xi}$ *.*

In eq. (1.7), $\delta W_{\perp}\left(\boldsymbol{\xi}^{*},\boldsymbol{\xi}\right)$ is the potential energy associated with **incompressible** displacements. In other words, ideal MHD stability, for this first family of modes and magnetic geometries, in inherently incompressible.

- *For closed field line systems (Z-pinch, Dipole, FRC, etc.), and modes which conserve the closed-line symmetry, a static ideal MHD equilibrium is linearly stable if and only if*

$$\delta W_{\perp}\left(\boldsymbol{\xi}^{*},\boldsymbol{\xi}\right)+\delta W_{C}\left(\boldsymbol{\xi}^{*},\boldsymbol{\xi}\right)=\delta W_{\perp}\left(\boldsymbol{\xi}^{*},\boldsymbol{\xi}\right)+\int \gamma p \,|\langle \nabla\cdot\boldsymbol{\xi}_{\perp}\rangle|^{2}\, d\mathbf{r} \geq 0 \tag{1.8}$$

for all allowable displacements $\boldsymbol{\xi}$ *.*

In eq. (1.8), $\langle\ \rangle$ represents the flux-tube averaging operation. $\delta W_{C}\left(\boldsymbol{\xi}^{*},\boldsymbol{\xi}\right)$, the compressible piece of $\delta W_{MHD}\left(\boldsymbol{\xi}^{*},\boldsymbol{\xi}\right)$ is present in the stability criterion, unlike the previous case. Since it is clear that $\delta W_{C}\left(\boldsymbol{\xi}^{*},\boldsymbol{\xi}\right)\geq 0$, the contribution from this term is stabilizing. This is what is known as MHD compressibility

stabilization. Some closed field line devices, such as the Levitated Dipole eXperiment (LDX), rely explicitly on MHD compressibility to stabilize their most dangerous MHD modes.

The ideal MHD model relies on the assumption that both the electrons and the ions are collisional on the MHD time scale. In this approximation, the plasma is isotropic, and kinetic effects are absent. In most modern magnetic confinement experiments and in future fusion reactors, this assumption is not justified, at least for the ions. Fusion grade plasmas behave in a fundamentally anisotropic manner, and kinetic effects are ubiquitous. One can therefore wonder how robust the ideal MHD stability analyses and the ideal MHD energy principle are in plasmas of fusion interest. For example, a question of interest for closed line systems such as the LDX is the reliability of the criterion (1.8). The factor γ in δW_C comes from the ideal MHD equation of state $d/dt\left(p/\rho^{\gamma}\right)=0$. Since this equation is derived assuming that the plasma behaves as an isotropic fluid, one may have doubts about the robustness of (1.8), and about the existence of MHD compressibility stabilization.

In Chapter 3 of this thesis, we assess the reliability of the ideal MHD energy principles for both ergodic and closed line systems. We introduce six models which more accurately describe the plasmas in the different collisionality regimes of fusion interest. Some of these models are new, while some others have already been used

extensively. They are presented in Table 1, in which they are organized according to the collisionality regime they are associated with, and to whether or not they allow for finite $k_\perp r_{L_i}$, where $k_\perp$ is the perpendicular wave number of the modes of interest, and r_{L_i} is the ion Larmor radius.

	$k_\perp r_{L_i} = 0$	$k_\perp r_{L_i}$ finite
Collisional electrons and Collisional ions	Two-Temperature MHD	
Collisional electrons and Collisionless ions	- CGL – Fluid MHD - Kinetic – Fluid MHD	Vlasov – Fluid
Collisionless electrons and collisionless ions	- CGL - Kinetic MHD	

Table 1.1 The six models which are compared to the ideal MHD model

For each of the models shown in Table 1, we derive new expressions for the potential energy of the plasma displacement, and new quadratic energy relations, valid in arbitrary 3-D configuration, which we compare with δW_{MHD} and with the ideal MHD energy principle. The results can be summarized as follows.

The stability boundaries predicted by ideal MHD are more conservative than those predicted by any of the models in Table 1.1 assuming $k_\perp r_{L_i} = 0$. In other words, ideal MHD linear stability implies linear stability in any of these models. The situation is different, however, when ideal MHD is compared with the Vlasov-Fluid (VF) model, a model which is constructed specifically to allow finite $k_\perp r_{L_i}$, and which assumes that the equilibrium ion distribution function depends only on the total energy (so that there is no equilibrium ion flow, as in ideal MHD). Indeed, in this thesis we prove the following statement:

For both ergodic and closed line magnetic geometries, the condition for the marginal stability in the VF model is:

$$\delta W_\perp = 0 \tag{1.9}$$

Two important consequences can be deduced from (1.9). First, note that for ergodic systems, the condition (1.9) is identical to the condition (1.7). In other words, for ergodic systems, the ideal MHD energy principle for incompressible displacements accurately predicts the linear stability boundaries. It is not a conservative estimate as has been thought in the past, but corresponds to the actual stability boundary.

Second, plasma compressibility is absent from the criterion (1.9). Thus, according to the VF model, in closed line systems, the linear stability boundaries determined with the ideal MHD model are not the most conservative. A plasma can VF unstable to an MHD mode, and yet found to be ideal MHD stable.

Physically, we find that for the equilibria under consideration in the VF model, in which the ions are electrostatically confined, kinetic effects associated with the drift of the particles perpendicular to the magnetic field lines are responsible for the vanishing of plasma compressibility. Of all the models shown in Table 1, only the VF model can treat resonant particle effects perpendicular to the field lines. In fluid models, kinetic effects are obviously absent, and in the other kinetic models, which assume $r_{L_i} = 0$, particles do not drift off the flux tubes they are attached to. This explains why the result given in (1.9) is new. Until now, there was a shared belief, supported by a large number of studies with the CGL and Kinetic MHD models, that ideal MHD stability boundaries were always the most conservative, both in ergodic and closed line systems.

Our new result may be most important for closed line configurations, such as the levitated dipole and the FRC, where MHD compressibility stabilization plays an important role in predicted plasma performance. Therefore, in Chapter 4 we illustrate its implications by studying the case of the hard-core Z-pinch, a closed line configuration which is the large aspect ratio limit of the levitated dipole.

Ideal MHD stability theory shows that in a hard-core Z-pinch, the most unstable mode is the compressible interchange mode. This mode is driven unstable by the pressure gradient in the unfavorable curvature of the field lines. However, for

small enough pressure gradients, the mode is stabilized by plasma compressibility. In low β plasmas, the condition on the pressure gradient is

$$-\frac{r}{p}\frac{dp}{dr} < 2\gamma = 10/3 \quad \text{for ideal MHD stability} \tag{1.10}$$

Based on our analysis in the previous section, we expect this condition to be violated in the VF model, and the instability to persist beyond the ideal MHD stability limit, once resonant particle effects perpendicular to the field lines are taken into account. Therefore, we derive the eigenvalue equation for the interchange mode in the VF model, and solve this equation numerically. The VF criterion for stability we obtain from our numerical analysis is the following:

$$-\frac{r}{p}\frac{dp}{dr} < 0 \qquad \text{for Vlasov-fluid stability} \tag{1.11}$$

Eq. (1.11) proves the absence of plasma compressibility stabilization in the VF model, which applies to the particular class of hard-core Z-pinch equilibria in which the ions are electrostatically confined. Thus, when ion kinetic effects perpendicular to the field lines are included, the instability persists beyond the ideal MHD limit, and only non-decaying pressure profiles are linearly stable. Such profiles are obviously not desirable for magnetic fusion concepts.

When $k_\perp r_{L_i}$ is small, the growth rate of the instability is small in the ideal MHD stable regime. This is expected, since the instability is only due to a few resonant ions in the tail of the distribution function. However, the growth rate

becomes larger as $k_\perp$ gets larger, and may be comparable to ideal MHD growth rates when $k_\perp r_{L_i} \sim 1$.

Additionally, our VF numerical studies show that to fully account for the resonant ion effects, it is crucial to solve the full eigenvalue equation. Often, this equation is simplified by assuming that the mode has scale lengths which are much shorter than those of the equilibrium quantities. This is the so-called local approximation. However, the results we obtain in this approximation are qualitatively different from the results we obtain solving the global eigenvalue equation, even when the approximation is justified. The reasons for this discrepancy are two-folds: 1) The details of the profiles (pressure, magnetic field) explicitly appear in the resonant denominators; 2) The real frequency of the mode given by the global eigenvalue equation is different from the one obtained by solving the equation at a given location, which modifies the resonance condition.

We conclude this thesis by discussing the experimental relevance of the VF results, and by suggesting ways to verify the robustness of these results with models allowing more general and more realistic ion equilibria.

Chapter 2

Static MHD equilibria and analytic solutions to the Grad-Shafranov equation

We focus, in this chapter, on one aspect of ideal MHD equilibrium theory, namely the calculation of *analytic* self-consistent MHD equilibria. What exactly do we mean by *analytic* equilibria? We will show in the first part of this chapter that for toroidally axisymmetric confinement concepts (i.e. almost all the magnetic confinement machines which show promise as future fusion reactors, except for the notable exception of the stellarator), the equation describing the equilibrium of the plasma can be cast in the form of a two-dimensional, nonlinear, elliptic partial differential equation called the Grad-Shafranov equation (GS equation). The solution of the GS equation, with its associated boundary conditions, fully determines the equilibrium. (Section 2.1). In general, the GS equation has to be solved numerically [1]. However, for particular, somewhat idealized equilibrium pressure and current profiles, analytic solutions to the GS equation can be obtained. This is what we mean by analytic equilibria. These analytic solutions are clearly desirable from a theoretical

point of view: we can use them to develop our intuition about a particular confinement concept, to perform analytic calculations of the stability and transport properties of that concept, or to benchmark numerical solvers of the GS equation.

Our new analytic solutions to the GS equation are presented in the second and third parts of this chapter. We first present new analytic solutions of the GS equation for the pressure and current profiles known as Solov'ev profiles [2], simple profiles which still retain most of the crucial physics involved in the theory of MHD equilibria in toroidally axisymmetric devices. The attractiveness of the solutions we propose lies in their simplicity, and versatility. Indeed, we show that by using a single, streamlined procedure, these solutions can be used to calculate MHD equilibria of tokamaks, spherical tokamaks (STs), spheromaks and field reversed configurations (FRCs), and we give examples for each configuration. (Section 2.2)

The difficulty with the Solov'ev profiles is that they are partially unrealistic experimentally, since they correspond to a situation where the pressure gradient and the current profiles have a jump at the plasma edge. The purpose of the third part of this chapter is to demonstrate that the procedure described in Section 2.2 can in fact be generalized to more realistic profiles. We find analytic solutions to the GS equation for profiles characterized by the vanishing of the pressure gradient and of the current at the plasma surface. These analytic solutions have the same number of degrees of freedom as the ones we propose in the Solov'ev case, so that the undetermined constants can be determined in exactly the same way as in Section 2.2.

With these solutions, we calculate tokamak and ST equilibria, with and without up-down symmetry.

2.1 Confined plasma equilibrium and Grad-Shafranov equation

2.1.1 Equilibrium equations in fusion plasmas

We start with the ideal MHD momentum equation:

$$\rho \frac{d\mathbf{v}}{dt} = \mathbf{J} \times \mathbf{B} - \nabla p \tag{2.1}$$

An equilibrium is defined by the fact that all the quantities involved in eq. (2.1) are time-independent, $\frac{\partial}{\partial t} \equiv 0$. In these conditions, eq. (2.1) becomes

$$\rho \mathbf{v} \cdot \nabla \mathbf{v} = \mathbf{J} \times \mathbf{B} - \nabla p \tag{2.2}$$

Furthermore, comparing the inertial term and the pressure gradient term, we have the following scaling:

$$\frac{\rho \mathbf{v} \cdot \nabla \mathbf{v}}{\nabla p} \sim \frac{\mathrm{v}^2}{\mathrm{v}_{T_i}^2} \equiv M_i^2 \tag{2.3}$$

where we have assumed that the ion and electron temperatures are comparable (a very good assumption in fusion grade plasmas), and where we have introduced the ion Mach number M_i as the ratio of the plasma velocity to the ion thermal velocity. In toroidally axisymmetric geometries, one usually distinguishes the poloidal velocity, which is in the plane parallel to the axis of symmetry, and the toroidal velocity, in

the plane perpendicular to the axis of symmetry. Consequently, one often separates the poloidal Mach number M_{iP} and the toroidal Mach number, M_{iT}. In magnetic fusion experiments, we typically have $M_{iP} \ll M_{iT}$ (e.g. [3]), so that the ordering in (2.3), and the question of keeping or neglecting the inertial term in eq. (2.2) essentially depends on M_{iT}.

In the absence of external momentum input, in particular from neutral beam injection systems, the upper bound $M_{iT} \leq 0.15$ is usually found in modern fusion experiments (e.g. [4] for the DIII-D tokamak [5] and [6] in the Alcator C-Mod tokamak [7]), so that the inequality $M_i^2 \ll 1$ is very well satisfied. In the presence of auxiliary torque input, through neutral beams for instance, as in the DIII-D tokamak and the NSTX spherical tokamak (ST) [8], the plasma flows can be larger. Still, the values typically observed are of the order $M_{iT} \sim 0.5$ ([9], [10]), so that the ordering $M_{iT}^2 \ll 1$ is still somewhat acceptable. It will most likely be even more acceptable in the ITER tokamak [11], where the momentum input from the neutral beam system is expected to be smaller, because of the large machine size, and the higher densities.

In conclusion, we can say that for almost all situations of fusion interest, neglecting the inertial term is justified, and we can focus on static equilibria, $\mathbf{v} = \mathbf{0}$, for which the equilibrium momentum equation takes the form:

$$\mathbf{J} \times \mathbf{B} = \nabla p \tag{2.4}$$

which is the well-known equation expressing the balance between the magnetic force $\mathbf{J} \times \mathbf{B}$ and the pressure gradient force.

The three components of Eq. (2.4) represent three equations for seven unknowns: p, the three components of $\mathbf{J}$ and the three components of $\mathbf{B}$. This is obviously not sufficient to fully determine the equilibrium. The remaining equations are obtained from the low-frequency version of Maxwell's equations, consistent with the ideal MHD ordering: $\nabla \cdot \mathbf{B} = 0$, and $\nabla \times \mathbf{B} = \mu_0 \mathbf{J}$. Thus, ideal MHD equilibria are calculated from the following system of equations

$$\begin{aligned} \nabla \cdot \mathbf{B} &= 0 \\ \nabla \times \mathbf{B} &= \mu_0 \mathbf{J} \\ \mathbf{J} \times \mathbf{B} &= \nabla p \end{aligned} \tag{2.5}$$

and we now indeed have seven equations for seven unknown, so that the problem is well-posed. In Section 2.1.2, we show that for toroidally axisymmetric plasmas, all the information contained in the seven equations given by eq. (2.5) can be expressed in a single equation for one variable: the Grad-Shafranov equation. This is our next task.

Before doing so, however, it is worth mentioning that although we derived eq. (2.5) from the set of equations defining the ideal MHD model, and although the computation of plasma equilibria in magnetic confinement concepts is usually

considered a part of ideal MHD theory, the equilibrium described by eq. (2.5) is in fact consistent with descriptions of the plasma which are more accurate than ideal MHD, and valid in regimes where ideal MHD is not, in particular in regimes of fusion interest, where the plasma ions are collisionless (cf. Chapter 3). This is shown as follows.

First, $\nabla \cdot \mathbf{B} = 0$ and $\nabla \times \mathbf{B} = \mu_0 \mathbf{J}$ are the equations of magnetostatics, the steady-state version of Maxwell's equations for the magnetic field. They are obviously exact equations when $\frac{\partial}{\partial t} = 0$, independently from any consideration about the collisionality of the plasma.

The discussion about the momentum equation is more subtle. Taking the exact second order moment of the electrons' and ions' Maxwell-Boltzmann equations, and adding them, we obtain the exact[1] momentum equation for the whole plasma:

$$\rho \frac{d\mathbf{v}}{dt} + \nabla \cdot \left(\mathbf{\Pi}_i + \mathbf{\Pi}_e \right) = \mathbf{J} \times \mathbf{B} - \nabla p \tag{2.6}$$

For the same reasons as the ones previously presented, we can neglect the inertial term in eq. (2.6): $\frac{d\mathbf{v}}{dt} \simeq 0$ in steady-state, and for flows which are subsonic. We also know that the viscosity tensors $\mathbf{\Pi}_i$ and $\mathbf{\Pi}_e$ vanish identically if the ion and electron

[1] to be more precise, we made an assumption to obtain eq. (2.6), namely that the electron inertia is negligible compared to the ion inertia, so that the plasma inertia can be identified to the ion inertia.

equilibrium distribution functions are exact Maxwell-Boltzmann distributions. The question about the validity of eq. (2.5) in collisionality regimes of fusion interest is then the following: what is the condition on the ion and electron collisionality for the distribution functions to be Maxwellian in equilibrium? In particular, can we assume that the ions are in thermal equilibrium (i.e. are well-represented by a Maxwell-Boltzmann distribution) when we know that ions are essentially collisionless in fusion grade plasmas?

The answer, perhaps surprisingly, is yes. The main reason is that, by definition, equilibrium equations describe the steady-state behavior of the plasma, or, in other words, its evolution on very long time scales. And on these long time scales, even weak collisions eventually Maxwellianize the plasma, and drive it towards thermal equilibrium [12]. Using an entropy production argument, it can be shown [13] that the condition for the ion and electron distribution functions to be Maxwellian to lowest order only relies on the fact that in magnetic confinement systems, the particles' Larmor radius is much smaller than the typical macroscopic size of the system. In fusion grade plasmas we therefore have $\mathbf{\Pi}_i \approx \mathbf{0}$, $\mathbf{\Pi}_e \approx \mathbf{0}$ in equilibrium, and $\mathbf{J} \times \mathbf{B} \approx \nabla p$.

The bottom line of all this discussion is that eq. (2.5) is valid far beyond the limits of ideal MHD, and in particular reliably represents equilibria of fusion grade plasmas, at least when neutral beam heating and current drive systems are turned off.

2.1.2 Equilibrium in toroidally axisymmetric plasmas: the Grad-Shafranov equation

As announced in the previous section, we now show how the set of seven equations for seven unknowns given in (2.5) reduces, for toroidally axisymmetric configuration, to a single two-dimensional, nonlinear, elliptic partial differential equation, whose solution contains all the information necessary to fully determine the nature of the equilibrium. This was first discovered by Lüst and Schlüter, Grad and Rubin, and Shafranov in the years 1957 to 1959 [14], [15], [16]. In this section, we rederive this equation, now known as the Grad-Shafranov equation (GS equation), following the presentation given in [17].

For toroidally axisymmetric geometries, the natural coordinates are the (R,ϕ,Z) cylindrical coordinates, where ϕ is the ignorable coordinate, i.e. $\partial/\partial\phi = 0$ for all the quantities. This is illustrated in Fig. 2.1, where for the example, we chose a torus with circular cross section.

We start with the first equation in (2.5): $\nabla \cdot \mathbf{B} = 0$. Of course, because of the toroidal axisymmetry, this equation does not give us any information about B_ϕ, the ϕ component of the magnetic field, which is usually called toroidal magnetic field. However, it gives us a very convenient way of writing the poloidal magnetic field, $\mathbf{B}_p$,

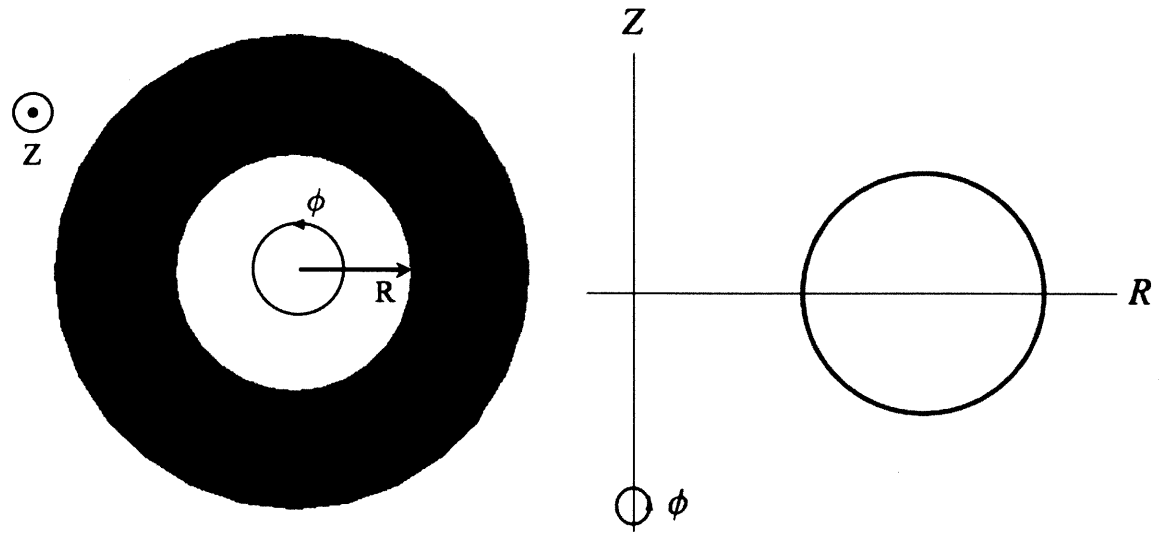

Fig. 2.1. Geometry for toroidally axisymmetric equilibria and cylindrical coordinates

which is the field in the (R,Z) plane. Indeed, $\nabla \cdot \mathbf{B} = 0$ implies that $\mathbf{B}$ can be written as $\mathbf{B} = \nabla \times \mathbf{A}$, where $\mathbf{A}$ is the vector potential. And with the axisymmetry, only A_ϕ appears in the expressions for B_R and B_Z:

$$B_R = -\frac{\partial A_\phi}{\partial Z} = -\frac{1}{R}\frac{\partial (RA_\phi)}{\partial Z}, \quad B_Z = \frac{1}{R}\frac{\partial (RA_\phi)}{\partial R} \tag{2.7}$$

As is often done in fluid dynamics, it is then very convenient to introduce a stream function Ψ, defined by $\Psi = RA_\phi$, to write

$$\mathbf{B} = B_\phi \mathbf{e}_\phi + \frac{1}{R}\nabla\Psi \times \mathbf{e}_\phi \tag{2.8}$$

where $\mathbf{e}_\phi$ is the unit vector in the ϕ direction, $\mathbf{e}_\phi = R\nabla\phi$.

The physical interpretation of the stream function Ψ is straightforward: it is the poloidal flux Ψ_P normalized by dividing by a factor 2π. This is shown as follows. The poloidal flux is defined by $\Psi_P = \int \mathbf{B}_P \cdot \mathbf{dS}$, where $\mathbf{dS}$ is an infinitesimal surface element. If we choose to calculate the poloidal flux through the area of a washer shaped surface in the plane $Z = 0$, extending from the magnetic axis, located at $R = R_a$, to an arbitrary Ψ contour, at $R = R_b$, we find:

$$\begin{aligned} \Psi_P &= \int_0^{2\pi} d\phi \int_{R_a}^{R_b} dR R B_Z(R, Z=0) = \int_0^{2\pi} d\phi \int_{R_a}^{R_b} dR \frac{\partial \Psi}{\partial R} \\ \Leftrightarrow \Psi_P &= 2\pi \left[\Psi(R_b, 0) - \Psi(R_a, 0) \right] \end{aligned} \tag{2.9}$$

As we can see from eq. (2.7), Ψ is defined to within an arbitrary integration constant. Choosing this arbitrary constant so that $\Psi(R_a, 0) = 0$[2], eq. (2.9) becomes:

$$\Psi_P = 2\pi\Psi \tag{2.10}$$

which proves our statement.

The next step in the derivation of the GS equation is to use the low-frequency version of Ampere's law, $\nabla \times \mathbf{B} = \mu_0 \mathbf{J}$, to obtain an expression of $\mathbf{J}$ in terms of the stream function Ψ. Ampere's law is formally identical to the equation linking the magnetic field and the vector potential, so that we immediately obtain, for the poloidal current,

---

[2] Note that we will choose the arbitrary constant in a different way in Section 2.2, where it will be more convenient to choose it such that $\Psi = 0$ on the plasma surface

$$\mu_0 \mathbf{J}_p = \frac{1}{R}\nabla\left(RB_\phi\right)\times \mathbf{e}_\phi \tag{2.11}$$

The toroidal current is

$$\begin{aligned}\mu_0 J_\phi &= \frac{\partial B_R}{\partial Z} - \frac{\partial B_Z}{\partial R} = -\frac{1}{R}\left[R\frac{\partial}{\partial R}\left(\frac{1}{R}\frac{\partial \Psi}{\partial R}\right)+\frac{\partial^2 \Psi}{\partial Z^2}\right] \\ &= -\frac{1}{R}\Delta^* \Psi\end{aligned} \tag{2.12}$$

where, as usually done in MHD equilibrium theory, we have introduced the elliptic operator Δ^* , given by :

$$\Delta^* X = R^2 \nabla\cdot\left(\frac{\nabla X}{R^2}\right) = R\frac{\partial}{\partial R}\left(\frac{1}{R}\frac{\partial X}{\partial R}\right)+\frac{\partial^2 X}{\partial Z^2} \tag{2.13}$$

We are now ready for the last three steps in the derivation of the GS equation, which consists in projecting the momentum equation $\mathbf{J}\times\mathbf{B} = \nabla p$ onto the three vectors $\mathbf{B}$, $\mathbf{J}$, and $\nabla\Psi$.

- Projection onto $\mathbf{B}$

  It is clear that the left-hand side of the momentum equation is orthogonal to $\mathbf{B}$. Because of the axisymmetry, ∇p has only R and Z components, so that the result of the projection is

$$\frac{1}{R}\left(\nabla\Psi\times\mathbf{e}_\phi\right)\cdot\nabla p = 0 \Leftrightarrow \mathbf{e}_\phi\cdot\nabla\Psi\times\nabla p = 0 \tag{2.14}$$

  Now, $\nabla\Psi\times\nabla p$ only has a ϕ component. Therefore, eq. (2.14) implies that

$$\nabla\Psi\times\nabla p = 0 \Leftrightarrow p = p\left(\Psi\right) \tag{2.15}$$

p depends on Ψ only, it is a surface quantity.

- Projection onto **J**

From the formal equivalence of the role played by **B** and **J** in the momentum equation, it is clear that the projection onto **J** leads to the following equation:

$$\begin{aligned} \frac{1}{R}\nabla\left(RB_\phi\right)\times\mathbf{e}_\phi\cdot\nabla p = 0 &\Leftrightarrow \mathbf{e}_\phi\cdot\nabla\left(RB_\phi\right)\times\nabla p = 0 \\ &\Leftrightarrow \mathbf{e}_\phi\cdot\nabla\left(RB_\phi\right)\times\nabla\Psi = 0 \end{aligned} \tag{2.16}$$

In the second line of eq. (2.16), we used the fact that $p = p\left(\Psi\right)$. We now are in the same situation as in eq. (2.14), and in the same way, we conclude that

$$RB_\phi = F\left(\Psi\right) \tag{2.17}$$

The quantity RB_ϕ depends on Ψ only, and is a surface quantity like p. As with Ψ, there is a physical interpretation for the quantity F: it is the net poloidal current flowing in the plasma and the toroidal field coils normalized by dividing by a factor -2π. To prove this, we calculate the flux of the poloidal current density through a disk-shaped surface lying in the $Z = 0$ plane, extending from $R = 0$ to an arbitrary Ψ contour at $R = R_b$. We find:

$$I_p = \int \mathbf{J}_p\cdot\mathbf{dS} = -\int_0^{2\pi} d\phi\int_0^{R_b} dRRJ_Z\left(R, Z=0\right) = -\int_0^{2\pi} d\phi\int_0^{R_b} dR\frac{\partial F}{\partial R} = -2\pi F(\Psi) \tag{2.18}$$

which proves our point. In (2.18), the – sign comes from the fact that the element of surface **dS** is oriented in the $+Z$ direction.

- Projection onto $\nabla\Psi$

We are now ready to calculate $\mathbf{J}\times\mathbf{B}=\left(J_\phi\mathbf{e}_\phi+\mathbf{J}_p\right)\times\left(B_\phi\mathbf{e}_\phi+\mathbf{B}_p\right)$. The cross product between the two toroidal components obviously vanishes. Furthermore, $\mathbf{J}_p\times\mathbf{B}_p=\mathbf{0}$ since $\nabla\Psi\times\mathbf{e}_\phi\cdot\mathbf{e}_\phi=0$, and $\nabla\Psi\times\mathbf{e}_\phi\cdot\nabla\Psi=0$. Therefore, the only contributions come from the cross terms between poloidal and toroidal components. Using the so-called "BAC-CAB" vector identity, it is easily to calculate that

$$\begin{aligned} J_\phi\mathbf{e}_\phi\times\mathbf{B}_p &= \frac{J_\phi}{R}\nabla\Psi=-\frac{1}{\mu_0R^2}\Delta^*\Psi\nabla\Psi \\ \mathbf{J}_p\times B_\phi\mathbf{e}_\phi &= -\frac{1}{\mu_0R^2}F\frac{dF}{d\Psi}\nabla\Psi \end{aligned} \tag{2.19}$$

For toroidally axisymmetric geometries, the momentum equation can therefore be written as

$$-\frac{1}{\mu_0R^2}\Delta^*\Psi\nabla\Psi-\frac{1}{\mu_0R^2}F\frac{dF}{d\Psi}\nabla\Psi=\frac{dp}{d\Psi}\nabla\Psi \tag{2.20}$$

We see here that the only non trivial information in the equilibrium force balance equation is contained in the $\nabla\Psi$ component, as expected. Eq. (2.20) is usually written in the form

$$\Delta^*\Psi=-\mu_0R^2\frac{dp}{d\Psi}-F\frac{dF}{d\Psi} \tag{2.21}$$

This second-order, nonlinear, elliptic partial differential equation is the Grad-Shafranov equation (GS equation). Once the two free functions p and F are chosen,

and the boundary conditions fixed, the GS equation can be solved, and the solution Ψ fully determines the nature of the equilibrium. In the next two sections (Sections 2.2 and 2.3), we focus on particular profiles for p and F, profiles for which we will be able to find analytic solutions to the GS equation.

2.2 Analytic solutions of the Grad-Shafranov equation with Solov'ev profiles[3]

2.2.1 Analytic solutions of the Grad-Shafranov equation

In general, the GS equation has to be solved numerically, and since the late 1950s and the first derivation of the equation, several excellent accurate and fast numerical Grad-Shafranov solvers have been proposed (see for instance [18] and references therein). Nevertheless, analytic solutions are always desirable from a theoretical point of view. They usually give more insights into the properties of a given equilibrium than numerical solvers do, for instance when used to derive scalings with the different geometric parameters (aspect ratio, elongation, triangularity). They can also be the basis of analytic stability and transport calculations. Finally, they can be used to test the numerical solvers.

In several confinement concepts of fusion interest, such as the tokamak and the stellarator for instance, the inverse aspect ratio is a small number which can be used as an expansion parameter in eq. (2.21). Analytic solutions are obtained by

[3] A significant portion of Section 2.2 can be found in A.J. Cerfon and J.P. Freidberg, *Phys. Plasmas* **17**, 032502 (2010).

expanding (2.21) order by order, as one usually does in asymptotic calculations. This method has led to a wealth of results, and a very deep analytic understanding of static equilibrium in tokamaks (See for instance [17] and [19]).

The problem, of course, is that asymptotic expansions break down in other confinement concepts of fusion interest, such as spherical tokamaks (STs), spheromaks, or Field Reverse Configurations (FRCs), in which the inverse aspect ratio is close to 1. In this case, of course, analytic solutions can only be found for specific, cleverly chosen profiles for the functions p and F. In 1968, Solov'ev [2] proposed simple pressure and poloidal current profiles which convert the GS equation into a linear, inhomogeneous partial differential equation, much simpler to solve analytically. Despite their simplicity, and the fact that the current density is finite, not zero, at the plasma edge, these profiles still retain much of the crucial physics that describes each configuration of interest, and have, therefore, been extensively studied, particularly for spherical tokamaks [17], [20], [21], [22]. The analytic solutions of the GS equation investigated in these papers have been used in the study of plasma shaping effects on equilibrium [23] and transport [24], [25] properties.

A general property of these analytic solutions is that they contain only a very few terms, thereby making them attractive from a theoretical analysis point of view. One down side is that while the solutions exactly satisfy the GS equation, one is not free to specify a desired shape for the plasma surface on which to impose boundary conditions. One simply has to take whatever the surface turns out to be after

optimizing over the small number of terms kept in the solution. Specifically, this mini-optimization results in limits on the class of equilibria that can be accurately described. For instance, reference [17] focuses solely on low-β equilibria, where the toroidal field is a vacuum field. It thus cannot describe the equilibrium β limit. The solution presented in [20] can describe the equilibrium β limit but only for small triangularities. It is ill behaved for moderate to large triangularities. In references [21] and [22], the solutions allow for an inboard separatrix for a wider range of triangularities, but appear to be over constrained in that the shape of the plasma (elongation and triangularity) depends on the choice of the location of the poloidal field null. Often trial and error is required to choose certain free coefficients that appear in the optimization in order to obtain an equilibrium with certain desired qualitative properties. Rarely, if ever, are non-tokamak configurations considered.

The goal of this section and of this chapter as a whole is to present a new, extended analytic solution to the GS equation with Solov'ev profiles which possesses sufficient freedom to describe a variety of magnetic configurations: the standard tokamak, the spherical tokamak, the spheromak, and the field reversed configuration. This new solution possesses a finite number of terms but includes several additional terms not contained in previous analyses. Our solution is valid for arbitrary aspect ratio, elongation, and triangularity. It is also allows a wide range of β: (1) $\beta = 0$ force free equilibria, (2) $\beta_p \approx 1$ equilibria where the toroidal field is a vacuum field

that could have the value zero, and (3) high β equilibria where a separatrix moves onto the inner plasma surface. Lastly, the solution allows the plasma surface to be either smooth or to possess a double or single null divertor X-point. Most importantly, no trial and error hunting is required. A simple, direct, non-iterative, one-pass methodology always yields the desired equilibrium solution.

In the remainder of this section, we describe how to derive the new extended solution (section 2.2.2), explain the procedure we use to systematically calculate the free coefficients in our solution (section 2.2.3), and use the solution to calculate equilibria and figures of merit in all the geometries of interest and for all the beta regimes mentioned previously (section 2.2.4 to section 2.2.9).

2.2.2 The Grad-Shafranov equation with Solov'ev profiles

The GS equation (eq. (2.21)) can be put in a non-dimensional form through the normalization $R = R_0 x$, $Z = R_0 y$, and $\Psi = \Psi_0 \psi$, where R_0 is the major radius of the plasma, and Ψ_0 is an arbitrary constant:

$$x\frac{\partial}{\partial x}\left(\frac{1}{x}\frac{\partial \psi}{\partial x}\right)+\frac{\partial^2 \psi}{\partial y^2} = -\mu_0 \frac{R_0^4}{\Psi_0^2} x^2 \frac{dp}{d\psi} - \frac{R_0^2}{\Psi_0^2} F \frac{dF}{d\psi} \tag{2.22}$$

The choices for p and F corresponding to the Solov'ev profiles are given by [2]

$$\begin{aligned} -\mu_0 \frac{R_0^4}{\Psi_0^2}\frac{dp}{d\psi} &= C \\ -\frac{R_0^2}{\Psi_0^2} F \frac{dF}{d\psi} &= A \end{aligned} \tag{2.23}$$

where A and C are constants. Since Ψ_0 is an arbitrary constant, one can, without loss in generality, choose it such that $A+C=1$[4]. This is formally equivalent to the rescaling $\Psi_0^2 \rightarrow (A+C)\Psi_0^2$. Under these conditions, the GS equation with Solov'ev profiles can be written in the following dimensionless form

$$x\frac{\partial}{\partial x}\left(\frac{1}{x}\frac{\partial \psi}{\partial x}\right)+\frac{\partial^2 \psi}{\partial y^2}=(1-A)x^2+A \tag{2.24}$$

The choice of A defines the β regime of interest for the configuration under consideration. In the following sections, we will calculate equilibria in various magnetic geometries for particular values of A corresponding to a range of β values.

The solution to eq. (2.24) is of the form $\psi(x,y)=\psi_P(x,y)+\psi_H(x,y)$ where ψ_P is the particular solution and ψ_H is the homogeneous solution. The particular solution can be written as

$$\psi_P(x,y)=\frac{x^4}{8}+A\left(\frac{1}{2}x^2\ln x-\frac{x^4}{8}\right) \tag{2.25}$$

The homogeneous solution satisfies

$$x\frac{\partial}{\partial x}\left(\frac{1}{x}\frac{\partial \psi_H}{\partial x}\right)+\frac{\partial^2 \psi_H}{\partial y^2}=0 \tag{2.26}$$

[4] The special case $A+C=0$ cannot occur for physical equilibria since it corresponds to a situation beyond the equilibrium limit where the separatrix moves onto the inner plasma surface.

A general arbitrary degree polynomial-like solution to this equation for plasmas with up-down symmetry has been derived by Zheng *et. al.* in [20]. We present here the details of this derivation.

Given the form of eq. (2.26), and the fact that we look for solutions which are even in the variable y (up-down symmetry), we assume that there exists a general solution of the form of the expansion

$$\psi_H(x,y) = \sum_{n=0,2,\ldots} \sum_{k=0}^{n/2} G(n,k,x) y^{n-2k} \tag{2.27}$$

where, the expansion can stop at any desired n, and where G is a function which is not yet determined, but which we expect to have a similar form as the particular solution ψ_P, namely either a power of x, or a power of x multiplying $\ln x$. Now, if (2.27) is a solution, it obviously has to satisfy the equation (2.26). Inserting (2.27) into (2.26), and identifying the terms where y has the same exponents for a given n, we obtain the following recurrence relations on the index k, for a given n:

$$\begin{aligned} x\frac{\partial}{\partial x}\left(\frac{1}{x}\frac{\partial G(n,0,x)}{\partial x}\right) &= 0 \\ x\frac{\partial}{\partial x}\left(\frac{1}{x}\frac{\partial G(n,k,x)}{\partial x}\right) &= -(n-2k+1)(n-2k+2)G(n,k-1,x) \qquad (k \neq 0) \end{aligned} \tag{2.28}$$

As can be seen by focusing for instance on the case $k = 0$, there are two types of solutions to eq. (2.28) (In the case $k = 0$, they are $G1(n,0,x) = 1$ and $G2\big(n,0,x\big) = x^2$). Thus, we write

$$G(n,k,x) = c_{n1}G1\big(n,k,x\big) + c_{n2}G2\big(n,k,x\big) \tag{2.29}$$

where the c_{n1} and c_{n2} are free constants. With a proof by induction, it is then easy to show that if $G1$ and $G2$ take the following general forms:

$$\begin{aligned} &G1\big(n,0,x\big) = 1 \\ &G1\big(n,k>0,x\big) = \big(-1\big)^k \frac{n!}{\big(n-2k\big)!}\frac{1}{2^{2k}k!\big(k-1\big)!}x^{2k}\left(2\ln x + \frac{1}{k} - 2\sum_{j=1}^{k}\frac{1}{j}\right) \\ &G2\big(n,k,x\big) = \big(-1\big)^k \frac{n!}{\big(n-2k\big)!}\frac{1}{2^{2k}k!\big(k+1\big)!}x^{2k+2} \end{aligned} \tag{2.30}$$

they satisfy the recurrence relation (2.28), so that the solution assumed in (2.27) does indeed solve the differential equation (2.26).

The solutions given by the form in $G1$ are what we call the polynomial-like solutions (since they involve $\ln x$), while the solutions obtained from $G2$ are obviously the polynomial solutions. Eq. (2.30) is extremely convenient, since we can use it to calculate solutions to the GS equation with Solov'ev profiles in the form of polynomials (and polynomial-like terms) of arbitrary degree. For our purposes we need only a finite number of terms in the possible infinite sum of polynomials and polynomial-like terms. We truncate the series such that the highest degree polynomials appearing are R^6 and Z^6. Previous studies have truncated the series at

R^4 and Z^4. The full solution for up-down symmetric ψ including the most general polynomial and polynomial-like solution for ψ_H satisfying eq. (2.26) and consistent with our truncation criterion is given by

$$\psi(x,y) = \frac{x^4}{8} + A\left(\frac{1}{2}x^2 \ln x - \frac{x^4}{8}\right) + c_1\psi_1 + c_2\psi_2 + c_3\psi_3 + c_4\psi_4 + c_5\psi_5 + c_6\psi_6 + c_7\psi_7$$

$$\begin{aligned}
\psi_1 &= 1 \\
\psi_2 &= x^2 \\
\psi_3 &= y^2 - x^2 \ln x \\
\psi_4 &= x^4 - 4x^2y^2 \\
\psi_5 &= 2y^4 - 9y^2x^2 + 3x^4 \ln x - 12x^2y^2 \ln x \\
\psi_6 &= x^6 - 12x^4y^2 + 8x^2y^4 \\
\psi_7 &= 8y^6 - 140y^4x^2 + 75y^2x^4 - 15x^6 \ln x + 180x^4y^2 \ln x - 120x^2y^4 \ln x
\end{aligned} \tag{2.31}$$

Equation (2.31) is the desired exact solution to the G-S equation that describes all the configurations of interest that possess up-down symmetry. The unknown constants c_n are determined from as yet unspecified boundary constraints on ψ. We note that the formulation can be extended to configurations which are up-down asymmetric. This formulation is described in Section 2.2.9. However, for simplicity the immediate discussion and examples are focused on the up-down symmetric case. Thus, our next task is to determine the unknown c_n appearing in eq. (2.31).

2.2.3 The boundary constraints

Assume for the moment that the constant A is specified (we show shortly how to choose A for various configurations). There are then seven unknown c_n to be determined. Note that, as stated, with a finite number of free constants it is not possible to specify the entire continuous shape of the desired plasma boundary. This would require an infinite number of free constants. We can only match seven properties of the surface since that is the number of free constants available.

Consider first the case where the plasma surface is smooth. A good choice for these properties is to match the function and its first and second derivative at three test points: the inner equatorial point, the outer equatorial point, and the high point (see Fig. 2.2 for the geometry). While this might appear to require nine free constants (i.e. three conditions at each of the three points), two are redundant because of the up-down symmetry.

Although it is intuitively clear how to specify the function and its first derivative at each test point, the choice for the second derivative is less obvious. To specify the second derivatives we make use of a well-known analytic model for a smooth, elongated, "D" shaped cross section, which accurately describes all the configurations of interest [26]. The boundary of this cross-section is given by the parametric equations

$$\begin{aligned} x &= 1 + \varepsilon \cos\left(\tau + \alpha \sin\tau\right) \\ y &= \varepsilon\kappa \sin\left(\tau\right) \end{aligned} \tag{2.32}$$

where τ is a parameter covering the range $0 \leq \tau \leq 2\pi$. Also, $\varepsilon = a / R_0$ is the inverse aspect ratio, κ is the elongation, and $\sin\alpha = \delta$ is the triangularity. These three parameters have been geometrically defined in Fig. 2.2. For convex plasma surfaces the triangularity is limited to the range $\delta \leq \sin(1) \approx 0.841$. The idea is simple: we match the curvature of the plasma surface determined by our solution with the curvature of the model surface (2.32) at each test point. We now show how this is done in practice.

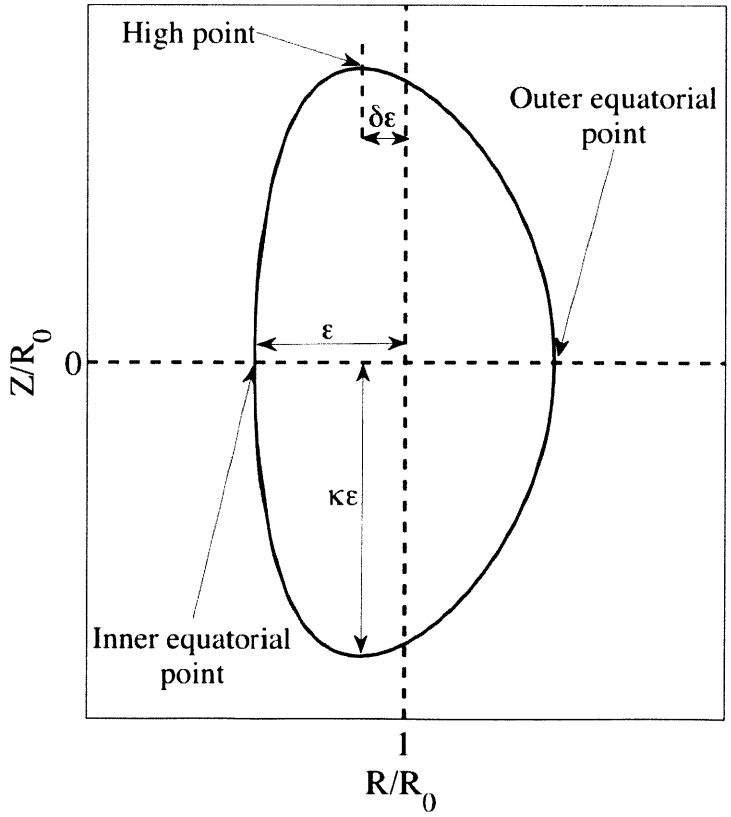

Fig. 2.2. Geometry of the problem and definition of the normalized geometric parameters ε, κ, and δ

Along the surface of constant ψ, we have, by definition,

$$d\psi = \psi_x dx + \psi_y dy = 0 \tag{2.33}$$

The first step is to use this equality to obtain expressions for the curvature at each point in terms of the partial derivatives of ψ at these points. For the inner and outer equatorial points, we write

$$\frac{d^2x}{dy^2} = -\frac{d}{dy}\left(\frac{\psi_y}{\psi_x}\right) = -\frac{\partial}{\partial y}\left(\frac{\psi_y}{\psi_x}\right) \qquad \text{(since } dx/dy = 0 \text{ at the two points)}$$

$$\Rightarrow \qquad \frac{d^2x}{dy^2} = -\frac{\psi_{yy}}{\psi_x} \qquad \text{(since } \psi_y = 0 \text{ at the two points)} \tag{2.34}$$

Similarly, at the top point, we find

$$\frac{d^2y}{dx^2} = -\frac{\psi_{xx}}{\psi_y} \tag{2.35}$$

The second step is to compute $\frac{d^2x}{dy^2}$ and $\frac{d^2y}{dx^2}$ for the model surface (2.32), so that we can indeed match the curvatures. After some mindless algebra starting from (2.32), we have

$$\frac{d^2x}{dy^2} = -\frac{1}{\varepsilon\kappa^2\cos^3\tau}\left[\sin\tau\sin\left(\tau+\alpha\sin\tau\right)\left(2\alpha\cos\tau+1\right)+\left(1+\alpha\cos\tau\right)^2\cos\tau\cos\left(\tau+\alpha\sin\tau\right)\right]$$

$$\frac{d^2y}{dx^2} = -\frac{\kappa}{\varepsilon}\frac{\sin\tau\sin\left(\tau+\alpha\sin\tau\right)+\left(1+\alpha\cos\tau\right)^2\cos\tau\cos\left(\tau+\alpha\sin\tau\right)}{\left(1+\alpha\cos\tau\right)^3\sin^3\left(\tau+\alpha\sin\tau\right)} \tag{2.36}$$

At the three points of interest, these expressions simplify substantially:

$$\left[\frac{d^2x}{dy^2}\right]_{\tau=0} = -\frac{\left(1+\alpha\right)^2}{\varepsilon\kappa^2} = N_1 \qquad \text{outer equatorial point}$$

$$\left[\frac{d^2x}{dy^2}\right]_{\tau=\pi} = \frac{\left(1-\alpha\right)^2}{\varepsilon\kappa^2} = N_2 \qquad \text{inner equatorial point} \tag{2.37}$$

$$\left[\frac{d^2y}{dx^2}\right]_{\tau=\pi/2} = -\frac{\kappa}{\varepsilon\cos^2\alpha} = N_3 \qquad \text{high point}$$

where we have named the three different curvatures N_1, N_2 and N_3 to simplify the expressions which will come later in this section.

We are now ready to introduce the seven geometric constraints, assuming that the free additive constant associated with the flux function is chosen so that $\psi = 0$ on the plasma surface (this implies that $\psi < 0$ in the plasma):

$\psi(1+\varepsilon,0) = 0$	outer equatorial point	
$\psi(1-\varepsilon,0) = 0$	inner equatorial point	
$\psi(1-\delta\varepsilon,\kappa\varepsilon) = 0$	high point	
$\psi_x(1-\delta\varepsilon,\kappa\varepsilon) = 0$	high point maximum	(2.38)
$\psi_{yy}(1+\varepsilon,0) = -N_1\psi_x(1+\varepsilon,0)$	outer equatorial point curvature	
$\psi_{yy}(1-\varepsilon,0) = -N_2\psi_x(1-\varepsilon,0)$	inner equatorial point curvature	
$\psi_{xx}(1-\delta\varepsilon,\kappa\varepsilon) = -N_3\psi_y(1-\delta\varepsilon,\kappa\varepsilon)$	high point curvature	

For a given value of A the conditions given by eq. (2.38) reduce to a set of seven linear inhomogeneous algebraic equations for the unknown c_n. This is a trivial numerical problem. We have found that even with only three test points the outer flux surface resulting from our analytic solution for ψ is smooth and remarkably close to the surface given by eq. (2.32) over the entire range of geometric parameters.

A similar formulation applies to the situation where the plasma surface has a double null divertor X-point. Here, we can imagine that the smooth model surface actually corresponds to the 95% flux surface. The location of the X-point usually occurs slightly higher and slightly closer to the inboard side of the plasma. Specifically we assume a 10% shift so that $x_{sep} = 1 - 1.1\delta\varepsilon$ and $y_{sep} = 1.1\kappa\varepsilon$. In terms of the boundary constraints, there is effectively only one change. At the X-point we can no longer impose the second derivative curvature constraint but instead require that both the tangential and normal magnetic field vanish. The conditions at the inboard and outboard equatorial points are left unchanged. The end result is that if one seeks an equilibrium solution where the plasma surface corresponds to a double null divertor and the 95% surface has an approximate elongation κ and triangularity δ then the constraint conditions determining the c_n are given by

$$
\begin{array}{ll}
\psi(1+\varepsilon,0) = 0 & \text{outer equatorial point} \\
\psi(1-\varepsilon,0) = 0 & \text{inner equatorial point} \\
\psi(x_{sep}, y_{sep}) = 0 & \text{high point} \\
\psi_x(x_{sep}, y_{sep}) = 0 & B_{normal} = 0 \text{ at the high point} \\
\psi_y(x_{sep}, y_{sep}) = 0 & B_{tangential} = 0 \text{ at the high point} \\
\psi_{yy}(1+\varepsilon,0) = -N_1\psi_x(1+\varepsilon,0) & \text{outer equatorial point curvature} \\
\psi_{yy}(1-\varepsilon,0) = -N_2\psi_x(1-\varepsilon,0) & \text{inner equatorial point curvature}
\end{array}
\tag{2.39}
$$

Hereafter, we assume that the c_n have been determined. The next step in the analysis is to evaluate the critical figures of merit describing the plasma equilibrium. This is the goal of section 2.2.4.

2.2.4 The plasma figures of merit

There are four figures of merit that are often used to describe the basic properties of Solov'ev MHD equilibria. These are defined as follows.

$$\begin{aligned} &\text{Total plasma beta} && \beta = \frac{2\mu_0 \langle p \rangle}{B_0^2 + \bar{B}_p^2} \\ &\text{Toroidal plasma beta} && \beta_t = \frac{2\mu_0 \langle p \rangle}{B_0^2} \\ &\text{Poloidal plasma beta} && \beta_p = \frac{2\mu_0 \langle p \rangle}{\bar{B}_p^2} \\ &\text{Kink safety factor} && q_* = \frac{\varepsilon B_0}{\bar{B}_p} \end{aligned} \tag{2.40}$$

The parameter B_0 is the vacuum toroidal field at $R = R_0$. The quantity $\bar{B}_p$ is the average poloidal magnetic field on the plasma surface

$$\bar{B}_p = \frac{\oint B_p \, dl_p}{\oint dl_p} = \frac{\int \mu_0 J_\phi \, dS_\phi}{\oint dl_p} = \frac{\mu_0 I}{R_0 C_p} \tag{2.41}$$

where C_p is the normalized poloidal circumference of the plasma surface

$$C_p = \frac{1}{R_0} \oint dl_p = 2 \int_{1-\varepsilon}^{1+\varepsilon} \left[1 + \left(dy / dx \right)^2 \right]^{1/2} dx \tag{2.42}$$

Lastly, $\langle p \rangle$ is the volume averaged pressure

$$\langle p \rangle = \frac{\int p \, d\mathbf{r}}{\int d\mathbf{r}} \tag{2.43}$$

The goal now is to derive explicit expressions for the figures of merit in terms of ψ, A, and the geometric parameters ε, κ, and δ. To do this we need the quantities p and $F^2 = R^2 B_\phi^2$ which are obtained by integrating eq. (2.23) and using the fact that $\psi = 0$ on the plasma surface.

$$\begin{aligned} p(x,y) &= -\frac{\Psi_0^2}{\mu_0 R_0^4}\left(1-A\right)\psi \\ B_\phi^2(x,y) &= \frac{R_0^2}{R^2}\left(B_0^2 - \frac{2\Psi_0^2}{R_0^4} A\,\psi\right) \end{aligned} \tag{2.44}$$

When evaluating the figures of merit the normalized quantity Ψ_0 / aR_0B_0 often appears in the results. It is convenient to replace this quantity with an equivalent quantity q_* which, after a short calculation, can be written as

$$\frac{1}{q_*} = -\left(\frac{\psi_0}{aR_0B_0}\right)\frac{1}{C_p}\int \frac{dx\,dy}{x}\left[A + (1-A)x^2\right] \tag{2.45}$$

The implication is that when describing MHD equilibria there are certain natural combinations of the figures of merit that appear which then depend only on the geometry and the for now free parameter A. This is convenient for determining general scaling relations.

Using this insight the desired form of the figures of merit are given by

$$\beta_p(\varepsilon,\kappa,\delta,A) = -2(1-A)\frac{C_p^2}{V}\left[\int \psi x\, dx\, dy\right]\left\{\int \frac{dx\, dy}{x}\left[A+(1-A)x^2\right]\right\}^{-2}$$

$$\beta_t = \frac{\varepsilon^2\beta_p}{q_*^2} \tag{2.46}$$

$$\beta = \frac{\varepsilon^2\beta_p}{q_*^2+\varepsilon^2}$$

where

$$V = \frac{1}{2\pi R_0^3}\int d\mathbf{r} = \int x\, dx\, dy \tag{2.47}$$

is the normalized plasma volume.

The analysis is now complete and ready to be applied to the magnetic configurations of interest.

2.2.5 ITER

A relatively simple case, which serves as a point of reference, is the International Thermonuclear Experimental Reactor (ITER) tokamak [11]. The baseline design [27] has the following parameters: $\varepsilon = 0.32$, $\kappa = 1.7$, and $\delta = 0.33$. The vacuum toroidal magnetic field at $R = R_0$ is $B_0 = 5.3$ T while the plasma current is $I = 15$ MA. Using the model surface given by eq. (2.32) yields a normalized circumference $C_p = 2.79$ and a normalized volume $V = 0.53$. These are approximate values used to estimate a value for $q_* = 1.57$. When evaluating the figures of merit the actual values of C_p and V from our Solov'ev equilibrium are

used. A wide range of beta values is possible for ITER. Choosing $A = -0.155$ yields $\beta_t = 0.05$ which is the baseline value.

The flux surfaces for the ITER example, assuming the smooth boundary constraints, are illustrated in Fig. 2.3. Observe that the shape of the surfaces and the magnetic axis shift are quite plausible as compared to full numerical solutions to the Grad-Shafranov equation.

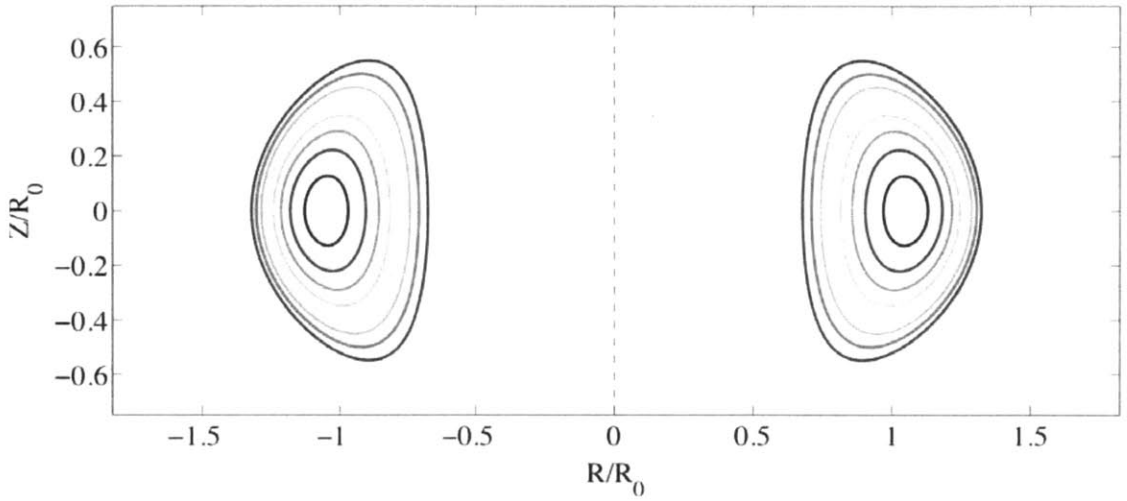

Fig. 2.3. ITER-like equilibrium with Solov'ev profiles $\varepsilon = 0.32, \kappa = 1.7, \delta = 0.33$

2.2.6 The spherical tokamak

The spherical tokamak (ST) is a much more challenging configuration to model because of the finite aspect ratio. It is in such a configuration that we best understand why our analytic solutions are useful. To show the range of possible ST equilibria we consider the flux surfaces for three qualitatively different regimes of

operation. These different regimes are characterized by different values of the free constant A.

The first regime corresponds to force free equilibria which, by definition, is equivalent to zero pressure. From eq. (2.23) this requires $A = 1$. In the second regime of interest we assume that B_ϕ, even with plasma, remains a vacuum toroidal field: that is, the free function $F(\psi) = R_0 B_0 = \text{const}$. This regime is usually referred to as the 'low-beta' regime. Again, referring to eq. (2.23) we see that this requires $A = 0$. The last regime to consider corresponds to the equilibrium beta limit where a separatrix moves onto the inner plasma surface. In this case A is determined by the condition

$$\psi_x\left(1-\varepsilon,0\right) = 0 \tag{2.48}$$

Equation (2.48) is to be added to the geometric boundary constraints given by eq. (2.38). The problem now requires the solution of eight (rather than seven) linear algebraic equations with the unknowns corresponding to the seven c_n plus A, still a trivial computational problem.

The flux surfaces for these three cases, assuming the smooth boundary constraints, are illustrated in Figs. 2.4 (a), (b), and (c), and for typical parameters corresponding to NSTX [28]: $\varepsilon = 0.78$, $\kappa = 2$, $\delta = 0.35$, and $q_* = 2$. Again, the surfaces appear quite plausible with the magnetic axis moving further out as beta

increases. This outward shift is known as the Shafranov shift [29]. For these three cases the figures of merit are summarized in Table 2.1.

	Force Free	Vacuum B_ϕ	Equilibrium Limit
β_p	0	1.07	4.20
β_t	0	0.16	0.64
β	0	0.14	0.55
Axis Shift: Δ / a	0.11	0.34	0.43

Table 2.1. Figures of merit for spherical tokamak equilibria

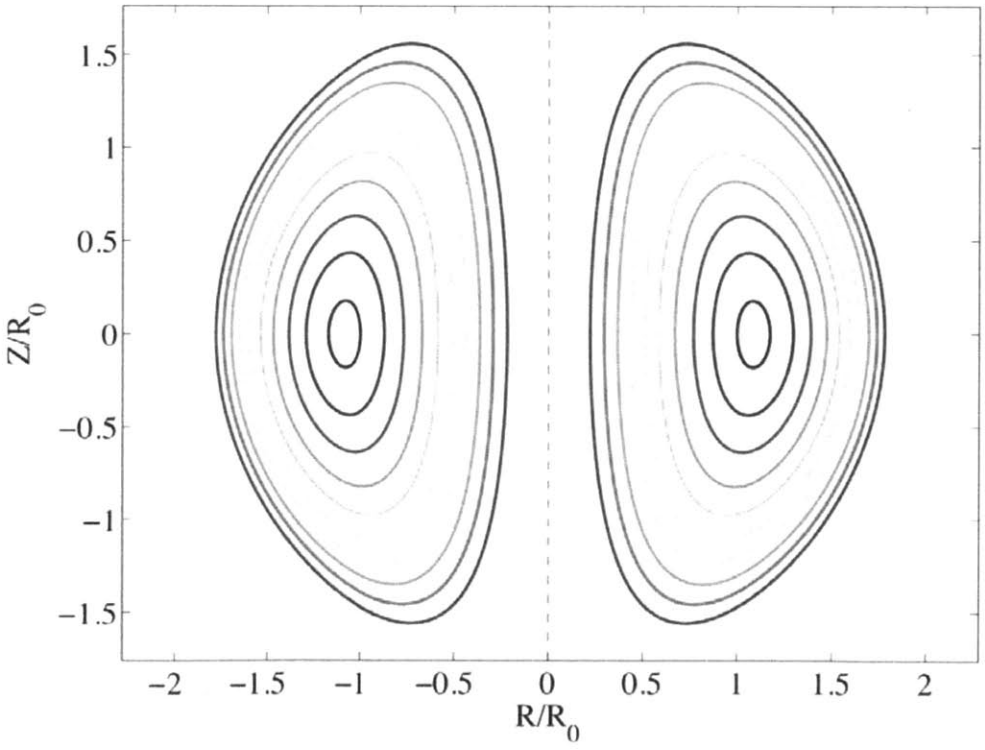

Fig. 2.4. (a) Force-free NSTX-like equilibrium ($\varepsilon = 0.78, \kappa = 2, \delta = 0.35$)

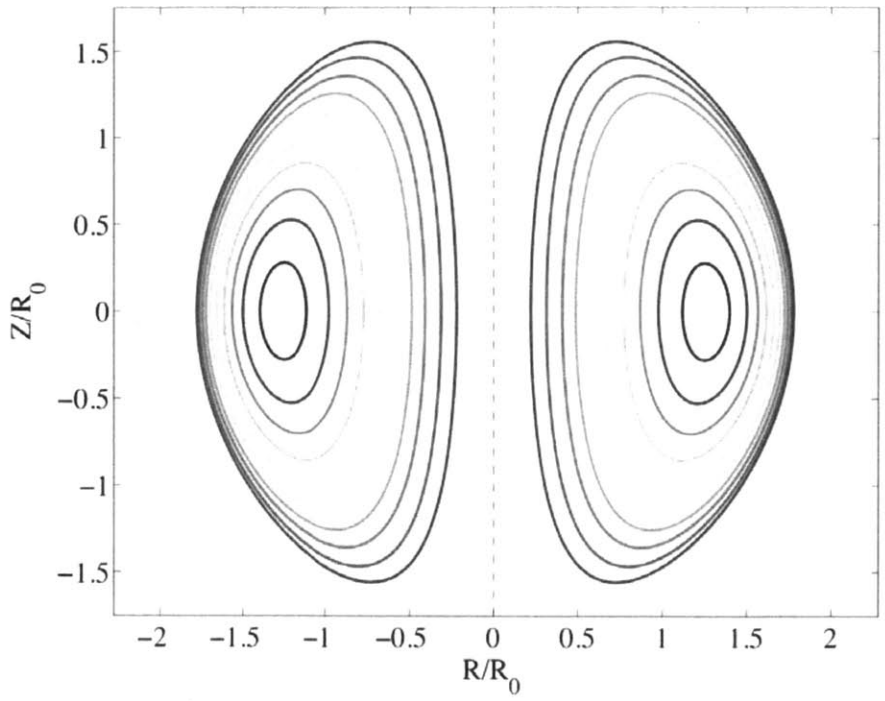

Fig. 2.4. (b) Low β NSTX-like equilibrium ($\varepsilon = 0.78, \kappa = 2, \delta = 0.35$)

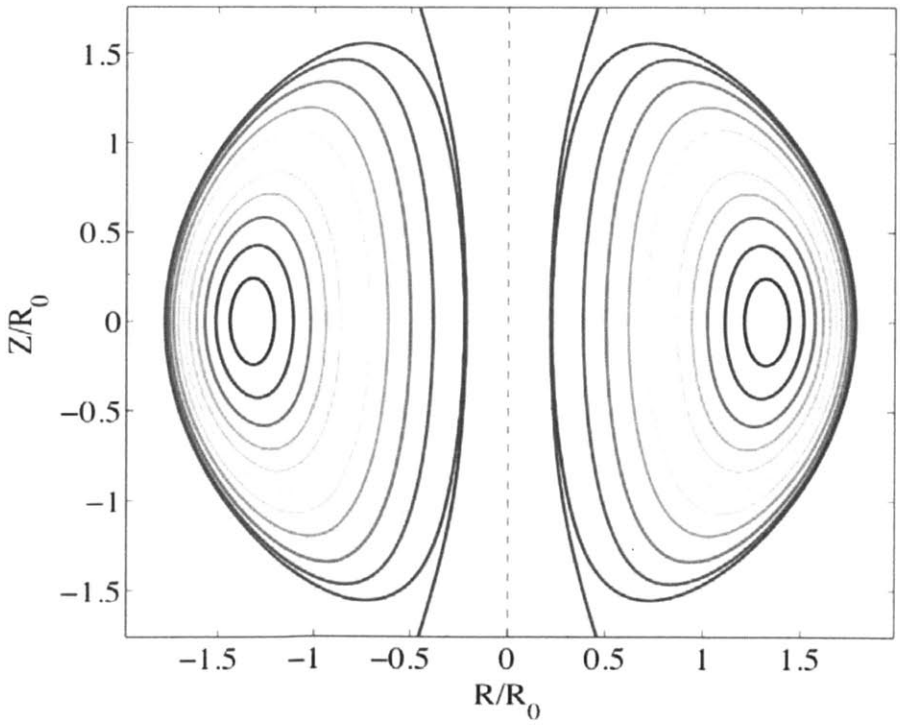

Fig. 2.4. (c) Equilibrium β limit NSTX-like equilibrium ($\varepsilon = 0.78, \kappa = 2, \delta = 0.35$). Note the separatrix on the inner surface of the plasma

Before calculating equilibria for other geometric configurations, we show how our analytic solution can be used to study equilibrium properties of the ST and get insights into the optimization of the design of a machine, perhaps before performing more computationally intensive numerical studies. It is for instance of interest to further examine the properties of the ST at the equilibrium limit. There are many ways to do this and one possible example is as follows. Consider an ST in which the inverse aspect ratio is fixed. For NSTX this value is $\varepsilon = 0.78$. The triangularity, for the sake of simplicity, is also held fixed at a typical NSTX value: $\delta = 0.35$. The kink safety factor is set to $q_* = 2$ to provide MHD stability against external kink modes. The goal now is to see how the value of beta at the equilibrium limit varies with the elongation κ.

Using the expressions (2.45) and (2.46), it is straightforward to use the analytic solution to plot a curve of β vs. κ. This curve is illustrated in Fig. 2.5. At $\kappa = 1$ the critical beta is $\beta = 0.38$, and this value increases with increasing κ, to reach $\beta = 0.55$ for $\kappa = 2$, a typical elongation in NSTX. From this particular point of view, the larger the elongation is, the better the equilibrium is. Of course, many other aspects have to be taken into consideration, both from an equilibrium and a stability point of view, and many such studies have to be performed during the process of optimization of a design.

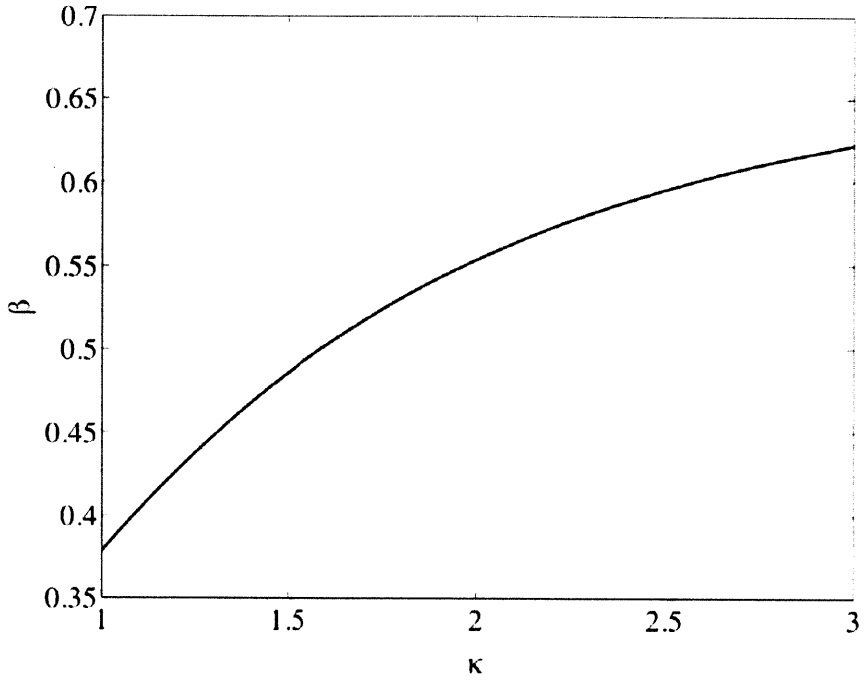

Fig. 2.5. β vs κ at the equilibrium beta limit, with ε, δ, and q_* held fixed ($\varepsilon = 0.78, \delta = 0.35$ and $q_* = 2$)

The last example of interest for the up-down symmetric spherical tokamak demonstrates that the analytical solution can be used to create a double null divertor. In this case we redo the intermediate case where $A = 0$ using the divertor constraints given by eq. (2.39). The resulting flux surfaces are illustrated in Fig. 2.6. Note that the solution has no difficulty generating a reasonable double null divertor equilibrium.

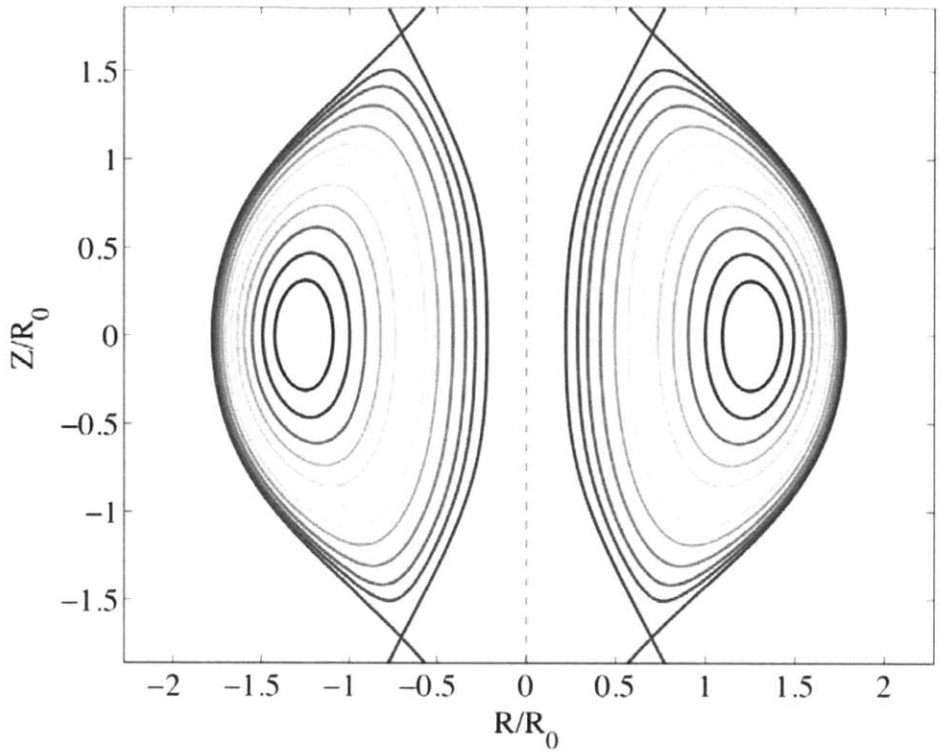

Fig. 2.6. Low β NSTX-like equilibrium with double null divertor.
$\varepsilon = 0.78, \kappa = 2, \delta = 0.35$

2.2.7 The spheromak

The calculation of the spheromak [30] flux surfaces closely parallels that of the ST. What is different is the evaluation of the figures of merit. Consider first the flux surfaces. Two interesting cases to consider are as follows. First, according to Taylor's theory of relaxation [16] the plasma should naturally evolve to a low beta force free state corresponding to $A = 1$. A set of flux surfaces for this case using the smooth surface constraints is illustrated in Fig. 2.7 (a) for typical spheromak parameters: $\varepsilon = 0.95$, $\kappa = 1$, and $\delta = 0.2$. They look reasonable, and obviously $\beta = 0$ since the plasma is force free.

The second case of interest recognizes that theoretically the spheromak also exhibits an equilibrium beta limit when the separatrix moves onto the inner plasma surface. This would not violate Taylor's theory since the plasma beta can be finite if it is externally heated. As for the ST the value of A for this case is determined by requiring that $\psi_x\left(1-\varepsilon,0\right)=0$. In terms of the corresponding figures of merit note that by definition $B_\phi = 0$ on the plasma surface since there is no toroidal field magnet. This implies that $q_* = 0$ for a spheromak. The conclusion is that the critical beta at the equilibrium limit can be written as

$$\beta = \beta_p = -2(1-A)\frac{C_p^2}{V}\left[\int \psi x\, dx\, dy\right]\left\{\int \frac{dx\, dy}{x}\left[A+(1-A)x^2\right]\right\}^{-2} \tag{2.49}$$

The flux surfaces for this case are illustrated in Fig. 2.7 (b) again assuming $\varepsilon = 0.95$, $\kappa = 1$, and $\delta = 0.2$. Note the larger shift of the magnetic axis as compared to the force free case. The value of beta at the equilibrium limit is given by $\beta = 2.20$.

2.2.8 The field reversed configuration

The final configuration of interest corresponds to the field reversed configuration (FRC) [31]. Here the plasma is very elongated (i.e. $\kappa \sim 10$) and has zero toroidal field implying that $A = 0$ and $B_0 = 0$. Therefore, $q_* = 0$ and $\beta = \beta_p$. Ideally an FRC has $\varepsilon = 1$ and $\delta = 1$.

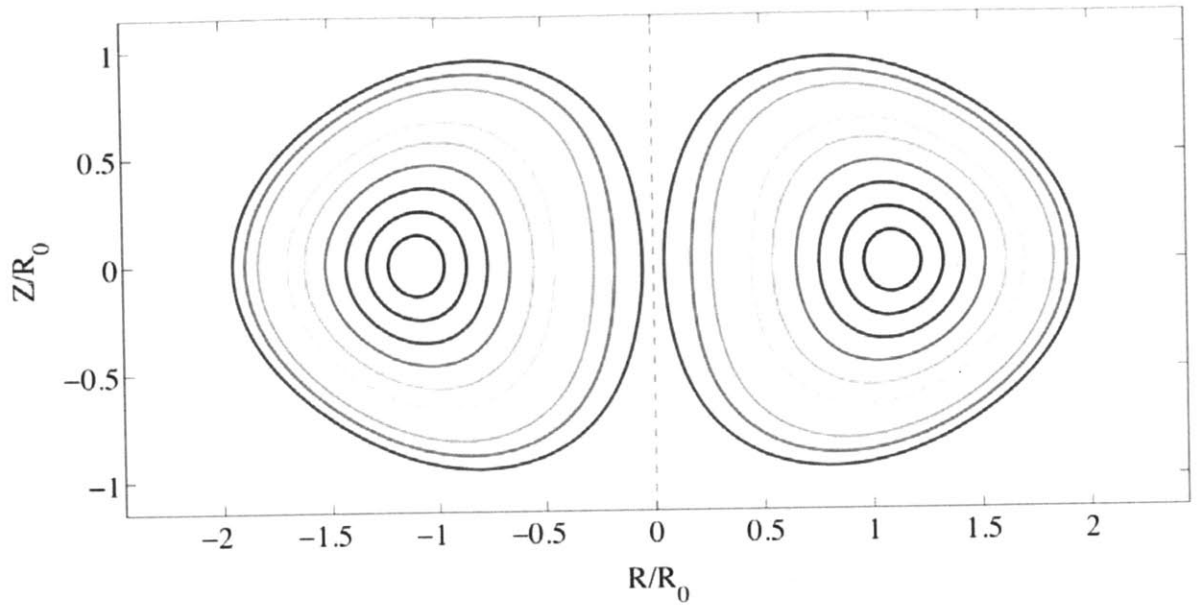

Fig. 2.7. (a) Force-free spheromak equilibrium ($\varepsilon = 0.95, \kappa = 1, \delta = 0.2$ and $\beta = 0$)

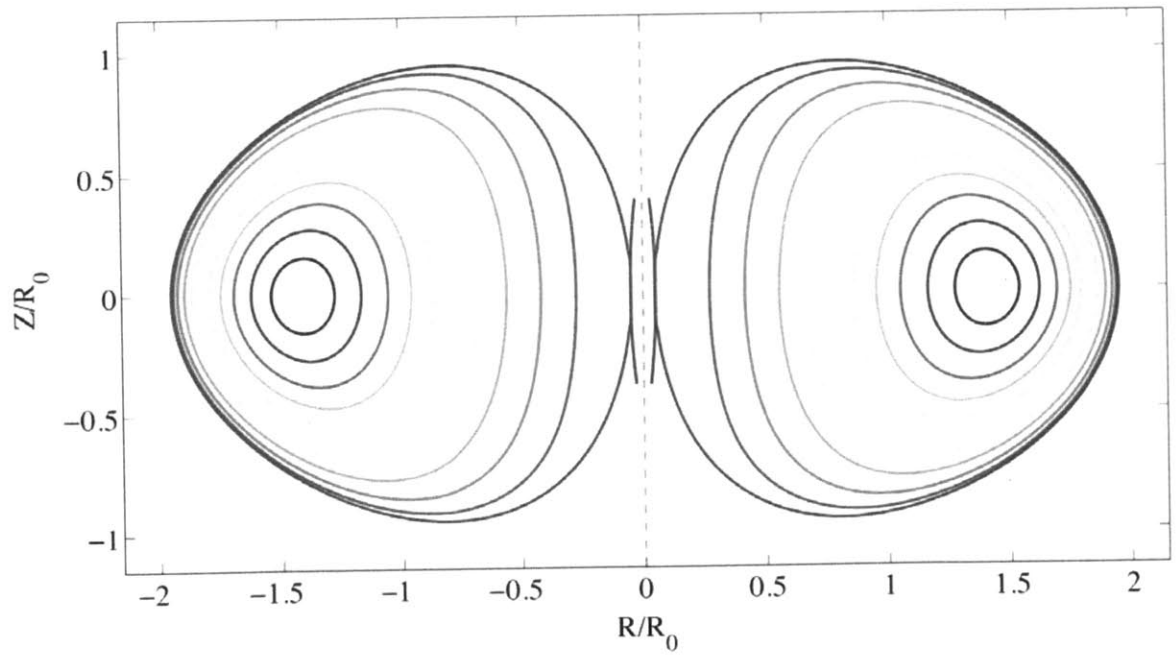

Fig. 2.7. (b) Equilibrium β limit spheromak equilibrium ($\varepsilon = 0.95, \kappa = 1, \delta = 0.2$, and $\beta = \beta_p = 2.2$). Note the separatrix on the inner surface of the plasma.

There are two ways to calculate the flux surfaces. The first method makes use of the solution already derived using the smooth surface constraints and

approximates the ideal FRC by choosing $\varepsilon = 0.99$ and $\delta = 0.7$. We cannot push the triangularity much higher, since the model surface we use comes with the requirement $\delta < 0.841$ for a convex plasma surface. The flux surfaces for the highly elongated case $\kappa = 10$ are illustrated in Fig. 2.8 (a). Observe that this is a reasonably good representation of an FRC. The value of beta is found to be $\beta = 1.20$.

The second way to calculate the flux surfaces is to explicitly make the plasma surface a separatrix. In this case $R = 0$ is the center line of the plasma thereby guaranteeing that $\varepsilon = 1$ and $\delta = 1$. To do this we must replace the model surface given by eq. (2.32) with one that is compatible with a separatrix. A convenient choice is a half-ellipse:

$$\begin{aligned} x &= 2\cos(\tau) \\ y &= \kappa \sin(\tau) \end{aligned} \tag{2.50}$$

with $-\pi / 2 \leq \tau \leq \pi / 2$.

The solution for the flux surfaces is again given by eq. (2.31) but in this case certain coefficients are automatically zero in order for $R = 0$ to correspond to the inner boundary of the flux surface: $\psi(0, y) = 0$. Specifically, $c_3 = c_5 = c_7 = 0$. The remaining non trivial surface constraints are now given by

$$\begin{aligned} &\psi(2,0) = 0 && \text{outer equatorial point} \\ &\psi(0,\kappa) = 0 && \text{high point} \\ &\psi_{yy}(2,0) = -N_1 \psi_x(2,0) && \text{outer equatorial point curvature} \\ &\psi_{xx}(0,\kappa) = -N_3 \psi_y(0,\kappa) && \text{high point curvature} \end{aligned} \tag{2.51}$$

For a half-ellipse the parameters N_1 and N_3 are easily evaluated :

$$N_1 = -2/\kappa^2$$
$$N_3 = -\kappa/4 \tag{2.52}$$

The flux surfaces for the second method are plotted in Fig. 2.8 (b) for $\kappa = 10$. The separatrix bounding the plasma is apparent. The value of beta is found to be $\beta = 1.05$ which is not too different from that obtained using the first method.

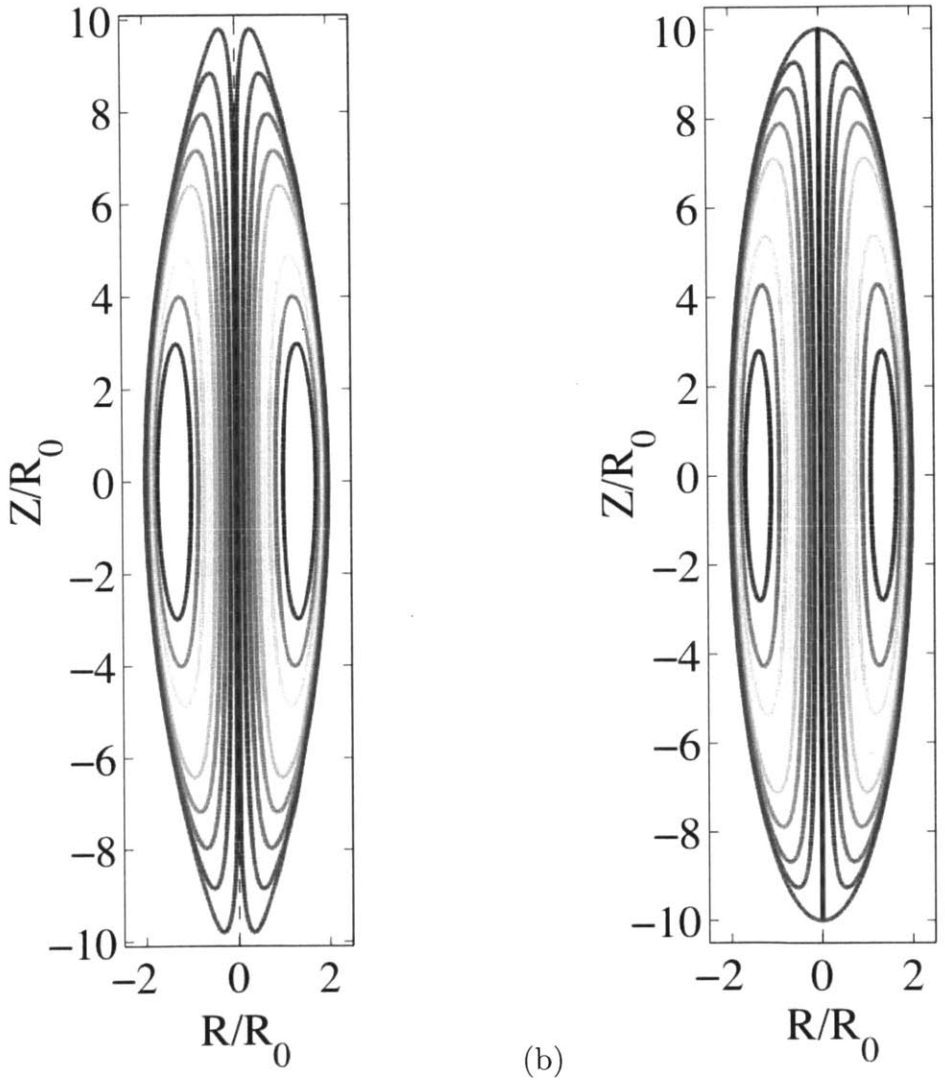

Fig. 2.8. (a) FRC equilibrium obtained with the first method, $\varepsilon = 0.99, \kappa = 10, \delta = 0.7$. (b) FRC equilibrium obtained with the second method, $\varepsilon = 1, \kappa = 10, \delta = 1$.

2.2.9 Up-down asymmetric formulation

Most of the modern fusion experiments operate with up-down asymmetric plasmas, with a single separatrix, or single 'null', and so will most of future experiments. In this section we show how the up-down symmetric formulation can be easily generalized to include the up-down asymmetric case, and in relation with the experiments, we will focus on cases with a single-null.

For up-down asymmetric configurations we once again assume that the reference surface of interest can be modeled parametrically as follows: $x = x(\tau)$, $y = y(\tau)$. In normalized units the inner and outer equatorial points are still located at $x = 1-\varepsilon,\ y = 0$ and $x = 1+\varepsilon,\ y = 0$ respectively. The upper portion of the surface is smooth and has a maximum at $x = 1-\delta\varepsilon,\ y = \kappa\varepsilon$. The lower portion of the surface is assumed to have a single null X-point located at $x = x_{sep}$ and $y = y_{sep} < 0$. The model surface can be specified either analytically or numerically. Under these assumptions the appropriate analytic solution to the Grad-Shafranov equation is now given by

$$\psi(x,y) = \frac{x^4}{8} + A\left(\frac{1}{2}x^2 \ln x - \frac{x^4}{8}\right) + c_1\psi_1 + c_2\psi_2 + c_3\psi_3 + c_4\psi_4 + c_5\psi_5 + c_6\psi_6 + c_7\psi_7 + c_8\psi_8 + c_9\psi_9 + c_{10}\psi_{10} + c_{11}\psi_{11} + c_{12}\psi_{12} \quad (2.53)$$

The terms on the first line have already been defined in eq. (2.31). The new terms on the second line have odd symmetry in y thereby allowing up-down asymmetric solutions. These terms can be written as

$$\begin{aligned}
\psi_8 &= y \\
\psi_9 &= yx^2 \\
\psi_{10} &= y^3 - 3yx^2 \ln x \\
\psi_{11} &= 3yx^4 - 4y^3x^2 \\
\psi_{12} &= 8y^5 - 45yx^4 - 80y^3x^2 \ln x + 60yx^4 \ln x
\end{aligned} \tag{2.54}$$

There are now 12 unknown coefficients. Following the procedure presented in the up-down symmetric case, there are 12 constraint relations (keeping in mind that the up-down symmetry conditions right at the inner and outer equatorial points no longer automatically apply). A good choice for the boundary constraints corresponding to a single null divertor are given by

$$\begin{aligned}
&\psi(1+\varepsilon,0) = 0 && \text{outer equatorial point} \\
&\psi(1-\varepsilon,0) = 0 && \text{inner equatorial point} \\
&\psi(1-\delta\varepsilon,\kappa\varepsilon) = 0 && \text{upper high point} \\
&\psi(x_{sep},y_{sep}) = 0 && \text{lower X-point} \\
&\psi_y(1+\varepsilon,0) = 0 && \text{outer equatorial point up-down symmetry} \\
&\psi_y(1-\varepsilon,0) = 0 && \text{inner equatorial point up-down symmetry} \\
&\psi_x(1-\delta\varepsilon,\kappa\varepsilon) = 0 && \text{upper high point maximum} \\
&\psi_x(x_{sep},y_{sep}) = 0 && B_y = 0 \text{ at lower X-point} \\
&\psi_y(x_{sep},y_{sep}) = 0 && B_x = 0 \text{ at lower X-point} \\
&\psi_{yy}(1+\varepsilon,0) = -N_1\psi_x(1+\varepsilon,0) && \text{outer equatorial point curvature} \\
&\psi_{yy}(1-\varepsilon,0) = -N_2\psi_x(1-\varepsilon,0) && \text{inner equatorial point curvature} \\
&\psi_{xx}(1-\delta\varepsilon,\kappa\varepsilon) = -N_3\psi_y(1-\delta\varepsilon,\kappa\varepsilon) && \text{high point curvature}
\end{aligned} \tag{2.55}$$

A simple practical choice for the N_j that works well is based on the model surface described by eq. (2.32). We assume initially that the configuration is up-down symmetric with κ and δ corresponding to the smooth upper portion of the surface. This assumption then leads to values for the N_j given by eq. (2.37). The location of the lower X-point is then chosen, as in section 2.2.3 : $x_{sep} = 1 - 1.1\delta\varepsilon$ and $y_{sep} = -1.1\kappa\varepsilon$.

The calculation of the unknown c_n is still a linear algebraic problem. Although it now involves 12 unknowns, it remains trivial computationally. Equations (2.53) - (2.55) represent the formulation of the up-down asymmetric problem.

To illustrate the procedure we show results for two examples. The first corresponds to ITER which is characterized by the following parameters: $\varepsilon = 0.32$, $\kappa = 1.7$, $\delta = 0.33$, $x_{sep} = 0.88$, $y_{sep} = -0.60$, and $q_* = 1.57$. The value of A is chosen as $A = -0.155$ which leads to a value of beta given by $\beta_t = 0.05$. The second example corresponds to a high beta spherical tokamak. Here, we use NSTX values for the geometry: $\varepsilon = 0.78$, $\kappa = 2$, $\delta = 0.35$, $x_{sep} = 0.70$, $y_{sep} = -1.71$, and $q_* = 2$. For this case A is chosen to correspond to a high value of beta but still below the equilibrium limit. Specifically we choose $A = -(1-\varepsilon)^2 / \varepsilon(2-\varepsilon) = -0.05$ which is the condition for the toroidal current density to vanish at the inner midplane, and leads to $\beta = 0.16$. The flux surfaces for these two examples are illustrated in Fig. 2.9 (a)

and Fig. 2.9 (b). Observe that the surfaces for both examples appear quite reasonable, thereby demonstrating the effectiveness of the procedure to model single null divertor configurations.

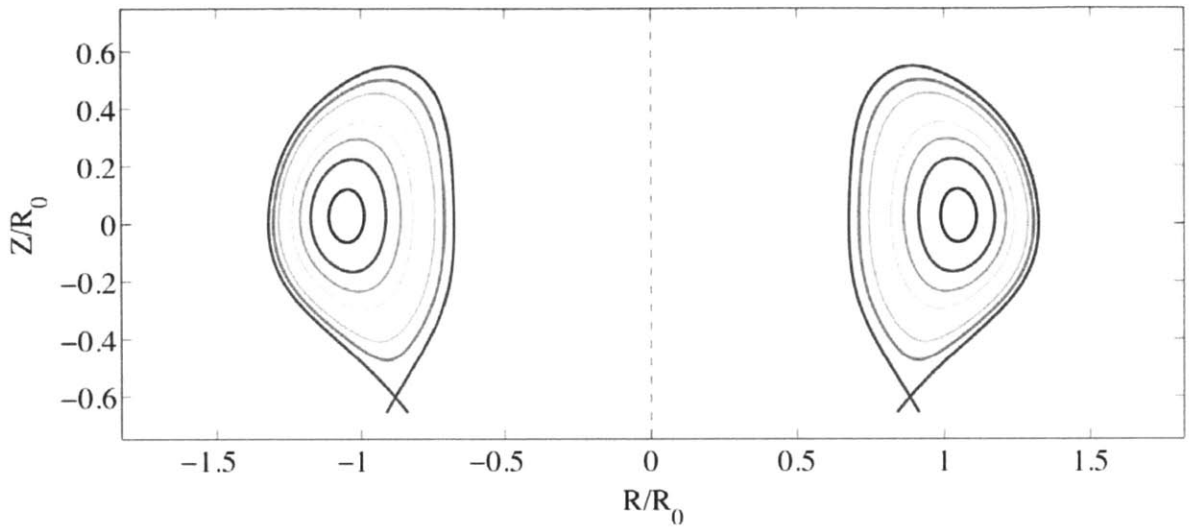

Fig. 2.9. (a) Lower single null ITER-like equilibrium ($\varepsilon = 0.32, \kappa = 1.7, \delta = 0.33$)

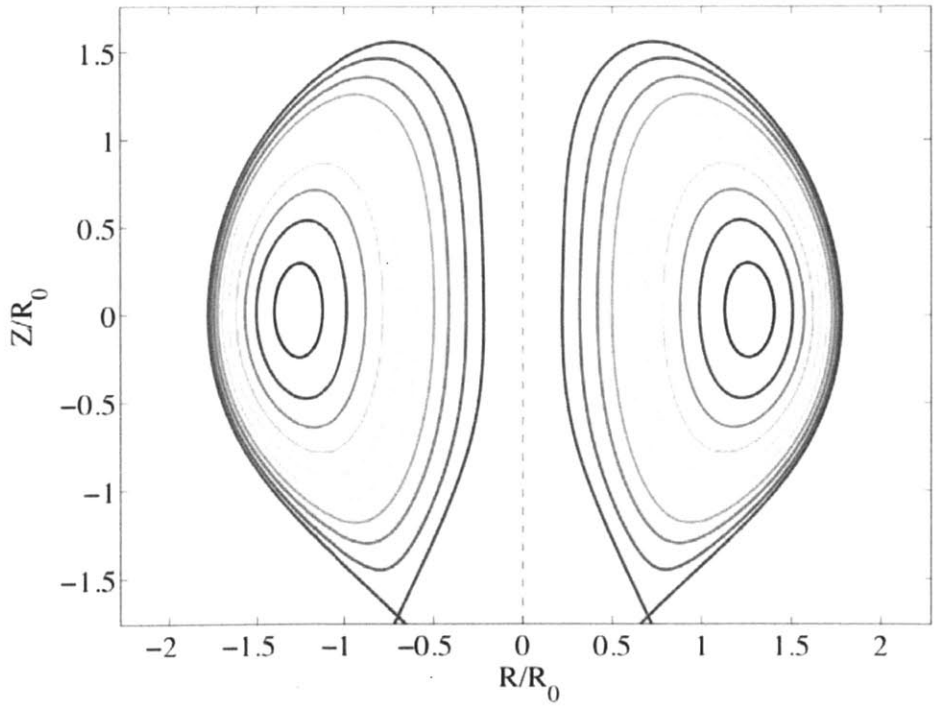

Fig. 2.9. (b) Lower single null NSTX-like equilibrium ($\varepsilon = 0.78, \kappa = 2, \delta = 0.35$)

2.3 Extension: Analytic solutions of the Grad-Shafranov equation with quadratic profiles

2.3.1 Solov'ev profiles and the discontinuity of the toroidal current density

The main problem with the Solov'ev profiles is that they correspond to the unrealistic situation where the toroidal current density has a jump at the plasma edge. Indeed, in eq. (2.12) we showed that the toroidal current density is given by

$$\mu_0 R J_\phi = -\Delta^* \Psi = \mu_0 R^2 \frac{dp}{d\Psi} + F \frac{dF}{d\Psi} \tag{2.56}$$

Normalizing eq. (2.56) as before, and using the Solov'ev profiles introduced in (2.23), we obtain

$$\frac{J_\phi}{J_0} = \left(A-1\right)x - \frac{A}{x} \tag{2.57}$$

where $J_0 = \left(\mu_0 R_0^3\right)^{-1} \Psi_0$. Using eq. (2.57), it is easy to see that for a given A, J_ϕ vanishes at the point x which solves the equation

$$x^2 = \frac{A}{A-1} \tag{2.58}$$

Of course, eq. (2.58) can not be satisfied at the inboard location ($x_{inboard} = 1-\varepsilon$) and the outboard location ($x_{outboard} = 1+\varepsilon$) simultaneously, and in general, it is satisfied at neither point, as illustrated in Figure 2.10, obtained for $A = 0.1$ and $\varepsilon = 0.78$.

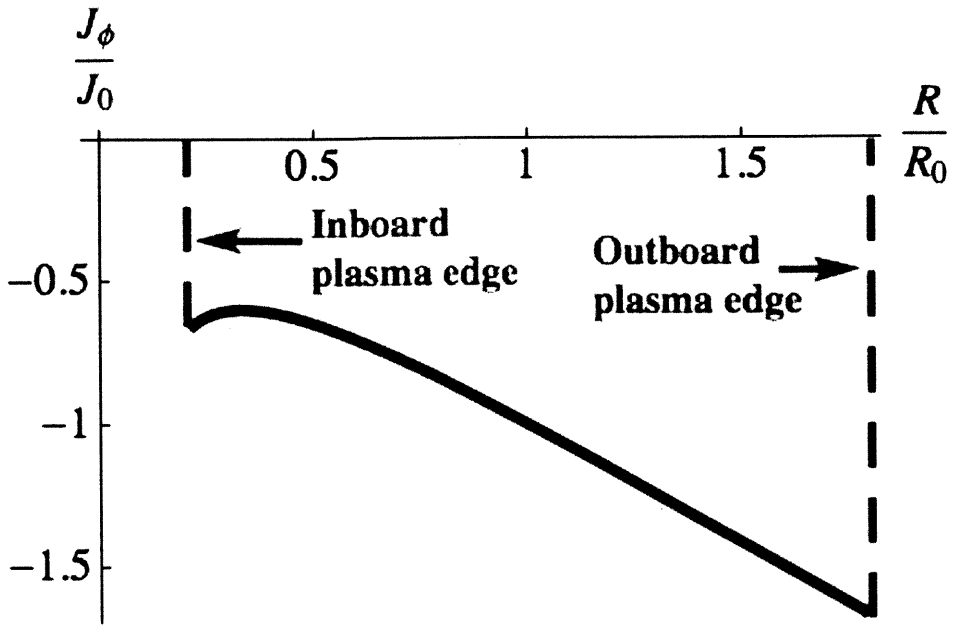

Fig. 2.10. Toroidal current density discontinuity for a Solov'ev equilibrium with

$$A = 0.1 \text{ and } \varepsilon = 0.78$$

In Fig. 2.10, the discontinuity of the toroidal current density appears clearly. Such a current profile is physically unrealistic.

Note that aside from the previous point, there is another problem with the current density calculated from Solov'ev profiles, which can be seen in eq. (2.57): J_ϕ does not depend on the variable y, or, in other words, on the coordinate Z in the original coordinate system $\left(R, \phi, Z\right)$.

For these reasons, our next task is to apply the strategy developed for Solov'ev type profiles in Section 2.2 to the more realistic case where p and F^2 are quadratic in the flux function Ψ.

2.3.2 Analytic solution of the Grad-Shafranov equation with quadratic profiles

We start from the normalized version of the GS equation, eq. (2.22), and consider profiles which are quadratic in the normalized flux function ψ. Specifically, we write $F^2 = R_0^2 B_0^2 \left(1 - \alpha\psi^2\right)$, and $p(\psi) = p_0\psi^2$. B_0 is the vacuum magnetic field, α represents the plasma diamagnetism ($\alpha > 0$) or paramagnetism ($\alpha < 0$), and p_0 is defined such that the pressure at the magnetic axis is $p_{axis} = p_0\psi_{axis}^2$. Defining the quantities

$$U = \frac{2\mu_0 R_0^4 p_0}{\Psi_0^2} \qquad \text{and} \qquad V = \alpha\frac{R_0^4 B_0^2}{\Psi_0^2} \tag{2.59}$$

equation (2.22) becomes

$$x\frac{\partial}{\partial x}\left(\frac{1}{x}\frac{\partial\psi}{\partial x}\right) + \frac{\partial^2\psi}{\partial y^2} + \left(Ux^2 - V\right)\psi = 0 \tag{2.60}$$

In all the regimes of interest, we have $U - V > 0$. Defining

$$k^2 = U - V = \frac{R_0^4 B_0^2}{\Psi_0^2}\left(\frac{2\mu_0 p_0}{B_0^2} - \alpha\right) \quad \text{and} \quad b = \frac{U}{U - V} = \left(1 - \frac{\alpha B_0^2}{2\mu_0 p_0}\right)^{-1} \tag{2.61}$$

equation (2.60) can be written in its final, desired form :

$$x\frac{\partial}{\partial x}\left(\frac{1}{x}\frac{\partial\psi}{\partial x}\right) + \frac{\partial^2\psi}{\partial y^2} + k^2\left[1 + b\left(x^2 - 1\right)\right]\psi = 0 \tag{2.62}$$

In eq. (2.62) k is treated as an unknown constant, which is determined from the boundary conditions, while b is chosen according to the β regime of operation (for example, $b = 1 \rightarrow \beta = 0$, $b = 0 \rightarrow \beta_p \approx 1$, $b = -1/2\varepsilon \rightarrow \varepsilon\beta \approx 1$).

We solve eq. (2.62) by separation of variables, writing $\psi(x,y) = \tilde{\psi}_1(x)\cos(k_y y) + \tilde{\psi}_2(x)\sin(k_y y)$, with $k_y^2 \leq k^2$ an undetermined separation constant. The first term corresponds to up-down symmetric solutions, while the second term corresponds to up-down asymmetric solutions. Also, for $k_y = 0$, $\sin(k_y y)$ has to be replaced by y, the simplest up-down asymmetric solution. Inserting this expression for $\psi(x,y)$ into eq. (2.62) leads to the same ordinary differential equation for $\tilde{\psi}_1(x)$ and $\tilde{\psi}_2(x)$:

$$x\frac{d}{dx}\left(\frac{1}{x}\frac{d\tilde{\psi}}{dx}\right) + \left[k^2(1-b) - k_y^2 + k^2 b x^2\right]\tilde{\psi} = 0 \tag{2.63}$$

The general solution to eq. (2.63) is:

$$\tilde{\psi}(x) = cW_{\lambda,\frac{1}{2}}\left(-ik\sqrt{b}x^2\right) + dM_{\lambda,\frac{1}{2}}\left(-ik\sqrt{b}x^2\right) \tag{2.64}$$

where W and M are the Whittaker functions, and $\lambda = i\left(4k\sqrt{b}\right)^{-1}\left[k^2(1-b) - k_y^2\right]$. The free constants c and d are determined from the boundary conditions. Theoretically, specifying the entire continuous shape of the plasma boundary would require an infinite number of free constants c, d, and k_y. This is the reason why the approach chosen by Atanasiu *et al.* [32] for the same problem (in fact, they allow p and F^2 to vary both linearly and quadratically with ψ, thereby combining the solutions presented in Sections 2.2 and 2.3) is to construct the analytic equilibrium by summing a large number of solutions of the form (2.64), and by determining the many free

constants c, d, and k_y from the minimization of the difference between the calculated plasma shape and the expected one. This approach is useful when trying to compare with experimental data, since it provides good accuracy and flexibility. However, the large number of terms retained make the equilibrium hard to use in practice for analytical stability or transport studies.

Fortunately, Guazzotto *et al.* [33] have shown that the following reduced, simpler expansion

$$\begin{aligned}\psi(x,y) = {} & W_{\lambda_0} + c_1 M_{\lambda_0} + \left(c_2 W_{\lambda_1} + c_3 M_{\lambda_1}\right)\cos(ky) + \left(c_4 W_{\lambda_2} + c_5 M_{\lambda_2}\right)\cos(k_2 y) \\ & + \left(c_6 W_{\lambda_0} + c_7 M_{\lambda_0}\right) y + \left(c_8 W_{\lambda_1} + c_9 M_{\lambda_1}\right)\sin(ky) + \left(c_{10} W_{\lambda_2} + c_{11} M_{\lambda_2}\right)\sin(k_2 y)\end{aligned} \tag{2.65}$$

leads to a very good match between a desired plasma shape and the actual shape obtained by solving for the finite number of unknown free constants using a corresponding number of boundary constraints. Eq. (2.65) is much more convenient for analytic equilibrium, stability and transport studies than the solution proposed in [32]. In eq. (2.65) the subscript 0 corresponds to $k_y = 0$, the subscript 1 to $k_y = k$, and the subscript 2 to $0 < k_y < k$.

The last task is to define the 13 boundary constraints required to determine the 13 free constants $c_1 - c_{11}$, k_y and k. A point of particular interest is the determination of the constants k_y and k. In Reference [33], they were determined empirically. We show in the next two sections that by applying the procedure presented in Section 2.2 to this problem, k_y and k no longer have to be guessed, but

are calculated from the appropriate boundary constraints, along with the coefficients $c_1 - c_{11}$. This simplifies the calculation of equilibria considerably.

2.3.3 Up-down symmetric solutions

The up-down symmetry automatically implies $c_6 = c_7 = c_8 = c_9 = c_{10} = c_{11} = 0$. The solution reduces to:

$$\psi(x,y) = W_{\lambda_0} + c_1 M_{\lambda_0} + \left(c_2 W_{\lambda_1} + c_3 M_{\lambda_1}\right)\cos(ky) + \left(c_4 W_{\lambda_2} + c_5 M_{\lambda_2}\right)\cos(k_2 y) \quad (2.66)$$

There are 7 unknowns: $c_1 - c_5, k, k_2$. In our study of Solov'ev equilibria, we presented 7 natural boundary constraints, for plasma equilibria with a limiter in eq. (2.38), or with a double-null divertor in eq. (2.39). We can directly reuse these 7 boundary constraints, which give us a system of 7 equations for the 7 unknowns. Such a system is easily solved numerically using typical nonlinear root solvers, provided one starts with an acceptable initial guess. The Whittaker functions are in the libraries of most commercial computational software programs.

In Fig 2.11, we show two double-null divertor equilibria calculated with this method. The first equilibrium corresponds to an ITER-like geometry, while the second corresponds to an NSTX-like geometry. Both are computed for a high plasma β corresponding to the vanishing of the toroidal current density gradient at the inboard midplane (i.e. for $b = 1/\varepsilon(2-\varepsilon)$), and the location of the X-points is given by $x_{sep} = 1 - 1.05\delta\varepsilon, y_{sep} = 1.05\delta\varepsilon$.

a)

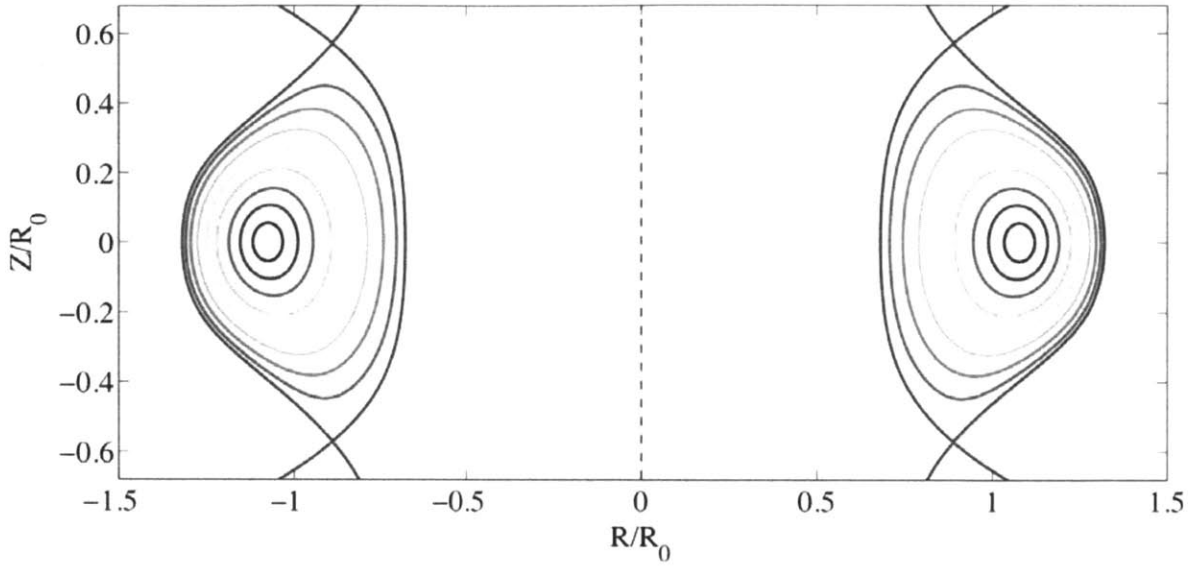

b)

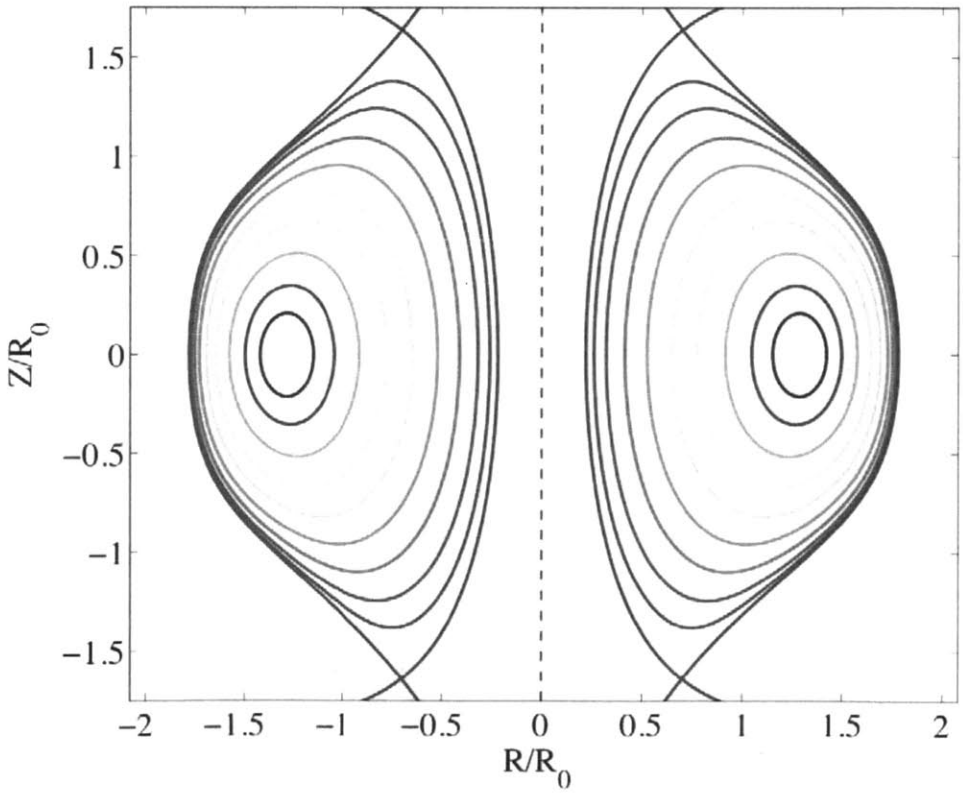

Fig. 2.12. a) ITER-like double-null equilibrium ($\varepsilon = 0.32, \kappa = 1.7, \delta = 0.33$). b) NSTX-like double-null equilibrium ($\varepsilon = 0.78, \kappa = 2.2, \delta = 0.2$). In both cases, b is chosen such that the toroidal current density gradient vanishes at the inboard midplane, and $x_{sep} = 1 - 1.05\delta\varepsilon, y_{sep} = 1.05\kappa\varepsilon$

2.3.4 Up-down asymmetric solutions

For up-down asymmetric equilibria, the solution is given by eq. (2.65). We now have to solve for 13 unknowns: c_1 to c_{11}, k and k_2. In the equivalent Solov'ev case, we have 12 boundary constraints, given by eq. (2.55). We thus need a 13th boundary constraint. We found that a simple choice, which gives good results, is to fix the location of a fifth point, aside from the outboard, inboard, top, and X points. If $\left(x\left(\tau\right),y\left(\tau\right)\right)$ is the model surface (2.32), we thus impose, for the 13th boundary condition:

$$\psi\left(x\left(\tau = 3\pi / 4\right),y\left(\tau = 3\pi / 4\right)\right) = 0 \tag{2.67}$$

The value $3\pi / 4$ is explicitly chosen because it lies between two points already fixed in the boundary constraints: the top and inboard points. We thus improve the sampling of the model surface, and optimize the match with our calculated solution.

In Fig. 2.12, we show two single-null divertor equilibria calculated with this method. The first equilibrium corresponds to an ITER-like geometry, while the second corresponds to an NSTX-like geometry. Both were computed for a low β plasma, $\beta \approx 0$, corresponding to $b = 1$. Also, the most realistic shapes were found for the following location of the lower X point: $x_{sep} = 1 - 1.05\delta\varepsilon, y_{sep} = -1.05\kappa\varepsilon$ for the ITER-like case, and $x_{sep} = 0.6, y_{sep} = -1.05\kappa\varepsilon$ for the NSTX-like case.

Note once more that the equilibria calculated in Fig. 2.11 and Fig. 2.12 appear quite plausible. Before closing this section, however, it is worthwhile to highlight the cost one pays for making the pressure and current profiles more realistic in Section 2.3 as compared to Section 2.2. It is found in the nature of the systems of equations one has to solve to determine the unknown constants.

In the solutions of the GS equation in Section 2.2, either (2.31) or (2.53), the unknown constants all appear linearly, so that the system of equations one has to solve to determine the coefficients is a *linear* system. Numerically, that means that the coefficients are simply obtained through a matrix inversion, and the system of equations always has solutions, very quickly calculated by any scientific computing program. There is no convergence issues. For extreme, unrealistic geometric parameters, these coefficients may lead to an unacceptable equilibrium, which may have to be ruled out, but in any case, the unknown constants can always be calculated.

The situation is different in the case of the quadratic profiles introduced in this section. Indeed, two of the unknowns, k and k_2 appear in a nonlinear way, inside the Whittaker function. In general, that does not cause any problem, and the same numerical solver can be called to solve the now *nonlinear* system of equations. However, as the parameters become more extreme (higher ε or δ, smaller κ), convergence issues may appear. We were for instance not able to compute acceptable equilibria which had $\varepsilon \geq 0.78$ while $\kappa = 1$.

a)

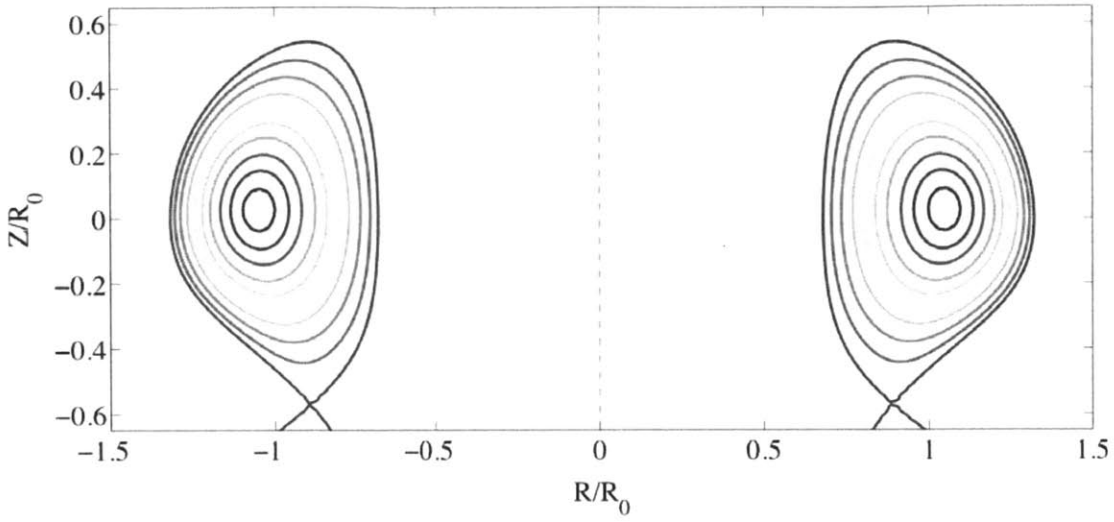

b)

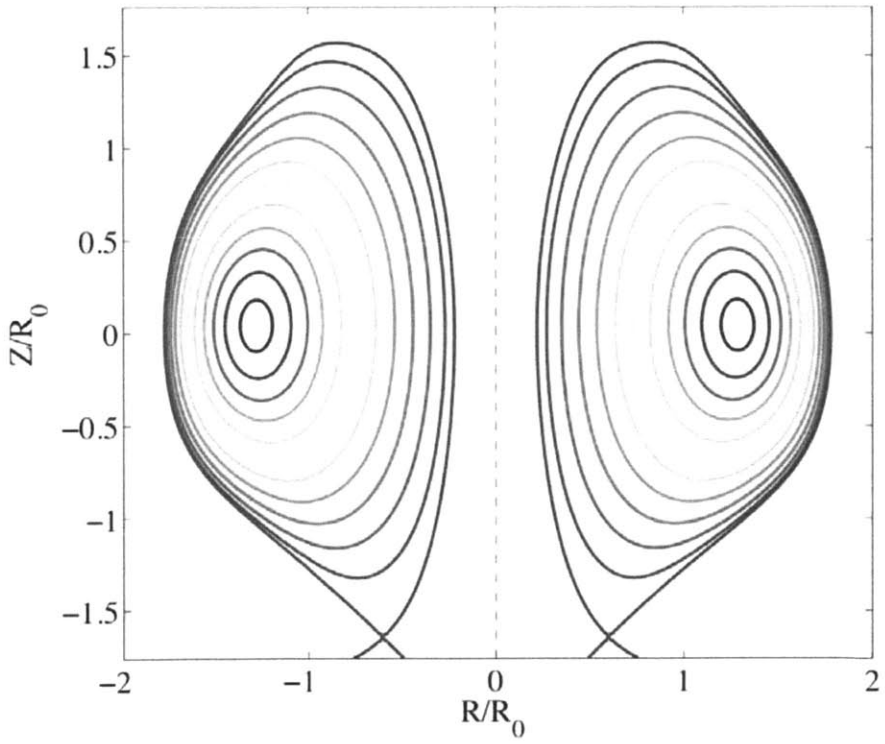

Fig. 2.12. a) ITER-like lower single-null equilibrium $(\varepsilon = 0.32, \kappa = 1.7, \delta = 0.33)$, $x_{sep} = 1 - 1.05\delta\varepsilon, y_{sep} = 1.05\kappa\varepsilon$. b) NSTX-like lower single null equilibrium $(\varepsilon = 0.78, \kappa = 2, \delta = 0.2)$, $x_{sep} = 0.6, y_{sep} = -1.05\kappa\varepsilon$. In both cases, $b = 1$.

2.4 Summary

In this chapter, we considered analytic solutions of the Grad-Shafranov equation for two types of pressure and current profiles: profiles which are linear in the flux function ψ, usually referred to as Solov'ev profiles, and profiles which are quadratic in ψ.

In the case of the Solov'ev profiles, we extended the previously known solutions by including additional terms in the usual polynomial expansion. These additional terms give additional degrees of freedom to our solution, which allow us to satisfy a correspondingly larger set of fitting boundary conditions. As a result, we can calculate analytic equilibria for a wider range of geometric parameters (ε, κ, and δ) figures of merit (β and q_*), and magnetic field line topologies. By choosing the boundary constraints according to the configuration of interest, we showed that with the same solution we can model equilibria for the standard tokamak and the ST (with or without up-down asymmetry), the spheromak and the FRC. To compute the equilibrium flux contours for all these configurations, one only has to solve the linear system formed by the equations for the boundary constraints. Since this system only consists of 7 equations in up-down symmetric geometries, and 12 otherwise, it is a trivial numerical problem.

The Solov'ev profiles unfortunately correspond to the unrealistic situation where the pressure gradient and the toroidal current density have a jump at the plasma surface. For this reason, we also calculated analytic solutions to the GS

equation for more realistic profiles, such that p and F^2 depend on ψ quadratically. These profiles are characterized by the vanishing of the pressure gradient and of the current at the plasma surface.

The solution of the GS equation which we find in this case is more complicated than the polynomial expansion of the Solov'ev case. Some of the undetermined constants now appear nonlinearly in the solution, namely in the argument of Whittaker functions. However, the procedure to determine the free constants which we presented in the Solov'ev case can be applied in exactly the same way. The only difference is that the system of equations for the boundary constraints is now nonlinear. Solving this system is a less trivial numerical problem than in the previous case, and convergence issues may be encountered if the chosen geometric and plasma parameters are too extreme. Nevertheless, in most cases the system can readily be solved by calling a built-in nonlinear solver in any scientific computing program. We have been able to compute very plausible tokamak and ST equilibria with this procedure, for a wide range of parameters.

Chapter 2 – References

[1] T. Takeda and Shinji Tokuda, Computation of MHD equilibrium of tokamak plasma, *Journal of Computational Physics*, Volume 93, Issue 1, March 1991, Pages 1-107

[2] L.S. Solov'ev, Zh. Eksp. Teor. Fiz. 53, 626 (1967)[Sov. Phys. JETP 26, 400 (1968)

[3] J.E. Rice, M. Greenwald, I.H. Hutchinson, E.S. Marmar, Y. Takase, S.M. Wolfe, F. Bombarda, *Nucl. Fusion* **38** 75 (1998)

[4] J.S. deGrassie, J.E. Rice, K.H. Burrell, R. J. Groebner, W. M. Solomon, *Phys. Plasmas* **14** 056115 (2007)

[5] J. L. Luxon, R. Anderson, F. Batty, C. B. Baxi, G. Bramson, N. H. Brooks, B. Brown, and the DIII-D Team, in Plasma Physics and Controlled Nuclear Fusion Research, 1986 (International Atomic Energy Agency, Vienna, 1987), Vol. I, p. 159.

[6] J.E. Rice, P.T. Bonoli, J.A. Goetz, M.J. Greenwald, I.H. Hutchinson, E.S. Marmar, M. Porkolab, S.M. Wolfe, S.J. Wukitch, C.S. Chang, *Nucl. Fusion* **39** 1175 (1999)

[7] I. H. Hutchinson, R. L. Boivin, F. Bombarda, P. Bonoli, S. Fairfax, C. Fiore, J. Goetz, S. Golovato, R. Granetz, M. Greenwald, S. Horne, A. Hubbard, J. Irby, B. LaBombard, B. Lipschultz, E. Marmar, G. McCracken, M. Porkolab, J. Rice, J. Snipes, Y. Takase, J. Terry, S. Wolfe, C. Christensen, D. Garnier, M. Graf, T. Hsu, T. Luke, M. May, A. Niemczewski, G. Tinios, J. Schachter, and J. Urbahn, *Phys. Plasmas* **1** 1511 (1994)

[8] M. Ono, S. M. Kaye, Y. -K. M. Peng, G. Barnes, W. Blanchard, M. D. Carter, J. Chrzanowski, L. Dudek, R. Ewig, D. Gates, R. E. Hatcher, T. Jarboe, S. C. Jardin, D. Johnson, R. Kaita, M. Kalish, C. E. Kessel, H. W. Kugel, R. Maingi, R. Majeski, J. Manickam, B. McCormack, J. Menard, D. Mueller, B. A. Nelson, B. E. Nelson, C. Neumeyer, G. Oliaro, F. Paoletti, R. Parsells, E. Perry, N. Pomphrey, S. Ramakrishnan, R. Raman, G. Rewoldt, J. Robinson, A. L. Roquemore, P. Ryan, S. Sabbagh, D. Swain, E. J. Synakowski, M. Viola, M. Williams, J. R. Wilson, and NSTX Team, Nucl. Fusion **40**, 557 (2000)

[9] J.S. deGrassie, J.E. Rice, K.H. Burrell, R. J. Groebner, W. M. Solomon, *Phys. Plasmas* **14** 056115 (2007)

[10] B.P. LeBlanc, R.E. Bell, S.M. Kaye, D. Stutman, M.G. Bell, M.L. Bitter, C. Bourdelle, D.A. Gates, R. Maingi, S.S. Medley, J.E. Menard, D. Mueller, S.F. Paul, A.L. Roquemore, A. Rosenberg, S.A. Sabbagh, V.A. Soukhanovskii, E.J. Synakowski, J.R. Wilson, and the NSTX Research Team, *Nucl. Fusion* **44** 513 (2004)

[11] R. Aymar, V. Chuyanov, M. Huguet, R. Parker, and Y. Shimomura, *Proceedings of the 16th International Conference on Fusion Energy*, Montreal, 1996 (International Atomic Energy Agency, Trieste, 1997), Vol. 1, p. 3.

[12] R. D. Hazeltine and J. D. Meiss, *Plasma Confinement*, Addison-Wesley, Redwood City, CA, 1992.

[13] P. Helander, D. J. Sigmar, *Collisional Transport in Magnetized Plasmas*, Cambridge University Press, Cambridge, United Kingdom, 2002, pp. 151-152

[14] R. Lüst, and A. Schlüter, 1957, Z. Naturforsch. A **12A**, 850

[15] V. D. Shafranov, 1958, Sov. Phys. JETP **6**, 545

[16] H. Grad and H. Rubin, in *Proceedings of the Second United Nations Conference on the Peaceful Uses of Atomic Energy* (United Nations, Geneva, 1958), Vol. 31, p.190

[17] J.P. Freidberg, *Ideal Magnetohydrodynamics* (Plenum, New York, 1985), pp. 108-111

[18] J.P. Goedbloed, R. Keppens, and Stefaan Poedts, *Advanced Magnetohydrodynamics with Applications to Laboratory and Astrophysical Plasmas*, Cambridge University Press (2010), pp. 293-299

[19] S.C. Cowley, P. K. Kaw, R. S. Kelly, and R. M. Kulsrud, *Phys. Fluids* B **3** (8), August 1991

[20] S. B. Zheng, A. J. Wootton, and E. R. Solano, *Phys. Plasmas* **3**, 1176 (1996)

[21] R. H. Weening, *Phys. Plasmas* **7**, 3654 (2000)

[22] B. Shi, *Phys. Plasmas* **12**, 122504 (2005)

[23] R. Srinivasan, K. Avinash, and P. K. Kaw, *Phys. Plasmas* **8**, 4483 (2001)

[24] Y. Xiao and P. J. Catto, *Phys. Plasmas* **13**, 082307 (2006)

[25] B. Shi, *Plasma Phys. Controlled Fusion* **49**, 2019 (2007)

[26] F. Troyon, R. Gruber, H. Saurenmann, S. Semenzato, S. Succi, *Plasma Phys. Control. Fusion* **26** 209 (1984)

[27] R. Aymar, P. Barabaschi, and Y. Shimomura, *Plasma Phys. Controlled Fusion* **44**, 519 (2002)

[28] S. M. Kaye, M. G. Bell, R. E. Bell, J. Bialek, T. Bigelow, M. Bitter, P. Bonoli, D. Darrow, P. Efthimion, J. Ferron, E. Fredrickson, D. Gates, L. Grisham, J. Hosea, D. Johnson, R. Kaita, S. Kubota, H. Kugel, B. LeBlanc, R. Maingi, J. Manickam, T. K. Mau, R. J. Maqueda, E. Mazzucato, J. Menard, D. Mueller, B. Nelson, N. Nishino, M. Ono, F. Paoletti, S. Paul, Y. -K. M. Peng, C. K. Phillips, R. Raman, P. Ryan, S. A. Sabbagh, M. Schaffer, C. H. Skinner, D. Stutman, D. Swain, E. Synakowski, Y. Takase, J. Wilgen, J. R. Wilson, W. Zhu, S. Zweben, A. Bers, M. Carter, B. Deng, C. Domier, E. Doyle, M. Finkenthal, K. Hill, T. Jarboe, S. Jardin, H. Ji, L. Lao, K. C. Lee, N. Luhmann, R. Majeski, S. Medley, H. Park, T. Peebles, R. I. Pinsker, G. Porter, A. Ram, M. Rensink, T. Rognlien, D. Stotler, B. Stratton, G. Taylor, W. Wampler, G. A. Wurden, X. Q. Xu, and L. Zeng, *Phys. Plasmas* **8**, 1977 (2001)

[29] V.D. Shafranov, *Journal of Nuclear Energy, Part C Plasma Phys.* **5** 251 (1963)

[30] P. M. Bellan, *Spheromaks: A Practical Application of Magnetohydrodynamic Dynamos and Plasma Self-Organization*, London: Imperial College Press, 2000

[31] J.P. Freidberg, *Plasma Physics and Fusion Energy*, Cambridge University Press (2007)

[32] C. V. Atanasiu, S. Günter, K. Lackner, and I. G. Miron, *Phys. Plasmas* **11**, 3510 (2004)

[33] L. Guazzotto and J.P. Freidberg, *Phys. Plasmas* **14**, 112508 (2007)

Chapter 3

Are fusion plasmas compressible? A new look at MHD comparison theorems

One of the key steps in the design of a new fusion experiment is the study of the stability of the confined plasma to the fast, macroscopic modes known as MHD modes. MHD instabilities are indeed experimentally known for considerably degrading the plasma properties, and can cause the termination of the plasma discharge. They have to be avoided.

By fast, we mean that the typical scale for the plasma velocity is the ion thermal velocity, v_{T_i}; by macroscopic we mean that the typical scale for the amplitude of the mode is the characteristic size of the confinement experiment, which we call a in the rest of this chapter. Unsurprisingly, the ideal MHD model is constructed so as to be relevant on these velocity and length scales, and their associated time scale $\tau_{MHD} = a / v_{T_i}$. Because of its simplicity and its very particular mathematical properties, it is the model most often used for macroscopic stability

analyses. Specifically, in ideal MHD, the problem of linear stability in any 3D magnetic configuration can be cast in a convenient form known as the MHD energy principle (Section 3.1 and 3.2), which is very commonly used to predict and understand stability boundaries in fusion systems.

The difficulty with using the ideal MHD model and its energy principle for the design of modern fusion experiments is that it relies on the assumption that both the ions and the electrons are very collisional on the MHD time scale τ_{MHD}. At the plasma temperatures and densities of fusion interest, this assumption is not justified, at least not for the ions (Section 3.3). One then naturally wonders how reliable the ideal MHD predictions are for the stability of fusion grade plasmas. The goal of this chapter is to answer this question by introducing six models which more accurately describe the plasmas in the different collisionality regimes of fusion interest (Sections 3.4 to Section 3.10). For each of these six models, we derive quadratic energy relations, which we compare with the ideal MHD energy principle. Those energy relations allow us to determine the stability boundaries in the six models of interest, and compare them to the ideal MHD boundaries. Using these comparison, we assess the reliability of the ideal MHD results on the time scale τ_{MHD}, in any 3-D configuration. The end result is a hierarchy between the models, from the most conservative to the least conservative. And the perhaps most important conclusions can be summarized in two points: (1) In ergodic systems, or closed line systems with modes which break the closed-line symmetry, ideal MHD is indeed the most

conservative model, even when the plasma is collisionless; (2) In closed line systems with modes which conserve the closed-line symmetry, the ideal MHD result is *not* the most conservative results, because it relies on plasma compressibility, which in fact vanishes in fusion grade plasmas.

3.1 Ideal MHD linear stability and the ideal MHD energy principle

3.1.1 Ideal MHD linear stability

All the stability analyses we will perform in Chapters 3 and 4, and the energy relations and comparison theorems we will derive, are solely concerned with the question of *linear stability.* By linear stability, we mean the stability of a given plasma equilibrium to *small* displacements of the plasma about this equilibrium. By restricting our work to small displacements and linear theory, we obviously leave aside the important topics of MHD turbulence and nonlinear evolution and saturation of MHD instabilities. While these topics are of great interest (see for instance [1]), in particular in astrophysical objects, our focus on linear stability is to be understood within the context of fusion research.

In magnetic confinement experiments and future fusion reactors, the macroscopic, fast and virulent ideal MHD instabilities can lead to significant plasma losses, major disruptions, and threaten the physical integrity of the fusion reactor. Therefore, one is not as much interested in the behavior of these instabilities on long

time scales, as in looking into ways to avoid them. In other words, the primary goal of ideal MHD stability studies for fusion applications is to determine the operational limits beyond which dangerous instabilities will be triggered. Such will be our goal in Chapters 3 and 4 as well, and in this context, linear stability theory is justified, even more so as it comes with an elegant and powerful mathematical formalism which we now describe, following the presentation given in [2].

We start with a static plasma equilibrium, to which we will add perturbations. As discussed in Chapter 2, the equilibrium equations are

$$\begin{aligned} \mathbf{J}_0 \times \mathbf{B}_0 &= \nabla p_0 \\ \nabla \times \mathbf{B}_0 &= \mu_0 \mathbf{J}_0 \\ \nabla \cdot \mathbf{B}_0 &= 0 \end{aligned} \tag{3.1}$$

and $\mathbf{B}_0(\mathbf{r}), \mathbf{J}_0(\mathbf{r})$, and $p_0(\mathbf{r})$ are time-independent quantities. We add small perturbations as follows:

$$\begin{aligned} \mathbf{v}(\mathbf{r},t) &= \tilde{\mathbf{v}}(\mathbf{r},t) \\ p(\mathbf{r},t) &= p_0(\mathbf{r}) + \tilde{p}(\mathbf{r},t) \\ \mathbf{B}(\mathbf{r},t) &= \mathbf{B}_0(\mathbf{r}) + \tilde{\mathbf{B}}(\mathbf{r},t) \\ \rho(\mathbf{r},t) &= \rho_0(\mathbf{r}) + \tilde{\rho}(\mathbf{r},t) \end{aligned} \tag{3.2}$$

where for each quantity A, we have $\left|\tilde{A}(\mathbf{r},t) / A_0(\mathbf{r})\right| \ll 1$. Inserting the expressions in (3.2) into the ideal MHD equations and keeping only the zeroth and first order terms, we find the following first order equations for the perturbations:

$$
\begin{aligned}
&\rho\frac{\partial\tilde{\mathbf{v}}}{\partial t} = \tilde{\mathbf{J}}\times\mathbf{B} + \mathbf{J}\times\tilde{\mathbf{B}} - \nabla\tilde{p} \\
&\frac{\partial\tilde{p}}{\partial t} + \tilde{\mathbf{v}}\cdot\nabla p + \gamma p\nabla\cdot\tilde{\mathbf{v}} \\
&\frac{\partial\tilde{\mathbf{B}}}{\partial t} = \nabla\times\left(\tilde{\mathbf{v}}\times\mathbf{B}\right), \quad \nabla\cdot\tilde{\mathbf{B}} = 0 \\
&\frac{\partial\tilde{\rho}}{\partial t} + \nabla\cdot\left(\rho\tilde{\mathbf{v}}\right) = 0
\end{aligned}
\tag{3.3}
$$

In (3.3), we suppressed the 0 subscript for the equilibrium quantities, to simplify the notation. We will keep this notation for the rest of the chapter.

The first equation, i.e. the momentum equation, is the one we need to solve to describe the evolution of the perturbed velocity $\tilde{\mathbf{v}}$. Once this is done, we can substitute $\tilde{\mathbf{v}}$ into the other equations to determine the evolution of the other quantities. Bernstein *et al* [3] were the first ones to use this fact to show that the set of equations (3.3) can be reduced to a very convenient form by introducing the small Lagrangian displacement $\boldsymbol{\xi}$ associated with the plasma perturbation, defined as

$$
\tilde{\mathbf{v}} = \frac{\partial\boldsymbol{\xi}}{\partial t} \tag{3.4}
$$

Indeed, substituting $\tilde{\mathbf{v}}$ in terms of $\boldsymbol{\xi}$ into the equations for $\tilde{p}$, $\tilde{\mathbf{B}}$, and $\tilde{\rho}$ and integrating each equation over time, we obtain

$$
\begin{aligned}
&\tilde{p} = -\boldsymbol{\xi}\cdot\nabla p - \gamma p\nabla\cdot\boldsymbol{\xi} \\
&\tilde{\mathbf{B}} = \nabla\times\left(\boldsymbol{\xi}\times\mathbf{B}\right) \\
&\tilde{\rho} = -\nabla\cdot\left(\rho\boldsymbol{\xi}\right)
\end{aligned}
\tag{3.5}
$$

(the equation $\nabla\cdot\tilde{\mathbf{B}} = 0$ has been dropped, since it now is redundant), and we can now use these expressions in the momentum equation, to find

$$\rho\frac{\partial^2\boldsymbol{\xi}}{\partial t^2}=\frac{1}{\mu_0}\left(\nabla\times\mathbf{B}\right)\times\left[\nabla\times\left(\boldsymbol{\xi}\times\mathbf{B}\right)\right]+\frac{1}{\mu_0}\left\{\nabla\times\left[\nabla\times\left(\boldsymbol{\xi}\times\mathbf{B}\right)\right]\right\}\times\mathbf{B}+\nabla\left(\boldsymbol{\xi}\cdot\nabla p+\gamma p\nabla\cdot\boldsymbol{\xi}\right)$$
$$=\mathbf{F}(\boldsymbol{\xi}) \tag{3.6}$$

As expected, eq. (3.6) only involves $\boldsymbol{\xi}$ and the equilibrium quantities. This equation, along with the initial conditions $\boldsymbol{\xi}\left(\mathbf{r},0\right)=0,\left.\frac{\partial\boldsymbol{\xi}}{\partial t}\right|_{t=0}=\tilde{\mathbf{v}}\left(\mathbf{r},0\right)$ and appropriate boundary conditions constitute the formulation of the general linearized stability equations. By solving this equation, and using the solution $\boldsymbol{\xi}\left(\mathbf{r},t\right)$ into eq. (3.5), we can determine everything we need to know about a given perturbation.

As we already discussed, however, what one is usually most interested in when performing MHD stability calculations is whether a given geometric configuration is stable to the most dangerous instabilities or not. The details of the time evolution of the instability may not matter as much. In these conditions, we can ask ourselves if solving the general initial value problem is the most efficient way, from a computational perspective, to determine if a given perturbation is stable or not. The answer is no. Indeed, there exists an elegant and powerful variational procedure, known as the ideal MHD energy principle [3] which is much more effective and convenient for testing ideal MHD stability in arbitrary three-dimensional geometries. We present and discuss this procedure in the next section.

3.1.2 Ideal MHD variational formulation

The first step in the derivation the variational formulation and the energy principle in the next section is to show that the force operator $\mathbf{F}$ is self-adjoint with respect to the scalar product defined by

$$\left\langle \mathbf{a}, \mathbf{b} \right\rangle = \int \mathbf{a} \cdot \mathbf{b}\, \mathbf{dr} \tag{3.7}$$

where $\mathbf{dr}$ is an infinitesimal element of volume, and the integral is over the whole plasma volume. This self-adjointness property will be needed several times in the derivation. There are many different ways to do prove it, all of them requiring substantial amounts of algebra and integrations by parts. A nice and detailed derivation can for instance be found in Appendix A of reference [4], where the following expression is derived for any two vectors $\boldsymbol{\eta}$ and $\boldsymbol{\xi}$ satisfying the boundary conditions (in this case $\boldsymbol{\eta} \cdot \mathbf{n} = \boldsymbol{\xi} \cdot \mathbf{n} = 0$ at the plasma surface, where $\mathbf{n}$ is the unit vector perpendicular to the surface; however the result can be generalized to other boundary conditions):

$$\begin{aligned} \int \boldsymbol{\eta} \cdot \mathbf{F}(\boldsymbol{\xi}) d\mathbf{r} = -\int d\mathbf{r} \Bigg[& \frac{1}{\mu_0} \left(\mathbf{B} \cdot \nabla \boldsymbol{\xi}_\perp \right) \cdot \left(\mathbf{B} \cdot \nabla \boldsymbol{\eta}_\perp \right) + \gamma p \left(\nabla \cdot \boldsymbol{\xi} \right) \left(\nabla \cdot \boldsymbol{\eta} \right) \\ & + \frac{B^2}{\mu_0} \left(\nabla \cdot \boldsymbol{\xi}_\perp + 2 \boldsymbol{\xi}_\perp \cdot \boldsymbol{\kappa} \right) \left(\nabla \cdot \boldsymbol{\eta}_\perp + 2 \boldsymbol{\eta}_\perp \cdot \boldsymbol{\kappa} \right) \\ & - \frac{4B^2}{\mu_0} \left(\boldsymbol{\xi}_\perp \cdot \boldsymbol{\kappa} \right) \left(\boldsymbol{\eta}_\perp \cdot \boldsymbol{\kappa} \right) + \left(\boldsymbol{\eta}_\perp \boldsymbol{\xi}_\perp : \nabla \nabla \right) \left(p + \frac{B^2}{2\mu_0} \right) \Bigg] \end{aligned} \tag{3.8}$$

In eq. (3.8), we have introduced several notations. $\boldsymbol{\xi} = \boldsymbol{\xi}_\perp + \xi_\parallel \mathbf{b}$ and $\boldsymbol{\eta} = \boldsymbol{\eta}_\perp + \eta_\parallel \mathbf{b}$, where $\mathbf{b}$ is the unit vector along the equilibrium magnetic field, and the $\perp$ and $\parallel$ subscripts refer to directions perpendicular and parallel to that equilibrium magnetic field. Also, $\boldsymbol{\kappa} = \mathbf{b} \cdot \nabla \mathbf{b}$ is the curvature vector of the magnetic field line. Eq. (3.8) is written in such a way that the self-adjointness of $\mathbf{F}$ is immediately apparent. Indeed, the roles of $\boldsymbol{\eta}$ and $\boldsymbol{\xi}$ are symmetric in the right-hand side of (3.8). Exchanging the two vectors would therefore not change this expression, which means that

$$\int \boldsymbol{\eta} \cdot \mathbf{F}(\boldsymbol{\xi}) d\mathbf{r} = \int \boldsymbol{\xi} \cdot \mathbf{F}(\boldsymbol{\eta}) d\mathbf{r} \tag{3.9}$$

The first place the self-adjointness of $\mathbf{F}$ is used is when defining the linearized potential energy associated with the displacement $\boldsymbol{\xi}$, which is one of the two physical quantities involved in the variational formulation of the eigenvalue problem and the energy principle. To define the linearized potential energy, we first introduce the linearized kinetic energy in the plasma

$$\delta T = \frac{1}{2} \int \rho \left| \frac{\partial \boldsymbol{\xi}}{\partial t} \right|^2 d\mathbf{r} \tag{3.10}$$

and calculate

$$\begin{aligned} \frac{d\delta T}{dt} &= \frac{1}{2} \int d\mathbf{r} \rho \left(\frac{\partial^2 \boldsymbol{\xi}}{\partial t^2} \cdot \frac{\partial \boldsymbol{\xi}^*}{\partial t} + \frac{\partial \boldsymbol{\xi}}{\partial t} \cdot \frac{\partial^2 \boldsymbol{\xi}^*}{\partial t^2} \right) \\ &= \frac{1}{2} \int d\mathbf{r} \left[\frac{\partial \boldsymbol{\xi}^*}{\partial t} \cdot \mathbf{F}(\boldsymbol{\xi}) + \frac{\partial \boldsymbol{\xi}}{\partial t} \cdot \mathbf{F}(\boldsymbol{\xi}^*) \right] \end{aligned} \tag{3.11}$$

In (3.11), we used the fact that $\boldsymbol{\xi}$ is a solution of the momentum equation (3.6) to go from the first line to the second line, and the superscript * indicates the complex conjugate of a quantity. Now that we have an expression for the time derivative of the kinetic energy, we can calculate the time derivative of the potential energy δW_{MHD} using the fact that the ideal MHD model conserves energy (e.g. Chapter 3 in reference [4]):

$$\begin{aligned}\frac{d\delta W_{MHD}}{dt} = -\frac{d\delta T}{dt} &= -\frac{1}{2}\int d\mathbf{r}\left[\frac{\partial \boldsymbol{\xi}^*}{\partial t}\cdot\mathbf{F}(\boldsymbol{\xi}) + \frac{\partial \boldsymbol{\xi}}{\partial t}\cdot\mathbf{F}(\boldsymbol{\xi}^*)\right] \\ &= -\frac{1}{2}\frac{d}{dt}\left[\int \boldsymbol{\xi}^*\cdot\mathbf{F}(\boldsymbol{\xi})\,d\mathbf{r}\right] + \frac{1}{2}\int \boldsymbol{\xi}^*\cdot\mathbf{F}\left(\frac{\partial \boldsymbol{\xi}}{\partial t}\right)d\mathbf{r} - \frac{1}{2}\int \frac{\partial \boldsymbol{\xi}}{\partial t}\cdot\mathbf{F}(\boldsymbol{\xi}^*)d\mathbf{r} \qquad (3.12) \\ &= -\frac{1}{2}\frac{d}{dt}\left[\int \boldsymbol{\xi}^*\cdot\mathbf{F}(\boldsymbol{\xi})\,d\mathbf{r}\right]\end{aligned}$$

where to go from the second line of (3.12) to the third line, we used the fact that the operator $\mathbf{F}$ is self-adjoint. Integrating eq. (3.12) we finally get the desired expression:

$$\delta W_{MHD}(\boldsymbol{\xi}^*, \boldsymbol{\xi}) = -\frac{1}{2}\int d\mathbf{r}\boldsymbol{\xi}^*\cdot\mathbf{F}(\boldsymbol{\xi}) \qquad (3.13)$$

δW_{MHD} has the expected form $W = \int \mathbf{F}\cdot d\mathbf{l}$ for a potential energy.

The next step in the derivation of the variational principle is to transform the initial value problem (3.6) into an eigenvalue problem. Since the equilibrium quantities $\rho(\mathbf{r})$, $p(\mathbf{r})$, and $\mathbf{B}(\mathbf{r})$ in eq. (3.6) are time-independent, we consider solutions of the equation in the form of normal modes:

$$\boldsymbol{\xi}(\mathbf{r}, t) = \boldsymbol{\xi}(\mathbf{r})e^{-i\omega t} \qquad (3.14)$$

and using this expression for $\boldsymbol{\xi}$ in eq. (3.6), the linearized momentum equation becomes

$$-\rho\omega^2\boldsymbol{\xi} = \mathbf{F}(\boldsymbol{\xi}) \tag{3.15}$$

which is the expected eigenvalue equation, for the eigenvalue ω^2.

The eigenvalue problem, consisting of eq. (3.15) and boundary conditions on $\boldsymbol{\xi}$ can now be recast in a variational form. Dotting both sides of eq. (3.15) with $\boldsymbol{\xi}^*$, integrating over the plasma volume, and multiplying $1/2$, we indeed find

$$\omega^2 = \frac{\delta W_{MHD}(\boldsymbol{\xi}^*, \boldsymbol{\xi})}{K_{MHD}(\boldsymbol{\xi}^*, \boldsymbol{\xi})} \tag{3.16}$$

where

$$K_{MHD}(\boldsymbol{\xi}^*, \boldsymbol{\xi}) = \frac{1}{2}\int \rho\left|\boldsymbol{\xi}\right|^2 d\mathbf{r} \tag{3.17}$$

is proportional to the linearized kinetic energy, and is identified to it.

Eq. (3.16) is the variational formulation of the eigenvalue problem (3.15). To show this, we let $\boldsymbol{\xi} \to \boldsymbol{\xi} + \delta\boldsymbol{\xi}$, and $\omega^2 \to \omega^2 + \delta\omega^2$ in (3.17). Since W_{MHD} and K_{MHD} are both bilinear,

$$\omega^2 + \delta\omega^2 = \frac{\delta W_{MHD}\left(\boldsymbol{\xi}^*, \boldsymbol{\xi}\right) + \delta W_{MHD}\left(\delta\boldsymbol{\xi}^*, \boldsymbol{\xi}\right) + \delta W_{MHD}\left(\boldsymbol{\xi}^*, \delta\boldsymbol{\xi}\right) + \delta W_{MHD}\left(\delta\boldsymbol{\xi}^*, \delta\boldsymbol{\xi}\right)}{K_{MHD}\left(\boldsymbol{\xi}^*, \boldsymbol{\xi}\right) + K_{MHD}\left(\delta\boldsymbol{\xi}^*, \boldsymbol{\xi}\right) + K_{MHD}\left(\boldsymbol{\xi}^*, \delta\boldsymbol{\xi}\right) + K_{MHD}\left(\delta\boldsymbol{\xi}^*, \delta\boldsymbol{\xi}\right)} \tag{3.18}$$

For small variations, we can Taylor the numerator and the denominator. Remembering that $\delta W_{MHD}\left(\boldsymbol{\xi}, \boldsymbol{\xi}^*\right) = \omega^2 K_{MHD}\left(\boldsymbol{\xi}, \boldsymbol{\xi}^*\right)$, we have

$$\delta\omega^2 = \frac{\delta W_{MHD}\left(\delta\boldsymbol{\xi}^*,\boldsymbol{\xi}\right)+\delta W_{MHD}\left(\boldsymbol{\xi}^*,\delta\boldsymbol{\xi}\right)}{K_{MHD}\left(\boldsymbol{\xi}^*,\boldsymbol{\xi}\right)} - \omega^2 \frac{K_{MHD}\left(\delta\boldsymbol{\xi}^*,\boldsymbol{\xi}\right)+K_{MHD}\left(\boldsymbol{\xi}^*,\delta\boldsymbol{\xi}\right)}{K_{MHD}\left(\boldsymbol{\xi}^*,\boldsymbol{\xi}\right)} \tag{3.19}$$

which, according to the definitions of δW_{MHD} and K_{MHD}, is :

$$\begin{aligned}\delta\omega^2 &= -\frac{1}{2}\frac{\int d\mathbf{r}\left\{\left[\delta\boldsymbol{\xi}^*\cdot\mathbf{F}\left(\boldsymbol{\xi}\right)+\omega^2\rho\delta\boldsymbol{\xi}^*\cdot\boldsymbol{\xi}\right]+\left[\boldsymbol{\xi}^*\cdot\mathbf{F}\left(\delta\boldsymbol{\xi}\right)+\omega^2\rho\delta\boldsymbol{\xi}\cdot\boldsymbol{\xi}^*\right]\right\}}{K_{MHD}\left(\boldsymbol{\xi},\boldsymbol{\xi}^*\right)} \\ &= -\frac{1}{2}\frac{\int d\mathbf{r}\left\{\delta\boldsymbol{\xi}^*\cdot\left[\mathbf{F}\left(\boldsymbol{\xi}\right)+\omega^2\rho\boldsymbol{\xi}\right]+\delta\boldsymbol{\xi}\cdot\left[\mathbf{F}\left(\boldsymbol{\xi}^*\right)+\omega^2\rho\boldsymbol{\xi}^*\right]\right\}}{K_{MHD}\left(\boldsymbol{\xi},\boldsymbol{\xi}^*\right)}\end{aligned} \tag{3.20}$$

To go from the first line to second line, we used the self-adjoint property of $\mathbf{F}$ once again. Now, ω^2 is an extremum iff for all allowable $\delta\boldsymbol{\xi}$, we have $\delta\omega^2 = 0$. Since $\delta\boldsymbol{\xi}$ is arbitrary, the condition for $\delta\omega^2$ to be zero in eq. (3.20) is

$$\omega^2\rho\boldsymbol{\xi} + \mathbf{F}\left(\boldsymbol{\xi}\right) = \mathbf{0} \tag{3.21}$$

In other words, the condition for ω^2 to be an extremum is that $\boldsymbol{\xi}$ is an eigenfunction. This completes our proof.

The variational formulation (3.16) is particularly useful for the efficient computation (either analytic or numerical) of the eigenvalue ω^2. Indeed, if we calculate the quotient $\lambda^2 = \dfrac{\delta W_{MHD}\left(\boldsymbol{\eta}^*,\boldsymbol{\eta}\right)}{K_{MHD}\left(\boldsymbol{\eta}^*,\boldsymbol{\eta}\right)}$, where $\boldsymbol{\eta} = \boldsymbol{\xi} + \delta\boldsymbol{\xi}$ is a trial function which differs from the actual eigenfunction $\boldsymbol{\xi}$ by $\delta\boldsymbol{\xi}$, then λ^2 will only differ from the actual eigenvalue ω^2 by $\left(\delta\boldsymbol{\xi}\right)^2$ (see for instance Chapter 8 in reference [4]).

However useful this variational formulation is, there are cases when it provides us with more information than we actually need. Given the short time scales on which ideal MHD instabilities develop, and given their dramatic effect on the plasma, the actual value of the growth rate of instabilities can sometimes only be a secondary concern, the central question being: is the system stable or not, and how can we design it to be stable? And to answer this question, the variational formulation can be further simplified, leading to a powerful principle, known as the *Ideal MHD energy principle* [3]. This is discussed in the next section.

3.1.3 Ideal MHD energy principle

The ideal MHD energy principle is summarized in the following statement, first proposed by Bernstein *et al.* [3], and Hain *et al.* [5] :

An ideal MHD equilibrium is stable if and only if

$$\delta W\left(\boldsymbol{\xi}^{*}, \boldsymbol{\xi}\right) \geq 0 \tag{3.22}$$

for all allowable displacements $\boldsymbol{\xi}$.

Intuition about why the energy principle is true can be gained by following the partly incomplete proof of it given by Bernstein *et al.* [3]. We assume that the force operator $\mathbf{F}$ only allows for discrete eigenvalues and discrete normal modes. Since $\mathbf{F}$ is self-adjoint, the eigenfunctions $\boldsymbol{\xi}_n$ associated with the eigenvalues ω_n can be chosen

so as to form an orthonormal basis, and any arbitrary displacement $\boldsymbol{\xi}$ can be written as

$$\boldsymbol{\xi} = \sum_n c_n \boldsymbol{\xi}_n \tag{3.23}$$

In these conditions, $\delta W_{MHD}\left(\boldsymbol{\xi}^*, \boldsymbol{\xi}\right)$ can be calculated in terms of the c_n and ω_n^2:

$$\begin{aligned} \delta W_{MHD}\left(\boldsymbol{\xi}^*, \boldsymbol{\xi}\right) &= -\frac{1}{2}\int \boldsymbol{\xi}^* \cdot \mathbf{F}\left(\boldsymbol{\xi}\right) d\mathbf{r} = \frac{1}{2}\sum_n \sum_m c_n^* c_m \omega_m^2 \int \boldsymbol{\xi}_n^* \cdot \boldsymbol{\xi}_m d\mathbf{r} \\ &= \sum_n \left|c_n\right|^2 \omega_n^2 \end{aligned} \tag{3.24}$$

where to go from the first line to the second line, we used the fact that the functions $\boldsymbol{\xi}_n$ are orthonormal, i.e. perpendicular to each other, and with norm 1. The energy principle can be understood in the light of eq. (3.23). Indeed, there exists a displacement $\boldsymbol{\xi}$ such that $\delta W_{MHD}\left(\boldsymbol{\xi}^*, \boldsymbol{\xi}\right) < 0$ if and only if there exists an eigenvalue such that $\omega_n^2 \leq 0$, i.e. if and only if the eigenmode $\boldsymbol{\xi}_n$ is exponentially unstable, and thus the system unstable.

If this proof helps us to intuitively understand why the energy principle may be true, it is not entirely complete. Indeed, as was unknown at the time of Bernstein *et al.*'s article, the spectrum of $\mathbf{F}$, also known as the ideal MHD spectrum, does not consist solely of discrete eigenvalues. The operator $\mathbf{F}$ also has a continuous spectrum (see for instance Chapter 6 in reference [2]), which makes the expansion in normal modes in (3.23) improper.

Fortunately, a correct proof of both necessity and sufficiency has been given by Laval *et al.* [6]. Their proof is elegantly based on the conservation of energy in the ideal MHD model, and carried out in the time domain, thereby avoiding any difficulty associated with the subtleties of the ideal MHD spectrum.

There are several advantages to the energy principle formulation of the ideal MHD stability problem. First, as we will see in the next sections for the particular case of plasma compressibility, the different terms in δW_{MHD} can be recast in more intuitive forms, highlighting the different physical roles they play. By looking at their sign, we can identify the physical mechanisms which are stabilizing, and those which are destabilizing, and get additional physical insight into the behavior of MHD instabilities. A second advantage, related to this, is that based on physical intuition, we may be able to construct a trial function which makes δW_{MHD} negative. According to the energy principle, this would be a sufficient proof that the system is unstable to certain types of perturbations. This method has been successfully used to derive necessary conditions for stability, such as Suydam's criterion, for instance [7]. Finally, if one is interested in studying the stability of a system more systematically, one may investigate the sign of δW_{MHD} by exploiting a complete set of trial functions, in order to obtain necessary and sufficient conditions for stability.

In the remainder of Chapter 3, we illustrate another aspect of the power of the energy principle approach. We use it to compare the stability boundaries

predicted by several different models, including ideal MHD, in order to investigate the reliability of ideal MHD predictions in fusion grade plasmas. Since particular attention will be given to the role of plasma compressibility, we now discuss its role in the ideal MHD energy principle.

3.2 Ideal MHD plasma compressibility

In order to see where plasma compressibility enters in the energy principle, we integrate by parts the last term in $\delta W_{MHD}\left(\boldsymbol{\xi}^*,\boldsymbol{\xi}\right)$. Focusing our attention on internal modes[5], i.e. modes such that $\mathbf{n}\cdot\boldsymbol{\xi}\big|_{S_P}=0$, where $\mathbf{n}$ is the unit vector normal to the plasma boundary, and S_P is the plasma boundary, we have, using the divergence theorem,

$$\int \boldsymbol{\xi}^*\cdot\nabla\left(\gamma p\nabla\cdot\boldsymbol{\xi}\right)d\mathbf{r}=-\int\gamma p\left|\nabla\cdot\boldsymbol{\xi}\right|^2 d\mathbf{r} \tag{3.25}$$

The term on the right hand side of (3.25), involving the divergence of the displacement, represents the energy required to compress the plasma. It is the expected plasma compressibility term. Using (3.25), the potential energy can be rewritten as

$$\begin{aligned}\delta W_{MHD}(\boldsymbol{\xi}^*,\boldsymbol{\xi}) &= \delta W_{\perp}(\boldsymbol{\xi}_{\perp}^*,\boldsymbol{\xi}_{\perp})+\delta W_C(\boldsymbol{\xi}^*,\boldsymbol{\xi})\\ \delta W_{\perp} &= -\int\boldsymbol{\xi}_{\perp}^*\cdot\left[(\tilde{\mathbf{J}}\times\mathbf{B}+\mathbf{J}\times\tilde{\mathbf{B}})+\nabla(\boldsymbol{\xi}_{\perp}\cdot\nabla p)\right]d\mathbf{r}\\ \delta W_C &= \int\gamma p\mid\nabla\cdot\boldsymbol{\xi}\mid^2 d\mathbf{r}\end{aligned} \tag{3.26}$$

[5] In the remaining of Chapter 3, we focus on internal modes to keep the expressions relatively simple, without the extra boundary terms. However, it is important to note that all the results derived here can be generalized to cover external modes as well.

We remind the reader that the perturbed magnetic field and current density are given by the relations (see previous section) $\tilde{\mathbf{B}} = \nabla \times \left(\boldsymbol{\xi}_\perp \times \mathbf{B} \right)$, $\mu_0 \tilde{\mathbf{J}} = \nabla \times \nabla \times \left(\boldsymbol{\xi}_\perp \times \mathbf{B} \right)$ and involve $\boldsymbol{\xi}_\perp$ only. Key features to observe from eq. (3.26) then are that $\delta W_\perp$ depends only on $\boldsymbol{\xi}_\perp$ and that the only appearance of $\boldsymbol{\xi}_\parallel$ is in the $\nabla \cdot \boldsymbol{\xi}$ stabilizing plasma compression term in δW_C.

The energy principle states that a mode is stable iff $\delta W_{MHD} \geq 0$ for all allowable plasma displacements. Therefore, stability is determined by minimizing δW_{MHD} with respect to $\boldsymbol{\xi}$, and then calculating the value of δW_{MHD} for the minimizing $\boldsymbol{\xi}$. If $\delta W_{MHD} \geq 0$ the plasma is stable whereas if $\delta W_{MHD} < 0$ the plasma is unstable. Now, since $\xi_\parallel$ appears only in the plasma compressibility term, it is convenient to first perform a universal minimization with respect to $\xi_\parallel$. The variation of δW_{MHD} with respect to $\xi_\parallel$ is:

$$\delta \left(\delta W_{MHD} \right)_{\xi_\parallel} = \int \gamma p \left[\nabla \cdot \left(\frac{\delta \xi_\parallel}{B} \mathbf{B} \right) \nabla \cdot \boldsymbol{\xi}^* + \nabla \cdot \left(\frac{\delta \xi_\parallel^*}{B} \mathbf{B} \right) \nabla \cdot \boldsymbol{\xi} \right] d\mathbf{r} \tag{3.27}$$

Since $\mathbf{B} \cdot \mathbf{n} = 0$, and $\mathbf{B} \cdot \nabla p = 0$, the divergence theorem can be used to rewrite (3.27) as

$$\delta \left(\delta W_{MHD} \right)_{\xi_\parallel} = -\int \gamma p \left[\frac{\delta \xi_\parallel}{B} \mathbf{B} \cdot \nabla \left(\nabla \cdot \boldsymbol{\xi}^* \right) + \frac{\delta \xi_\parallel^*}{B} \mathbf{B} \cdot \nabla \left(\nabla \cdot \boldsymbol{\xi} \right) \right] d\mathbf{r} \tag{3.28}$$

δW_{MHD} is minimized with respect to $\xi_{\|}$ if $\delta\left(\delta W_{MHD}\right)_{\xi_{\|}} = 0$ for any arbitrary $\delta\xi_{\|}$. According to eq. (3.28), this requires

$$\mathbf{B}\cdot\nabla(\nabla\cdot\boldsymbol{\xi}) = 0 \tag{3.29}$$

To solve this equation, two different cases have to be distinguished: (1) systems where $\mathbf{B}\cdot\nabla \neq 0$ which include ergodic field line geometries as well as closed line systems undergoing perturbations that break the closed line symmetry, and (2) closed line systems undergoing perturbations that do not break the closed line symmetry.

- *Case 1 : Ergodic systems, or closed field lines systems with modes which do not conserve the closed-line symmetry*

For this first case, $\mathbf{B}\cdot\nabla$ is not singular, so that the equation $\mathbf{B}\cdot\nabla(\nabla\cdot\boldsymbol{\xi}) = 0$ is trivially solved, yielding $\nabla\cdot\boldsymbol{\xi} = 0$. The minimization with respect to $\xi_{\|}$ thus implies that

$$\delta W_{MHD}(\boldsymbol{\xi},\boldsymbol{\xi}^*) = \delta W_{\perp}(\boldsymbol{\xi}_{\perp},\boldsymbol{\xi}_{\perp}^*) \tag{3.30}$$

Ideal MHD stability for ergodic systems is incompressible: $\delta W_C = 0$

- *Case 2 : Closed field lines systems, and modes which conserve the closed-line symmetry*

For this second case, there is a periodicity constraint $\xi_{\|}(l) = \xi_{\|}(l+L)$, where l is any point along the arc length of the field line and L is the length of the line. This

periodicity constraint can only be satisfied by adding a homogeneous solution to the solution $\nabla \cdot \boldsymbol{\xi} = 0$ of eq. (3.29):

$$\nabla \cdot \boldsymbol{\xi} = G(p) \tag{3.31}$$

(G is indeed a solution, since $\mathbf{B} \cdot \nabla p = 0$). The periodicity constraint determines the function G. Indeed, eq. (3.31) can be rewritten as

$$G(p) - B\frac{\partial}{\partial l}\left(\frac{\xi_{\parallel}}{B}\right) = \nabla \cdot \boldsymbol{\xi}_{\perp} \tag{3.32}$$

where the notation $\partial / \partial l$ indicates a derivative along the magnetic field line. Dividing eq. (3.32) by B and integrating the equation over the entire length of a closed field line, we see that the second term on the left-hand side vanishes because of the periodicity constraint. Thus, we find:

$$G(p)\oint \frac{dl}{B} = \oint \nabla \cdot \boldsymbol{\xi}_{\perp} \frac{dl}{B} \tag{3.33}$$

and the minimizing condition (3.31) is

$$\nabla \cdot \boldsymbol{\xi} = \oint \nabla \cdot \boldsymbol{\xi}_{\perp} \frac{dl}{B} \Big/ \oint \frac{dl}{B} \tag{3.34}$$

Minimizing with respect to $\xi_{\parallel}$ thus leads to the following expression for the compressibility contribution:

$$\delta W_C = \int \gamma p \mid \nabla \cdot \boldsymbol{\xi} \mid^2 d\mathbf{r} = \int \gamma p \mid \langle \nabla \cdot \boldsymbol{\xi}_{\perp} \rangle \mid^2 d\mathbf{r} \tag{3.35}$$

where Q indicates the field line average of the quantity Q:

$$\langle Q \rangle = \frac{\oint Q \frac{dl}{B}}{\oint \frac{dl}{B}} \tag{3.36}$$

For this case the plasma compressibility term must be maintained and included in the final minimization with respect to $\boldsymbol{\xi}_\perp$. And since clearly $\delta W_C \geq 0$, δW_C makes a positive contribution to δW_{MHD}: plasma compressibility is stabilizing. Several closed field line configurations, such as the field-reversed configuration [8] and the levitated dipole [9] explicitly rely on this term to stabilize some of their potentially most violent modes.

The difficulty with these fusion concepts relying on plasma compressibility to stabilize macroscopic instabilities is that the compressibility term is obtained from the ideal MHD equation for energy conservation

$$\frac{d}{dt}\left(\frac{p}{\rho^\gamma}\right) = 0 \tag{3.37}$$

as indicated by the presence of the ratio of the specific heats γ in (3.35). Eq. (3.37) relies on two critical assumptions: 1) that energy equilibration occurs on a faster time scale then the typical time scale of the instability, so that the ion and electron temperatures are identical during the evolution of the instability: $T_e = T_i$; 2) that we can neglect the heat flux normally on the right-hand side of eq. (3.37), and in

particular the electron parallel heat flux, which has the largest contribution. Both assumptions are justified if the following ordering is satisfied

$$\left(\frac{m_i}{m_e}\right)^{1/2} \frac{\mathrm{v}_{T_i}\tau_{ii}}{a} \ll 1 \Leftrightarrow \left(\frac{m_i}{m_e}\right)^{1/2} \omega\tau_{ii} \ll 1 \tag{3.38}$$

where m_i and m_e are the ion and electron masses, v_{T_i} is the ion thermal speed, τ_{ii} is the typical ion-ion collision time, and a is the characteristic size of the magnetic confinement device. $\omega \sim \mathrm{v}_{T_i}/a$ is the typical MHD time scale, as explained in Chapter 1. The ordering (3.38) requires the ions to be very collisional on the fast MHD time scale. This is never satisfied in the high-temperature, fusion-grade plasmas, as we will quantitatively show in the next section. We can therefore wonder about the validity of the plasma compressibility stabilization prediction.

Our task in the remainder of this chapter will be to introduce several models which are more accurate than ideal MHD in the different regimes relevant to nuclear fusion, and derive energy relations, which will be compared to the ideal MHD energy principle. Through these comparisons, we will be able to assess the reliability of the compressibility stabilization.

We start by discussing the different collisionality regimes of fusion interest, and by introducing these different new models in this context.

3.3 Collisionality regimes in plasmas of fusion interest and alternate MHD models

From the MHD stability point of view, there are four different characteristic collisionality regimes to consider when assessing the reliability of the ideal MHD predictions.

The first regime corresponds to the ordering

$$\omega\tau_{eq} \ll 1 \tag{3.39}$$

where $\omega \sim \mathrm{v}_{T_i} / a$ is the typical MHD frequency, and τ_{eq} is the characteristic temperature equilibration time. As discussed at the end of the previous section, if (3.39) is satisfied, the equations of ideal MHD are well justified, including the ideal MHD conservation of energy equation, eq. (3.37) included. In these conditions, there is indeed compressibility stabilization, as already discussed.

The second regime of interest corresponds to the case where the electron-ion and electron-electron characteristic collision times (τ_{ei} and τ_{ee} respectively), and the ion-ion characteristic collision time (τ_{ii}) are much shorter than the MHD time scale, but the temperature equilibration time is longer than the MHD time scale. Mathematically, this is

$$\omega\tau_{ee} \sim \omega\tau_{ei} \ll \omega\tau_{ii} \ll 1 \ll \omega\tau_{eq} = \omega\tau_{ie} \qquad \text{(Regime 2)} \tag{3.40}$$

If the ordering (3.40) is satisfied, both ions and electrons essentially behave as fluids, and the whole plasma dynamics is well described by the first two equations of ideal MHD: conservation of mass, and conservation of momentum. However, the ideal MHD equation of state is not justified anymore, and we must allow the temperatures of the ions and electrons to evolve according to separate equations. The appropriate model then is what we call *Two-Temperature MHD*, a model which we describe in detail in Sec. 3.5, and for which we will derive quadratic energy forms which will be compared to the ideal MHD energy principle.

The third regime corresponds to the case where the characteristic ion collision time τ_{ii} is also longer than the MHD time scale, while the electron collision times remain much shorter:

$$\omega\tau_{ee} \sim \omega\tau_{ei} \ll 1 \ll \omega\tau_{ii} \ll \omega\tau_{eq} = \omega\tau_{ie} \qquad \text{(Regime 3)} \tag{3.41}$$

In regime 3, the electrons keep their fluid behavior, while the ions do not undergo enough collisions to maintain the behavior of an isotropic fluid. A kinetic description of the ions is then necessary. We will consider three such descriptions. The first two make use of the fact that in usual magnetic confinement concepts, the ion Larmor radius is much smaller than the typical size of the device, which is also the typical wavelength of the MHD instability: $\delta_i = r_{L_i} / a \ll 1$, where r_{L_i} is the ion Larmor radius. The first model, the simplest, takes the $\delta_i \to 0$ limit of the Vlasov equation

for the ions, and neglects the ion heat fluxes. Fluid-like equations are then obtained for the ions, allowing for non-isotropic evolution, unlike the Two-Temperature MHD model. This is the so-called Chew-Goldberger-Low [10] description for the ions, and we therefore call the full model, with CGL ions and MHD electrons the *CGL – Fluid MHD* model. It is perhaps the simplest model one can think of for collisionless ions and collision dominated electrons.

The CGL – Fluid MHD model is simple, but unfortunately unsatisfactory, since there is no justification for neglecting the ion heat fluxes. In the second model, known as Kinetic MHD [11], the quantities of interest for the ions are calculated by solving the Vlasov equation in the limit $\delta_i \to 0$ and taking the appropriate moments. No assumption is made concerning the heat fluxes, so that the equations do not reduce to fluid-like equations. What one loses in simplicity as compared to the CGL model, one gains in accuracy: the Kinetic MHD model is an exact description for collisionless ions, in the limit of infinite magnetic field, i.e. in the limit $\delta_i \to 0$. We call this model, with Kinetic MHD ions and MHD electrons the *Kinetic - Fluid MHD* model.

For certain fusion configurations (most often closed line configurations and when compressibility plays a critical role), the most unstable MHD modes have very short wavelengths, with the perpendicular wave number $k_\perp$ of the order $k_\perp r_{L_i} \sim 1$. When this is the case, taking the limit $\delta_i \to 0$ is not a good approximation. The

approach we then choose is to calculate the ion quantities of interest by solving the exact Vlasov equation. The full model, with the MHD electrons, is then called *Vlasov-Fluid* model [12]. Of course, the Vlasov equation is too complex to be solved in the most general case. As we will see, the price we will pay for solving this equation which is exact for arbitrary δ_i is that we will have to restrict the class of equilibria we allow ourselves to study. Fortunately, the static ideal MHD equilibrium belongs to the class of equilibria which are tractable.

The last collisionality regime of interest, regime 4, corresponds to the case where even the electrons are collisionless on the MHD time scale:

$$1 \ll \omega\tau_{ee} \sim \omega\tau_{ei} \ll \omega\tau_{ii} \ll \omega\tau_{eq} = \omega\tau_{ie} \qquad \text{(Regime 4)} \tag{3.42}$$

In that case, both species have to be treated kinetically. In this chapter, we will consider two models. In the first model, both species are described by the simple, yet ill-justified CGL equations. This is the original *CGL* model [10]. In the second model, both species are described by the Kinetic MHD equations. This is the original *Kinetic MHD* model [11], which is exact whenever the approximation $\delta_i \ll 1$ is well justified.

Ideally, we would want a fully collisionless model which treats the case $k_\perp r_{L_i} \sim 1$ accurately, in other word a full Vlasov model, to study plasma compressibility in this regime. However, none are satisfactory. The first reason for this is practical: we have not been able to derive, for a full Vlasov model, the same

energy relations which we have derived with the other models, and which can be compared to the ideal MHD energy principle. The second reason is more fundamental: if both species are described by the Vlasov equation, and $k_\perp$ is allowed to be large, the plasma is not tied to the magnetic field lines. Since this a critical characteristic of an MHD mode, we could wonder whether any instability that is found is indeed an MHD instability.

Now that we have introduced the 4 collisionality regimes of interest, and the six models we will study in detail in the next sections, it is interesting to see which of them are relevant for fusion grade plasmas. The two physical parameters which determine the collisionality regime of a plasma are the plasma temperature and the plasma density. In his classic paper, Braginskii [13] calculates the following expressions for the different collisional time scales of interest:

$$\begin{aligned}
\tau_{ee} &= 3\left(2\pi\right)^{3/2} \frac{\varepsilon_0^2 m_e^{1/2} T^{3/2}}{n e^4 \ln\Lambda} = 1.09\times 10^{-4} \frac{T_k^{3/2}}{n_{20} \ln\Lambda} \\
\tau_{ii} &= \sqrt{\frac{2m_i}{m_e}} \tau_{ee} \\
\tau_{eq} &= \frac{m_i}{2m_e} \tau_{ee}
\end{aligned} \tag{3.43}$$

In (3.43), m_e and m_i are the electron and ion mass, respectively, ε_0 is the vacuum permittivity, e is the charge of the proton, n is the density in m^{-3} units, n_{20} is the density in 10^{20} m^{-3} units, T is the temperature in eV, and T_k the temperature in

keV. $\ln\Lambda$ is the Coulomb logarithm [14], a quantity which weakly depends on temperature and density, and typically has values between 10 and 20. Setting the Coulomb logarithm to $\ln\Lambda = 19$ and the ion mass to that of deuterium, and multiplying all the expressions in (3.43) by $\omega = \mathrm{v}_{T_i} / a$, we obtain the following dependences on n_{20} and T_k for the collisionality boundaries:

$$\begin{aligned} \omega\tau_{eq} &= 3.3\times10^{3}\frac{T_k^2}{an_{20}} \\ \omega\tau_{ii} &= 1.5\times10^{2}\frac{T_k^2}{an_{20}} \\ \omega\tau_{ee} &= 1.8\frac{T_k^2}{an_{20}} \end{aligned} \tag{3.44}$$

Using (3.44), we can now represent the collisionality boundaries in $n_{20} - T_k$ parameter space, and see where they stand with respect to the rectangle $\left\{10^{18}\ \mathrm{m}^{-3} < n < 10^{22}\ \mathrm{m}^{-3}; 0.5\ \mathrm{keV} < T < 50\ \mathrm{keV}\right\}$ corresponding to the region of fusion interest. This is shown below, in Fig. 3.1, obtained for $a = 1$.

As can be seen in Fig. 3.1, on the MHD time scale, the ions are essentially collisionless in fusion grade plasmas. Several conclusions can be drawn. First, it is clear that the ideal MHD equation of state, requiring $\omega\tau_{eq} \ll 1$, is not a good approximation in regimes relevant to nuclear fusion. Second, when the approximation $\delta_i \ll 1$ is justified, the Kinetic MHD and Kinetic - Fluid MHD models appear to be relevant models for MHD stability studies. When $k_\perp$ becomes large, the Vlasov-Fluid

model is required in the region between the green and the red curve which is crossing the "Fusion grade plasmas" rectangle. As discussed, another model would be desirable for large $k_{\perp}$ in the region of this rectangle where the electrons are also collisionless, but we could not find any which was satisfactory.

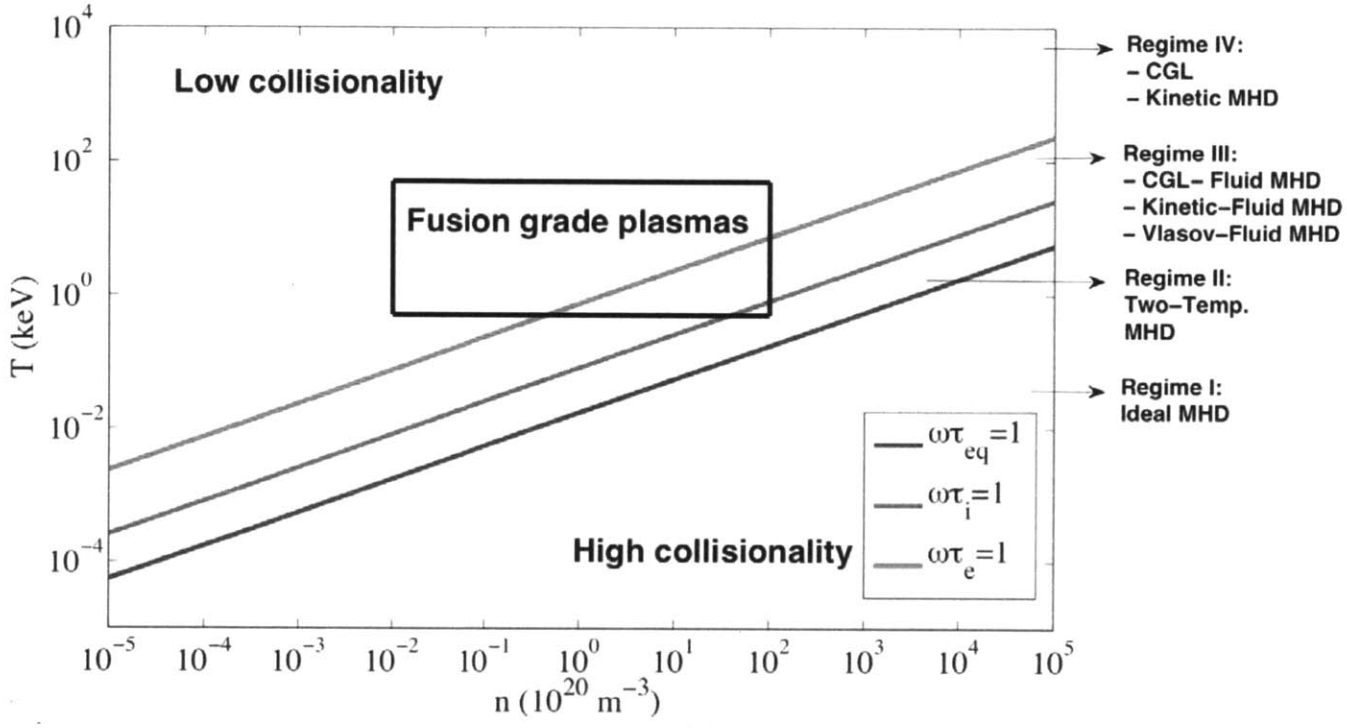

Fig. 3.1. Collisionality regimes in fusion grade plasmas

One could wonder why we choose to derive results for the Two-Temperature MHD, CGL – Fluid MHD, and CGL models. Indeed, according to Fig. 9.1 the Two-Temperature MHD model is hardly relevant in fusion plasmas, or perhaps only at very high densities and very low temperatures, and while the CGL – Fluid MHD and

CGL models describe more relevant regimes, they do it inaccurately. The answer to this question is that these models allow us to work our way gradually from ideal MHD to more relevant models. With the Two-Temperature MHD model, we allow the ion and electron temperatures to evolve separately. With the CGL – Fluid MHD model, we allow the ions to be collisionless, on our way to the Kinetic - Fluid MHD and the Vlasov-fluid models. With the CGL model, we treat the plasma as fully collisionless, on our way to the Kinetic MHD model.

The structure for the remainder of this chapter is as follows. Since the Vlasov-Fluid model is fundamentally different from the other five models in that it allows for finite δ_i, we will clearly separate our treatment of these two classes of models. From Section 3.4 to Section 3.9 we introduce the five models which assume $\delta_i \to 0$, and derive energy relations for each of them. Then, in Section 3.10 we introduce the Vlasov-Fluid model, and also derive an energy relation in this model. Based on all the energy relations, we will be able to reach conclusions about the reliability of ideal MHD stability analyses in fusion systems, and the existence – or not of plasma compressibility stabilization.

3.4 Five models, one general formulation

With the exception of the Vlasov-Fluid model, each of the other plasma models has the same starting point, which consists of an identical form of the mass and momentum moments of the Boltzmann-Maxwell equations, which are coupled to the low frequency, quasi neutral form of Maxwell's equations. Recalling that all the five models are defined in the limit $\delta_i \to 0$, the starting point is written as follows:

$$\begin{aligned}
&\frac{\partial n}{\partial t} + \nabla \cdot \left(n\mathbf{v} \right) = 0 \\
&m_i n \frac{d\mathbf{v}}{dt} = \mathbf{J} \times \mathbf{B} - \nabla \cdot \left(\mathbf{P}_e + \mathbf{P}_i \right) \\
&\frac{\partial \mathbf{B}}{\partial t} = \nabla \times \left(\mathbf{v} \times \mathbf{B} \right) \\
&\nabla \cdot \mathbf{B} = 0 \\
&\nabla \times \mathbf{B} = \mu_0 \mathbf{J} \\
&n_e = n_i = n
\end{aligned} \tag{3.45}$$

Note that to derive the first two equations in (3.45), the only approximation made is to assume that the center of mass inertia can be identified with the ion inertia, because of the large mass difference between electrons and ions. The assumption $\delta_i \to 0$ is not necessary. Likewise, the last two equations only depend on the following requirements

$$\begin{aligned}
&\frac{\omega}{k} \ll c \quad \text{and } \mathrm{v}_{T_i}, \mathrm{v}_{T_e} \ll c \quad \text{(neglect displacement current in Ampere's law)} \\
&\omega \ll \omega_{pe}, \quad \mathrm{a} \gg \lambda_D, \quad k\lambda_D \ll 1 \quad \text{(Charge neutrality condition)}
\end{aligned} \tag{3.46}$$

where $\omega_{pe} = \left(ne^2 / \varepsilon_0 m_e\right)^{1/2}$ is the electron plasma frequency, and $\lambda_D = \mathrm{v}_{T_e} / \omega_{pe}$ is the Debye length. The orderings in (3.46) are very well satisfied for fusion plasmas over a wide range of densities and temperatures. And obviously, $\nabla \cdot \mathbf{B} = 0$ is always true. Thus, the only place where the limit of small δ_i is taken is in the third equation, the so-called frozen-in law. This equation is derived in the following way. Neglecting electron inertia, the exact electron momentum equation is

$$\mathbf{E} + \mathbf{v} \times \mathbf{B} = \frac{1}{en}\left(\mathbf{J} \times \mathbf{B} - \nabla \cdot \mathbf{P}_e + \mathbf{R}_e\right) \tag{3.47}$$

where $\mathbf{R}_e$ represents the momentum loss of the electrons due to collisions with the ions. The largest contribution to the pressure tensor $\mathbf{P}_e$ comes from its diagonal, isotropic piece, and we have the ordering

$$\frac{1}{en}\left|\frac{\mathbf{J} \times \mathbf{B}}{\mathbf{v} \times \mathbf{B}}\right| \sim \frac{1}{en}\left|\frac{\nabla \cdot \mathbf{P}_e}{\mathbf{v} \times \mathbf{B}}\right| \sim \delta_i \ll 1 \tag{3.48}$$

Furthermore, according to Braginskii [13],

$$\frac{1}{en}\left|\frac{\mathbf{R}_e}{\mathbf{v} \times \mathbf{B}}\right| \sim \sqrt{\frac{m_e}{m_i}}\frac{1}{\omega\tau_{ii}}\delta_i^2 \ll 1 \tag{3.49}$$

Therefore, in the limit $\delta_i \to 0$, we have $\mathbf{E} + \mathbf{v} \times \mathbf{B} = \mathbf{0}$, ideal Ohm's law. Substituting ideal Ohm's law into Faraday's law results in the simple form given in (3.45). This

form of Faraday's law guarantees that the magnetic field lines are frozen into the plasma [4], the basic condition for ideal MHD behavior.

The set of equations in (3.45) has more unknowns than equations. We need additional information to determine the pressure tensors $\mathbf{P}_e$ and $\mathbf{P}_i$. This is what is known as a closure problem, and where the differences between the five models are found.

3.5 Two-Temperature MHD energy principle

As described in Section 3.3, the Two-Temperature MHD model aims at describing collisionality regimes such that $\omega\tau_{ee} \sim \omega\tau_{ei} \ll \omega\tau_{ii} \ll 1 \ll \omega\tau_{eq} = \omega\tau_{ie}$. Both the electrons and the ions still behave as fluids, so that we can use the Braginskii [13] transport coefficients to evaluate the ordering of each term in the exact energy equations, and obtain closure from the simplified energy equations.

According to Braginskii, we have

$$\left|\frac{\nabla\cdot\boldsymbol{\Pi}_i}{\nabla p_i}\right| \sim \omega\tau_{ii}; \quad \left|\frac{\nabla\cdot\boldsymbol{\Pi}_e}{\nabla p_e}\right| \sim \omega\tau_{ee} \tag{3.50}$$

where for both ions and electrons $\boldsymbol{\Pi}$ is the anisotropic part of the pressure tensor $\mathbf{P}$, and p is the isotropic part, $\boldsymbol{\Pi} = \mathbf{P} - p\mathbf{I}$. From (3.50) and our ordering, we conclude that we can assume that the pressure tensors of both species are isotropic. The next step is to find an expression for p_i and p_e in terms of the lower moments. This is

done separately for the ions and for the electrons because the electron parallel heat flux is so dominant in the electron energy equation.

3.5.1 Electron energy equation

Taking the energy moment of the Boltzmann equation for electrons, we have:

$$\frac{d}{dt}\left(\frac{p_e}{n^{\gamma_e}}\right) = \frac{\gamma_e - 1}{n^{\gamma_e}}\left[Q_e - \nabla\cdot\mathbf{h}_e - \boldsymbol{\Pi}_e : \nabla\left(\mathbf{v} - \frac{\mathbf{J}}{en}\right)\right] + \frac{1}{en}\mathbf{J}\cdot\nabla\left(\frac{p_e}{n^{\gamma_e}}\right) \tag{3.51}$$

In (3.51), $Q_e \equiv \frac{1}{2}\int \mathbf{dw} m_e \mathrm{w}^2 C_{ei}$ is the heat generated due to collisions, and $\mathbf{h}_e = \frac{1}{2}\int m_e \mathrm{w}^2 \mathbf{w} f_e d\mathbf{w}$ is the heat flux due to random motion, C_{ei} being the electron-ion collision operator, f_e the electron distribution function, and $\mathbf{w}$ the relative velocity. We evaluate the orders of magnitude of the different terms in (3.51), from the right to the left. First, according to Braginskii [13],

$$\begin{aligned}
\frac{\mathbf{J}\cdot\nabla p_e}{en\omega p_e} &\sim \frac{p_e^2}{enBa^2\omega p_e} \sim \delta_i \ll 1 \\
\frac{\boldsymbol{\Pi}_e : \nabla\mathbf{J}}{en\omega p_e} &\sim \frac{nT_e\tau_{ee}\mathrm{v}_{T_i}}{eBna^3\omega} \sim \delta_i\omega\tau_{ee} \ll 1 \\
\frac{\boldsymbol{\Pi}_e : \nabla\mathbf{v}}{\omega p_e} &\sim \frac{\boldsymbol{\Pi}_e}{p_e} \sim \omega\tau_{ee} \ll 1
\end{aligned} \tag{3.52}$$

Now, neglecting Joule heating (which is the same condition as neglecting the $\mathbf{R}_e / en$ term in the electron momentum equation), the main contribution to Q_e is electron and ion energy equilibration. We have

$$\frac{Q_e}{\omega p_e} \sim \frac{nT_e}{\tau_{eq}\omega p_e} \sim \frac{1}{\omega\tau_{eq}} \ll 1 \tag{3.53}$$

Therefore, on the right hand side of equation (3.51) we only have to keep the heat flux $\mathbf{h}_e$. The largest contribution to $\mathbf{h}_e$ comes from the parallel conductivity, so that in the end, we write

$$\frac{d}{dt}\left(\frac{p_e}{n^{\gamma_e}}\right) = \frac{\gamma_e - 1}{n^{\gamma_e}}\left[\nabla_\parallel \cdot \left(\kappa_{\parallel e}\nabla_\parallel T_e\right)\right] \tag{3.54}$$

where $\kappa_\parallel$ is the parallel thermal conductivity. Now, from Braginskii's transport theory [13], we know that $\kappa_{\parallel e} \sim nT_e\tau_{ee} / m_e$. Comparing the left and right hand side of (3.54) then leads to:

$$\frac{\nabla_\parallel \cdot \left(\kappa_{\parallel e}\nabla_\parallel T_e\right)}{\omega p_e} \sim \frac{m_i}{m_e}\omega\tau_{ee} \sim \omega\tau_{eq} \gg 1 \tag{3.55}$$

Thus, the heat flux tends to dominate the electron energy equation. It is tempting to write it as $\nabla_\parallel \cdot \left(\kappa_{\parallel e}\nabla_\parallel T_e\right) = 0$. As we will now see, the correct form for eq. (3.54) in fact depends on the field line geometry.

- *Case 1 : Ergodic systems, or closed-field line systems with modes which do not conserve the closed-line symmetry*

In this case, the right-hand side of eq. (3.54) does not naturally cancel. Since $\kappa_{\|e}$ is so large, it dominates the entire equation:

$$\nabla_{\|} \cdot \left(\kappa_{\|e} \nabla_{\|} T_e \right) = 0 \tag{3.56}$$

which we write in a more convenient way :

$$\mathbf{B} \cdot \nabla \left(\frac{\kappa_{\|e}}{B^2} \mathbf{B} \cdot \nabla T_e \right) = 0 \tag{3.57}$$

If we introduce a general coordinate system (l, χ, ψ) where l is the coordinate along a given field line, the general solution of eq. (3.57) can be written as

$$\frac{\kappa_{\|e}}{B^2} B \frac{\partial T_e}{\partial l} = G(\chi, \psi) \tag{3.58}$$

where G is an unknown function for the moment. Now, multiplying both sides of eq. (3.58) by $B^2 / \kappa_{\|e}$ and integrating along a given flux tube ($\int dl / B$), we obtain

$$\int dl \frac{\partial T_e}{\partial l} = G(\chi, \psi) \int dl \frac{B}{\kappa_{\|e}} \tag{3.59}$$

Now, the term on the left-hand side of eq. (3.59) is bounded : it is simply the difference between the temperatures at two different points along the flux tube. For ergodic field lines, however, the term on the right-hand side of (3.59) is unbounded, since it includes the infinite integral of a definite positive term which does not

converge to zero. Consequently, for (3.59) to hold, we must have $G(\chi,\psi)=0$. And we conclude that the proper equation of state for electrons in ergodic systems is

$$\mathbf{B}\cdot\nabla T_e = 0 \tag{3.60}$$

This is the equation of state we will use for the fluid electrons in ergodic systems.

- *Case 2: Closed field lines systems, and modes which conserve the closed-line symmetry*

In this case, eq. (3.59) still holds, and because of the closed-line symmetry, the left-hand side of the equation is identically zero if one integrates along the full length of a given flux tube. As a consequence, we have $G(\chi,\psi)=0$ once again, and $\mathbf{B}\cdot\nabla T_e = 0$. The difference with the previous case, however, is that taking the flux tube average of eq. (3.54), we have the additional constraint

$$\left\langle n^{\gamma_e}\frac{d}{dt}\left(\frac{p_e}{n^{\gamma_e}}\right)\right\rangle = 0 \tag{3.61}$$

Taking the partial derivative with respect to time of $\mathbf{B}\cdot\nabla T_e = 0$, we can write:

$$\frac{\partial\mathbf{B}}{\partial t}\cdot\nabla\left(\frac{p_e}{n}\right)+\mathbf{B}\cdot\nabla\left[\frac{\partial}{\partial t}\left(\frac{p_e}{n}\right)\right]=0 \tag{3.62}$$

Using the frozen-in law, $\partial\mathbf{B}/\partial t = \nabla\times\left(\mathbf{v}\times\mathbf{B}\right)$, and simple vector algebra formulas, eq. (3.62) can be rewritten as

$$\mathbf{B}\cdot\nabla\left[\frac{d}{dt}\left(\frac{p_e}{n}\right)\right]=0 \tag{3.63}$$

Combining the equation for the conservation of mass with eq. (3.63), we finally get

$$\mathbf{B}\cdot\nabla\left[\frac{1}{n}\left(\frac{dp_e}{dt}+p_e\nabla\cdot\mathbf{v}\right)\right]=0 \tag{3.64}$$

The general solution of eq. (3.64) is

$$\frac{1}{n}\left(\frac{dp_e}{dt}+p_e\nabla\cdot\mathbf{v}\right)=H(\chi,\psi) \tag{3.65}$$

where H is an unknown function of the two coordinates χ and ψ which is determined from the constraint given in eq. (3.61). Indeed, taking the flux tube average of eq. (3.65), we find

$$\left\langle\frac{dp_e}{dt}+p_e\nabla\cdot\mathbf{v}\right\rangle=H(\chi,\psi)\langle n\rangle \tag{3.66}$$

and according to (3.61),

$$\left\langle\frac{dp_e}{dt}+\gamma_e p_e\nabla\cdot\mathbf{v}\right\rangle=0 \tag{3.67}$$

Therefore, (3.66) implies

$$H(\chi,\psi)=-\left(\gamma_e-1\right)\frac{\langle p_e\nabla\cdot\mathbf{v}\rangle}{\langle n\rangle} \tag{3.68}$$

Substituting this expression for H into (3.65), we have our equation of state for the case of closed-field line symmetry :

$$\frac{dp_e}{dt}+p_e\nabla\cdot\mathbf{v}+\left(\gamma_e-1\right)\frac{n}{\langle n\rangle}\langle p_e\nabla\cdot\mathbf{v}\rangle=0 \tag{3.69}$$

This is the expression we will use for the fluid electrons in closed line systems, and concludes our derivation of approximate equations of state for the fluid electrons.

3.5.2 Ion energy equation

Taking the $\frac{m_i v^2}{2}$ moment of the ion Boltzmann equation, we find the following exact energy equation for the ions

$$\frac{d}{dt}\left(\frac{p_i}{n^{\gamma_i}}\right) = \frac{\gamma_i - 1}{n^{\gamma_i}}\left(Q_i - \nabla \cdot \mathbf{h}_i - \boldsymbol{\Pi}_i : \nabla \mathbf{v}\right) \tag{3.70}$$

Based on Braginskii's transport coefficients [13], we can compare the orders of magnitude of the terms in (3.70):

$$\begin{aligned} \frac{\boldsymbol{\Pi}_i : \nabla \mathbf{v}}{\omega p_i} &\sim \omega \tau_{ii} \ll 1 \\ \frac{Q_i}{\omega p_i} &\sim \frac{1}{\omega \tau_{eq}} \ll 1 \end{aligned} \tag{3.71}$$

Therefore, what is left on the right-hand side of (3.70) is the heat flux term, dominated by the parallel heat flux:

$$\frac{d}{dt}\left(\frac{p_i}{n^{\gamma_i}}\right) = \frac{\gamma_i - 1}{n^{\gamma_i}} \nabla_{\parallel} \cdot \left(\kappa_{\parallel i} \nabla T_i\right) \tag{3.72}$$

The ion parallel thermal conductivity is smaller than the electron thermal conductivity by the ratio $\left(m_e / m_i\right)^{1/2}$. Comparing both sides of eq. (3.72), we find

$$\frac{\nabla_{\parallel} \cdot \left(\kappa_{\parallel i} \nabla_{\parallel} T_i\right)}{\omega p_i} \sim \left(\frac{m_e}{m_i}\right)^{1/2} \omega\tau_{eq} \sim \omega\tau_{ii} \ll 1 \tag{3.73}$$

Consequently, the equation of state to use for fluid ions, in both ergodic and closed-line systems is:

$$\frac{d}{dt}\left(\frac{p_i}{n^{\gamma_i}}\right) = 0 \tag{3.74}$$

3.5.3 Two-Temperature MHD static equilibrium

In order to compare the Two-Temperature MHD stability predictions with those of static ideal MHD, we focus on the same class of equilibria: 1) static, i.e. $\mathbf{v}_0 = \mathbf{0}$, and 2) isotropic, so that $\mathbf{P}_{i0} = p_{i0}\mathbf{I}, \mathbf{P}_{e0} = p_{e0}\mathbf{I}$, with $p_0 = p_{i0} + p_{e0}$. With these choices, the non-trivial equilibrium equations in eq. (3.45) take the form:

$$\begin{aligned} \mathbf{J}_0 \times \mathbf{B}_0 &= \nabla p_0 \\ \nabla \cdot \mathbf{B}_0 &= 0 \\ \nabla \times \mathbf{B}_0 &= \mu_0 \mathbf{J}_0 \end{aligned} \tag{3.75}$$

These three equations are exactly identical to those of static ideal MHD, as expected. We are indeed comparing stability for the same class of equilibria.

3.5.4 Two-Temperature MHD stability and energy principle

As in ideal MHD, we introduce the displacement $\boldsymbol{\xi}$ defined by $-i\omega\boldsymbol{\xi} = \tilde{\mathbf{v}}$ and write the linearized momentum equation in terms of $\boldsymbol{\xi}$:

$$-m_i n\omega^2\boldsymbol{\xi} = \mathbf{J}\times\tilde{\mathbf{B}} + \tilde{\mathbf{J}}\times\mathbf{B} - \nabla\tilde{p} \tag{3.76}$$

The linearized version of the equations of state derived in 3.5.3 and 3.5.4 is

$$\tilde{p}_i = -\boldsymbol{\xi}\cdot\nabla p_i - \gamma_i p_i \nabla\cdot\boldsymbol{\xi} \qquad \text{(ions)} \tag{3.77}$$

and

$$\begin{cases} \tilde{p}_e = -\boldsymbol{\xi}\cdot\nabla p_e - p_e\nabla\cdot\boldsymbol{\xi} & \text{(electrons, ergodic systems)} \\ \tilde{p}_e = -\boldsymbol{\xi}_\perp\cdot\nabla p_e - p_e\nabla\cdot\boldsymbol{\xi} - \left(\gamma_e - 1\right)\left\langle\nabla\cdot\boldsymbol{\xi}_\perp\right\rangle & \text{(electrons, closed line systems)} \end{cases} \tag{3.78}$$

It is clear that the only terms in eq. (3.76) which differ from the ideal MHD case are the terms in (3.77) and (3.78) involving the compressibility, i.e. $\nabla\cdot\boldsymbol{\xi}$ and $\nabla\cdot\boldsymbol{\xi}_\perp$. Therefore, we can readily write

$$\omega^2 = \frac{\delta W_{TT}(\boldsymbol{\xi}^*,\boldsymbol{\xi})}{K_{MHD}(\boldsymbol{\xi}^*,\boldsymbol{\xi})} \tag{3.79}$$

where $\delta W_{TT}(\boldsymbol{\xi}^*,\boldsymbol{\xi}) = \delta W_\perp(\boldsymbol{\xi}_\perp^*,\boldsymbol{\xi}_\perp) + \delta W_{tt}(\boldsymbol{\xi}^*,\boldsymbol{\xi})$ is the potential energy associated with the displacement $\boldsymbol{\xi}$. $\delta W_\perp(\boldsymbol{\xi}_\perp^*,\boldsymbol{\xi}_\perp)$ is exactly identical to the incompressible part of $\delta W_{MHD}(\boldsymbol{\xi}_\perp^*,\boldsymbol{\xi}_\perp)$ defined previously. The exact form of $\delta W_{tt}(\boldsymbol{\xi}_\perp^*,\boldsymbol{\xi}_\perp)$ depends on the electron and ion equations of state, and therefore on the magnetic geometry.

- *Case 1: Ergodic systems or closed line systems undergoing symmetry breaking perturbations*

In this case, the electron and ion equations of state lead to

$$\delta W_{tt}(\boldsymbol{\xi},\boldsymbol{\xi}^*) = \int \left(\gamma_i p_i + p_e\right) |\nabla\cdot\boldsymbol{\xi}|^2 \, d\mathbf{r} \tag{3.80}$$

We notice that $\delta W_{TT}(\boldsymbol{\xi}^*,\boldsymbol{\xi})$ has exactly the same mathematical properties as $\delta W_{MHD}(\boldsymbol{\xi}^*,\boldsymbol{\xi})$. Using the same mathematical tools as in section 3.1.2 and 3.1.3, we could in particular prove that:

A system is stable in the Two-Temperature MHD model iff $\delta W_{TT}(\boldsymbol{\xi}^*,\boldsymbol{\xi}) \geq 0$ *for all allowable displacement* $\boldsymbol{\xi}$.

The most unstable modes are therefore found by minimizing $\delta W_{TT}(\boldsymbol{\xi}^*,\boldsymbol{\xi})$. Since $\xi_\parallel$ only appears $\delta W_{tt}(\boldsymbol{\xi}^*,\boldsymbol{\xi})$, we first perform the minimization with respect to $\xi_\parallel$ in this term. The form of $\delta W_{tt}(\boldsymbol{\xi}^*,\boldsymbol{\xi})$ is similar to that of $\delta W_C(\boldsymbol{\xi}^*,\boldsymbol{\xi})$ in ideal MHD. Therefore, following the same analysis, we find that the minimizing condition is $\nabla\cdot\boldsymbol{\xi} = 0$. In other words, the worst modes in ergodic systems in the Two-Temperature MHD model are incompressible modes. Modes are stable iff $\delta W_\perp(\boldsymbol{\xi}_\perp^*,\boldsymbol{\xi}_\perp) \geq 0$, which is equivalent to the following very powerful statement:

In ergodic systems or closed line systems undergoing symmetry breaking perturbations, a plasma is Two-Temperature MHD stable iff it is ideal MHD stable.

This completes our study of Two-Temperature MHD linear stability in ergodic systems.

- *Case 2: Closed field lines systems, and modes which conserve the closed-line symmetry*

Here, the ion and electron equations of state yield

$$\delta W_{tt}(\boldsymbol{\xi},\boldsymbol{\xi}^*) = \int \left(\gamma_i p_i + p_e\right) |\nabla\cdot\boldsymbol{\xi}|^2 \, d\mathbf{r} + \int \left(\gamma_e - 1\right) p_e \left|\left\langle \nabla\cdot\boldsymbol{\xi}_\perp \right\rangle\right|^2 d\mathbf{r} \tag{3.81}$$

As in the previous case, the mathematical properties of $\delta W_{TT}(\boldsymbol{\xi},\boldsymbol{\xi}^*)$ are identical to those of $\delta W_{MHD}(\boldsymbol{\xi},\boldsymbol{\xi}^*)$, so that the necessary and sufficient condition for stability is $\delta W_{TT}(\boldsymbol{\xi},\boldsymbol{\xi}^*) \geq 0$. $\xi_\parallel$ only appears in the first term of $\delta W_{tt}(\boldsymbol{\xi},\boldsymbol{\xi}^*)$, and following the ideal MHD treatment, we know that in closed line systems with modes which keep the closed line symmetry, the minimizing condition on $\xi_\parallel$ is

$$\nabla\cdot\boldsymbol{\xi} = \left\langle \nabla\cdot\boldsymbol{\xi}_\perp \right\rangle \tag{3.82}$$

Consequently,

$$\delta W_{tt}(\boldsymbol{\xi},\boldsymbol{\xi}^*) = \int \left(\gamma_i p_i + \gamma_e p_e\right) \left|\left\langle \nabla\cdot\boldsymbol{\xi}_\perp \right\rangle\right|^2 d\mathbf{r} \tag{3.83}$$

and for $\gamma_i = \gamma_e = \gamma = 5/3$ (adiabatic isotropic compression), (3.83) implies $\delta W_{TT}(\boldsymbol{\xi}, \boldsymbol{\xi}^*) = \delta W_{MHD}(\boldsymbol{\xi}, \boldsymbol{\xi}^*)$, which once again proves the statement:

In closed-line magnetic geometries, modes which conserve the closed-line symmetry are Two-Temperature MHD stable iff they are ideal MHD stable.

Returning to the question of compressibility, we conclude from the study of Case 2 that the Two-Temperature MHD model agrees with the ideal MHD predictions: in closed-line systems the plasma is compressible, and compressibility is stabilizing.

This concludes our study of the collisionality regime which we called Regime 2. We now look into Regime 3, with two models for collisionless ions and collisional electrons: the simple, fluid-like, but ill justified CGL - Fluid MHD model, and the more complex Kinetic – Fluid MHD model.

3.6 CGL – Fluid MHD energy principle

3.6.1 CGL – Fluid MHD closure

The collisionality regime which we called Regime 3 is defined by the ordering $\omega\tau_{ee} \sim \omega\tau_{ei} \ll 1 \ll \omega\tau_{ii} \ll \omega\tau_{eq} = \omega\tau_{ie}$. In these conditions, the electrons still behave

as an isotropic fluid, $\mathbf{P}_e = p_e \mathbf{I}$, and since all the orderings calculated in Section 3.5.1 still hold, the equations of state for the evolution of p_e in the CGL – Fluid MHD model are the same as in the previous model.

The ions, however, are not collisional anymore. The consequence of this is that without collisions, there is no physical mechanism to drive the ion pressure tensor towards an isotropic state. The first simplification made by the CGL description of the ions is to assume $\delta_i \to 0$. This implies that the off-diagonal components of the pressure tensor are negligible as compared to the diagonal components, since they are smaller by δ_i [11]. The ion pressure tensor is written as

$$\mathbf{P}_i = p_{i\perp}\left(\mathbf{I} - \mathbf{bb}\right) + p_{i\parallel}\mathbf{bb} \tag{3.84}$$

Furthermore, Chew, Goldberger, and Low [10] noticed that by taking the perpendicular and parallel energy moments of the Boltzmann equation for the ions, and neglecting the heat fluxes (besides neglecting the temperature equilibration term because $\omega\tau_{eq} \gg 1$ and the off-diagonal components of the pressure tensor, for the reasons mentioned above), fluid-like expressions could be found for the evolution of $p_{i\perp}$ and $p_{i\parallel}$:

$$\frac{d}{dt}\left(\frac{p_{i\parallel}B^2}{n^3}\right) = 0 \qquad \text{and} \qquad \frac{d}{dt}\left(\frac{p_{i\perp}}{nB}\right) = 0 \tag{3.85}$$

Note that there is no real justification for neglecting the heat fluxes when $\omega\tau_{ii} \gg 1$. The CGL model is commonly used nevertheless, since it is the simplest description of a collisionless, anisotropic plasma. Indeed, all the equations are fluid-like, unlike the next model we will treat, Kinetic MHD, which chooses accuracy at the expense of simplicity.

3.6.2 CGL – Fluid MHD static equilibrium

Once again, we can only compare the CGL – Fluid MHD predictions with those of ideal MHD if we focus on the same class of equilibria: 1) static, i.e. $\mathbf{v}_0 = \mathbf{0}$, and 2) isotropic, so that $\mathbf{P}_{i0} = p_{i0}\mathbf{I}, \mathbf{P}_{e0} = p_{e0}\mathbf{I}$, with $p_0 = p_{i0} + p_{e0}$. With these choices, the non-trivial equilibrium equations in eq. (3.45) take the form:

$$\begin{aligned} \mathbf{J}_0 \times \mathbf{B}_0 &= \nabla p_0 \\ \nabla \cdot \mathbf{B}_0 &= 0 \\ \nabla \times \mathbf{B}_0 &= \mu_0 \mathbf{J}_0 \end{aligned} \tag{3.86}$$

These three equations are exactly identical to those of static ideal MHD, as expected. We are indeed comparing stability for the same class of equilibria.

Focusing on isotropic equilibria does not contradict our desire to study the behavior of essentially collisionless, anisotropic ions, which is the whole purpose of the CGL model. The basic idea behind our stability studies in Regime 3 of collisionality is the following: on the long equilibrium time scale, the ions undergo enough collisions to make their equilibrium pressure isotropic. However, on the fast

MHD time scale during which perturbations develop, the ions are collisionless, so that their behavior is essentially anisotropic.

3.6.3 CGL – Fluid MHD stability and energy principle

Following the usual procedure, we first introduce the displacement $\boldsymbol{\xi}$ such that $\tilde{\mathbf{v}} = -i\omega\boldsymbol{\xi}$, and write the linearized momentum equation:

$$-\omega^2 m_i n\boldsymbol{\xi} = \mathbf{J}\times\tilde{\mathbf{B}} + \tilde{\mathbf{J}}\times\mathbf{B} - \nabla\tilde{p}_e - \nabla\tilde{p}_{i\perp} - \left(\tilde{p}_{i\parallel} - \tilde{p}_{i\perp}\right)\boldsymbol{\kappa} - \mathbf{bB}\cdot\nabla\left(\frac{\tilde{p}_{i\parallel} - \tilde{p}_{i\perp}}{B}\right) \quad (3.87)$$

Linearizing the equations of state (3.85), we find:

$$\tilde{p}_{i\parallel} = -\boldsymbol{\xi}\cdot\nabla p_i - p_i\nabla\cdot\boldsymbol{\xi} - 2p_i\mathbf{bb}:\nabla\boldsymbol{\xi} \quad (3.88)$$

and

$$\tilde{p}_{i\perp} = -\boldsymbol{\xi}\cdot\nabla p_i - 2p_i\nabla\cdot\boldsymbol{\xi} + p_i\mathbf{bb}:\nabla\boldsymbol{\xi} \quad (3.89)$$

$\tilde{p}_e$ is given by the same equations as in the Two-Temperature MHD case, and depends on the geometry under consideration. Dotting eq. (3.87) with $\boldsymbol{\xi}^*$, and integrating over the plasma volume, we find the variational form

$$\omega^2 = \frac{\delta W_{CF}(\boldsymbol{\xi}^*,\boldsymbol{\xi})}{K_{MHD}(\boldsymbol{\xi}^*,\boldsymbol{\xi})} \quad (3.90)$$

where $\delta W_{CF}(\boldsymbol{\xi}^*,\boldsymbol{\xi}) = \delta W_\perp(\boldsymbol{\xi}_\perp^*,\boldsymbol{\xi}_\perp) + \delta W_{cf}(\boldsymbol{\xi}^*,\boldsymbol{\xi})$ is the potential energy associated with the displacement $\boldsymbol{\xi}$. $\delta W_\perp(\boldsymbol{\xi}_\perp^*,\boldsymbol{\xi}_\perp)$ is exactly identical to the incompressible part of $\delta W_{MHD}(\boldsymbol{\xi}_\perp^*,\boldsymbol{\xi}_\perp)$ defined previously. The exact form of $\delta W_{cf}(\boldsymbol{\xi}_\perp^*,\boldsymbol{\xi}_\perp)$ depends on the electron and ion equations of state, and therefore on the magnetic geometry.

- *Case 1*: *Ergodic systems or closed line systems undergoing symmetry breaking perturbations*

Using (3.78) for the electrons, and (3.88), and (3.89) for the ions, we find the following expression for $\delta W_{cf}(\boldsymbol{\xi}_\perp^*, \boldsymbol{\xi}_\perp)$, after using the divergence theorem a few times:

$$\begin{aligned}\delta W_{cf}(\boldsymbol{\xi}_\perp^*, \boldsymbol{\xi}_\perp) = &\int d\mathbf{r}\left(p_e + 2p_i\right)\left|\nabla\cdot\boldsymbol{\xi}\right|^2 + \int d\mathbf{r} p_i\left(\nabla\cdot\boldsymbol{\xi} - 3\mathbf{bb}:\nabla\boldsymbol{\xi}\right)\boldsymbol{\xi}^*\cdot\boldsymbol{\kappa} \\ &- \int d\mathbf{r} p_i\left(\mathbf{bb}:\nabla\boldsymbol{\xi}\right)\nabla\cdot\boldsymbol{\xi}^* + \int d\mathbf{r} p_i\left(3\mathbf{bb}:\nabla\boldsymbol{\xi} - \nabla\cdot\boldsymbol{\xi}\right)\mathbf{b}\cdot\nabla\xi_\parallel^*\end{aligned} \tag{3.91}$$

Now, since $\boldsymbol{\xi}^*\cdot\boldsymbol{\kappa} = \mathbf{b}\cdot\nabla\xi_\parallel^* - \mathbf{bb}:\nabla\boldsymbol{\xi}^*$, natural cancellations occur in (3.91):

$$\begin{aligned}\delta W_{cf}(\boldsymbol{\xi}_\perp^*, \boldsymbol{\xi}_\perp) = &\int d\mathbf{r}\left(p_e + 2p_i\right)\left|\nabla\cdot\boldsymbol{\xi}\right|^2 + 3\int d\mathbf{r} p_i\left|\mathbf{bb}:\nabla\boldsymbol{\xi}\right|^2 \\ &- \int d\mathbf{r} p_i\nabla\cdot\boldsymbol{\xi}\left(\mathbf{bb}:\nabla\boldsymbol{\xi}^*\right) - \int d\mathbf{r} p_i\nabla\cdot\boldsymbol{\xi}^*\left(\mathbf{bb}:\nabla\boldsymbol{\xi}\right)\end{aligned} \tag{3.92}$$

Writing $2p_i = \frac{5}{3}p_i + \frac{1}{3}p_i$, $\delta W_{cf}(\boldsymbol{\xi}_\perp^*, \boldsymbol{\xi}_\perp)$ can finally be written in desired form:

$$\delta W_{cf}(\boldsymbol{\xi}_\perp^*, \boldsymbol{\xi}_\perp) = \int d\mathbf{r}\left(p_e + \frac{5}{3}p_i\right)\left|\nabla\cdot\boldsymbol{\xi}\right|^2 + 3\int d\mathbf{r} p_i\left|\frac{1}{3}\nabla\cdot\boldsymbol{\xi} - \mathbf{bb}:\nabla\boldsymbol{\xi}\right|^2 \tag{3.93}$$

The CGL equations conserve energy, and the CGL force operator is self-adjoint [3]. Consequently, we can reuse all the ideal MHD machinery to derive the CGL – Fluid MHD energy principle, and state:

A system is stable in the CGL – Fluid MHD model iff $\delta W_{CF}(\boldsymbol{\xi}^*, \boldsymbol{\xi}) \geq 0$ *for all allowable displacement* $\boldsymbol{\xi}$.

Note that $\xi_\parallel$, which appears only in $\delta W_{cf}(\boldsymbol{\xi}^*, \boldsymbol{\xi})$, does so in a more complicated way than in ideal MHD. Therefore, the minimization with respect to $\xi_\parallel$ does not lead to an immediate condition on $\nabla \cdot \boldsymbol{\xi}$. Instead, it is a complicated integro-differential equation, which we do not need to derive here. Indeed, the point is that we are not interested in the exact details of the CGL – Fluid MHD stability thresholds. We just want to verify that ideal MHD, the simpler model, leads to conservative estimates as compared to CGL – Fluid MHD, which allows for the anisotropic behavior of the ions. And this is very easily done, using the CGL – Fluid MHD energy principle just stated.

The first step is to notice that $\delta W_{cf}(\boldsymbol{\xi}^*, \boldsymbol{\xi}) \geq 0$, as obviously shown by eq. (3.93). Therefore,

$$\delta W_{CF}(\boldsymbol{\xi}^*, \boldsymbol{\xi}) \geq \delta W_{\perp}(\boldsymbol{\xi}^*, \boldsymbol{\xi}) \tag{3.94}$$

The next step is to assume that the ergodic system is ideal MHD stable. According to the ideal MHD energy principle for ergodic magnetic geometries, this means that $\delta W_{\perp}(\boldsymbol{\xi}^*, \boldsymbol{\xi}) \geq 0$ for any $\boldsymbol{\xi}$. And using eq. (3.94), this implies:

$$\text{For any } \boldsymbol{\xi},\ \delta W_{CF}(\boldsymbol{\xi}^*, \boldsymbol{\xi}) \geq 0 \tag{3.95}$$

According to the CGL – Fluid MHD energy principle, this means that the system is CGL – Fluid MHD stable. Thus, we just proved the following powerful result:

In ergodic systems or closed line systems undergoing symmetry breaking perturbations, if a plasma is ideal MHD stable, it is CGL – Fluid MHD stable.

- *Case 2 : Closed field lines systems, and modes which conserve the closed-line symmetry*

In this case, we can reuse most of the results from Case 1, and simply change the electron term, since in closed-line systems, with modes which keep the closed-line symmetry, the electron equation of state takes a different form. We find:

$$\delta W_{cf}(\boldsymbol{\xi}_\perp^*, \boldsymbol{\xi}_\perp) = \int d\mathbf{r}\left(p_e + \frac{5}{3}p_i\right)\left|\nabla\cdot\boldsymbol{\xi}\right|^2 + \int\left(\gamma_e - 1\right)p_e\left|\left\langle\nabla\cdot\boldsymbol{\xi}_\perp\right\rangle\right|^2 d\mathbf{r} + 3\int d\mathbf{r}p_i\left|\frac{1}{3}\nabla\cdot\boldsymbol{\xi} - \mathbf{bb}:\nabla\boldsymbol{\xi}\right|^2 \tag{3.96}$$

Now, from Schwarz's inequality, $\int d\mathbf{r}\left(p_e + \frac{5}{3}p_i\right)\left|\nabla\cdot\boldsymbol{\xi}\right|^2 \geq \int d\mathbf{r}\left(p_e + \frac{5}{3}p_i\right)\left|\left\langle\nabla\cdot\boldsymbol{\xi}_\perp\right\rangle\right|^2$, so that

$$\delta W_{cf}(\boldsymbol{\xi}_\perp^*, \boldsymbol{\xi}_\perp) \geq \int\left(\gamma_e p_e + \frac{5}{3}p_i\right)\left|\left\langle\nabla\cdot\boldsymbol{\xi}_\perp\right\rangle\right|^2 d\mathbf{r} + 3\int d\mathbf{r}p_i\left|\frac{1}{3}\nabla\cdot\boldsymbol{\xi} - \mathbf{bb}:\nabla\boldsymbol{\xi}\right|^2 \tag{3.97}$$

The second term on the right-hand side of eq. (3.97) is clearly positive definite. Furthermore, for isotropic electrons, $\gamma_e = 5/3$, so eq. (3.97) implies

$\delta W_{cf}(\boldsymbol{\xi}_\perp^*, \boldsymbol{\xi}_\perp) \geq \delta W_C(\boldsymbol{\xi}_\perp^*, \boldsymbol{\xi}_\perp)$, and $\delta W_{CF}(\boldsymbol{\xi}_\perp^*, \boldsymbol{\xi}_\perp) \geq \delta W_{MHD}(\boldsymbol{\xi}_\perp^*, \boldsymbol{\xi}_\perp)$. Hence, using the same arguments as in Case 1, we can formulate the following statement:

In closed-line magnetic geometries, if modes which conserve the closed-line symmetry are ideal MHD stable, they are CGL – Fluid MHD stable.

And as far as compressibility is concerned, the CGL – Fluid MHD predictions confirm the ideal MHD predictions: there is compressibility stabilization, even when the ions are collisionless.

Of course, as mentioned in the beginning of Section 3.6, the CGL – Fluid MHD results are at least as suspicious as the ideal MHD results, since the CGL equations of state for the ions are poorly justified when the ions are collisionless. It is for this reason that we now turn to a more accurate model: the Kinetic – Fluid MHD model.

3.7 Kinetic – Fluid MHD energy principle

3.7.1 Kinetic – Fluid MHD closure

In the Kinetic – Fluid MHD model, the electrons behave as a collision dominated fluid, so that the electron equations of state derived for the previous models in Section 3.5 and 3.6 still hold. For the collisionless ions, however, the

closure is quite different than that of the CGL model. We still study the plasma in the limit $\delta_i \to 0$, so that the ion pressure tensor can be written as

$$\mathbf{P}_i = p_{i\perp}\left(\mathbf{I} - \mathbf{bb}\right) + p_{i\parallel}\mathbf{bb} \tag{3.98}$$

but the difference with the previous model is that instead of calculating $p_{i\perp}$ and $p_{i\parallel}$ from approximate, fluid-like equations of state, we calculate these quantities from the drift-kinetic equation [15] with large $\mathbf{E}\times\mathbf{B}$ flow (i.e. $\mathrm{v}_{\mathbf{E}\times\mathbf{B}} \sim \mathrm{v}_{T_i}$ as in ideal MHD) and in the limit $\delta_i \to 0$. Namely,

$$\begin{aligned} p_{i\perp} &= \int \frac{mw_\perp^2}{2} f_i \, d\mathbf{w} = \frac{2^{1/2}\pi B}{m^{3/2}} \int \frac{\mu B}{\left(\varepsilon - \mu B\right)^{1/2}} f_i \, d\varepsilon \, d\mu \\ p_{i\parallel} &= \int m w_\parallel^2 \, f_i \, d\mathbf{w} = \frac{2^{3/2}\pi B}{m^{3/2}} \int \left(\varepsilon - \mu B\right)^{1/2} f_i \, d\varepsilon \, d\mu \end{aligned} \tag{3.99}$$

where $\varepsilon = (m/2)(w_\perp^2 + w_\parallel^2)$ and $\mu = mw_\perp^2/2B$ are the basic velocity variables describing the distribution function $f_i(\mathbf{r},\varepsilon,\mu,t)$, which is the solution of the equation

$$\frac{\partial f}{\partial t} + (\mathbf{v} + w_\parallel \mathbf{b})\cdot\nabla f + \bar{\dot{\varepsilon}}\frac{\partial f}{\partial \varepsilon} = 0 \tag{3.100}$$

with

$$\bar{\dot{\varepsilon}} = q w_\parallel E_\parallel - m w_\parallel \mathbf{b}\cdot\frac{d\mathbf{v}}{dt} - \frac{mw_\perp^2}{2}\nabla\cdot\mathbf{v} + m\left(\frac{w_\perp^2}{2} - w_\parallel^2\right)\mathbf{b}\cdot\left(\mathbf{b}\cdot\nabla\right)\mathbf{v} \tag{3.101}$$

In eqs. (3.99), (3.100), and (3.101), $\mathbf{w}$ is the random component of the particle velocity while $\mathbf{v} = \mathbf{v}(\mathbf{r},t)$ is the macroscopic plasma velocity (in this ordering, it consists of two pieces : the parallel velocity and the $\mathbf{E}\times\mathbf{B}$ velocity). A very good

derivation of equations (3.100) and (3.101) can be found in [11]. There are two things to note: 1) Eq. (3.100) is an exact consequence of the Vlasov equation in the mentioned limit, i.e. $\delta_i \to 0$ and $\mathrm{v}_{\mathbf{E}\times\mathbf{B}} \sim \mathrm{v}_{T_i}$; 2) Although $E_\parallel / E_\perp \sim \delta_i$ as seen from the ideal Ohm's law $\mathbf{E} + \mathbf{v}\times\mathbf{B} = \mathbf{0} + O(\delta_i)$, it enters in eq. (3.101). It is calculated from the parallel component of the electron momentum equation. Indeed, neglecting the terms which are small in the electron mass, and all the terms in the friction force, the electron momentum equation takes the form $\mathbf{E} + \mathbf{v}_e \times \mathbf{B} + \dfrac{\nabla p_e}{en} = \mathbf{0}$, so that

$$E_\parallel = -(\mathbf{b}\cdot\nabla p_e)/en \tag{3.102}$$

3.7.2 Kinetic – Fluid MHD equilibrium

The equilibria of interest are static (i.e. $\mathbf{v} = 0$) with isotropic pressure. This corresponds to requiring the ion distribution function to be of the form $f_i = f_i(\psi, \varepsilon)$. For these choices, $\mathbf{P}_{i0} = p_{i0}(\psi)\mathbf{I}$, and the equilibrium equations take the form:

$$\begin{aligned} \mathbf{J}_0 \times \mathbf{B}_0 &= \nabla p_0 \\ \nabla\cdot\mathbf{B}_0 &= 0 \\ \nabla\times\mathbf{B}_0 &= \mu_0\mathbf{J}_0 \end{aligned} \tag{3.103}$$

The first equation in (3.103) implies $p_0 = p_0(\psi)$. Since $p_{i0} = p_{i0}(\psi)$, we necessarily have $p_{e0} = p_{e0}(\psi)$. Using eq. (3.102) we conclude that $E_{\parallel 0} = 0$. Furthermore, from the ideal Ohm's law with $\mathbf{v} = \mathbf{0}$, we know that $\mathbf{E}_{\perp 0} = \mathbf{0}$. Consequently, $\mathbf{E}_0 = \mathbf{0}$, and the class of equilibria described by (3.103) is identical to that of static ideal MHD.

3.7.3 Kinetic – Fluid MHD energy principle

What the Kinetic – Fluid MHD model gains in accuracy as compared to the CGL-MHD model, it obviously loses in simplicity. The kinetic effects associated with the kinetic treatment of the ions indeed make the analysis much more complicated. For the clarity of the presentation, we focus here solely on the key results of the derivation. The details of the calculation can be found in Appendix B.

Since the electron equation of state takes a different form in ergodic and closed line systems, and since the ion trajectories also have different periodicity properties in the two systems, we need to distinguish the two geometries once again.

- *Case 1*: *Ergodic systems or closed line systems undergoing symmetry breaking perturbations*

For ergodic systems, we find the following energy relation

$$\left|\omega\right|^2 = -\frac{\delta W_\perp(\boldsymbol{\xi}_\perp,\boldsymbol{\xi}_\perp^*) + \delta W_{kf}(\boldsymbol{\xi},\boldsymbol{\xi}^*)}{K_\perp(\boldsymbol{\xi}_\perp,\boldsymbol{\xi}_\perp^*)} \tag{3.104}$$

Here, $\boldsymbol{\xi}$ is the plasma displacement, $-i\omega\boldsymbol{\xi} = \tilde{\mathbf{v}}$, $K_\perp(\boldsymbol{\xi}_\perp,\boldsymbol{\xi}_\perp^*) = \int \rho\left|\boldsymbol{\xi}_\perp\right|^2 d\mathbf{r}$ is the perpendicular kinetic energy, and δW_{kf} is the contribution to the potential energy associated with the ion kinetic effects. For any ion distribution function satisfying $\frac{\partial f_i}{\partial \varepsilon} < 0$, δW_{kf} is given by:

$$\delta W_{kf}(\boldsymbol{\xi},\boldsymbol{\xi}^*) = \left|\omega\right|^2 \int \frac{d\mathbf{r}}{n}(U_i + U_h)$$
$$U_i = \hat{T}_i \left[\int \frac{\partial f_i}{\partial \varepsilon} d\mathbf{w} \int \frac{\partial f_i}{\partial \varepsilon} \left|\tilde{s}_i\right|^2 d\mathbf{w} - \left| \int \frac{\partial f_i}{\partial \varepsilon} \tilde{s}_i \, d\mathbf{w} \right|^2 \right] \tag{3.105}$$
$$U_h = \frac{1}{\left(\hat{T}_i + T_e\right)} \left| \hat{T}_i \int \frac{\partial f_i}{\partial \varepsilon} \tilde{s}_i d\mathbf{w} \right|^2$$

where $T_e = p_e / n$ and

$$\frac{1}{\hat{T}_i} = -\frac{1}{n} \int \frac{\partial f_i}{\partial \varepsilon} d\mathbf{w} > 0$$
$$\tilde{s}_i(\varepsilon,\mu,\mathbf{r},t) = \int_{-\infty}^{t} \left[\frac{m_i w_\perp^2}{2} \nabla \cdot \boldsymbol{\xi}_\perp + m_i \left(\frac{w_\perp^2}{2} - w_\parallel^2 \right) \boldsymbol{\xi}_\perp \cdot \boldsymbol{\kappa} + T_e \nabla \cdot \boldsymbol{\xi} \right] e^{-i\omega t'} dt' \tag{3.106}$$

The quantity $\hat{T}_i(\psi)$ has the dimensions of temperature and is indeed equal to the temperature for the case of a local Maxwellian distribution function.

Using Schwarz's inequality in eq. (3.105), we clearly see that $\delta W_{kf} \geq 0$. We can then deduce two conclusions from the energy relation. First ideal MHD stability implies kinetic MHD-fluid stability. Indeed, for an ergodic system which is ideal MHD stable, we have the inequality

$$\delta W_{KF} \equiv \delta W_\perp + \delta W_{kf} \geq \delta W_\perp(\boldsymbol{\xi}^*_{\perp KF}, \boldsymbol{\xi}_{\perp KF}) \geq \delta W_\perp(\boldsymbol{\xi}^*_{\perp MHD}, \boldsymbol{\xi}_{\perp MHD}) > 0 \tag{3.107}$$

The quantity $\boldsymbol{\xi}_{\perp KF}$ is the exact eigenfunction for the hybrid model, and the next to last inequality in eq. (3.107) holds because by definition $\boldsymbol{\xi}_{\perp MHD}$ minimizes $\delta W_\perp$ in

ergodic systems. Eq. (3.107) leads to a contradiction in eq. (3.104), which can only be resolved by recognizing that the assumption $\mathrm{Im}(\omega) \geq 0$ made when integrating back to $t' = -\infty$ in the orbit integrals to derive eq. (3.105) is incorrect. Therefore, we must have $\mathrm{Im}(\omega) \leq 0$, which implies stability. We just proved the following result:

In ergodic systems or closed line systems undergoing symmetry breaking perturbations, if a plasma is ideal MHD stable, it is Kinetic – Fluid MHD stable.

The second conclusion involves the limit $\omega^2 = 0$ which we assume corresponds to marginal stability[6]. In this limit $\delta W_{kf} = 0$ for a straight cylinder and is positive in a torus because of trapped particle compressibility stabilization; that is, $\delta W_{kf} > 0$.

This can be demonstrated explicitly by examining the parallel motion in the trajectory integral in eq. (3.106). Qualitatively, since eq. (3.100) is a zero gyroradius approximation of the Vlasov equation, the integrand is proportional to $\exp[-i\omega t + ik_{\|}l(t')]$ where $l(t')$ is the parallel trajectory of a particle. For a passing particle $l(t') \approx w_{\|}t'$ and the trajectory integral $s \propto 1/(\omega - k_{\|}w_{\|})$ which is finite in the limit of $\omega^2 \to 0$.

---

[6] It has been proven [16] that $\omega^2 = 0$ indeed corresponds to the marginal stability boundary in the Kinetic MHD model, which we treat in Section 3.9. We assume here that this result holds for the Kinetic – Fluid MHD model.

However, for a trapped particle $l(t') \approx l_0 \cos(\omega_B t')$ where $\omega_B(\varepsilon, \mu, \mathbf{r})$ is the bounce frequency of the orbit. The integrand in eq. (3.106) can therefore be expanded in a Fourier series and the zeroth harmonic yields a contribution proportional to $1/\omega$ [17]. Specifically, as $\omega^2 \to 0$ the orbit integral reduces to

$$\begin{aligned} \tilde{s} &\to \frac{i}{\omega \tau_B} \bar{s} \\ \bar{s} &= \int_0^{\tau_B} \left[\frac{m_i w_\perp^2}{2} \nabla \cdot \boldsymbol{\xi}_\perp + m_i \left(\frac{w_\perp^2}{2} - w_\parallel^2 \right) \boldsymbol{\xi}_\perp \cdot \boldsymbol{\kappa} + T_e \nabla \cdot \boldsymbol{\xi} \right] dt' \end{aligned} \tag{3.108}$$

Here, $\tau_B = 2\pi / \omega_B$ is the bounce period. The $1/\omega$ factor in the denominator leads to a finite value for δW_{kf} given by

$$\begin{aligned} \delta W_{kf}(\boldsymbol{\xi}, \boldsymbol{\xi}^*) &= \frac{4}{\pi^2} \int \frac{d\mathbf{r}}{n} (U_i + U_h) \\ U_i &= \hat{T}_i \left[\int \frac{\partial f_i}{\partial \varepsilon} d\mathbf{w} \int_T \frac{\partial f_i}{\partial \varepsilon} \left| \omega_{Bi} \bar{s}_i \right|^2 d\mathbf{w} - \left| \int_T \frac{\partial f_i}{\partial \varepsilon} \omega_{Bi} \bar{s}_i \, d\mathbf{w} \right|^2 \right] \\ U_h &= \frac{1}{\left(\hat{T}_i + T_e \right)} \left| \hat{T}_i \int_T \frac{\partial f_i}{\partial \varepsilon} \omega_{Bi} \bar{s}_i \, d\mathbf{w} \right|^2 \end{aligned} \tag{3.109}$$

where the subscript T on the integrals denotes integration over the region of velocity space corresponding to trapped particles.

Thus, the second conclusion is that a toroidal kinetic MHD system is positively stable when the ideal MHD system is marginally stable. This behavior corresponds to trapped particle compressibility stabilization [18], an effect obviously not present in a straight cylinder. The results for ergodic Kinetic – Fluid MHD systems at $\omega^2 = 0$ can be conveniently summarized as follows.

$$\begin{aligned} \delta W_{KF} &= \delta W_{\perp} = \delta W_{MHD} && \text{straight cylinder} \\ \delta W_{KF} &= \delta W_{\perp} + \delta W_{kf} > \delta W_{MHD} && \text{torus} \end{aligned} \tag{3.110}$$

- *Case 2 : Closed field lines systems, and modes which conserve the closed-line symmetry*

The analysis presented in Case 1 also applies to this case but is not directly useful for determining MHD stability comparison theorems. The reason is that for closed line systems $\delta W_{MHD} = \delta W_{\perp} + \delta W_{C}$ and there is no way to show whether δW_{kf} in its present form is bigger or smaller than the MHD compression stabilization term δW_{C}. What is needed is a quantitative estimate of δW_{kf}, and not just a determination of its sign. This requires a substantial amount of analysis, which is given in Appendix B. The bottom line is that in the limit $\omega^2 \to 0$, a lower bound for δW_{kf} can be calculated analytically. We can write

$$\delta W_{KF} = \delta W_{\perp} + \delta W_{kf} \tag{3.111}$$

where (for $\gamma_e = 5/3$)

$$\delta W_{kf} \geq \delta W_{C} = \int \frac{5}{3} p \left| \left\langle \nabla \cdot \boldsymbol{\xi}_{\perp} \right\rangle \right|^2 d\mathbf{r} \tag{3.112}$$

Therefore, for a closed-line system which is ideal MHD stable, we have the inequality

$$\delta W_{KF} \equiv \delta W_{\perp} + \delta W_{kf} \geq \delta W_{MHD}(\boldsymbol{\xi}^*_{\perp KF}, \boldsymbol{\xi}_{\perp KF}) \geq \delta W_{MHD}(\boldsymbol{\xi}^*_{\perp MHD}, \boldsymbol{\xi}_{\perp MHD}) > 0 \tag{3.113}$$

In other words,

In closed-line magnetic geometries, if modes which conserve the closed-line symmetry are ideal MHD stable, they are Kinetic – Fluid MHD stable.

As far as plasma compressibility is concerned, the Kinetic – Fluid MHD model thus confirms the ideal MHD result in that it also finds compressibility stabilization for models with closed-line symmetry.

The issue with the Kinetic – Fluid MHD results on plasma compressibility stabilization is that they rely on the exact periodicity of the particles' motion – the trapped particles in ergodic systems, and both passing and trapped particles in closed-line geometries for modes which conserve this symmetry. In the limit $\delta_i \to 0$, the particles' motion is indeed exactly periodic. But this is not true anymore for finite δ_i since the particles' precession motion due to their drifts off flux tubes then has to be taken into account. For most MHD instabilities, the neglect of these drifts is justified, since $k_\parallel w_\parallel \gg k_\perp \mathrm{v}_d$, where v_d is the drift velocity. However, in ideal MHD, the compressible modes are often the most unstable in the limit $k_\perp \to \infty$, so that $k_\perp \mathrm{v}_d$ may compete with $k_\parallel \mathrm{v}_\parallel$ even if $\mathrm{v}_d / w_\parallel \sim \delta_i$. Another case where the neglect of the drifts may not be justified corresponds to modes which have $k_\parallel = 0$, such as the compressible interchange modes in a Z-pinch for instance.

Thus, it is crucial to look into the MHD compressibility stabilization result in the Regime 3 of collisionality with a model which allows for finite $k_\perp r_{L_i}$. This is the purpose of the Vlasov-Fluid model, which we study in Section 3.10. Before doing so, we finish our study of the models described by eq. (3.45), by looking into the collisionality regime which we called Regime 4.

3.8 CGL energy principle

3.8.1 CGL closure

The collisionality regime which we called Regime 4 is defined by the ordering $1 \ll \omega\tau_{ee} \sim \omega\tau_{ei} \ll \omega\tau_{ii} \ll \omega\tau_{eq} = \omega\tau_{ie}$. In these conditions, neither the electrons nor the ions are collisional. The CGL model [10] is a simple, fluid-like model constructed to describe such a collisionality regime. It takes the limit $\delta_i \to 0$, so that the total plasma pressure is gyrotropic [11]:

$$\mathbf{P} = p_\perp \left(\mathbf{I} - \mathbf{bb}\right) + p_\parallel \mathbf{bb} \tag{3.114}$$

where $\mathbf{P} = \mathbf{P}_i + \mathbf{P}_e$, $p_\perp = p_{i\perp} + p_{e\perp}$, and $p_\parallel = p_{i\parallel} + p_{e\parallel}$. Furthermore, it neglects the heat fluxes and the temperature equilibration term in the second-order moment of the Boltzmann equation for the ions and for the electrons. Adding these two equations, one finds that $p_\perp$ and $p_\parallel$ are linked to lower order moments through simple equations of state:

$$\frac{d}{dt}\left(\frac{p_{\parallel}B^2}{n^3}\right)=0 \qquad \text{and} \qquad \frac{d}{dt}\left(\frac{p_{\perp}}{nB}\right)=0 \tag{3.115}$$

Note that there is no real justification for neglecting the heat fluxes when $\omega\tau_{ii} \gg \omega\tau_{ee} \gg 1$. The CGL model is commonly used nevertheless, since it is the simplest description of a collisionless, anisotropic plasma. In Section 3.9, we will have a better idea of the accuracy of the CGL model by deriving energy relations for the more exact Kinetic MHD model.

3.8.2 CGL static equilibrium

As always in this work, we focus on the same class of equilibria as in ideal MHD, namely static, i.e. $\mathbf{v}_0 = \mathbf{0}$, and isotropic equilibria, so that $\mathbf{P}_{i0} = p_{i0}\mathbf{I}, \mathbf{P}_{e0} = p_{e0}\mathbf{I}$, with $p_0 = p_{i0} + p_{e0}$. With these choices, the non-trivial equilibrium equations in eq. (3.45) take the form:

$$\begin{aligned} &\mathbf{J}_0 \times \mathbf{B}_0 = \nabla p_0 \\ &\nabla \cdot \mathbf{B}_0 = 0 \\ &\nabla \times \mathbf{B}_0 = \mu_0 \mathbf{J}_0 \end{aligned} \tag{3.116}$$

These three equations are indeed exactly identical to those of static ideal MHD.

Recall here that while we study isotropic equilibria, the plasma is not forced to behave in an isotropic manner as the perturbation develops. As emphasized previously, one of the strengths of the CGL model is that it allows the collisionless plasma to have an anisotropic behavior.

3.8.3 CGL stability and energy principle

Introducing the displacement $\boldsymbol{\xi}$ such that $\tilde{\mathbf{v}} = -i\omega\boldsymbol{\xi}$, the linearized CGL momentum equation is:

$$-\omega^2 m_i n\boldsymbol{\xi} = \mathbf{J}\times\tilde{\mathbf{B}} + \tilde{\mathbf{J}}\times\mathbf{B} - \nabla\tilde{p}_\perp - \left(\tilde{p}_\parallel - \tilde{p}_\perp\right)\boldsymbol{\kappa} - \mathbf{bB}\cdot\nabla\left(\frac{\tilde{p}_\parallel - \tilde{p}_\perp}{B}\right) \tag{3.117}$$

where the evolution of $\tilde{p}$ is once again given by the linearized CGL equations of state:

$$\tilde{p}_\parallel = -\boldsymbol{\xi}\cdot\nabla p - p\nabla\cdot\boldsymbol{\xi} - 2p\mathbf{bb}:\nabla\boldsymbol{\xi} \tag{3.118}$$

and

$$\tilde{p}_\perp = -\boldsymbol{\xi}\cdot\nabla p - 2p\nabla\cdot\boldsymbol{\xi} + p\mathbf{bb}:\nabla\boldsymbol{\xi} \tag{3.119}$$

Given the similarity between the CGL equations and the CGL – Fluid MHD equations, the results for the CGL model are readily obtained from Section 3.6 by replacing the ion pressure with the total plasma pressure, and setting the electron terms to zero. Dotting eq. (3.117) with $\boldsymbol{\xi}$, and integrating over the plasma volume, we thus find the variational form

$$\omega^2 = \frac{\delta W_{CGL}(\boldsymbol{\xi}^*,\boldsymbol{\xi})}{K_{MHD}(\boldsymbol{\xi}^*,\boldsymbol{\xi})} \tag{3.120}$$

where $\delta W_{CGL}(\boldsymbol{\xi}^*,\boldsymbol{\xi}) = \delta W_\perp(\boldsymbol{\xi}_\perp^*,\boldsymbol{\xi}_\perp) + \delta W_{cgl}(\boldsymbol{\xi}^*,\boldsymbol{\xi})$ is the potential energy associated with the displacement $\boldsymbol{\xi}$. $\delta W_\perp(\boldsymbol{\xi}_\perp^*,\boldsymbol{\xi}_\perp)$ is exactly identical to the incompressible part of $\delta W_{MHD}(\boldsymbol{\xi}_\perp^*,\boldsymbol{\xi}_\perp)$ defined previously, and $\delta W_{cgl}(\boldsymbol{\xi}^*,\boldsymbol{\xi})$ has the following form:

$$\delta W_{cgl}(\boldsymbol{\xi}_{\perp}^{*},\boldsymbol{\xi}_{\perp}) = \frac{5}{3}\int p\left|\nabla\cdot\boldsymbol{\xi}\right|^{2} d\mathbf{r} + 3\int d\mathbf{r} p\left|\frac{1}{3}\nabla\cdot\boldsymbol{\xi} - \mathbf{bb}:\nabla\boldsymbol{\xi}\right|^{2} \qquad (3.121)$$

The CGL force operator is self-adjoint [3], and using the fact that there is conservation of energy in this model, one can derive an energy principle that is similar to that of ideal MHD:

A system is stable in the CGL model iff $\delta W_{CGL}(\boldsymbol{\xi}^{*},\boldsymbol{\xi}) \geq 0$ *for all allowable displacement* $\boldsymbol{\xi}$.

Now, for the same reasons as the ones already discussed in Section 3.6, it is clear from eq. (3.121) that we have

$$\delta W_{cgl}(\boldsymbol{\xi}^{*},\boldsymbol{\xi}) \geq \delta W_{C}(\boldsymbol{\xi}^{*},\boldsymbol{\xi}) \geq 0 \qquad (3.122)$$

and consequently, for both ergodic and closed-line systems,

$$\text{For all } \boldsymbol{\xi},\ \delta W_{CGL}(\boldsymbol{\xi}^{*},\boldsymbol{\xi}) \geq \delta W_{MHD}(\boldsymbol{\xi}^{*},\boldsymbol{\xi}) \qquad (3.123)$$

Using the CGL energy principle just stated, and the same reasoning as in the previous sections, it is then easy to see that eq. (3.123) implies the following sufficient condition for stability in the CGL model:

In both ergodic and closed-line magnetic geometries, if a plasma is ideal MHD stable, it is CGL stable.

With regards to compressibility, this result shows that collisionless plasmas in the CGL approximation are indeed compressible, and that compressibility is stabilizing.

3.9 Kinetic MHD energy principle

3.9.1 The Kinetic MHD closure

Instead of arbitrarily assuming that the heat fluxes vanish, as it is done in the CGL model, the idea in the Kinetic MHD model is to calculate the ion and electron pressure tensors from the solution of the Vlasov equation in the limit $\delta_i \to 0$ and with strong electric field ($\mathbf{v}_{\mathbf{E}\times\mathbf{B}} \sim \mathbf{v}_{T_i}$). This equation, already presented in Section 3.7 for the ions, is repeated here for convenience: the ion and electron distribution functions, $f_i\left(\mathbf{r},\varepsilon,\mu,t\right)$ and $f_e\left(\mathbf{r},\varepsilon,\mu,t\right)$ are solutions of the equation

$$\frac{\partial f}{\partial t} + (\mathbf{v} + w_{\|}\mathbf{b})\cdot\nabla f + \dot{\bar{\varepsilon}}\frac{\partial f}{\partial \varepsilon} = 0 \tag{3.124}$$

with

$$\dot{\bar{\varepsilon}} = q w_{\|} E_{\|} - m w_{\|}\mathbf{b}\cdot\frac{d\mathbf{v}}{dt} - \frac{m w_{\perp}^2}{2}\nabla\cdot\mathbf{v} + m\left(\frac{w_{\perp}^2}{2} - w_{\|}^2\right)\mathbf{b}\cdot\left(\mathbf{b}\cdot\nabla\right)\mathbf{v} \tag{3.125}$$

and where we have kept the same notations as in Section 3.7. In particular, $\mathbf{w}$ is the random component of particle velocity while $\mathbf{v} = \mathbf{v}(\mathbf{r},t)$ is the macroscopic plasma velocity (which consists of the parallel flow and the $\mathbf{E}\times\mathbf{B}$ drift). The charge q and the mass m in eq. (3.125) obviously depend on whether we solve for the ion or the electron distribution function. The pressure tensors are given by

$$\begin{aligned}
\mathbf{P} &= p_{\perp}\left(\mathbf{I}-\mathbf{bb}\right)+p_{\parallel}\mathbf{bb} \\
p_{\perp} &= \frac{2^{1/2}\pi B}{m^{3/2}}\int \frac{\mu B}{\left(\varepsilon-\mu B\right)^{1/2}} f\, d\varepsilon\, d\mu \\
p_{\parallel} &= \frac{2^{3/2}\pi B}{m^{3/2}}\int \left(\varepsilon-\mu B\right)^{1/2} f\, d\varepsilon\, d\mu
\end{aligned} \tag{3.126}$$

Note once again that the parallel electric field $E_{\parallel}$ appears in eq. (3.125) even though it scales as $E_{\parallel}\sim\delta_i E_{\perp}$. It is calculated from the parallel electron momentum equation

$$E_{\parallel} \equiv -\mathbf{b}\cdot\nabla\phi - \frac{\partial A_{\parallel}}{\partial t} = -\frac{\mathbf{B}\cdot(\nabla\cdot\mathsf{P}_e)}{enB} \tag{3.127}$$

or, when it is more convenient, from the charge neutrality condition $n_i = n_e$, where the densities are calculated from the distribution functions:

$$n = \int f\, d\mathbf{w} = \frac{2^{1/2}\pi B}{m^{3/2}}\int \frac{1}{\left(\varepsilon-\mu B\right)^{1/2}} f\, d\varepsilon\, d\mu \tag{3.128}$$

The set of equations (3.45), (3.124), (3.125), (3.126), (3.127), and (3.128) define what is usually called the Kinetic MHD model [11],[19], or the 'beads on a wire' approximation [20], since it is a kinetic model restricting the motion of the particles to that of beads 'sliding' along the magnetic field lines of force. The first kinetic

comparison theorems [21], [22] were derived using this model, albeit assuming $E_{\|} = 0$. Later works have generalized these comparison theorems, by using the same Kinetic MHD model but allowing for electrostatic perturbations: $\tilde{E}_{\|} = -\mathbf{b} \cdot \nabla \tilde{\phi}$ [20], [23], [16]. As we will see in Section 3.9.3, we generalize all these results one step further, by allowing for electromagnetic perturbations: $\tilde{E}_{\|} = -\mathbf{b} \cdot \nabla \tilde{\phi} + i\omega \tilde{A}_{\|}$.

3.9.2 Kinetic MHD static equilibrium

Consider now equilibrium in the kinetic MHD model. In order to compare macroscopic stability thresholds with those of ideal MHD we choose equilibrium distribution functions that are independent of the adiabatic invariant μ; that is both the electron and ion equilibrium distribution functions are of the form $f_0(\mathbf{r}, \varepsilon, \mu) \rightarrow f_0(\psi, \varepsilon)$ where $\psi(\mathbf{r})$ is the usual flux function satisfying $\mathbf{b} \cdot \nabla \psi = 0$. The equilibrium pressure tensor is then isotropic: $p_{\perp 0}(\psi) = p_{\|0}(\psi) = p_{e,i0}(\psi)$. For static equilibrium (i.e. $\mathbf{v} = 0$) the plasma momentum equation therefore becomes

$$\begin{aligned} \mathbf{J}_0 \times \mathbf{B}_0 &= \nabla p_0 \\ \nabla \cdot \mathbf{B}_0 &= 0 \\ \nabla \times \mathbf{B}_0 &= \mu_0 \mathbf{J}_0 \end{aligned} \tag{3.129}$$

Furthermore, since $E_{\|0} = -\mathbf{B}_0 \cdot (\nabla \cdot \mathsf{P}_{e0}) / en_0 B_0 = -\mathbf{B}_0 \cdot \nabla p_{e0} / en_0 B_0$ it follows that $E_{\|0} = 0$. Similarly for static equilbria $\mathbf{E}_{\perp 0} = 0$, since $\mathbf{v} \times \mathbf{B} = \mathbf{0}$. The conclusion is that the equilibria of interest are identical to those in ideal MHD.

3.9.3 Kinetic MHD energy principle

As in Section 3.7, we leave the details of the derivation of the energy relations to Appendix A, and for the clarity of the presentation just focus on the main results in this section. Some of the results presented here have been originally derived in [16], [20], [21], [22], [23]. We bring two new elements to this well-studied problem: 1) we generalize the derivation of the energy relations by allowing a non-zero value for the perturbed parallel vector potential, $\tilde{A}_{\parallel}$, representing electromagnetic effects; 2) we explicitly distinguish between ergodic and closed-line systems, and identify the differences in stability criteria that arise between these two families.

- <u>*Case 1*</u>: *Ergodic systems or closed line systems undergoing symmetry breaking perturbations*

In this case the energy relation can be written as

$$\left|\omega\right|^2 = -\frac{\delta W_{\perp}(\boldsymbol{\xi}_{\perp}, \boldsymbol{\xi}_{\perp}^*) + \delta W_{kk}(\boldsymbol{\xi}, \boldsymbol{\xi}^*)}{K_{\perp}(\boldsymbol{\xi}_{\perp}, \boldsymbol{\xi}_{\perp}^*)} \tag{3.130}$$

where $\delta W_{\perp}(\boldsymbol{\xi}_{\perp}, \boldsymbol{\xi}_{\perp}^*)$ is identical to that corresponding to ideal MHD and $K_{\perp}(\boldsymbol{\xi}_{\perp}, \boldsymbol{\xi}_{\perp}^*)$ has already been defined in Section 3.7.

The modification to the potential energy δW_{kk} is evaluated for arbitrary equilibrium distribution functions $f(\varepsilon, \psi)$ that need only satisfy the constraint:

$$\frac{\partial f}{\partial \varepsilon} < 0 \tag{3.131}$$

for both species. The result is a complicated expression which has the form

$$\begin{aligned}
\delta W_{kk}(\boldsymbol{\xi},\boldsymbol{\xi}^*) &= \left|\omega\right|^2 \int \frac{d\mathbf{r}}{n}(U_i + U_e + U_h) \\
U_i &= \hat{T}_i\left[\int \frac{\partial f_i}{\partial \varepsilon} d\mathbf{w} \int \frac{\partial f_i}{\partial \varepsilon}\left|\tilde{s}_i\right|^2 d\mathbf{w} - \left|\int \frac{\partial f_i}{\partial \varepsilon}\tilde{s}_i\, d\mathbf{w}\right|^2\right] \\
U_e &= \hat{T}_e\left[\int \frac{\partial f_e}{\partial \varepsilon} d\mathbf{w} \int \frac{\partial f_e}{\partial \varepsilon}\left|\tilde{s}_e\right|^2 d\mathbf{w} - \left|\int \frac{\partial f_e}{\partial \varepsilon}\tilde{s}_e\, d\mathbf{w}\right|^2\right] \\
U_h &= \frac{1}{\left(\hat{T}_i + \hat{T}_e\right)}\left|\hat{T}_i \int \frac{\partial f_i}{\partial \varepsilon}\tilde{s}_i d\mathbf{w} + \hat{T}_e \int \frac{\partial f_e}{\partial \varepsilon}\tilde{s}_e d\mathbf{w}\right|^2
\end{aligned} \tag{3.132}$$

where $\hat{T}(\psi)$ and the orbit integral $\tilde{s}$ for each species are given by

$$\begin{aligned}
\frac{1}{\hat{T}} &= -\frac{1}{n}\int \frac{\partial f}{\partial \varepsilon} d\mathbf{w} > 0 \\
\tilde{s}(\varepsilon,\mu,\mathbf{r},t) &= \int_{-\infty}^{t}\left[\frac{m w_\perp^2}{2}\nabla\cdot\boldsymbol{\xi}_\perp + m\left(\frac{w_\perp^2}{2} - w_\parallel^2\right)\boldsymbol{\xi}_\perp\cdot\boldsymbol{\kappa} + q\left(\tilde{\phi} - w_\parallel\tilde{A}_\parallel\right)\right]e^{-i\omega t'}dt'
\end{aligned} \tag{3.133}$$

Note that unlike the Kinetic – Fluid MHD case, the trajectory integrals do not only involve the plasma displacement $\boldsymbol{\xi}$, but also the unknowns $\tilde{\phi}$ and $\tilde{A}_\parallel$. In fact, these two quantities can be expressed in terms of the plasma displacement $\boldsymbol{\xi}$, although the relations involve a set of coupled integral equations (see Appendix A). Fortunately, these complicated relations are not required for the analysis, as we show next.

A simple application of Schwarz's inequality implies that $\delta W_{kk} \geq 0$. This allows us to draw two conclusions. First, assume that the system is ideal MHD stable:

$$\delta W_{MHD} = \delta W_\perp(\boldsymbol{\xi}^*_{\perp MHD}, \boldsymbol{\xi}_{\perp MHD}) > 0 \tag{3.134}$$

where $\boldsymbol{\xi}_{\perp MHD}$ is the ideal MHD eigenfunction. It immediately follows that

$$\delta W_{KK} \equiv \delta W_{\perp} + \delta W_{kk} \geq \delta W_{\perp}(\boldsymbol{\xi}^{*}_{\perp KK}, \boldsymbol{\xi}_{\perp KK}) \geq \delta W_{\perp}(\boldsymbol{\xi}^{*}_{\perp MHD}, \boldsymbol{\xi}_{\perp MHD}) > 0 \qquad (3.135)$$

Here, $\boldsymbol{\xi}_{\perp KK}$ is the kinetic MHD eigenfunction and the last inequality holds because of the minimizing energy principle associated with the ideal MHD potential energy. Equation (3.135), however, leads to a contradiction in eq. (3.130): $|\omega|^2 < 0$. This is exactly the same contradiction as the one already encountered in Section 3.7, coming from the fact that we assumed $\mathrm{Im}(\omega) > 0$ to derive eq. (3.132) (see Appendix A). The resolution of the problem is that $\mathrm{Im}(\omega) \leq 0$ which implies that the system is linearly stable. We have just proved the following result:

In ergodic systems or closed line systems undergoing symmetry breaking perturbations, if a plasma is ideal MHD stable, it is Kinetic MHD stable.

The second conclusion comes from taking the limit $\omega^2 \to 0$ in eq. (3.132), a limit which as we know [16] corresponds to the marginal stability boundary. Using, as in the Kinetic-Fluid MHD case, the periodicity of the trapped particles' motion in toroidal devices, we can Fourier expand the integrand in the orbit integrals, and evaluate these integrals in the limit $\omega^2 \to 0$. As in Section 3.7, we find that while δW_{kk} vanishes in the limit $\omega^2 \to 0$ in cylindrical systems, it is finite in the same limit in toroidal systems, and given by

$$
\begin{aligned}
\delta W_{kk}(\boldsymbol{\xi},\boldsymbol{\xi}^*) &= \frac{4}{\pi^2}\int \frac{d\mathbf{r}}{n}(U_i + U_e + U_h) \\
U_i &= \hat{T}_i\left[\int \frac{\partial f_i}{\partial \varepsilon} d\mathbf{w} \int_T \frac{\partial f_i}{\partial \varepsilon}\left|\omega_{Bi}\bar{s}_i\right|^2 d\mathbf{w} - \left|\int_T \frac{\partial f_i}{\partial \varepsilon}\omega_{Bi}\bar{s}_i\, d\mathbf{w}\right|^2\right] \\
U_e &= \hat{T}_e\left[\int \frac{\partial f_e}{\partial \varepsilon} d\mathbf{w} \int_T \frac{\partial f_e}{\partial \varepsilon}\left|\omega_{Be}\bar{s}_e\right|^2 d\mathbf{w} - \left|\int_T \frac{\partial f_e}{\partial \varepsilon}\omega_{Be}\bar{s}_e\, d\mathbf{w}\right|^2\right] \\
U_h &= \frac{1}{\left(\hat{T}_i + \hat{T}_e\right)}\left|\hat{T}_i\int_T \frac{\partial f_i}{\partial \varepsilon}\omega_{Bi}\bar{s}_i\, d\mathbf{w} + \hat{T}_e\int_T \frac{\partial f_e}{\partial \varepsilon}\omega_{Be}\bar{s}_e\, d\mathbf{w}\right|^2
\end{aligned}
\tag{3.136}
$$

where the subscript T on the integrals denotes integration over the region of velocity space corresponding to trapped particles.

Thus, the second conclusion is that a toroidal Kinetic MHD system is positively stable when the ideal MHD system is marginally stable. This behavior corresponds to trapped particle compressibility stabilization ([24, [25]), an effect obviously not present in a straight cylinder. The results for ergodic Kinetic MHD systems at $\omega^2 = 0$ can be conveniently summarized as follows.

$$
\begin{aligned}
&\delta W_{KK} = \delta W_{\perp} = \delta W_{MHD} && \text{straight cylinder} \\
&\delta W_{KK} = \delta W_{\perp} + \delta W_{kk} > \delta W_{MHD} && \text{torus}
\end{aligned}
\tag{3.137}
$$

- *Case 2 : Closed field lines systems, and modes which conserve the closed-line symmetry*

Here, we need to compare δW_{kk} with δW_C, the compressible piece of δW_{MHD}. Even though eq. (3.132) is valid for closed field lines systems and modes which conserve the

closed-line symmetry, the form of δW_{kk} in this equation is not directly useful for comparing it to δW_C. Indeed, knowing the sign of δW_{kk} is not sufficient, and we now need a quantitative estimate for δW_{kk}. The calculation of this estimate can be done analytically only in the limit $\omega^2 \to 0$. It consists of several complicated steps, and the details of the derivation are left to Appendix A. The end result is an inequality expression for δW_{KK}, valid in the limit of marginal stability $\omega^2 \to 0$.

$$\delta W_{KK} = \delta W_{\perp}(\boldsymbol{\xi}_{\perp}, \boldsymbol{\xi}_{\perp}^*) + \delta W_{kk}(\boldsymbol{\xi}, \boldsymbol{\xi}^*) \tag{3.138}$$

with

$$\delta W_{kk} \geq \int \frac{5}{3} p \left| \left\langle \nabla \cdot \boldsymbol{\xi}_{\perp} \right\rangle \right|^2 d\mathbf{r} \tag{3.139}$$

For a system that is ideal MHD stable, $\delta W_{MHD} = \delta W_{\perp} + \delta W_C > 0$. It then follows from eqs. (3.138) and (3.139) that

$$\delta W_{KK} \equiv \delta W_{\perp} + \delta W_{kk} \geq \delta W_{MHD}(\boldsymbol{\xi}_{\perp KK}^*, \boldsymbol{\xi}_{\perp KK}) \geq \delta W_{MHD}(\boldsymbol{\xi}_{\perp MHD}^*, \boldsymbol{\xi}_{\perp MHD}) > 0 \tag{3.140}$$

This proves the following statement about Kinetic MHD linear stability in closed line systems:

In closed-line magnetic geometries, if modes which conserve the closed-line symmetry are ideal MHD stable, they are Kinetic MHD stable.

From this result, we conclude that there is indeed plasma compressibility stabilization in the Kinetic MHD model. In fact, eq. (3.139) indicates that Kinetic MHD predicts additional sources of compressibility as compared to ideal MHD.

As in the Kinetic – Fluid MHD model, the plasma compressibility stabilization is due to the exact periodicity of the particles' motion in closed-line systems. This is only true in the 'beads on a wire' description of the motion. Only the parallel motion is accounted for. One then naturally wonders what would happen to the compressibility stabilization prediction if finite $k_\perp$ terms were kept, so that the particles are allowed to drift off their flux tubes.

Unfortunately, we have not found a model in which both ions and electrons could be described by a kinetic equation which allows for finite $k_\perp$, and which would allow us to derive MHD comparison theorems. The main difficulty comes from the fact that in such a model, neither the ions nor the electrons are tied to the magnetic field lines. It then becomes difficult to define what one means by an MHD mode. Thus, our only way to study the effects on MHD stability of particle drifts off flux tubes is through a hybrid model, with ions described by the exact Vlasov equation, and electrons described as a fluid. This is the purpose of the next section.

3.10 Energy relations for comparison theorems: Vlasov ions, fluid electrons

The last model of interest is a hybrid model with Vlasov ions and fluid electrons. The motivation for using the Vlasov equation for the ions is to allow us to consider stability for arbitrary $k_\perp$ including both $k_\perp a \sim 1$ and $k_\perp r_{L_i} \sim 1$. The regime $k_\perp r_{L_i} \sim 1$ is important for closed line systems such as the levitated dipole and the field reversed configuration as well as ballooning modes in ergodic systems. The crucial feature included in the Vlasov, but not the kinetic MHD, description is the possibility of particle resonances with the perpendicular guiding center velocity as well as the parallel velocity. Specifically the resonance condition changes from $\omega - k_\| w_\| = 0$ to $\omega - k_\| w_\| - \mathbf{k}_\perp \cdot \mathbf{v}_d = 0$ where $\mathbf{v}_d$ includes the $\mathbf{E}\times\mathbf{B}$, curvature, and grad-B guiding center drifts.

Ideally we would like to be able to treat the electrons with the Vlasov equation but this becomes too complicated mathematically. The basic difficulty is that a dual Vlasov model contains far more physics than just MHD behavior. Thus some simplifications are needed to restrict the physical content of the overall model such that attention can be focused on MHD phenomena. A fluid model for electrons meets this purpose. It is also possible to treat the electrons as collisionless by using the simpler kinetic MHD description. This, however, is deceptive and corresponds to an

inconsistent mathematical ordering. The reason is that even in the limit $m_e \to 0$ the perpendicular guiding center drifts of the electrons (for $T_e \sim T_i$) are important when $k_\parallel \approx 0$ and $k_\perp r_{L_i} \sim 1$.

In carrying out the analysis there are three issues that arise that are worth noting. First, a simplified energy equation must be used for the electrons in order to focus on MHD modes which are defined as modes in which the magnetic field is frozen into the plasma. Second, a special choice must be made for the form of the equilibrium ion distribution function in order to guarantee zero macroscopic fluid velocity, corresponding to static equilibrium. This choice also has the feature of making the analysis valid for arbitrary 3-D geometries. Third, the analysis is carried out using a procedure which is traditionally and wisely thought to be highly inefficient and mathematically complex when applied to models that make use of a gyro radius expansion (e.g. gyrokinetics [26],[27] and kinetic MHD). The "forbidden" approach that we use directly calculates the perpendicular ion current from the distribution function rather than using moments. There is no problem doing this with the Vlasov equation since no gyro radius expansion is used and, as is shown, leads to a simplified analysis if attention is focused solely on obtaining an energy integral. Each of these points is discussed in more detail as the analysis progresses.

3.10.1 The electron model

The electrons are treated as a massless isotropic fluid. The mass and momentum equations are written as follows:

$$\begin{aligned} &\frac{\partial n_e}{\partial t} + \nabla \cdot \left(n_e \mathbf{v}_e \right) = 0 \\ &\mathbf{E} + \mathbf{v}_e \times \mathbf{B} + \frac{\nabla p_e}{e n_e} = 0 \end{aligned} \tag{3.141}$$

where $\mathbf{v}_e$ is the electron fluid velocity, and where we have neglected all the terms due to friction in the momentum equation. While the set of equations (3.141) is the same as in the Kinetic MHD-Fluid model, the electron energy equations has to be changed. This can be seen by substituting the momentum equation into Faraday's law.

$$\frac{\partial \mathbf{B}}{\partial t} = \nabla \times \left(\mathbf{v}_e \times \mathbf{B} + \frac{\nabla p_e}{e n_e} \right) \tag{3.142}$$

In order to focus on MHD modes, we require by definition, that the magnetic field be frozen into the plasma. This requires that the $\nabla \times (\nabla p_e / e n_e)$ term be zero or small. However, when $k_\perp r_{L_i} \sim 1$, the term is comparable in magnitude to the other terms. We could assume an intermediate ordering such as $k_\perp r_{L_i} \ll 1 \ll k_\perp L$ but this leaves us in the awkward position of making a gyro radius expansion in Faraday's law but not the ion Vlasov equation.

Our approach is to postulate an alternative energy equation which must have three desirable properties: (1) it must be mathematically simple, (2) it must include

electron plasma compressibility effects, and (3) it must guarantee that the magnetic field is tied to the electron fluid. A model which has these features is as follows.

$$p_e = K n_e^{\gamma_e} \tag{3.143}$$

Our model looks very similar to the usual adiabatic energy relation but there is one important difference. In our model both the equilibrium and perturbed pressure satisfy the same relation. In the usual adiabatic relation, $d(p_e / n_e^{\gamma_e})/dt = 0$ the equilibrium pressure and density profiles are independent of each other and it is only the perturbations that are non-trivially governed by eq. (3.143). Thus, our model is a special case of the more general adiabatic relation. The main consequence of eq. (3.143) is that in the stability analysis only the pressure gradient can drive instabilities. In contrast, for the general adiabatic relation the parameter $\eta_e = d\ln T_e / d\ln n_e$ also appears which can drive instabilities such as the entropy mode. Specifically, when $\gamma_e = 5/3$, our model implies that $\eta_e = 2/3$ and for this value the entropy mode is always stable, as shown in cylindrical and point-dipole magnetic geometries in references [28], and [29]. Thus, choosing eq. (3.143) as the energy relation for electrons allows us to focus on MHD modes, which is the topic of interest.

3.10.2 The Vlasov-Fluid model

The basic equations describing the Vlasov-Fluid model are obtained by evaluating the quantity $\mathbf{J}\times\mathbf{B}$ with the electron current calculated from $\mathbf{v}_e$ and the ion current

by the usually inefficient process of integrating over the distribution function. A short calculation leads to the following model.

$$
\begin{aligned}
&\mathbf{J}\times\mathbf{B} = \nabla p_e + e\int\left(\mathbf{E}+\mathbf{u}\times\mathbf{B}\right)f_i\,d\mathbf{u}\\
&\frac{\partial f_i}{\partial t} + \mathbf{u}\cdot\nabla f_i + \frac{e}{m_i}\left(\mathbf{E}+\mathbf{u}\times\mathbf{B}\right)\cdot\nabla_u f_i = 0\\
&\frac{\partial n_e}{\partial t} + \nabla\cdot(n_e\mathbf{v_e}) = 0\\
&p_e = Kn_e^{\gamma_e}\\
&\frac{\partial\mathbf{B}}{\partial t} = \nabla\times(\mathbf{v_e}\times\mathbf{B})\\
&\nabla\times\mathbf{B} = \mu_0\mathbf{J}\\
&\nabla\cdot\mathbf{B} = 0\\
&E_{\|} = -(\mathbf{b}\cdot\nabla p_e)/en\\
&n_i = n_e \equiv n
\end{aligned}
\tag{3.144}
$$

Here, $\mathbf{u}$ represents the total (not random) particle velocity.

3.10.3 Vlasov-Fluid Equilibrium

An exact analytic equilibrium satisfying the Vlasov-Fluid equations can be found that is valid for arbitrary 3-D geometries. The key point to recognize is that our primary interest is in *static* equilibria. The motivation for focusing on static equilibria is to enable a mathematically consistent comparison with static ideal MHD equilibria which is the usual "gold" standard for macroscopic stability analyses. We emphasize that equilibria with flow are possible and often necessary when comparing with detailed experimental data. However, when comparing with other theoretical models it is necessary to focus on the identical class of equilibria - those that have zero equilibrium flow.

The condition of identically zero macroscopic equilibrium flow implies that the equilibrium ion distribution function be of the form

$$\begin{aligned} f_{i0} &= f(\varepsilon) \\ \varepsilon &= \frac{m_i u^2}{2} + e\phi(\mathbf{r}) \end{aligned} \tag{3.145}$$

where $\phi(\mathbf{r})$ is the electrostatic potential. From eq. (3.145) it follows that the ions are electrostatically confined and that the ion pressure is isotropic. A short calculation also shows that the pressure and density are related by

$$\begin{aligned} p_{i0}(\phi) &= \int \frac{m_i u^2}{3} f_{i0}\, d\mathbf{u} \\ n_{i0}(\phi) &= -\frac{1}{e}\frac{dp_{i0}}{d\phi} \end{aligned} \tag{3.146}$$

Now, since there is no equilibrium ion flow,

$$\mathbf{J}_0 \times \mathbf{B}_0 = \nabla p_{e0} + e n_0 \mathbf{E}_0 = \nabla p_{e0} - e n_0 \nabla \phi_0 \tag{3.147}$$

Here, we have set $n_{e0} = n_{i0} \equiv n_0$. Substituting eq. (3.146) into eq. (3.147) then yields

$$\mathbf{J}_0 \times \mathbf{B}_0 = \nabla p_0 \tag{3.148}$$

where $p_0 = p_{e0} + p_{i0}$.

Moreover, since $p_{e0} = K n_0^{\gamma} = K[n_0(\phi_0)]^{\gamma}$, the total pressure also has the form $p_0 = p_0(\phi)$. The condition $\mathbf{B}_0 \cdot \nabla p_0 = (dp_0 / d\phi_0)\mathbf{B}_0 \cdot \nabla \phi_0 = -(dp_0 / d\phi_0)\mathbf{B}_0 \cdot \mathbf{E}_0 = 0$ then implies that $E_{\|0} = 0$ in equilibrium. The overall conclusion is that the choice $f_i = f_0(\varepsilon)$ leads to Vlasov-Fluid equilibria that are identical to ideal MHD equilibria.

3.10.4 Vlasov-Fluid Stability

Linear stability in the Vlasov-Fluid model is carried out in terms of the electron displacement vector $\boldsymbol{\xi}$. The relationship between $\tilde{\mathbf{v}}_e$ and $\boldsymbol{\xi}$ in a system in which there is an equilibrium flow $\mathbf{v}_{e0}$ is given by $\tilde{\mathbf{v}}_e = -i\omega\boldsymbol{\xi} + \mathbf{v}_{e0}\cdot\nabla\boldsymbol{\xi} - \boldsymbol{\xi}\cdot\nabla\mathbf{v}_{e0}$ [30]. Using this definition it follows that most of the perturbed quantities can be easily expressed in terms of $\boldsymbol{\xi}$.

$$\begin{aligned}
\tilde{n}_e &= -\boldsymbol{\xi}_\perp\cdot\nabla n - n\nabla\cdot\boldsymbol{\xi} \\
\tilde{p}_e &= -\boldsymbol{\xi}_\perp\cdot\nabla p_e - \gamma_e p_e\nabla\cdot\boldsymbol{\xi} \\
\tilde{\mathbf{B}} &= \nabla\times\left(\boldsymbol{\xi}_\perp\times\mathbf{B}\right) \\
\tilde{\mathbf{E}} &= i\omega\boldsymbol{\xi}_\perp\times\mathbf{B} - \nabla\left[\left(\boldsymbol{\xi}_\perp\cdot\nabla p_i - \gamma_e p_e\nabla\cdot\boldsymbol{\xi}\right)/en\right]
\end{aligned} \tag{3.149}$$

The remaining unknown is the perturbed distribution function which, as shown in Appendix C, can be written as

$$\begin{aligned}
\tilde{f}_i &= \left[\frac{1}{n}\left(\boldsymbol{\xi}_\perp\cdot\nabla p_i - \gamma_e p_e\nabla\cdot\boldsymbol{\xi}\right) + i\omega\tilde{s}\right]\frac{\partial f_i}{\partial\varepsilon} \\
\tilde{s} &= \int_{-\infty}^{t}\left[e(\mathbf{E}+\mathbf{u}\times\mathbf{B})\cdot\boldsymbol{\xi}_\perp - (\gamma_e p_e/n)\nabla\cdot\boldsymbol{\xi}\right]dt'
\end{aligned} \tag{3.150}$$

where $p = p_i + p_e$.

As for the other models, an energy integral can be obtained for the Vlasov-Fluid model. The details are presented in Appendix C. A critical point regarding this energy integral is that unlike for the other models, there is no need to distinguish between ergodic and closed field line geometries for the VF equilibria, which assume that the ion equilibrium distribution function only depends on the total energy. The reason is that the orbit integral $\tilde{s}$ does not have any terms that are proportional to

$1/\omega$. It is the $1/\omega$ terms in $\tilde{s}$ that yield a finite contribution in the product $i\omega\tilde{s}$, giving rise to trapped particle compressibility stabilization and closed line periodicity stabilization.

The $1/\omega$ terms are absent because the resonant denominator arising from the trajectory integral is modified from its kinetic MHD form $\omega - k_{\|}w_{\|}$ to its Vlasov-Fluid form $\omega - k_{\|}w_{\|} - \mathbf{k}_{\perp}\cdot\mathbf{v}_{d}$ where $\mathbf{v}_{d}$ is the guiding center drift velocity comprised of the grad-B, curvature, and $\mathbf{E}\times\mathbf{B}$ drifts. Thus, even when $k_{\|}=0$ the resonant denominator in the Vlasov-Fluid model does not vanish as $\omega\to 0$ because there is always a non-zero precession drift.

This behavior can be seen explicitly by examining the Vlasov-Fluid energy integral

$$\left|\omega\right|^{2} = -\frac{\delta W_{\perp}}{K_{VF}} \tag{3.151}$$

where

$$\begin{aligned} K_{VF} &= \int d\mathbf{r}\frac{\hat{T}_{i}}{n}\left(V_{1}+V_{2}\right) \\ V_{1} &= \int\frac{\partial f_{i}}{\partial\varepsilon}d\mathbf{w}\int\frac{\partial f_{i}}{\partial\varepsilon}\left|\tilde{s}\right|^{2}d\mathbf{w} - \left|\int\frac{\partial f_{i}}{\partial\varepsilon}\tilde{s}\,d\mathbf{w}\right|^{2} \\ V_{2} &= \frac{\gamma_{i}p_{i}}{\gamma_{i}p_{i}+\gamma_{e}p_{e}}\left|\int\frac{\partial f_{i}}{\partial\varepsilon}\tilde{s}\,d\mathbf{w}\right|^{2} \end{aligned} \tag{3.152}$$

and $\gamma_{e,i}(\psi) = d\ln p_{e,i}/d\ln n$. Clearly, $K_{VF}>0$ by Schwarz's inequality.

A sufficient condition for instability can now easily be obtained. Assume the plasma, for any type of geometry, is ideal MHD stable for incompressible displacements: $\delta W_\perp \geq 0$. Then, eq. (3.151) is a contradiction, similar to that derived for the other models, which can only be resolved by recognizing that the original assumption $\mathrm{Im}(\omega) > 0$ is violated. In other words the system is linearly stable. This conclusion makes use of the fact that K_{VF} remains finite as $\omega \to 0$. Therefore, incompressible stability in ideal MHD implies stability in the Vlasov-Fluid model for any type of geometry.

Consider next unstable behavior corresponding to $\delta W_\perp < 0$ for ideal MHD. Since the Vlasov-Fluid operator is not self-adjoint it is not possible to rigorously conclude that the plasma is also unstable in this model. However, there is strong motivation to conjecture that this is indeed the case. The reason is that the ideal MHD incompressible eigenfunction at marginal stability is also an exact eigenfunction of the Vlasov-Fluid model. Then, once any plasma parameter, for example β, is changed, the presence of resonant particles strongly suggests that the resulting eigenvalue will be complex. Changing β in the appropriate direction (presumably by increasing it) should then produce a positive growth rate. Assuming the conjecture to be correct, then the stability results as $\omega^2 \to 0$ can be summarized as follows

$$\begin{aligned} \delta W_{VF} &= \delta W_\perp(\boldsymbol{\xi}^*_{\perp MHD}, \boldsymbol{\xi}_{\perp MHD}) = \delta W_{MHD}(\boldsymbol{\xi}^*_{\perp MHD}, \boldsymbol{\xi}_{\perp MHD}) \qquad \text{ergodic systems} \\ \delta W_{VF} &\equiv \delta W_\perp(\boldsymbol{\xi}^*_{\perp MHD}, \boldsymbol{\xi}_{\perp MHD}) \leq \delta W_{MHD}(\boldsymbol{\xi}^*_{\perp MHD}, \boldsymbol{\xi}_{\perp MHD}) \qquad \text{closed line systems} \end{aligned} \tag{3.153}$$

In other words, the Vlasov-Fluid model, which applies to equilibria for which the equilibrium ion distribution function only depends on the total energy, does not exhibit any form of compressibility stabilization. The absence of compressibility stabilization is likely to be more important for closed line configurations such as the levitated dipole and the field reversed configuration which depend on this effect for good plasma performance. For these geometries, our Vlasov-Fluid results motivate further investigations in two different areas. First, it would be interesting to see if the absence of compressibility stabilization for MHD modes persists for more general equilibria than the ones allowed in the VF model, in particular equilibria in which the ions are magnetically confined, instead of electrostatically confined. Second, we point out that the nonlinear effects may be very important since modifications to the distribution function may lead to stabilization without the severe consequences usually associated with ideal MHD. Even if so, it is still very worthwhile to understand the predictions of linear stability as is contained in each of the models under consideration.

3.11 Summary

We have derived a series of MHD stability comparison theorems corresponding to different plasma physics models, varying from collisional to collisionless in their physical content. Some of the results are generalizations and clarifications of existing results. Other results involve the introduction of new models and the derivation of

new comparison theorems. In general we have shown that it is necessary to distinguish between ergodic systems and closed line systems. Also, cylindrical systems must sometimes be distinguished from toroidal systems.

Below, we summarize in the form of four tables the results of our analysis. Specifically, we present the comparison results for each energy relation valid in the marginal stability limit $\omega^2 \to 0$. The first two tables correspond to ergodic systems including closed line systems undergoing symmetry breaking perturbations, first for models with fluid electrons, and then for models with kinetic electrons (except, of course, for ideal MHD). The last two tables correspond to closed line systems undergoing perturbations that maintain the closed line symmetry, once again first for fluid electrons, and then for kinetic electrons (except for ideal MHD). In all tables the entries are arranged in ascending order with the most conservative model appearing first. The comparisons for ergodic systems are made against the reference model corresponding to the ideal MHD potential energy for incompressible displacements $\delta W_\perp$. For closed line systems the comparisons are made with respect to the compressible ideal MHD potential energy $\delta W_{MHD} = \delta W_\perp + \delta W_C$. Note that the comparisons between the CGL model and the Kinetic MHD model (and between the CGL-Fluid MHD and Kinetic-Fluid MHD models) are not derived in this chapter, but can be found in reference [22].

Model	Comparison Theorem
Ideal MHD	$\delta W_{MHD} = \delta W_{\perp}$
Vlasov-Fluid	$\delta W_{VF} = \delta W_{\perp}$
Two-Temperature MHD	$\delta W_{TT} = \delta W_{\perp}$
Kinetic -Fluid MHD	$\delta W_{KF} = \delta W_{\perp}$ cylindrical $\delta W_{KF} > \delta W_{\perp}$ toroidal
CGL-Fluid MHD	$\delta W_{CF} > \delta W_{KF} \geq \delta W_{\perp}$

Table 3.1. Summary of comparison theorems for ergodic systems and for models with fluid electrons.

Model	Comparison Theorem
Ideal MHD	$\delta W_{MHD} = \delta W_{\perp}$
Kinetic MHD	$\delta W_{KK} = \delta W_{\perp}$ cylindrical $\delta W_{KK} > \delta W_{\perp}$ toroidal
CGL	$\delta W_{CGL} > \delta W_{KK} \geq \delta W_{\perp}$

Table 3.2. Summary of comparison theorems for ergodic systems and for models with kinetic electrons (except for ideal MHD).

Model	Comparison Theorem
Vlasov-Fluid	$\delta W_{VF} = \delta W_{\perp}$
Ideal MHD	$\delta W_{MHD} = \delta W_{\perp} + \delta W_{C}$
Two Temperature MHD	$\delta W_{TT} = \delta W_{MHD} + \delta W_{C}$
Kinetic – Fluid MHD	$\delta W_{KF} > \delta W_{MHD}$ cylindrical $\delta W_{KF} > \delta W_{MHD}$ toroidal
CGL-Fluid MHD	$\delta W_{CF} > \delta W_{KF} > \delta W_{MHD} > \delta W_{VF}$

Table 3.3. Summary of comparison theorems for closed line systems and for models with fluid electrons

Model	Comparison Theorem
Ideal MHD	$\delta W_{MHD} = \delta W_{\perp} + \delta W_{C}$
Kinetic MHD	$\delta W_{KK} > \delta W_{MHD}$ cylindrical $\delta W_{KK} > \delta W_{MHD}$ toroidal
CGL	$\delta W_{CGL} > \delta W_{KK} > \delta W_{MHD}$

Table 3.4. Summary of comparison theorems for closed line systems and for models with kinetic electrons (except for ideal MHD).

The overall conclusions are as follows. For ergodic systems stability boundaries are accurately predicted by the ideal MHD energy principle for incompressible displacements: $\delta W_{\perp} = 0$. The trapped particle compressibility stabilization arising in the kinetic MHD model may be an artifact since the more accurate (in terms of gyro

radius approximations) Vlasov-Fluid model also predicts marginal stability when $\delta W_{\perp} = 0$.

For closed line systems, however, the usual statement that ideal MHD represents the most conservative stability estimate even in collisionless plasmas does not hold in every situation. While the statement is true for any equilibrium in the Kinetic MHD models, it is incorrect in the Vlasov-Fluid model, which allows finite $k_{\perp} r_{L_i}$, and assumes that the ions are electrostatically confined in equilibrium. In this model resonant particles moving with the perpendicular precession drift velocity eliminate all compressibility stabilization effects so that the stability boundary is again given by $\delta W_{\perp} = 0$.

The results presented here may be more important for closed line configurations such as the levitated dipole and the field reversed configuration where compressibility stabilization plays an important role in predicted plasma performance. Even so, it is important to recognize the limitations of the VF result and of its experimental relevance. First, in plasma equilibria of fusion interest, the ions are typically magnetically confined, and not electrostatically confined as they are in VF equilibria. Second, the comparisons theorems only apply to linear stability and the nonlinear MHD behavior may not be catastrophic, particularly for modes driven by a small class of resonant particles. These limitations should motivate further theoretical studies in closed field line systems, with kinetic models allowing more general

equilibria. If the vanishing of compressibility stabilization is confirmed in these studies, it will be very interesting to look at the nonlinear behavior of the instability responsible for the absence of plasma compressibility, in order to determine its experimentally observable characteristics, and understand if it can lead to a major loss of plasma confinement, as incompressible MHD instabilities tend to do in ergodic systems.

Chapter 3 – References

[1] D. Biskamp, *Nonlinear Magnetohydrodynamics*, Cambridge Monographs on Plasma Physics, Cambridge University Press, 1993

[2] H. Goedbloed and S. Poedts, *Principles of Magnetohydrodynamics with Applications to Laboratory and Astrophysical Plasmas*, Cambridge University Press, 2004

[3] I.B. Bernstein, E.A. Frieman, M.D. Kruskal and R.M. Kulsrud, *Proc. Roy. Soc. (London)* **A244** (1958) pp. 17-40

[4] J.P. Freidberg, *Ideal Magnetohydrodynamics*, (Plenum, New York, 1987)

[5] K. Hain, R. Lüst, and A. Schlüter, *Z. Naturforsch.* **12a** (1957), pp. 833-941

[6] G. Laval, C. Mercier, and R.M. Pellat, *Nucl. Fusion* **5** (1965), pp. 156-158

[7] B.R. Suydam, *Proceedings of the Second United Nations International Conference on the Peaceful Uses of Atomic Energy*, United Nations, Geneva, Vol. 31, p.157

[8] J.P. Freidberg, *Plasma Physics and Fusion Energy*, Cambridge University Press (2007)

[9] J. Kesner, L. Bromberg, M.E. Mauel, and D. Garnier, Proceedings of the Seventeenth International Conference on Plasma Physics and Controlled Fusion Research, Yokahama, Japan, 1998 (IAEA, Vienna, 1999)

[10] G.F. Chew, M.L. Goldberger, and F.E. Low, *Proc. R. Soc. Lond. A* **236** (1956) pp. 112-118

[11] R.D. Hazeltine and F.L. Waelbroeck, *The Framework of Plasma Physics*, (Perseus Books, Reading, MA, 1998)

[12] J.P. Freidberg, *Phys. Fluids*, **15**, 1102 (1972)

[13] S.I. Braginskii, *Reviews of Plasma Physics*, edited by M. A. Leontovich (Consultants Bureau, New York, 1965), Vol. 1, p.205

[14] L. Spitzer, Jr., *Physics of Fully Ionized Gases*, Interscience, New York, 1962

[15] R. D. Hazeltine, Plasma Phys. **15**, 77 (1973)

[16] T.M. Antonsen, Jr. and Y.C. Lee, *Phys. Fluids* **25**, 142 (1982)

[17] T.M. Antonsen, Jr, *Proc. of International School of Plasma Physics*, Piero Caldirola, 1987

[18] A.B. Mikhailovskii, *Instabilities in a Confined Plasma* (IOP, Bristol, 1998)

[19] R.D. Hazeltine and J.D. Meiss, *Plasma Confinement*, Addison-Wesley, Redwood City, CA, 1992

[20] H. Grad, *Phys. Fluids*, **9**, 225 (1966)

[21] M.D. Kruskal and C. R. Oberman, *Phys. Fluids*, **1**, 275 (1958)

[22] M.N. Rosenbluth and N. Rostoker, *Phys. Fluids*, **2**, 23 (1959)

[23] R. Kulsrud, in *Proceedings of the International School of Physics "Enrico Fermi": Advanced Plasma Theory*, edited by M. Rosenbluth (Academic, New York, 1964)

[24] J. W. Connor and R. J. Hastie, *Phys. Rev. Lett.*, **33**, 202 (1974).

[25] F. Porcelli and M. N. Rosenbluth, *Plasma Phys. Control. Fusion*, **40** (1998), pp. 481-492

[26] P.H. Rutherford and E.A. Frieman, *Physics Fluids* **11**, 569 (1968)

[27] P.J. Catto, *Plasma Phys.* **20** 719 (1978)

[28] A.N. Simakov, P.J. Catto, and R.J. Hastie, *Physics of Plasmas* **8** 4414 (2001)

[29] A.N.Simakov, R.J. Hastie, and P.J. Catto, *Physics of Plasmas* **9** 201 (2002)

[30] E. Frieman and M. Rotenberg, *Rev. Modern Physics* **32**, 898 (1960)

Chapter 4

The vanishing of MHD compressibility stabilization: illustration in the hard-core Z-pinch

The energy relation (3.151) derived for the Vlasov-fluid (VF) model in Chapter 3 suggests that in plasmas with electrostatically confined collisionless ions, MHD compressibility stabilization vanishes in closed field line magnetic configurations. Eq. (3.151) cannot be considered as a rigorous proof, however, since the VF force operator is not self-adjoint, and we are not able to prove that marginal stability in the VF model implies $\omega^2 = 0$.

The purpose of Chapter 4 is to give a rigorous proof of the vanishing of compressibility stabilization in a specific magnetic geometry: the hardcore Z-pinch. Using the VF equations, we derive the eigenvalue differential equation for the $m = 0$ interchange mode, which is the compressible mode in ideal MHD. We will show that this eigenvalue equation is very similar to the equivalent one in ideal MHD, and the role of the resonant particles, which are absent in ideal MHD, appears clearly. Solving this eigenvalue equation, we determine the VF stability boundaries for this

particular geometry, compare them to the ideal MHD stability boundaries, and draw new conclusions about MHD plasma compressibility.

There are two reasons why we choose to study the hard-core Z-pinch in particular. First, the Z-pinch is perhaps the simplest closed field line magnetic geometry one can think of. The equilibrium quantities only depend on the radial variable, making the problem 1-D. This makes the comparison with the ideal MHD results particularly easy.

The second reason is that the hard-core Z-pinch can be considered to be a large aspect ratio approximation to the Levitated Dipole Experiment (LDX), an innovative plasma confinement experiment jointly undertaken by the Massachusetts Institute of Technology and Columbia University [1]. A large body of theoretical studies (e.g. [2], [3], [4], [5], [6]) have successfully used the Z-pinch approximation to improve our understanding of the levitated dipole. In fact, recent gyrokinetic simulations [7] have shown that the transport properties of the plasma are both qualitatively and quantitatively similar in a hard-core Z-pinch and ring-dipole geometry, suggesting that the physics is very similar in both configurations. This is what one would intuitively expect, since in a dipole, the trapped particles do not have banana orbits, and do not have large departures from their flux surfaces, unlike in tokamaks for instance.

The structure of this chapter is as follows. In Section 4.1 we briefly present LDX, and introduce the hard-core Z-pinch as its large aspect ratio approximation. In the next section (Section 4.2), we focus on the mode of interest in the Z-pinch, the only compressible mode in this geometry: the $m = 0$ interchange mode. We look into the ideal MHD eigenvalue equation for this mode, and use this differential equation to determine the stability picture of the mode in the ideal MHD model. In the last section (Section 4.3), we derive the eigenvalue equation for that same mode in the VF model, and solve it. Comparing the VF and the ideal MHD results, we are able to understand the role of the resonant ions on plasma compressibility (or on the absence it).

4.1 LDX and the hard-core Z-pinch

4.1.1 The Levitated Dipole experiment (LDX)

The motivation behind the Levitated Dipole experiment is the discovery, starting in 1958 with the Van Allen radiation belts around the earth, of well-confined plasmas within the magnetospheres of planets and other astrophysical objects. Inspired by these observations, Akira Hasegawa suggested, in 1987, the idea of a dipole fusion reactor, where the dipolar magnetic field would be produced by a single, levitated current ring [8]. The design of the LDX is remarkably close to Hasegawa's concept. The goal of the machine is to demonstrated the feasibility of the

confinement of a stable, long-lasting plasma in a dipole field in a laboratory size experiment.

The construction of the experiment was completed in 2004, and the first plasma obtained in August of that year [9]. For these first plasma experiments, the central current ring was not levitated, but supported. This is not a desirable situation from a fusion perspective. Indeed, when the plasma particles hit the supports, they deposit their energy onto them, which heats them, and more importantly, cools the plasma down. The first levitated experiments took place in the fall 2007, and several successful experimental campaigns have been conducted since then [10]. When the central coil is levitated, the LDX configuration is as shown in Fig. 4.1.

What are the possible advantages of a dipole configuration as compared to a tokamak? The most fundamental and least controversial ones are related to the toroidal current.

In tokamaks, the toroidal current has to be driven in the plasma. Since the available methods for external non-inductive (i.e. steady-state) current drive are not very efficient when converting power to current, one would like to rely as much as possible on the naturally occurring transport driven current known as the 'bootstrap current'. In principle, this current can indeed represent a very large fraction of the total toroidal current in the plasma. However, the amount of bootstrap current is highly dependent on the details of the pressure profile, and unfortunately, to achieve a large enough fraction of bootstrap current for a favorable power balance for the

tokamak as a fusion reactor, the required plasma pressure is such that MHD stability limits are crossed if the wall surrounding the plasma is not perfectly conducting but instead has a finite resistivity (as realistic walls do). These MHD instabilities which are stabilized by a perfectly conducting wall surrounding the plasma but unstable for resistive walls are known as resistive wall modes [11]. Their growth times tend to be long (typically of the order of a few milliseconds), and on these slow time scales, feedback stabilization may be possible [12]. Thus, ultimately, in a tokamak, achieving steady-state operation with a favorable power balance involves the demonstration of the feasibility of accurate profile control (for instance to optimize the bootstrap fraction) and feedback stabilization. This remains to be done experimentally, and raises physics issues which have not been fully understood yet, either theoretically or experimentally. It certainly adds to the physics complexity of the tokamak concept. In LDX, there is no such problem. The experiment is inherently steady-state, since the magnetic field is due to the superconducting floating coil. Of course, levitating a superconducting coil in a hot plasma in which nuclear reactions occur involves serious engineering challenges, some of which will be mentioned later in this chapter. Still, as compared to the tokamak, the LDX shifts the constraint of steady-state operation from a physics issue to an engineering issue.

Furthermore, in the Levitated Dipole configuration, the toroidal current is always perpendicular to the magnetic field lines: $J_{\parallel} = 0$. According to ideal MHD theory [13], it means that there is no drive for the external and internal kink

instabilities, which are known to be responsible for violent disruptions in tokamaks. One can therefore expect disruption-free operations in the LDX.

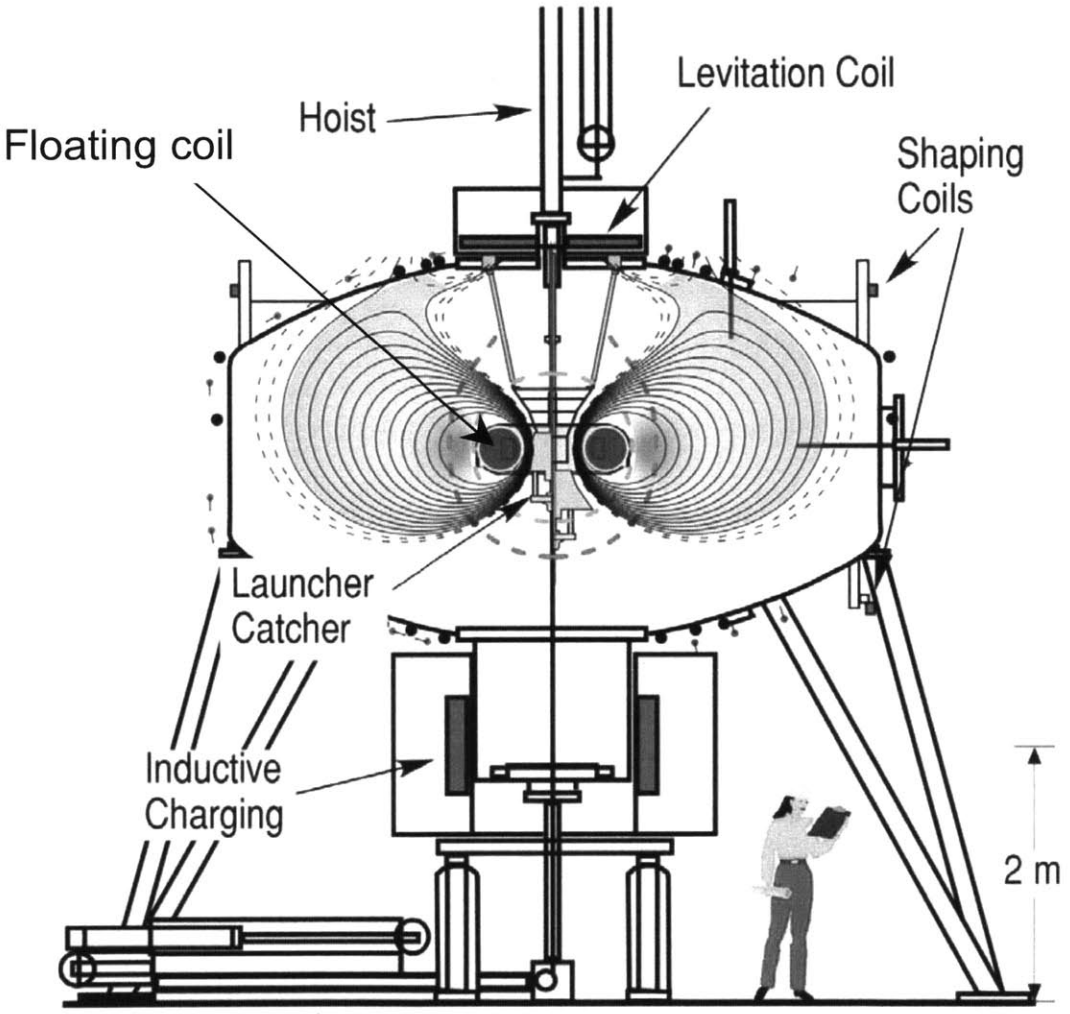

Fig. 4.1. Schematic of LDX showing a vertical cross-section of the experiment. In the left half of the figure, the launcher-catcher is supporting the floating coil; on the right half, it is removed: the floating coil is levitating.

The other advantages of the Levitated Dipole are more disputed. The first one is associated with the transport properties of the dipole configuration. With the magnetic field solely in the poloidal direction, the direction of the particles' drifts is

entirely in the toroidal direction. This implies that trapped particles do not follow banana orbits, or, to say it differently, that the bananas in a dipole configuration are infinitely thin. Consequently, there are no neoclassical effects on transport in a dipole, because there are no radial drifts off flux surfaces. This would indeed be an advantage, if it were true that tokamak transport was well described by neo-classical theory. However, we know that transport in a tokamak is largely dominated by what is known as 'anomalous' transport, and one may expect that such is the case the Levitated Dipole as well. And the question would then become: Is anomalous transport in a dipole more favorable than in a tokamak? The answer is not clear, and requires additional theoretical and experimental work.

The second argument in favor of the dipole is the ideal MHD prediction that a plasma β of the order $\beta \sim 50\%$ could be reached in stable operation, where β is defined as the ratio of plasma pressure to magnetic pressure: $\beta \equiv 2\mu_0 p / B^2$. This value can be compared with the tokamak regime of stable operation: $\beta \sim 5\%$. Thus, according to ideal MHD theory, the comparison is very favorable for the dipole. However, this result has to be taken with a grain of salt. As discussed in [11], the instability setting the limit on the maximum β in a levitated dipole is the $m = 0$ interchange mode, a compressible mode. In Chapter 3, we showed that the ideal MHD predictions may not be reliable for compressible modes when the plasma does not behave as a fluid. One of the purposes of this chapter thus is to reevaluate the theoretical β limit for the MHD interchange mode.

Along with these possible advantages over the tokamak, which is the most promising confinement concept, the dipole concept also comes with drawbacks which have to be taken into account. The main challenge comes from the fact that the D-T fusion reaction is not an acceptable choice for the Levitated Dipole. Indeed, this reaction produces an energetic 14.1 MeV neutron which is not trapped magnetically, and which can therefore penetrate the superconducting coil, heat it and damage it. The coil would then surely lose its super conductivity. Unfortunately, the D-T reaction is the fusion reaction which has by far the highest cross-section.

The next fusion reaction of interest, in decreasing order of the size of the cross-section, is the D-^{3}He reaction. This reaction has the advantage of producing an energetic proton instead of a neutron, which is kept off the floating coil by the magnetic field. However, it is not a valid option for a fusion reactor, since ^{3}He is only present in very small quantities on earth.

Thus, the only fusion reaction really acceptable for the Levitated Dipole concept is the D-D reaction, which has a smaller cross-section than the D-^{3}He reaction, much smaller than that of the D-T reaction. This is a serious drawback for dipoles. It means that the energy confinement time in such a device has to be much longer than in tokamaks. This remains to be proven experimentally.

Aside from this physics issue, there also is an engineering issue of the highest importance: how to thermally insulate the inner core of the floating coil from the surrounding hot plasma, so that the coil remains superconducting? The positive

results obtained during the operation of the LDX [14] are promising, but it remains to be seen whether they can be easily reproduced with the much hotter fusion grade plasmas, and in a nuclear environment.

In conclusion of this discussion, the Levitated Dipole is an innovative concept which may offer advantages as a fusion reactor as compared to the most promising concept: the tokamak. However, it also comes with serious drawbacks. In order to better assess the potential of the dipole configuration, we need to look in more detail at each of the advantages one by one. One of the purposes of this chapter is to have a closer look at one of the assumed strong points of the dipole, namely the ideal MHD prediction that stable plasmas with a β an order of magnitude larger than typical tokamak β limits may be confined in a Levitated Dipole. We will do so in a simplified geometry, corresponding to the large aspect ratio limit of the Levitated Dipole: the hard-core Z-pinch. We introduce this magnetic configuration in the next section.

4.1.2 The hard-core Z-pinch

In a Levitated Dipole, the axisymmetry implies that the equilibrium quantities are independent of ζ, the azimuthal coordinate. The equilibrium is essentially two-dimensional. Theoretical studies in dipole configurations can be greatly simplified by working in the very large aspect ratio, cylindrical limit. In this limit, the equilibrium

becomes one-dimensional, and the magnetic configuration is known as the hard-core Z-pinch (see Fig. 4.2).

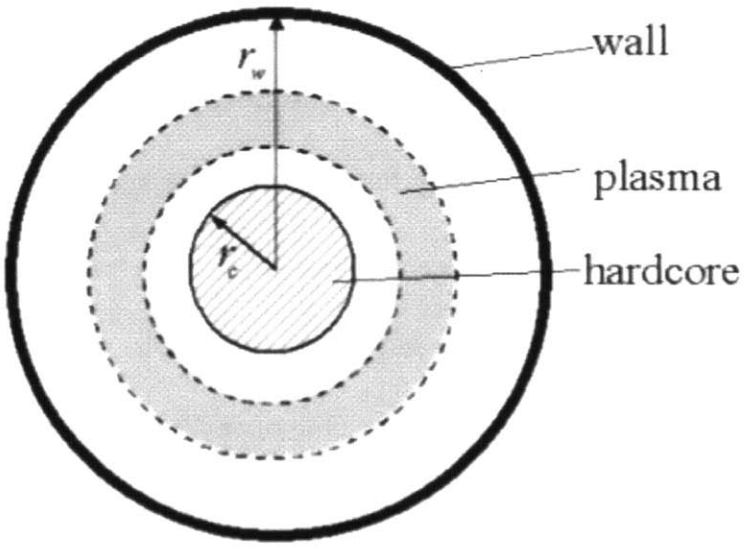

Fig. 4.2. Vertical cross-section (i.e. at fixed z, where z is the coordinate along the axis of the cylinder) of a hard-core Z-pinch. (Figure taken from [2])

The fact that in the hard-core Z-pinch the equilibrium quantities depend solely on r, the radial coordinate, greatly simplifies the calculations. The Z-pinch limit of the dipole has therefore been used in a large number of theoretical studies (e.g. [2], [3], [4], [5], [6]). Interestingly, numerical transport calculations in the dipole [7] have given results which were both qualitatively and quantitatively similar to the same calculations in a hard-core Z-pinch [6], suggesting that the latter indeed represents a good approximation of the physics in a dipole, and that toroidal effects are not crucial. In the rest of this chapter, we consequently focus on the hard-core Z-pinch geometry for our study of the stability of MHD modes.

According to ideal MHD stability theory [15], a simple Z-pinch without an equilibrium flow is potentially unstable to two modes: the $m = 1$ helical mode, and the $m = 0$ interchange mode (also known as the sausage instability). Here, m is the number of oscillations of the mode along the magnetic field line (i.e. in the θ direction). These two modes are illustrated in Fig. 4.3.

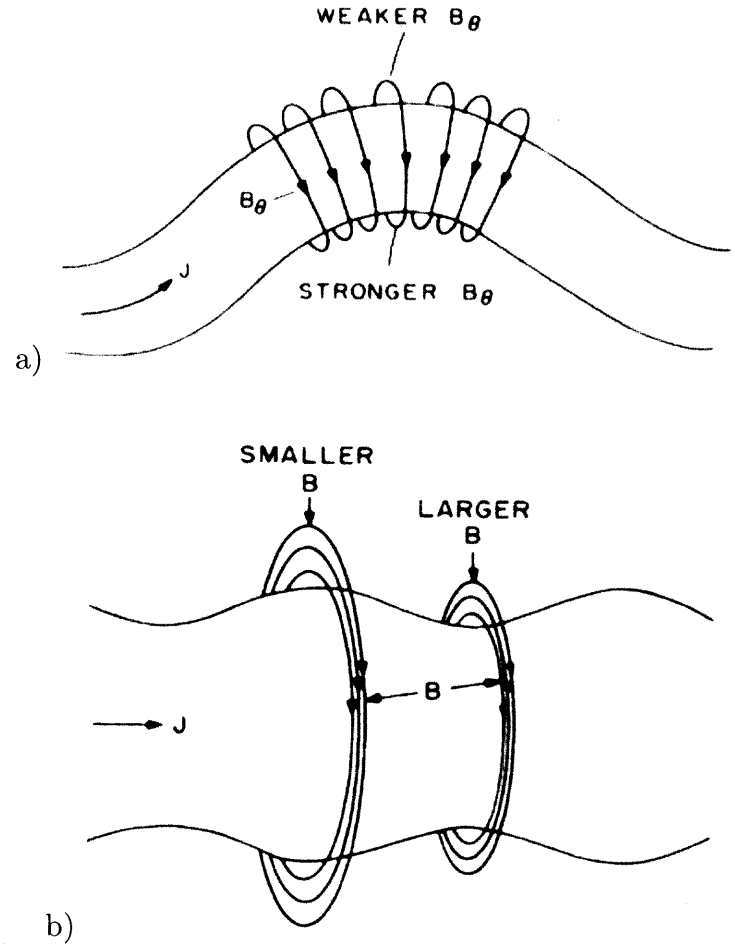

Fig. 4.3. a) Physical mechanism of the $m = 1$ instability in a pure Z-pinch. b) Physical mechanism of the $m = 0$ instability in a pure Z-pinch. (Illustrations from reference [13])

Freidberg has shown in [11] that in the hard-core Z-pinch, the $m = 1$ mode is always stable when the $m = 0$ mode is stable, so that the ideal MHD stability limit is set by the $m = 0$ mode. Moreover, the $m = 1$ mode is incompressible, and does not conserve the closed-line symmetry. As shown in the previous chapter, this implies that the ideal MHD limit for the $m = 1$ mode is more conservative than the limits calculated with models which are more relevant in fusion grade plasmas. For these two reasons, we only need to verify the reliability of the ideal MHD result for the $m = 0$ mode. This mode indeed has the characteristics which make the ideal MHD result suspicious: it is a compressible mode, which conserves the closed-line symmetry (since the perturbation has no variation in the θ direction, i.e. along the magnetic field line).

In the next section (Section 4.2), we give a short review of the ideal MHD stability picture for the $m = 0$ mode. This will facilitate the comparison with the Vlasov-fluid calculation for the same mode, which we present in the last section of the chapter (section 4.3).

4.2 Ideal MHD stability of the interchange mode in the hard-core Z-pinch

In this section, we review the eigenvalue equation one obtains with the ideal MHD model for the $m = 0$ interchange mode in a Z-pinch geometry. We then apply

it to the particular case of the hard-core Z-pinch, with typical LDX density and pressure profiles.

Starting from the full eigenmode equation for the general screw pinch and static equilibria [16], setting $m = 0$ and $B_z = 0$, and taking the low β limit, it easy to find the eigenvalue equation for the $m = 0$ ideal MHD interchange mode in a Z-pinch:

$$\frac{\omega^2}{k_\perp^2}\frac{d}{dr}\left[\rho r^3 \frac{d}{dr}\left(\frac{\xi}{r}\right)\right] - r\left[\omega^2 \rho r^2 - 2pK\right]\left(\frac{\xi}{r}\right) = 0 \tag{4.1}$$

In eq. (4.1), r is the radial coordinate in the natural cylindrical coordinate system associated with the Z-pinch geometry, $\rho = \rho(r)$ is the ion mass density, $p = p(r)$ is the plasma pressure, and $K(r) = \frac{r}{p}\frac{dp}{dr} + 2\gamma$ is the Kadomtsev function [15] in the low β limit, with $\gamma = 5/3$ the ratio of specific heats. ξ is the radial component of the plasma displacement $\boldsymbol{\xi}$, defined by $\boldsymbol{\xi} = \partial\tilde{\mathbf{v}} / \partial t$, where $\tilde{\mathbf{v}}$ is the plasma flow due to the perturbation. In the derivation of eq. (4.1), the plasma displacement $\boldsymbol{\xi}$ is Fourier expanded in both space and time: $\boldsymbol{\xi}(\mathbf{r}, t) = \boldsymbol{\xi}(r)e^{i(k_\perp z + m\theta - \omega t)}$. Thus, ω is the (complex) mode frequency, $k_\perp$ is the wave number in the z-direction (the z axis being the axis of the cylinder). It is well known [15] that if the pressure profile is such that the Kadomtsev function becomes negative at some location in the plasma, the ideal MHD interchange mode will be unstable. Ideal MHD stability thus sets a limit on the acceptable pressure profiles in Z-pinch geometries; they must be such that the pressure gradient at any point in the plasma satisfies the inequality

$$-\frac{r}{p}\frac{dp}{dr} < 2\gamma = \frac{10}{3} \tag{4.2}$$

We illustrate this requirement with the following example, inspired by LDX. A simple choice for the pressure and density profiles that captures the essential physics of the levitated dipole is given by

$$\rho(r) = \rho_{\max}\frac{2}{1+\left(\frac{r}{r_c}\right)^2} \qquad p(r) = p_{\max}\frac{\nu^2}{4}\left(\frac{\nu}{\nu-2}\right)^{\nu-2}\frac{\left[\left(\frac{r}{r_c}\right)^2-1\right]^2}{\left(\frac{r}{r_c}\right)^{2\nu}} \tag{4.3}$$

where r_c is the outer radius of the floating coil, and ν is unspecified for the moment. With these profiles, it is easy to see that the Kadomtsev function is a continuously decreasing function of r. This is illustrated in Fig. 4.4, for the particular case $\nu = 4$. Therefore, the minimum value of the Kadomtsev function over the whole plasma profile will be reached on the outside, at large r. Taking the limit $r \to \infty$, one easily finds a condition on the exponent ν for the pressure profile to be MHD stable. Indeed, $K(r) \xrightarrow[r\to\infty]{} 4 - 2\nu + 2\gamma$, so the condition expressed in eq. (4.3) becomes $\nu < 2 + \gamma = 11/3 \simeq 3.67$.

This condition can be verified by solving the eigenvalue equation (4.1) numerically. Using a shooting method, and the profiles introduced in eq. (4.3), we solved eq. (4.1) for values of ν ranging from 6 to 2. The reason we stop at $\nu = 2$ is that this value corresponds to a flat, non-decaying pressure profile at large radii. The

results are plotted in Figure 4.5, in which we show the normalized ideal MHD growth rate $\omega_I / \omega_{MHD} = \sqrt{\rho_{\max} / p_{\max}} r_c \omega_I$ as a function of ν, for the case $k_\perp r_c = 2.5$. In the simulations, we assumed that the wall facing the plasma was at a location r_w such that $r_w / r_c = 13$, in agreement with the typical situation in LDX.

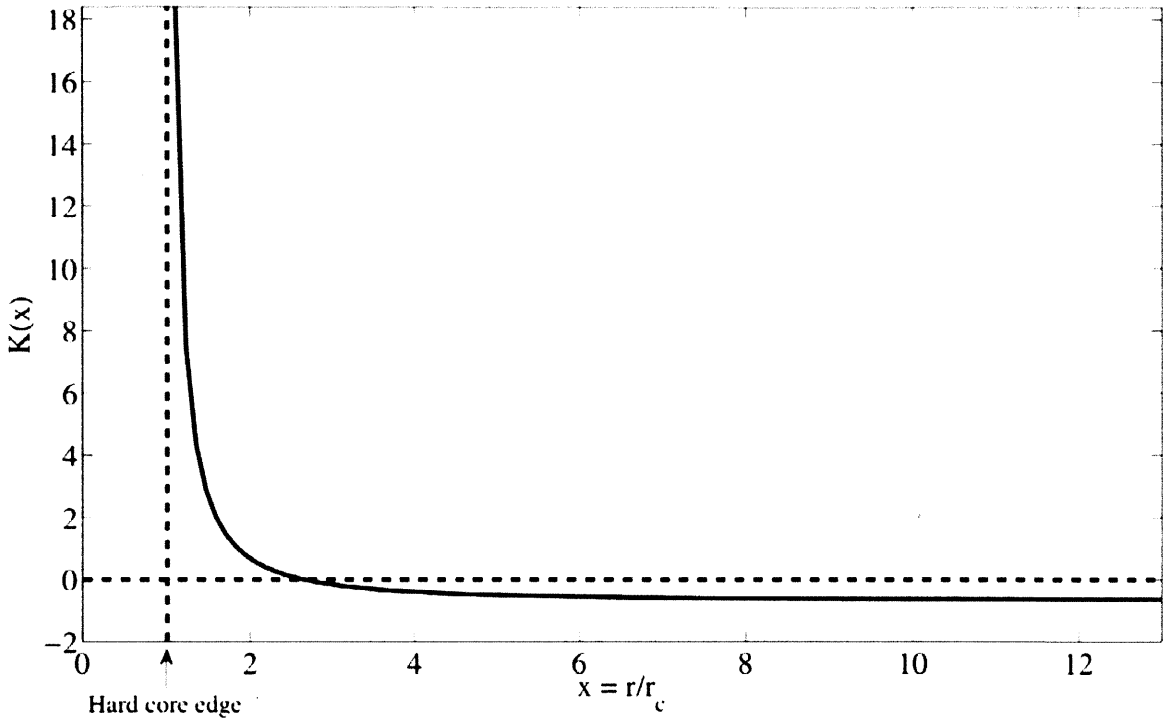

Fig. 4.4. Profile of the Kadomtsev function for the typical LDX pressure profiles given in eq. (4.3). Here $\nu = 4$. Note that the Kadomtsev function is a decreasing function of radius.

The numerical simulation confirms our analytic result. In the ideal MHD model, the pressure profile given in eq. (4.3) is stable to the $m = 0$ mode if $\nu \leq 11/3$. This range of allowable pressure profiles is due to the stabilizing role of MHD plasma

compressibility, as the presence of γ indicates in the criterion (4.2). This is the standard situation with which the Vlasov-fluid results will be compared.

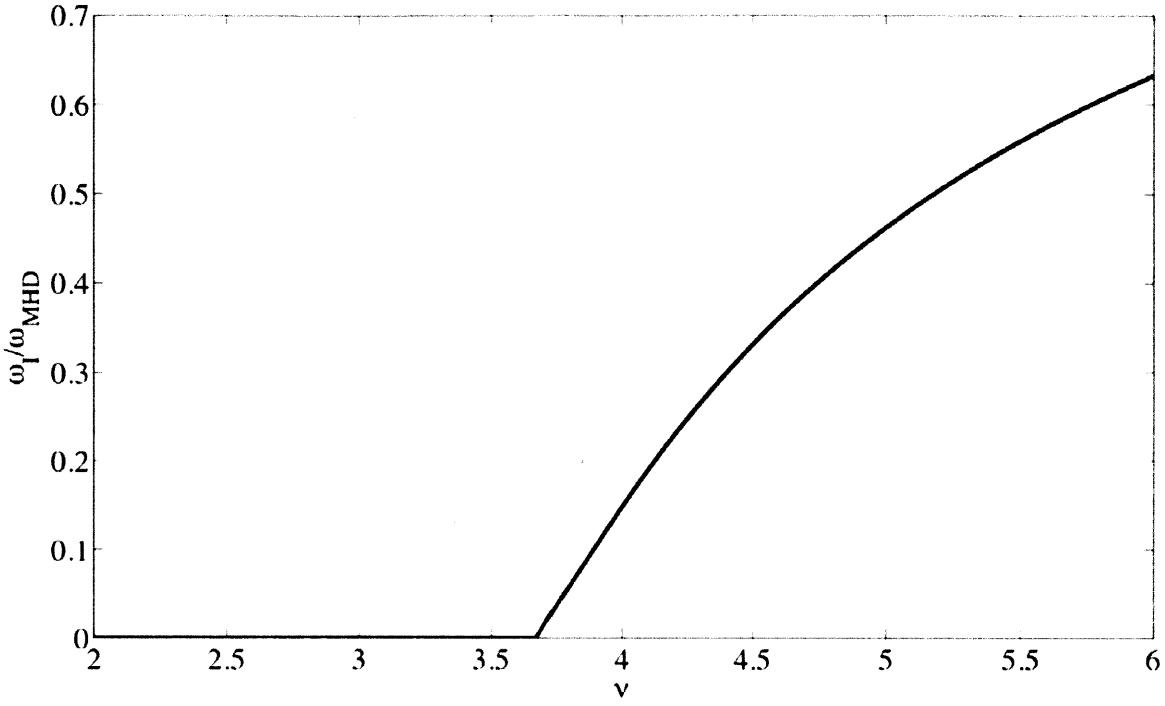

Fig. 4.5. Normalized ideal MHD growth rate $\omega_I / \omega_{MHD} = \sqrt{\rho_{\max} / p_{\max}} r_c \omega_I$ as a function of ν as defined in eq. (4.3). $k_\perp r_c = 2.5$ and $r_w / r_c = 13$.

4.3 Vlasov-Fluid stability of the interchange mode in the hard-core Z-pinch

4.3.1 Previous kinetic studies of the interchange mode in Z-pinch and point dipole geometries

The construction of the LDX generated new interest in the stability of plasmas in closed line magnetic geometries, and in particular in the Z-pinch and dipole configurations. The weaknesses of the MHD model in such geometries (which we

described in Chapter 3) being well known, the most recent stability studies used kinetic descriptions of the plasma, and focused on the most unstable mode: the interchange mode.

Simakov, Catto and Hastie used the gyrokinetic equations to study the interchange mode in both a point dipole and a Z-pinch configuration, in a collisional regime where the collision frequency is smaller than transit or bounce frequencies, but larger than the mode, magnetic drift and diamagnetic frequencies, both in the electrostatic limit [17], and allowing for electromagnetic perturbations [18]. They found that the interchange mode had a different character in the high-frequency (i.e. MHD) and low-frequency (i.e. drift wave) regime. In the high-frequency regime, the mode has the same characteristics as the ideal MHD sausage mode, and Simakov *et al.* obtained the same stability criterion as eq. (4.2). As the frequency of the mode decreases, and as one gets closer and closer to ideal MHD marginal stability, there is a coupling of this branch of the mode with the low-frequency branch, corresponding to the entropy mode. And because of the entropy mode, ideal MHD stability criterion can be violated: ideal MHD stable pressure gradients are found to be unstable.

Kesner and Hastie [19] also used the gyrokinetic equations to study the interchange mode in a dipole geometry, in a more realistic collisionality regime for the LDX experiment, corresponding to collisionless ions and collisional electrons (the collision frequency being smaller than the transit and bounce frequencies, but larger than the mode frequency, and the drift and diamagnetic frequencies). They did not

consider the MHD branch of the interchange mode, and only focused on the low-frequency entropy mode. The results they obtained were quantitatively different but qualitatively similar to those obtained by Simakov *et al.* for a more collisional plasma: the Kadomtsev criterion can be violated, and ideal MHD stable pressure profiles are unstable because of the entropy mode.

Finally, Ricci, Rogers, Dorland, and Barnes [6] used the code GS2 [20], [21] to solve the gyrokinetic system and evaluate the linear growth rates of the interchange modes in a Z-pinch geometry. They considered various collisionality regimes, including a regime in which both species are collisionless. The results are qualitatively similar to those obtained by Simakov *et al.* [17], [18] and Kesner *et al.* [19]: the entropy mode is unstable for pressure gradients which are lower than the marginal stability of the ideal mode. Furthermore, their work showed that kinetic effects were critical, since they found a stability threshold for the pressure gradient which is two times lower than the threshold obtained from fluid theories.

Since virtually all the collisionality regimes of interest are considered in the kinetic studies described in the previous paragraphs, one may wonder about the usefulness of the VF calculation presented in the next section. There are three different aspects to the answer.

First, remember that the goal of the VF analysis is to determine the reliability of the ideal MHD model for the stability of fast, macroscopic modes, where the plasma is tied to the magnetic field lines. In the gyrokinetic model and in the drift

ordering of the entropy mode, the magnetic field lines are not 'frozen in'. The VF calculation is the only calculation allowing us to study the role of kinetic effects and resonant particles while still focusing entirely on MHD modes, since the electron fluid is tied to the field lines in this model.

Second, as Kesner and Hastie [19] looked into the collisionality regime corresponding to the LDX, with collisional electrons and collisionless ions, they ignored the term in their dispersion relation for the interchange mode which corresponds to the high frequency, MHD branch, in order to focus on the entropy mode. With the VF model, we will be able to focus on the MHD branch of the interchange mode in the collisionality regime of greatest interest for LDX.

Lastly, all the kinetic studies described previously investigated the *local* behavior of the interchange mode, and effectively used the so-called local approximation [6], which turns the global eigenvalue equation into a local algebraic equation for the mode frequency ω. As we will see, one of the advantages of the calculation presented here is that one naturally obtains a global eigenvalue equation for ω, which can be directly compared with the ideal MHD eigenvalue equation, eq. (4.1). The similarity between the ideal MHD and VF formulations facilitates the interpretation of the VF results, and the identification of the role of the kinetic effects. Additionally, by taking the local approximation of the VF global eigenvalue equation, and comparing the local results with the global results, we can analyze the potential differences between the two approaches.

4.3.2 Vlasov-fluid stability analysis

We now derive the dispersion relation for the $m = 0$ interchange mode in the VF model. As discussed in Chapter 3, the VF model is mostly appropriate for a plasma with collisionless ions and collisional electrons. This is exactly the collisionality regime of interest for the LDX [19].

Based on the general energy relation derived for the VF model in Section 3.10 of Chapter 3, we expect the stability criterion to differ from the ideal MHD criterion because of wave-particle resonances in the collisionless ions. Therefore, we will give particular attention to the plasma compressibility term and to the ion resonant denominators.

We start with the general momentum equation for the VF plasma, obtained by adding the ion and electron momentum equations together:

$$mn\frac{d\mathbf{v}_i}{dt} = \mathbf{J}\times\mathbf{B} - \nabla p_e - \nabla\cdot\mathbf{P}_i \tag{4.4}$$

In (4.4) m is the ion mass, $\mathbf{v}_i$ is the ion fluid flow, defined by $n\mathbf{v}_i = \int \mathbf{u} f_i \, d\mathbf{u}$, and $\mathbf{P}_i$ is the ion pressure tensor, defined by $\mathbf{P}_i = m_i \int \mathbf{uu} f_i d\mathbf{u}$. f_i is the ion distribution function, and $\mathbf{u}$ represents the total particle velocity. For the derivation, we consider the same static equilibrium ($\mathbf{v}_{i0} = \mathbf{0}$) as in Section 3.10 of Chapter 3. We repeat it here for convenience:

$$
\begin{aligned}
&\mathbf{J}_0 \times \mathbf{B}_0 = \nabla p_0 \\
&p_0 = p_{i0} + p_{e0}, \text{ with } p_{i0} = \int \frac{m_i u^2}{3} f_{i0}\, d\mathbf{u} \quad \text{and } p_{e0} = K n_0^{\gamma_e} \\
&f_{i0} = f_{i0}(\varepsilon) \quad \text{with} \quad \varepsilon = \frac{m_i u^2}{2} + e\phi_0(\mathbf{r}) \\
&n_0 = \int f_{i0}\, d\mathbf{u} = -\frac{1}{e}\frac{dp_{i0}}{d\phi_0} \\
&\mathbf{E}_0 = -\nabla \phi_0
\end{aligned}
\tag{4.5}
$$

In the remainder of the calculation, we will drop the 0 subscripts for the equilibrium quantities, in order to simplify the notations. The momentum equation for the linear perturbation about the static equilibrium (4.5) is then given by:

$$
mn\frac{\partial \tilde{\mathbf{v}}_i}{\partial t} = \tilde{\mathbf{J}} \times \mathbf{B} + \mathbf{J} \times \tilde{\mathbf{B}} - \nabla \tilde{p}_e - \nabla \cdot \tilde{\mathbf{P}}_i \tag{4.6}
$$

where the sign $\tilde{A}$ refers to the linear perturbation of the quantity A.

We follow here the usual normal mode procedure, in which the perturbation $\tilde{A}$ is expanded as $\tilde{A}(\mathbf{r},t) = \tilde{A}(\mathbf{r})e^{-i\omega t}$, with ω is the complex mode frequency. As in Chapter 3, we introduce the electron fluid displacement $\boldsymbol{\xi}$ according to $\tilde{\mathbf{v}}_e = -i\omega\boldsymbol{\xi} + \mathbf{v}_e \cdot \nabla\boldsymbol{\xi} - \boldsymbol{\xi} \cdot \nabla \mathbf{v}_e$. All the perturbed quantities can be expressed in terms on $\boldsymbol{\xi}$ and equilibrium quantities only. In Chapter 3, we have already obtained

$$
\begin{aligned}
&\tilde{n}_e = -\boldsymbol{\xi}_\perp \cdot \nabla n - n\nabla \cdot \boldsymbol{\xi} \\
&\tilde{p}_e = -\boldsymbol{\xi}_\perp \cdot \nabla p_e - \gamma_e p_e \nabla \cdot \boldsymbol{\xi} \\
&\tilde{\mathbf{B}} = \nabla \times (\boldsymbol{\xi}_\perp \times \mathbf{B}) \\
&\tilde{\mathbf{E}} = i\omega\boldsymbol{\xi}_\perp \times \mathbf{B} - \nabla\left(\boldsymbol{\xi}_\perp \cdot \mathbf{E} - \frac{\gamma_e p_e}{en}\nabla \cdot \boldsymbol{\xi}\right)
\end{aligned}
\tag{4.7}
$$

and $\tilde{\mathbf{J}}$ is immediately calculated from $\tilde{\mathbf{B}}$ through Ampere's law. The last perturbed quantity we need to express in terms of $\boldsymbol{\xi}$ and the equilibrium quantities is $\tilde{f}$, the ion perturbed distribution function, which we need in order to calculate $\tilde{\mathbf{v}}_i$ and $\tilde{\mathbf{P}}_i$. Assuming that $\tilde{f}(t=-\infty)=0$, and using eqs. (C.2), and (4.7), $\tilde{f}$ can be rewritten as, after some algebra

$$\begin{aligned}\tilde{f} &= e f_\varepsilon \left\{ \boldsymbol{\xi}\cdot\mathbf{E} - \frac{\gamma_e p_e}{en}\nabla\cdot\boldsymbol{\xi} + i\omega\int_{-\infty}^{t} dt' \left[\boldsymbol{\xi}\cdot(\mathbf{E}+\mathbf{u}\times\mathbf{B}) - \frac{\gamma_e p_e}{en}\nabla\cdot\boldsymbol{\xi} \right] \right\} \\ &= f_\varepsilon \left\{ e\boldsymbol{\xi}\cdot\mathbf{E} - \frac{\gamma_e p_e}{n}\nabla\cdot\boldsymbol{\xi} + i\omega\int_{-\infty}^{t} dt' \left[m\boldsymbol{\xi}\cdot\frac{d\mathbf{u}}{dt} - \frac{\gamma_e p_e}{n}\nabla\cdot\boldsymbol{\xi} \right] \right\}\end{aligned} \tag{4.8}$$

In eq. (4.8), the time integral is taken along the ions' orbits, and $f_\varepsilon \equiv \partial f_i / \partial\varepsilon$ is the partial derivative of the ion equilibrium distribution function with respect to the total energy. Integrating the first term in the integrand by parts, we find

$$\tilde{f}_i = f_\varepsilon \left(e\boldsymbol{\xi}\cdot\mathbf{E} - \frac{\gamma_e p_e}{n}\nabla\cdot\boldsymbol{\xi} + i\omega m\boldsymbol{\xi}\cdot\mathbf{u} + \tilde{s} \right) \tag{4.9}$$

$$\text{with} \qquad \tilde{s} = i\omega\int_{-\infty}^{t} dt' \left[i\omega m\boldsymbol{\xi}\cdot\mathbf{u} - m\mathbf{u}\cdot\left(\mathbf{u}\cdot\nabla\boldsymbol{\xi}\right) - \frac{\gamma_e p_e}{n}\nabla\cdot\boldsymbol{\xi} \right] \tag{4.10}$$

The first three terms in eq. (4.9) are fluid-like. Their contributions to $\tilde{\mathbf{v}}_i$ and $\tilde{\mathbf{P}}_i$ are readily evaluated by using the following equalities:

$$
\begin{aligned}
e\int f_\varepsilon \mathbf{u} d\mathbf{u} &= \frac{d}{d\phi}\left(\int f_i \mathbf{u}\, d\mathbf{u}\right) = \mathbf{0} \\
em\int f_\varepsilon \mathbf{uu} d\mathbf{u} &= \mathbf{I}\frac{d}{d\phi}\left(m\int f_i \frac{u^2}{3} d\mathbf{u}\right) = \frac{dp_i}{d\phi}\mathbf{I} \\
e\int f_\varepsilon \mathbf{uuu} d\mathbf{u} &= \frac{d}{d\phi}\left(\int f_i \mathbf{uuu}\, d\mathbf{u}\right) = \mathbf{0}
\end{aligned}
\tag{4.11}
$$

In eq. (4.11), $\mathbf{I}$ is the identity matrix. Combining eqs. (4.6), (4.7), (4.9), (4.11), the linearized momentum equation becomes

$$
-\rho\omega^2\boldsymbol{\xi} = \tilde{\mathbf{J}}\times\mathbf{B} + \mathbf{J}\times\tilde{\mathbf{B}} + \nabla\left(\boldsymbol{\xi}\cdot\nabla p\right) + m\left(i\omega\int \tilde{s} f_\varepsilon \mathbf{u}\, d\mathbf{u} - \nabla\cdot\int \tilde{s} f_\varepsilon \mathbf{uu}\, d\mathbf{u}\right) \tag{4.12}
$$

where we have introduced the quantity $\rho = mn$ as in section 4.2. So far, we did not choose any ordering, and did not have to make any approximations other than those included in the equations for the electron fluid. Furthermore, eq. (4.12) is valid for any 3-D geometry, and arbitrary β.

We now evaluate this equation for the particular case of the $m = 0$ mode in a hard-core Z-pinch. In the remainder of this section, all the quantities will therefore be evaluated in the appropriate cylindrical coordinates (r, θ, z). For the $m = 0$ mode, the perturbed quantities have no dependence on θ. We Fourier expand them in the z coordinate, so that a Fourier mode is written $\tilde{A} = \tilde{A}(r)e^{ik_\perp z - i\omega t}$, as we have already seen in section 4.2 for the ideal MHD case. Finally, we adopt the following ordering:

$$
\omega \sim \omega_{MHD} \sim \frac{\mathrm{v}_{T_i}}{a} \ll \omega_c \tag{4.13}
$$

In eq. (4.13), $v_{T_i} = \sqrt{2T_i / m}$ is the ion thermal velocity, and a is the typical radius of the plasma. In the hard-core Z-pinch, the ion velocity is written as $\mathbf{u} = u_r \mathbf{e}_r + u_\parallel \mathbf{e}_\theta + u_z \mathbf{e}_z$, where $(\mathbf{e}_r, \mathbf{e}_\theta, \mathbf{e}_z)$ is the natural orthonormal basis of our coordinate system, $u_r = u_\perp \sin(\omega_c t + \varphi)$ and $u_z = u_\perp \cos(\omega_c t + \varphi) + \mathbf{v}_d \cdot \mathbf{e}_z$. $\omega_c = eB(r)/m$ is the ion cyclotron frequency, φ is the phase depending on the ion's trajectory initial conditions, $\mathbf{v}_d = \mathbf{E} \times \mathbf{B} / \mathrm{B}^2 - u_\perp^2 / 2\omega_c \nabla \mathrm{B} \times \mathbf{B} / \mathrm{B}^2 - u_\parallel^2 / \omega_c \boldsymbol{\kappa} \times \mathbf{B} / \mathrm{B}$ is the sum of the $\mathbf{E} \times \mathbf{B}$, $\nabla \mathrm{B}$, and curvature drifts respectively, and $\boldsymbol{\kappa}$ is the curvature vector. Note that in a Z-pinch geometry, we have $\mathbf{v}_d = v_d \mathbf{e}_z$. The ion trajectories are readily integrated:

$$
\begin{aligned}
r(t) &= -\frac{u_\perp}{\omega_c} \cos[\omega_c (t - t_0) + \varphi] + r(t_0) \\
\theta(t) &= \frac{u_\parallel}{r} (t - t_0) + \theta_0 \\
z(t) &= \frac{u_\perp}{\omega_c} \sin[\omega_c (t - t_0) + \varphi] + v_d (t - t_0) + z(t_0)
\end{aligned}
\tag{4.14}
$$

This is all the information we need to evaluate the trajectory integrals in the quantities $n\tilde{\mathbf{v}}_{i,kin} = \int \tilde{s} f_\varepsilon \mathbf{u}\, d\mathbf{u}$ and $\tilde{\mathbf{P}}_{i,kin} = m \int \tilde{s} f_\varepsilon \mathbf{u}\mathbf{u}\, d\mathbf{u}$. For the analytic evaluation of these two quantities, we assume that $k_\perp r_{L_i} \equiv k_\perp \frac{v_{T_i}}{\omega_c} \ll 1$, and only keep the terms to lowest order in the parameter $\lambda \equiv k_\perp u_\perp / \omega_c$. After some long but mindless algebra, we find, using the fact that $\omega \ll \omega_c$,

$$
\begin{aligned}
n\tilde{\mathbf{v}}_{i,kin} &= \mathbf{0} \\
\tilde{\mathbf{P}}_{i,kin} &= \pi m^2 \omega \begin{pmatrix} \hat{P}_\perp & 0 & 0 \\ 0 & \hat{P}_\parallel & 0 \\ 0 & 0 & \hat{P}_\perp \end{pmatrix} = \begin{pmatrix} P_\perp & 0 & 0 \\ 0 & P_\parallel & 0 \\ 0 & 0 & P_\perp \end{pmatrix}
\end{aligned} \tag{4.15}
$$

with

$$
\begin{aligned}
\hat{P}_\perp = (\xi' + ik_\perp \xi_z) \int_0^{+\infty}\int_{-\infty}^{+\infty} f_\varepsilon \frac{u_\perp^4}{4(\omega - k_\perp \mathrm{v}_d)} du_\perp^2 du_\parallel + \frac{\xi}{r} \int_0^{+\infty}\int_{-\infty}^{+\infty} f_\varepsilon \frac{u_\perp^2 u_\parallel^2}{2(\omega - k_\perp \mathrm{v}_d)} du_\perp^2 du_\parallel \\
+ \frac{1}{m}\frac{\gamma_e p_e}{n} \nabla \cdot \boldsymbol{\xi} \int_0^{+\infty}\int_{-\infty}^{+\infty} f_\varepsilon \frac{u_\perp^2}{2(\omega - k_\perp \mathrm{v}_d)} du_\perp^2 du_\parallel
\end{aligned}
$$

$$
\begin{aligned}
\hat{P}_\parallel = (\xi' + ik_\perp \xi_z) \int_0^{+\infty}\int_{-\infty}^{+\infty} f_\varepsilon \frac{u_\perp^2 u_\parallel^2}{2(\omega - k_\perp \mathrm{v}_d)} du_\perp^2 du_\parallel + \frac{\xi}{r} \int_0^{+\infty}\int_{-\infty}^{+\infty} f_\varepsilon \frac{u_\parallel^4}{\omega - k_\perp \mathrm{v}_d} du_\perp^2 du_\parallel \\
+ \frac{1}{m}\frac{\gamma_e p_e}{n} \nabla \cdot \boldsymbol{\xi} \int_0^{+\infty}\int_{-\infty}^{+\infty} f_\varepsilon \frac{u_\parallel^2}{\omega - k_\perp \mathrm{v}_d} du_\perp^2 du_\parallel
\end{aligned} \tag{4.16}
$$

In eq. (4.16) and for the remainder of this section, the symbol B' represents a derivative of the quantity B with respect to r, ξ is the component of the electron displacement $\boldsymbol{\xi}$ in the r direction, and ξ_z its component in the z direction. Using the low-β form of the magnetic drifts and eq. (4.5) we express $k_\perp \mathrm{v}_d$ as follows:

$$
k_\perp \mathrm{v}_d = \frac{k_\perp \mathrm{v}_{T_i}^2}{r\omega_c}\left(\frac{u_\perp^2}{2\mathrm{v}_{T_i}^2} + \frac{u_\parallel^2}{\mathrm{v}_{T_i}^2} + \frac{1}{2}\frac{r p_i'}{p_i}\right) \tag{4.17}
$$

The pressure gradient in (4.17) comes from the $\mathbf{E}\times\mathbf{B}$ drift term, which can be written in this form by using the equilibrium relations (4.5). We now choose f_i to be

Maxwellian: $f_i = n_i\left(m / 2\pi T_i\right)^{3/2} \exp(-mu^2 / 2T_i)$. Note that while this choice may seem natural, it has important implications on the type of equilibrium profiles which can be considered in our analysis of the $m = 0$ in the hard-core Z-pinch. Remember from eq. (4.5) that in the VF model, the equilibrium ion distribution function only depends on the energy, $\frac{mu^2}{2} + e\phi\left(\mathbf{r}\right)$, and that the only space dependence in the energy is in the electrostatic potential ϕ. If the Maxwellian distribution function is to satisfy this condition, T_i cannot depend on the space coordinates. In other words, by choosing a Maxwellian distribution function to evaluate the velocity integrals, we restrict ourselves to flat, isothermal equilibrium ion temperature profiles. One of the advantages of the gyrokinetic approach [22] is that there is no such constraint on the equilibrium Maxwellian distribution. The ion temperature can be a function of the radial coordinate.

With our choice for the ion distribution function, and the normalizations $\overline{u}_\perp = u_\perp / \mathrm{v}_{T_i}$, $\overline{u}_\parallel = u_\parallel / \mathrm{v}_{T_i}$, and $\Omega = r\omega_c\omega / (k_\perp \mathrm{v}_{T_i}^2)$, the kinetic contribution to the pressure tensor is

$$\tilde{\mathbf{P}}_{i,kin} = -p_i\Omega\begin{pmatrix} \widehat{P}_{i\perp} & 0 & 0 \\ 0 & \widehat{P}_{i\parallel} & 0 \\ 0 & 0 & \widehat{P}_{i\perp} \end{pmatrix} - \gamma_e p_e\Omega\begin{pmatrix} \widehat{P}_{e\perp} & 0 & 0 \\ 0 & \widehat{P}_{e\parallel} & 0 \\ 0 & 0 & \widehat{P}_{e\perp} \end{pmatrix} \tag{4.18}$$

where

$$\widehat{P}_{i\perp} = \frac{1}{\sqrt{\pi}}\left[(\xi' + ik_{\perp}\xi_z)\int_0^{+\infty}\int_{-\infty}^{+\infty}\frac{\overline{u}_{\perp}^4 e^{-\overline{u}_{\perp}^2-\overline{u}_{\parallel}^2}}{\Omega - \left(\frac{\overline{u}_{\perp}^2}{2} + \overline{u}_{\parallel}^2 + \frac{1}{2}r\frac{p_i'}{p_i}\right)} d\overline{u}_{\perp}^2\, d\overline{u}_{\parallel} + 2\frac{\xi}{r}\int_0^{+\infty}\int_{-\infty}^{+\infty}\frac{\overline{u}_{\perp}^2\overline{u}_{\parallel}^2 e^{-\overline{u}_{\perp}^2-\overline{u}_{\parallel}^2}}{\Omega - \left(\frac{\overline{u}_{\perp}^2}{2} + \overline{u}_{\parallel}^2 + \frac{1}{2}r\frac{p_i'}{p_i}\right)} d\overline{u}_{\perp}^2\, d\overline{u}_{\parallel}\right]$$

$$\widehat{P}_{i\parallel} = \frac{2}{\sqrt{\pi}}\left[(\xi' + ik_{\perp}\xi_z)\int_0^{+\infty}\int_{-\infty}^{+\infty}\frac{\overline{u}_{\perp}^2\overline{u}_{\parallel}^2 e^{-\overline{u}_{\perp}^2-\overline{u}_{\parallel}^2}}{\Omega - \left(\frac{\overline{u}_{\perp}^2}{2} + \overline{u}_{\parallel}^2 + \frac{1}{2}r\frac{p_i'}{p_i}\right)} d\overline{u}_{\perp}^2\, d\overline{u}_{\parallel} + 2\frac{\xi}{r}\int_0^{+\infty}\int_{-\infty}^{+\infty}\frac{\overline{u}_{\parallel}^4 e^{-\overline{u}_{\perp}^2-\overline{u}_{\parallel}^2}}{\Omega - \left(\frac{\overline{u}_{\perp}^2}{2} + \overline{u}_{\parallel}^2 + \frac{1}{2}r\frac{p_i'}{p_i}\right)} d\overline{u}_{\perp}^2\, d\overline{u}_{\parallel}\right]$$

$$\widehat{P}_{e\perp} = \frac{1}{\sqrt{\pi}}\nabla\cdot\boldsymbol{\xi}\int_0^{+\infty}\int_{-\infty}^{+\infty}\frac{\overline{u}_{\perp}^2 e^{-\overline{u}_{\perp}^2-\overline{u}_{\parallel}^2}}{\Omega - \left(\frac{\overline{u}_{\perp}^2}{2} + \overline{u}_{\parallel}^2 + \frac{1}{2}r\frac{p_i'}{p_i}\right)} d\overline{\mathrm{u}}_{\perp}^2\, d\overline{\mathrm{u}}_{\parallel}$$

$$\widehat{P}_{e\parallel} = \frac{2}{\sqrt{\pi}}\nabla\cdot\boldsymbol{\xi}\int_0^{+\infty}\int_{-\infty}^{+\infty}\frac{\overline{u}_{\parallel}^2 e^{-\overline{u}_{\perp}^2-\overline{u}_{\parallel}^2}}{\Omega - \left(\frac{\overline{u}_{\perp}^2}{2} + \overline{u}_{\parallel}^2 + \frac{1}{2}r\frac{p_i'}{p_i}\right)} d\overline{u}_{\perp}^2\, d\overline{u}_{\parallel}$$

Biglari *et al.* [23] presented a very convenient method for calculating all the velocity integrals in the previous expressions. Defining $\overline{\Omega} = \Omega - \frac{1}{2}rp_i' / p_i$ and the function

$$F_{\alpha,\beta}(\overline{\Omega}) = -i\pi^{-1/2}\int_0^{\infty} d\tau \int d\overline{u}_{\perp}^2\, d\overline{u}_{\parallel} \exp\left[-\alpha\overline{u}_{\parallel}^2 - \beta\overline{u}_{\perp}^2 + i\tau\left(\overline{\Omega} - \frac{\overline{u}_{\perp}^2}{2} - \overline{u}_{\parallel}^2\right)\right] \qquad (4.19)$$

$\widehat{P}_{i\perp}$, $\widehat{P}_{i\parallel}$, $\widehat{P}_{e\perp}$, and $\widehat{P}_{e\parallel}$ become

$$\widehat{P}_{i\perp} = \partial^2_{\beta} F_{\alpha,\beta}\Big|_{\alpha=1,\beta=1} \nabla\cdot\boldsymbol{\xi} + \left(2\partial^2_{\alpha\beta} F_{\alpha,\beta}\Big|_{\alpha=1,\beta=1} - \partial^2_{\beta} F_{\alpha,\beta}\Big|_{\alpha=1,\beta=1}\right)\frac{\xi}{r}$$

$$\widehat{P}_{i\parallel} = 2\partial^2_{\alpha\beta} F_{\alpha,\beta}\Big|_{\alpha=1,\beta=1} \nabla\cdot\boldsymbol{\xi} + \left(4\,\partial^2_{\alpha} F_{\alpha,\beta}\Big|_{\alpha=1,\beta=1} - 2\partial^2_{\alpha\beta} F_{\alpha,\beta}\Big|_{\alpha=1,\beta=1}\right)\frac{\xi}{r} \tag{4.20}$$

$$\widehat{P}_{e\perp} = -\partial_{\beta} F_{\alpha,\beta}\Big|_{\alpha=1,\beta=1} \nabla\cdot\boldsymbol{\xi}$$

$$\widehat{P}_{e\parallel} = -2\partial_{\alpha} F_{\alpha,\beta}\Big|_{\alpha=1,\beta=1} \nabla\cdot\boldsymbol{\xi}$$

The advantage of this procedure is that Biglari *et al.* [23] have been able to evaluate the function $F_{\alpha=1,\beta=1}$ and its partial derivatives involved in eq. (4.20). They found

$$\begin{aligned}
&F_{\alpha,\beta}\Big|_{\alpha=1,\beta=1} = Y^2 \\
&\partial_{\alpha} F_{\alpha,\beta}\Big|_{\alpha=1,\beta=1} = 1 - \bar{\Omega} F_{1,1} - \frac{1}{2}\partial_{\beta} F_{\alpha,\beta}\Big|_{\alpha=1,\beta=1} \\
&\partial_{\beta} F_{\alpha,\beta}\Big|_{\alpha=1,\beta=1} = -2\left[\left(\bar{\Omega} + \frac{1}{2}\right)F_{1,1} - 2\bar{\Omega}^{-\frac{1}{2}} Y + 1\right] \\
&\partial^2_{\beta} F_{\alpha,\beta}\Big|_{\alpha=1,\beta=1} = -2\left(\bar{\Omega} + \frac{1}{2}\right)\partial_{\beta} F_{\alpha,\beta}\Big|_{\alpha=1,\beta=1} + 2F_{1,1} - 8\bar{\Omega}^{-\frac{1}{2}} Y + 6 \\
&\partial^2_{\alpha\beta} F_{\alpha,\beta}\Big|_{\alpha=1,\beta=1} = -1 - \bar{\Omega}\partial_{\beta} F_{\alpha,\beta}\Big|_{\alpha=1,\beta=1} - \frac{1}{2}\partial^2_{\beta} F_{\alpha,\beta}\Big|_{\alpha=1,\beta=1} \\
&\partial^2_{\alpha} F_{\alpha,\beta}\Big|_{\alpha=1,\beta=1} = \bar{\Omega}(\bar{\Omega} Y^2 - 1 + \partial_{\beta} F_{\alpha,\beta}\Big|_{\alpha=1,\beta=1}) + \frac{1}{4}\partial^2_{\beta} F_{\alpha,\beta}\Big|_{\alpha=1,\beta=1} \\
&Y(\bar{\Omega}) = \exp(-\bar{\Omega})\left(-i\pi^{1/2} + \int_0^{\bar{\Omega}} dz z^{-1/2}\exp(z)\right) = -i\pi^{1/2}\exp(-\bar{\Omega})\left[1 + \mathrm{erf}(i\bar{\Omega}^{1/2})\right]
\end{aligned} \tag{4.21}$$

Note that our definition of Y is slightly different from the one given by Biglari *et al.* [23]; the one proposed here was found to be slightly more convenient. Since we evaluated all the components of the tensor $\tilde{\mathbf{P}}_{i,kin}$, we can now write down the radial dispersion relation for the $m = 0$ mode. The θ component of eq. (4.12) is $\xi_{\theta} = 0$,

which is what we physically expect for the $m = 0$ mode. The z component of eq. (4.12) can be written under the following form:

$$B\tilde{B} = \xi p' - P_{\perp} - \frac{\omega^2}{k_{\perp}^2}\rho\left[\nabla\cdot\boldsymbol{\xi} - \frac{(r\xi)'}{r}\right] \tag{4.22}$$

Using this expression for $B\tilde{B}$ in the r component of eq. (4.12), we find, after some algebra:

$$\frac{\omega^2}{k_{\perp}^2}\left[r^3\rho\left(\frac{\xi}{r}\right)'\right]' - \omega^2 r^2\rho\xi + 2rp'\xi - r\left(P_{\perp} + P_{\parallel}\right) = 0 \tag{4.23}$$

$P_{\perp}$ and $P_{\parallel}$ involve two components of the displacement $\boldsymbol{\xi}$: ξ and $\nabla\cdot\boldsymbol{\xi}$. Fortunately, for low-$\beta$ plasmas, there exists a simple expression for $\nabla\cdot\boldsymbol{\xi}$ in terms of ξ, which greatly simplifies (4.23). We start by calculating $\tilde{B}\mathbf{e}_{\theta} = \nabla\times\left(\xi B\mathbf{e}_{z} - \xi_{z}B\mathbf{e}_{r}\right)$:

$$\tilde{B} = B\frac{\xi}{r} - \xi B' - B\nabla\cdot\boldsymbol{\xi} \tag{4.24}$$

In low-β plasmas, $B' \simeq -\dfrac{B}{r}$ and $\tilde{B} \simeq 0$, so that

$$\nabla\cdot\boldsymbol{\xi} \simeq 2\xi / r \tag{4.25}$$

and with the expressions from eqs. (4.20) and (4.21), we finally find the following eigenvalue equation for the $m = 0$ mode:

$$\frac{\omega^2}{k_\perp^2}\left[r^3\rho\left(\frac{\xi}{r}\right)'\right]' - \left[\omega^2\rho r^2 - 2rp' - 4\left(\Gamma_e p_e + \Gamma_i p_i\right)\right]\xi = 0$$

with (4.26)

$$\Gamma_e = \gamma_e\Omega(\overline{\Omega}Y^2 - 1)$$

$$\Gamma_i = \Omega\left(\overline{\Omega}^2 Y^2 - \overline{\Omega} - 1\right)$$

We now clearly see the advantage of both not making the local approximation at the beginning of the derivation as it is often done, and of following the moment procedure presented here. Indeed, in this calculation the global eigenvalue equation for the mode frequency ω comes as the natural consequence of the projection of the momentum equation on the three vectors of the basis $\left(\mathbf{e}_r, \mathbf{e}_\theta, \mathbf{e}_z\right)$, and the very strong similarity between the ideal MHD eigenvalue equation, eq. (4.1), and the VF equation, eq. (4.26) allows for the direct comparison between the two models. This similarity is even more explicit in the limit where the MHD mode is very unstable, i.e. when $\Omega \gg 1$. In this limit, we have

$$Y^2 \underset{\Omega\gg 1}{\sim} \frac{1}{\overline{\Omega}} + \frac{1}{\overline{\Omega}^2} + \frac{7}{4}\frac{1}{\overline{\Omega}^3} \tag{4.27}$$

so that, when $\Omega \gg 1$, eq. (4.26) becomes

$$\frac{\omega^2}{k_\perp^2}\left[r^3\rho\left(\frac{\xi}{r}\right)'\right]' - \left[\omega^2\rho r^2 - 2rp' - 4\left(\gamma_e p_e + \frac{7}{4}p_i\right)\right]\xi = 0 \tag{4.28}$$

Eq. (4.28) would be exactly identical to the ideal MHD equation (4.1) if the factor 7/4 multiplying p_i was replaced by 5/3, and if we assumed $p_i = p_e = p/2$. We obtained 7/4 instead of 5/3 because the ions are collisionless instead of being collision dominated as in ideal MHD. In fact, it is easy to show [24] that eq. (4.28) is the eigenvalue equation one would obtain for the $m = 0$ mode in a Z-pinch in a hybrid model where the electron pressure is given by the MHD equation of state, and the ion pressure by the Chew-Golberger-Low double adiabatic equations of state [25].

By comparing eq. (4.1) and eq. (4.26), we can identify the role of the kinetic effects associated with the ion drift resonance on MHD plasma compressibility. While the functions Γ_i and Γ_e, containing these kinetic effects, are almost purely real when the MHD mode is very unstable, their imaginary parts become more and more important as the MHD growth rate decreases, and as one nears ideal MHD marginal stability. And because of the imaginary parts of Γ_i and Γ_e, the interchange instability persists beyond the ideal MHD limit for the equilibria under consideration in the VF model, in which the ions are electrostatically confined. In the next section, we show that kinetic effects are indeed responsible for the vanishing of MHD compressibility stabilization by numerically solving eq. (4.26).

4.3.3 The vanishing of MHD compressibility stabilization: a numerical example

In order to demonstrate the role of the kinetic effects in the persistence of the interchange instability beyond the ideal MHD limit, and the vanishing of

compressibility stabilization, we solve eq. (4.26) numerically, using a shooting method.

Unfortunately, we cannot directly use the model density and pressure profiles which we used in the ideal MHD case (eq. (4.3)) to solve eq. (4.26). The difficulty comes from our choice of a Maxwellian distribution function for the ions (which was solely motivated by our desire to calculate the velocity integrals analytically, and is not a requirement of the VF model), and from the special form of the electron equation of state. First, as we already discussed, by choosing to calculate the velocity integrals using a Maxwellian distribution function, we restricted our analysis to isothermal equilibrium profiles for the ion temperature: $T_i = cst$ in the plasma. Since $p_i = nT_i$, this means that the density and pressure profiles are now correlated, unlike the profiles in eq. (4.3). In ideal MHD, the details of the density profile have little impact on the stability picture, which almost entirely depends on the details of the pressure profile, as we have shown in Section 4.2. For this reason, for our numerical example we choose to solve eq. (4.26) for model pressure profiles in eq. (4.3), which we repeat here for convenience:

$$p_i(r) = p_{i,\max} \frac{\nu^2}{4} \left(\frac{\nu}{\nu - 2} \right)^{\nu-2} \frac{\left[\left(\frac{r}{r_c} \right)^2 - 1 \right]^2}{\left(\frac{r}{r_c} \right)^{2\nu}} \tag{4.29}$$

and we let the density profiles be given by the relation

$$n = p_i / T_i \tag{4.30}$$

with T_i, the ion temperature, a simple normalizing constant.

The second difficulty comes from the fact that the equilibrium electron pressure is given by the electron equation of state: $p_e = Kn^{\gamma_e}$, K being a normalizing constant. Now, with n given by $n = p_i / T_i$ as discussed in the previous paragraph, and $\gamma_e = 5/3$, we obtain very steep electron pressure profiles, which are always ideal MHD unstable. This is clearly not a regime of interest to us, since we would like to focus on the region where MHD plasma compressibility stabilizes the ideal mode. For this reason, we consider only cold electrons in our numerical example, with the equation of state given by:

$$T_e = 0 \tag{4.31}$$

Eqs. (4.30) and (4.31) clearly limit the experimental relevance of the VF results as far as the LDX is concerned. Indeed, in the LDX, the equilibrium ion temperature is not a constant across the plasma, and electrons tend to have a higher equilibrium temperature than ions. Therefore, the numerical results we present below are not a theoretical prediction of the stability limits in the LDX, and should not be seen as such. Instead, they are an illustration in a practical case of the limitations of the ideal MHD model, and of the role of resonant particles on MHD modes in collisionless plasmas. Our focus thus is mostly theoretical: we highlight some of the flaws of ideal MHD in fusion grade plasmas with a model which has its own

limitations, and with special equilibrium profiles which make the mathematical analysis more tractable.

Once the density and pressure profiles are chosen, we can readily solve eq. (4.26) using a shooting method, as in the ideal MHD case. In Figure 4.6, we show the normalized growth rate ω_I / ω_{MHD} of the Vlasov-Fluid interchange mode as a function of ν, and, for comparison, the normalized ideal MHD growth rate, which we obtained with the same profiles. For this numerical calculation, we had $k_\perp r_{L_i} = 0.1$, $k_\perp r_c = 5$ and $r_w / r_c = 13$.

We can draw two important conclusions from our numerical calculations. First, we proved that it is crucial, in plasmas in which the ions are essentially collisionless, to properly treat the ion kinetic effects. As exemplified in Fig. 4.6, when the ion resonance $\omega - k_\perp v_d$ is taken into account in the calculation, the $m = 0$ instability in a hard-core Z-pinch persists well beyond the ideal MHD stability limit. For the equilibria which we considered, in which the ions are electrostatically confined, the mode is only stable for $\nu \leq 2$, i.e. for non-decaying pressure profiles: there is no plasma compressibility stabilization! Since the hard-core Z-pinch represents the large aspect ratio limit of the levitated dipole, and since the physics of the ion wave-particle resonance is not fundamentally different in both configurations, we expect this result to hold for the same equilibria in the dipole geometry. As an

extension to this work, it may be interesting to verify this hypothesis, and derive the equivalent of the dispersion relation (4.26) in the dipole geometry.

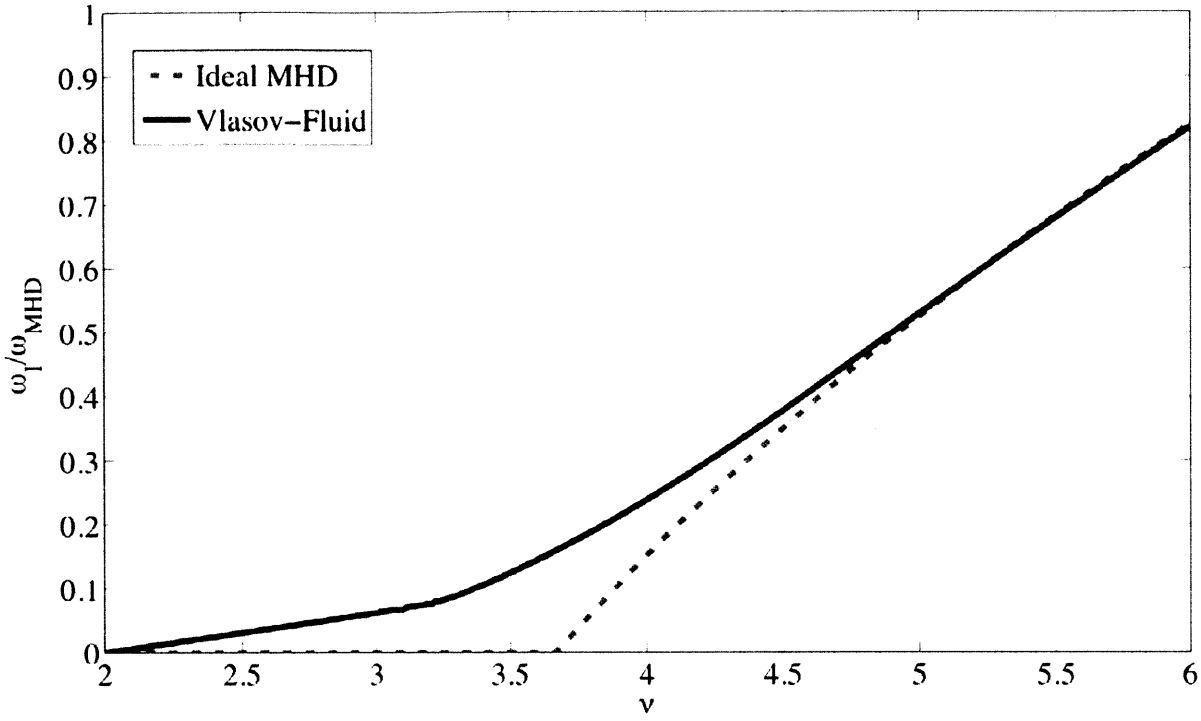

Fig. 4.6. Normalized Vlasov-fluid and ideal MHD growth rates $\omega_I / \omega_{MHD} = \sqrt{\rho_{\max} / p_{\max}} r_c \omega_I$ of the interchange mode as a function of ν as defined in eq. (4.3). $k_\perp r_{L_i} = 0.1$, $k_\perp r_c = 5$ and $r_w / r_c = 13$.

More importantly, it would be interesting to look at the nonlinear evolution of the instability, and to investigate the behavior and the characteristics of the instability in its fully developed stage. Indeed, in its ideal MHD stable regime, the interchange instability is driven by a rather small class of resonant ions. It is not

clear whether such an instability can lead to the same kind of dramatic loss of plasma confinement, as purely fluid MHD instability tend to do.

Note that for $k_\perp r_{L_i} \ll 1$ and $k_\perp r_c \sim 1$, the growth rate of the instability is small, as can be seen in Fig. 4.6. This is to be expected, since for small $k_\perp$, the wave particle resonance $\omega - k_\perp v_d$ only affects ions with very large velocities. When the ion distribution function is a Maxwellian, the ions with such velocities only represent a small fraction of the whole ion population.

As $k_\perp$ gets larger, however, the wave-particle resonance affects a larger fraction of the ion population, and we expect the growth rate of the instability to be larger. This is confirmed by the results shown in Fig. 4.7, in which we plot the VF growth rate as a function of ν for two different values of $k_\perp$: $k_\perp r_{L_i} = 0.1$ and $k_\perp r_{L_i} = 0.2$ (with all the other quantities fixed: $r_w / r_c = 13$ and $r_c / r_{L_i} = 50$). We see that the growth rate of the instability is indeed larger for the larger $k_\perp$.

It is well-known (e.g. [11]) that the largest growth rates of the ideal MHD interchange mode are found for large $k_\perp$, such that $k_\perp a \gg 1$. Thus, one would expect the kinetic effects observed in Fig. 4.6 to become very important in this limit, and the growth rate of the instability to be of the same order as the ideal MHD growth rate, even in the ideal MHD stable region. Unfortunately, we have not been able to verify this hypothesis, and did not explore the VF interchange instability in this

regime, for two reasons. First, eq. (4.26) is only valid in the regime $k_\perp r_{L_i} \ll 1$, since we have only kept the terms to lowest order in $k_\perp r_{L_i}$. To go into the regime $k_\perp r_{L_i} \sim 1$, we would need to include a lot more terms in the derivation of eq. (4.26). For example, we have ignored the off-diagonal elements of the ion pressure tensor, which become important as one approaches $k_\perp r_{L_i} \sim 1$.

The second reason is numerical: it is extremely hard obtain proper convergence beyond $k_\perp r_c \approx 10$ with the shooting method we use to solve eq. (4.26).

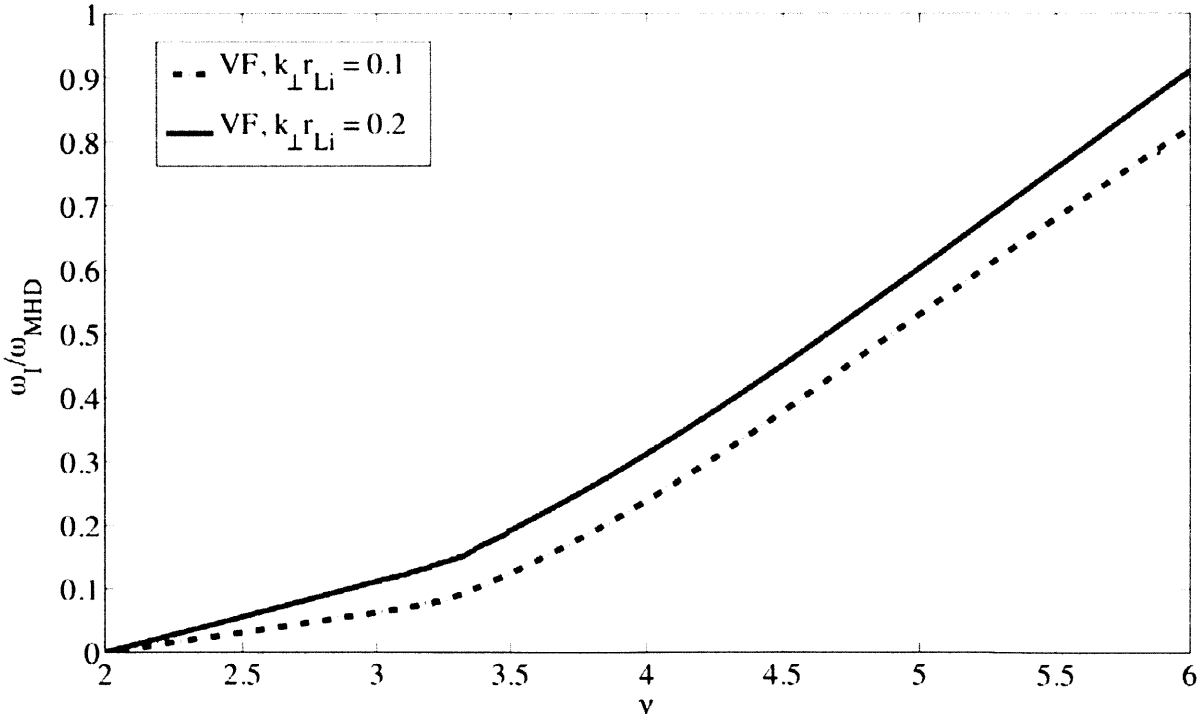

Fig. 4.7. Normalized Vlasov-fluid growth rate of the interchange instability as a function of ν as defined in eq. (4.3) and as a function of the perpendicular wave number $k_\perp$. ($r_w / r_c = 13$ and $r_c / r_{L_i} = 50$).

The second point of interest in our numerical example is that at the stability boundary, $\omega_I = 0$, $\nu = 2$, $p'\left(r \to \infty\right) = 0$, we also obtained $\omega_R = 0$ in our numerical calculation. In other words, the marginal stability condition is $\omega^2 = 0$, or, according to the general energy relation (3.151) in Chapter 3, $W_\perp = 0$. Thus, for equilibria such that the ion distribution function is only a function of the total energy, $f_i = f_i\left(\varepsilon\right)$, marginal stability is indeed inherently incompressible in a closed-line system such as the hard-core Z-pinch, and the conjecture which we proposed for general 3-D geometries in Section 3.10 of Chapter 3 is verified in this particular example. This gives us confidence that our conjecture may be true in any closed-line system.

4.3.4 Local approximation vs. global eigenvalue equation

When the perpendicular wave number $k_\perp$ is such that $k_\perp r_{L_i} \ll 1 \ll k_\perp r_c$ (as in the numerical examples in the previous section for instance), the second term in eq. (4.26) is much larger than the first term, so that the latter can be neglected. With this approximation, known as the local approximation, eq. (4.26) becomes

$$\omega^2 \rho r^2 - 2rp' - 4\left(\Gamma_e p_e + \Gamma_i p_i\right) = 0 \tag{4.32}$$

Eq. (4.32) is fundamentally different from eq. (4.26). In eq. (4.26), ω is the eigenvalue associated with the eigenfunction ξ, and does therefore not depend on the radial coordinate r. In eq. (4.32), however, ω is the solution of an algebraic equation, which depends on the radial location r, and on the local values of $p'\left(r\right)$,

$p_e(r)$, $p_i(r)$, and $\rho(r)$. What is usually done, once the local approximation leading to (4.32) is made, is to look at a given location r in the plasma, and to consider $p'(r)$, $p_e(r)$, $p_i(r)$, and $\rho(r)$ as parameters, which one can freely vary to determine the stability boundaries from (4.32). These inputs can indeed take any value locally, since one does not need to make them agree with global profiles in eq. (4.32), the equation being local itself.

In order to compare the results from the local approximation with those obtained with the eigenvalue equation (4.26), we solved eq. (4.32) for the case we considered in the previous section: isothermal equilibrium for the ions, $T_i = cst$, and zero temperature electrons, $p_e(r) = 0$, $p'(r) = p_i'(r)$. The results are shown in Figure 4.8, for $k_\perp r_{L_i} = 0.1$. In the local approximation, the growth rate is normalized by $\omega_{MHD} = \mathrm{v}_{T_i} / r$, where r is the generic location at which we solve eq. (4.32). Note that since in the local approximation we do not consider global profiles, it would be more natural to plot the growth rate versus $-rp_i' / p_i$ instead of $\nu = 2 - \frac{1}{2}\frac{rp_i'}{p_i}$. This is indeed what is generally done. Nevertheless, we chose to plot our curves versus ν to facilitate the comparison with the previous figures.

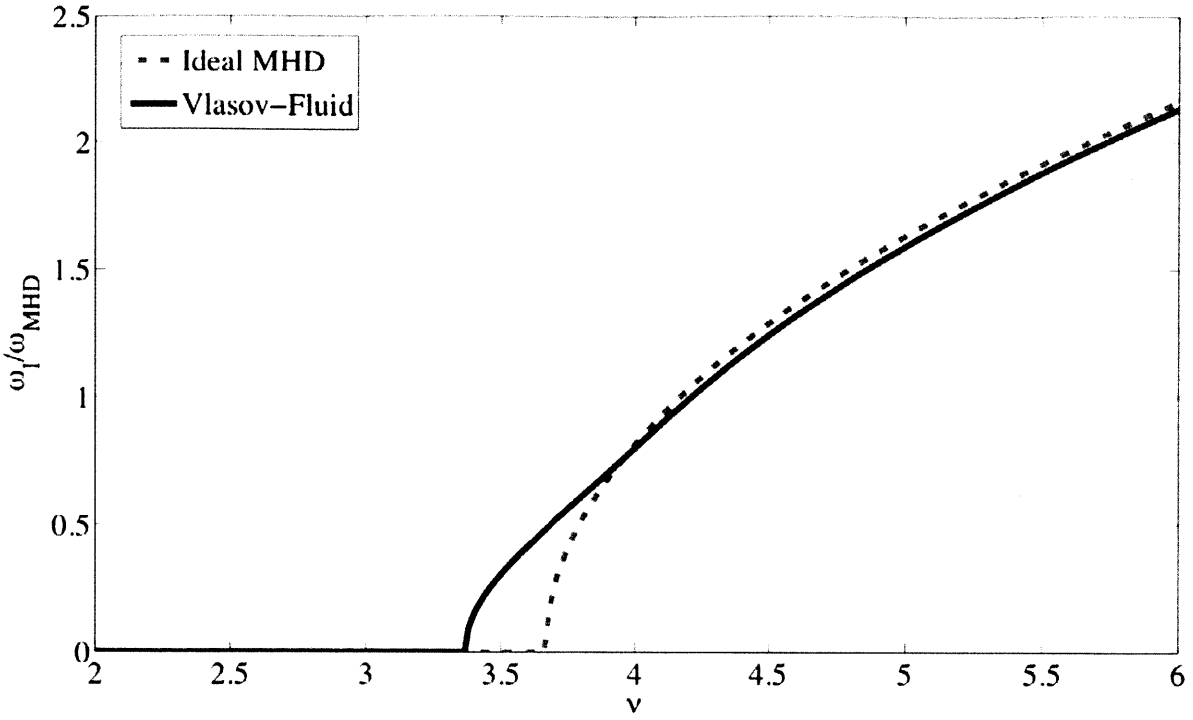

Fig. 4.8. Normalized Vlasov-fluid and ideal MHD growth rates of the interchange instability in the local approximation as a function of $\nu = 2 - \frac{1}{2}\frac{rp_i'}{p_i}$. ($k_\perp r_{L_i} = 0.1$).

Comparing Fig. 4.6 and Fig. 4.8, we see that in the ideal MHD unstable regime, the local and global VF growth rates have the same qualitative behavior. However, this not remain the case in the ideal MHD stable regime. While in the global case, the instability persists all the way to $\nu = 2$ because of the ion resonant effects, in the local case the VF interchange mode is stable for $\nu \leq 3.3$ (the exact boundary depends on the value of $k_\perp r_{L_i}$). In other words, the resonant particle effects are not entirely captured in the local approximation. The reason for the discrepancy is that the resonance condition,

$$\omega - \frac{1}{2}\frac{k_\perp \mathrm{v}_{T_i}^2}{r\omega_c}\frac{rp_i'}{p_i} - \frac{k_\perp \mathrm{v}_{T_i}^2}{r\omega_c}\left(\frac{u_\perp^2}{2\mathrm{v}_{T_i}^2} + \frac{u_\parallel^2}{\mathrm{v}_{T_i}^2}\right) = 0 \tag{4.33}$$

which requires that

$$\omega - \frac{1}{2}\frac{k_\perp \mathrm{v}_{T_i}^2}{r\omega_c}\frac{rp_i'}{p_i} > 0 \tag{4.34}$$

depends on the details of the equilibrium profiles in two different ways. The first way these details enter in (4.34) is explicit, namely through the quantity rp_i' / p_i, which varies across the plasma. The second way it enters is somewhat more implicit: when we solve the global eigenvalue equation, the value of ω also depends on the details of the equilibrium profiles. For instance, when we solve the global ideal MHD global eigenvalue equation, the growth rate in the ideal MHD unstable regime is smaller than that from the local approximation, because in the global calculation, there are parts of the pressure profile which are not as steep, and therefore not ideal MHD unstable.

The discrepancy between the global and the local approaches within the VF model suggests that it may be interesting to go beyond the local approximation when a kinetic equation other than the VF equation is used to study the stability properties of Z-pinches and levitated dipoles. To further motivate the need for global kinetic studies, we show that in the limit $k_\perp r_{L_i} \ll 1$, the VF and gyrokinetic local approximations agree.

For this comparison, we consider a more standard case for the VF equilibrium: $p_e = p_i = p/2$, $T_e = T_i = T$, $T_i' = 0$, $p_e' = \gamma_e p_i'$. Electrons can now have a finite temperature without causing difficulties because the analysis is local, and we do not have to worry about the consistency of the global profiles.

We obtain the gyrokinetic equivalent of the VF equation by following the derivation by Kesner and Hastie [19] for collisionless ions and collisional electrons, with two modifications: 1) we consider the hard-core Z-pinch geometry instead of a dipole configuration 2) we keep the Finite Larmor Radius (FLR) terms which are responsible for the MHD mode (Kesner and Hastie neglect them, as they focus on the entropy mode). In order to compare identical equilibria, we choose $\eta_i = 0$ and $\eta_e = \gamma_e - 1$, where for both species η is defined by $\eta = d\ln T / d\ln n$. In these conditions, the gyrokinetic analysis leads to the following local dispersion relation:

$$2 - \left(\Omega + \frac{1}{2}\frac{rp_i'}{p_i}\right)\left[F(\Omega) + \frac{k_\perp^2 r_{L_i}^2}{2}\partial_\beta F(\Omega)\right] - \frac{\Omega^2 - \Omega\left(\frac{1}{2}\frac{rp_i'}{p_i} - \frac{7}{3}\right) - \frac{1}{2}\frac{rp_i'}{p_i}\left(\frac{10}{3} - \gamma_e\right)}{\Omega^2 + \frac{10}{3}\Omega + \frac{5}{3}} = 0 \quad (4.35)$$

We solve eq. (4.32) and eq. (4.35), and plot the interchange growth rate in each model as a function of $\nu = 2 - \frac{1}{2}\frac{rp'}{p}$. The results are illustrated in Figure 4.9, for $k_\perp r_{L_i} = 0.05$. They confirm the agreement between the local VF and gyrokinetic equations in the limit $k_\perp r_{L_i} \ll 1$.

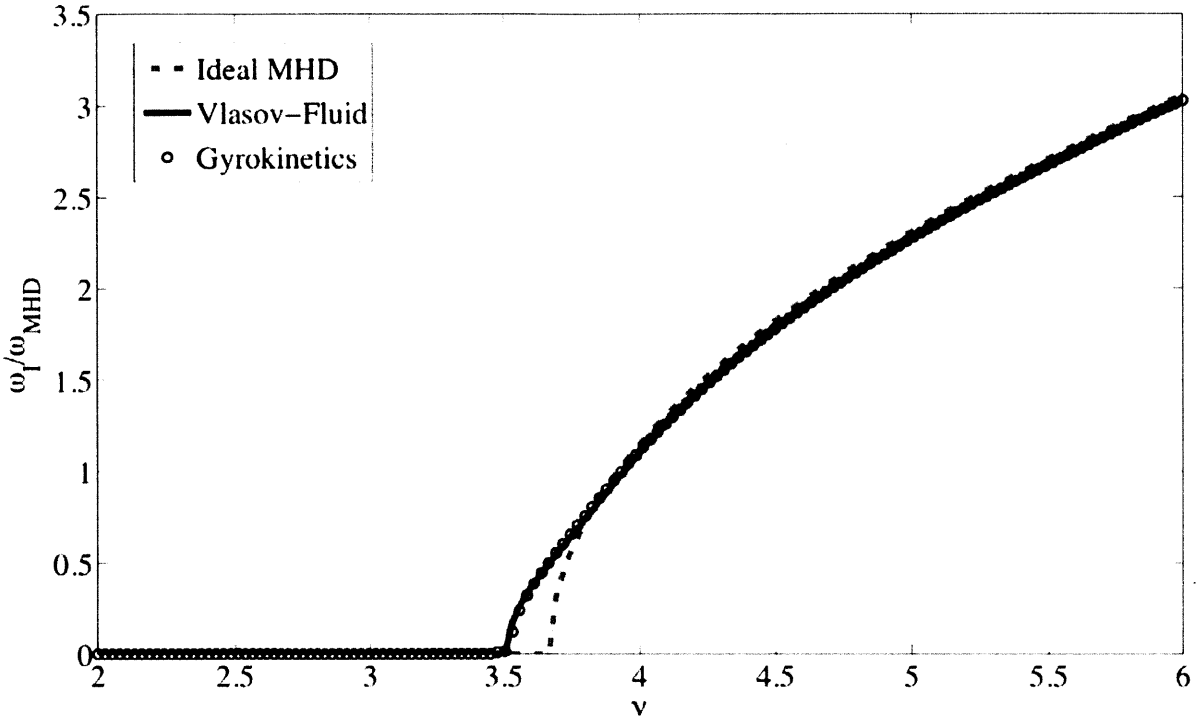

Fig. 4.9. Normalized Vlasov-fluid, gyrokinetics and ideal MHD growth rates of the interchange instability in the local approximation as a function of $\nu = 2 - \frac{1}{2}\frac{rp'}{p}$.

$(k_\perp r_{L_i} = 0.05)$.

4.4 Conclusion

We have demonstrated rigorously, in the hard-core Z-pinch geometry, the result which we had conjectured for general 3-D geometries in Chapter 3: even in a closed field line system, the stability boundary in the Vlasov-Fluid model is given by the incompressible condition $\delta W_\perp = 0$. We found that the $m = 0$ interchange instability, which is stabilized by plasma compressibility in the ideal MHD model, persists beyond the ideal MHD stability limit in the VF model. The absence of

plasma compressibility in the VF model is due to the wave-particle resonance associated with the perpendicular precession drift motion of the ions (i.e. the $\mathbf{E} \times \mathbf{B}$ drift and magnetic drifts). Consequently, the Vlasov-Fluid interchange mode, which is associated with equilibria for which the ion equilibrium distribution function only depends on the total energy, is only stable for pressure profiles which do not decay. Such profiles do not correspond to confined equilibria.

Since the hard-core Z-pinch represents the large aspect ratio limit of the levitated dipole, we expect that a similar calculation with the VF model, for the same class of allowable equilibria, in which the ions are electrostatically confined, would find that the VF interchange instability also persists beyond the ideal MHD limit in the dipole geometry.

In order to know if an instability of this nature could be observed in the LDX, and if the possible absence of plasma compressibility could negatively affect the behavior of the plasma in the experiment, further theoretical investigation is necessary, in two directions.

First, the role of resonant particles on the interchange mode has to be studied with models which describe more general ion distribution functions than the VF model, such as a gyrokinetics model for instance. With such models, equilibria which are experimentally relevant to LDX could be considered, in particular equilibria in which the ions are magnetically confined. As Section 4.3.4 shows, however, it will be

crucial in these new kinetic calculations to look at the *global* behavior of the interchange mode. Indeed, with the VF model, the persistence of the instability for any decaying pressure profile was observed by solving the global eigenvalue equation, but not found in the solution of the local approximation of this eigenvalue equation.

Finally, it is important to keep in mind that in all our discussions, we were only concerned with the question of *linear* stability. As an extension of our work, it would be interesting to look into the nonlinear evolution of the VF interchange instability (or its equivalent in a more experimentally relevant kinetic model), in order to better understand its behavior and its characteristics (thereby facilitating its experimental observation), and to determine if it can lead to catastrophic MHD behavior, and the loss of plasma confinement.

Chapter 4 – References

[1] J. Kesner, L. Bromberg, D. Garnier, and M. Mauel, 17th IAEA Conference of Plasma Physics and Controlled Nuclear Fusion, Yokohama, Japan 1998, (IAEA Vienna 1999), paper IAEA-F1-CN-69/ICP/09

[2] A. Kouznetsov, J.P. Freidberg, and J. Kesner, *Phys. Plasmas* **14**, 012503 (2007)

[3] A. Kouznetsov, J.P. Freidberg, and J. Kesner, *Phys. Plasmas* **14**, 102501 (2007)

[4] A. Kouznetsov, J.P. Freidberg, and J. Kesner, *Phys. Plasmas* **14**, 102502 (2007)

[5] P. Ricci, B.N. Rogers, and W. Dorland, *Phys. Rev. Lett.* **97**, 245001 (2006)

[6] P. Ricci, B.N. Rogers, W. Dorland, and M. Barnes, *Phys. Plasmas* **13**, 062102 (2006)

[7] S. Kobayashi, B.N. Rogers, and W. Dorland, *Phys. Rev. Lett.* **103**, 055003 (2009)

[8] A. Hasegawa, *Comments on Plasma Physics and Controlled Fusion*, **11**, 147 (1987)

[9] D.T. Garnier, A.K. Hansen, J. Kesner, M.E. Mauel, P.C. Michael, J.V. Minervini, A. Radovinsky, A. Zhukovsky, A. Boxer, J.L. Ellsworth, I. Karim, E.E. Ortiz, *Fusion Engineering and Design* **81** (2006) 2371-2380

[10] A.C. Boxer, R. Bergmann, J.L. Ellsworth, D.T. Garnier, J. Kesner, M. Mauel, and P. Woskov, *Nature Physics* **6**, 207-212 (2010)

[11] J.P. Freidberg, *Plasma Physics and Fusion Energy*, Cambridge University Press (2007)

[12] M. Okabayashi, J. Bialek, M.S. Chance, M.S. Chu, E.D. Fredrickson, A.M. Garofalo, M. Gryaznevich, R.E. Hatcher, T.H. Jensen, L.C. Johnson, R.J. La Haye, E.A. Lazarus, M.A. Makowski, J. Manickam, G.A. Navratil, J.T. Scoville, E.J. Strait, A.D. Turnbull, and M.L. Walker, *Phys. Plasmas* **8**, 2071 (2001)

[13] J.P. Freidberg, *Rev. Mod. Phys.*, Vol. 54, No. 3, July 1982

[14] A. Zhukovsky and D.T. Garnier, *IEEE Transactions on Applied Superconductivity*, Vol. 16, No. 2, pp. 898-901, June 2006

[15] B.B. Kadomtsev, in *Reviews of Plasma Physics*, edited by M.A. Leontovich, Consultants Bureau, New York, Vol. II (1966)

[16] J.P. Freidberg, *Ideal Magnetohydrodynamics*, (Plenum, New York, 1987)

[17] A.N. Simakov, P.J. Catto, and R.J. Hastie, *Phys. Plasmas* **8**, 4414 (2001)

[18] A.N.Simakov, R.J. Hastie, and P.J. Catto, *Phys. Plasmas* **9**, 201 (2002)

[19] J. Kesner and R.J. Hastie, *Phys. Plasmas* **9**, 395 (2002)

[20] M. Kotschenreuther, G. Rewoldt, and W. M. Tang, *Comput. Phys. Commun.* **88**, 128 (1995)

[21] W. Dorland, F. Jenko, M. Kotschenreuther, and B. N. Rogers, *Phys. Rev. Lett.* **85**, 5579 (2000)

[22] T.M. Antonsen, Jr. and B. Lane, *Phys. Fluids* **23**, 1205 (1980)

[23] H. Biglari, P. H. Diamond, and M. N. Rosenbluth, *Phys. Fluids B* **1**, 109 (1989)

[24] M. Coppins, *Phys. Fluid B* **1**, 591 (1989)

[25] G.F. Chew, M.L. Goldberger, and F.E. Low, *Proc. R. Soc. Lond. A* **236** (1956) pp. 112-118

Chapter 5

Summary and Conclusions

In the first part of this thesis, we presented new analytic solutions of the Grad-Shafranov equation with source functions which are linear in the flux function Ψ and with source functions which are quadratic in Ψ. These solutions have several degrees of freedom, in the form of free constants which are to be determined from the boundary constraints on the plasma surface. Depending on the choice of the boundary constraints, our solutions can be used to calculate equilibria in standard tokamaks and spherical tokamaks, with or without up-down asymmetry, for plasma surfaces which can be smooth or have divertor X-points, and for arbitrary aspect ratio, elongation, and triangularity.

In the case of source functions which are linear in Ψ, the so-called Solov'ev case, the same solutions can even be used to calculate spheromak and FRC equilibria. The more complex solutions obtained for source functions which are quadratic in Ψ are more realistic, but do not always converge for the extreme geometric parameters associated with spheromaks and FRCs (very large inverse aspect ratio for spheromaks, and very large elongation for FRCs).

Importantly, the versatility of our solutions does not come at the expense of computational complexity. Indeed, the determination of the free constants only involves the numerical resolution of a system of at most 13 algebraic equations, and most of the constants appear linearly in the solutions, as multiplying coefficients. In the worst case, only two constants appear nonlinearly in the system of equations. This is a trivial computational problem, which is easily solved with any built-in root solver.

In the second part of this thesis, we showed with the Vlasov-Fluid model that in both ergodic and closed field line magnetic geometries, the marginal stability condition for MHD modes in plasmas with electrostatically confined collisionless ions is given by $\delta W_{\perp} = 0$, where $\delta W_{\perp}$ is the ideal MHD potential energy associated with *incompressible* displacements. This condition is exactly identical to the ideal MHD condition for marginal stability in ergodic systems. In other words, in ergodic systems, ideal MHD linear stability theory accurately predicts the behavior of macroscopic modes. Given the relative simplicity of the ideal MHD model as compared to the models constructed to describe collisionless plasmas, this result speaks in favor of the continued use of ideal MHD for the study of large scale modes and instabilities in such configurations as the tokamaks and spherical tokamaks.

In closed line systems, the VF result means that the ideal MHD marginal stability criterion can be inaccurate and optimistic, since it predicts extra stability

coming from plasma compressibility, which is entirely absent in the Vlasov-Fluid criterion. Both criteria can be directly compared because the VF criterion is derived assuming that the ion equilibrium distribution function only depends on the total energy, so that the ions are in static equilibrium, as in ideal MHD. The absence of plasma compressibility in the VF equilibria, which describe electrostatically confined ions, is associated with ion kinetic effects perpendicular to the magnetic field lines, and is noteworthy for two reasons. First, it may affect the plasma performance in closed line configurations such as the levitated dipole, which explicitly rely on plasma compressibility by design. Second, from a theoretical point of view, it highlights the fact that drift resonances play a crucial role, which implies that kinetic models only allowing resonances parallel to the magnetic field lines, such as kinetic MHD, give an incomplete picture of MHD stability.

Our Vlasov-Fluid study of the hard-core Z-pinch, a closed line configuration, confirmed these results, which we had first derived for general 3-D geometries. While in ideal MHD plasma compressibility stabilizes the interchange mode, allowing stable and well confined equilibria with steep pressure profiles, in the Vlasov-Fluid model, which applies to equilibria with electrostatically confined ions, the interchange instability persists for any decaying pressure profile. When the wavelength of the mode is large, $k_\perp r_{L_i} \ll 1$, the growth rate of the instability in the ideal MHD stable regime is exponentially small. However, the growth rate increases with increasing $k_\perp$,

and for $k_\perp r_{L_i} \sim 1$, it may be comparable with the ideal MHD growth rate, even in the ideal MHD stable regime. Since interchange modes typically have short wavelengths, this instability may be observed in closed line confinement experiments, provided that the plasma is hot enough for the ions to be collisionless, and that the ions are in electrostatic equilibrium. It would therefore be interesting to study the nonlinear, fully developed stage of the instability, in order to better characterize it, and facilitate its experimental identification.

Ideally, such a nonlinear study would be performed using the gyrokinetic equation, and gyrokinetic codes, since the gyrokinetic model allows for plasma equilibria which are more general than the Vlasov-Fluid equilibria, and contains more physics than the VF model (which explains its relative complexity). However, a word of caution is necessary. When we make the same local approximation in the Vlasov-Fluid model as is usually made in kinetic calculations, the linear stability picture we find is qualitatively different from the picture obtained without the approximation. Specifically, in the local approximation, the wave-particle resonances are not accurately captured, and extra regions of stability are found. Thus, our results seem to call for a non-local gyrokinetic study of the stability properties of the LDX. As far as we know, this remains to be done.

Appendix A

Kinetic MHD Energy Relation

In this appendix, we rederive and extend the Kinetic MHD stability results derived in references [16], [20], [21], [22], [23] of Chapter 3.

General formulation

The desired energy relation is formulated in terms of the familiar perturbed fluid displacement $\boldsymbol{\xi}$ defined by $\tilde{\mathbf{v}} = \partial\boldsymbol{\xi} / \partial t = -i\omega\boldsymbol{\xi}$. The analysis is carried out by (1) linearizing the momentum equation, (2) solving for the perturbed kinetic MHD distribution function, (3) forming an energy integral, and (4) rewriting the energy integral in a form from which it is possible to deduce a comparison theorem.

- **The linearized momentum equation**

The linearized form of the momentum equation is straightforward to derive from eq. (3.45), and is given by

$$-\omega^2\rho\boldsymbol{\xi} = \mathbf{J}\times\tilde{\mathbf{B}} + \tilde{\mathbf{J}}\times\mathbf{B} - \sum_j \nabla\cdot\tilde{\mathsf{P}}_j \tag{A.1}$$

where $\sum_j$ indicates a sum over the two species, and for each species

$$\nabla\cdot\tilde{\mathsf{P}} = \nabla\tilde{p}_{\perp} + \left(\tilde{p}_{\parallel} - \tilde{p}_{\perp}\right)\boldsymbol{\kappa} + \mathbf{b}\left[\mathbf{B}\cdot\nabla\left(\frac{\tilde{p}_{\parallel} - \tilde{p}_{\perp}}{B}\right)\right] \tag{A.2}$$

- **The perturbed distribution function**

Consider next the perturbed distribution function which satisfies the linearized form of the kinetic MHD equation (eqs. (3.124) and (3.125)).

$$-i\omega\tilde{f} + w_{\parallel}\mathbf{b}\cdot\nabla\tilde{f} - i\omega\boldsymbol{\xi}_{\perp}\cdot\nabla f + w_{\parallel}\tilde{\mathbf{b}}\cdot\nabla f + \tilde{\varepsilon}\frac{\partial f}{\partial\varepsilon} = 0 \tag{A.3}$$

Remember that $\mathbf{w}$ is the random component of particle velocity while $\mathbf{v} = \mathbf{v}(\mathbf{r},t)$ is the macroscopic plasma velocity (which consists of the parallel flow and the $\mathbf{E}\times\mathbf{B}$ drift). Also, the velocity variables used in the Kinetic MHD equation are ε and μ, defined by $\varepsilon = \frac{mw^2}{2}$ and $\mu = \frac{mw_{\perp}^2}{2B}$. Eq. (A.3) is simplified as follows. First, note that the total time derivative along the unperturbed orbit for any quantity $g(\mathbf{r},\varepsilon,\mu,t) = \hat{g}(\mathbf{r},\varepsilon,\mu)\exp(-i\omega t)$ is defined by

$$\frac{dg}{dt} \equiv \left(\frac{\partial}{\partial t} + w_{\parallel}\mathbf{b}\cdot\nabla\right)g = \left(-i\omega + w_{\parallel}\mathbf{b}\cdot\nabla\right)g \tag{A.4}$$

Second, using the linearized form of Faraday's law it can easily be shown that $\tilde{\mathbf{b}}\cdot\nabla\psi = \mathbf{b}\cdot\nabla(\nabla\psi\cdot\boldsymbol{\xi}_{\perp})$. Third, the linearized quantity $\tilde{\varepsilon}$ can be written as

$$\tilde{\varepsilon} = qw_{\parallel}\tilde{E}_{\parallel} + i\omega m\left[-i\omega w_{\parallel}\xi_{\parallel} + \frac{w_{\perp}^2}{2}\nabla\cdot\boldsymbol{\xi} - \left(\frac{w_{\perp}^2}{2} - w_{\parallel}^2\right)\left(\mathbf{b}\cdot\nabla\xi_{\parallel} - \boldsymbol{\xi}_{\perp}\cdot\boldsymbol{\kappa}\right)\right] \tag{A.5}$$

Now, keeping in mind that that the basic velocity variables are ε, μ it follows that $dw_{\|} / dt = \pm d\left[(2/m)(\varepsilon - \mu B)\right]^{1/2} / dt = -\left(w_{\perp}^2 / 2B\right)\mathbf{b} \cdot \nabla B$. Thus, after grouping all the $\xi_{\|}$ terms together, we can rewrite eq. (A.5) as

$$\tilde{\varepsilon} = q w_{\|} \tilde{E}_{\|} + \frac{d}{dt}\left(i\omega m w_{\|} \xi_{\|}\right) + i\omega m \left[\frac{w_{\perp}^2}{2} \nabla \cdot \boldsymbol{\xi}_{\perp} + \left(\frac{w_{\perp}^2}{2} - w_{\|}^2\right)\left(\boldsymbol{\xi}_{\perp} \cdot \boldsymbol{\kappa}\right)\right] \tag{A.6}$$

The last step is to introduce scalar and vector potentials into the expression for $\tilde{E}_{\|}$: $\tilde{E}_{\|} = -\mathbf{b} \cdot \nabla \tilde{\phi} + i\omega \tilde{A}_{\|}$. Combining the results from all of these sub-steps leads to the following equation for $\tilde{f}$.

$$\begin{aligned} &\frac{d}{dt}\left(\tilde{f} + \boldsymbol{\xi}_{\perp} \cdot \nabla f + i\omega m w_{\|} \xi_{\|} \frac{\partial f}{\partial \varepsilon} - q\tilde{\phi} \frac{\partial f}{\partial \varepsilon}\right) + \\ &\qquad i\omega \left[q\left(w_{\|} \tilde{A}_{\|} - \tilde{\phi}\right) + \frac{m w_{\perp}^2}{2} \nabla \cdot \boldsymbol{\xi}_{\perp} + m\left(\frac{w_{\perp}^2}{2} - w_{\|}^2\right)\left(\boldsymbol{\xi}_{\perp} \cdot \boldsymbol{\kappa}\right)\right] \frac{\partial f}{\partial \varepsilon} = 0 \end{aligned} \tag{A.7}$$

The desired expression for $\tilde{f}$ is obtained by integrating along the unperturbed orbits assuming that $\mathrm{Im}(\omega) > 0$,

$$\begin{aligned} \tilde{f}\left(\mathbf{r}, \varepsilon, \mu, t\right) &= \tilde{f}_F + \tilde{f}_K \\ \tilde{f}_F &= -\boldsymbol{\xi}_{\perp} \cdot \nabla f - i\omega m w_{\|} \xi_{\|} \frac{\partial f}{\partial \varepsilon} + q\tilde{\phi} \frac{\partial f}{\partial \varepsilon} \\ \tilde{f}_K &= -i\omega \tilde{s} \frac{\partial f}{\partial \varepsilon} \end{aligned} \tag{A.8}$$

where

$$\tilde{s} = \int_{-\infty}^{t} \left[q\left(w_{\|} \tilde{A}_{\|} - \tilde{\phi}\right) + \frac{m w_{\perp}^2}{2} \nabla \cdot \boldsymbol{\xi}_{\perp} + m\left(\frac{w_{\perp}^2}{2} - w_{\|}^2\right)\left(\boldsymbol{\xi}_{\perp} \cdot \boldsymbol{\kappa}\right)\right] dt' \tag{A.9}$$

The quantities $\tilde{f}_F$ and $\tilde{f}_K$ represent the fluid and kinetic contributions to $\tilde{f}$ respectively.

- **The energy integral**

To begin, observe that the fluid contributions to the density and pressure are given by

$$\begin{aligned}
\tilde{n}_F &= \int \tilde{f}_F \, d\mathbf{w} = -\boldsymbol{\xi}_\perp \cdot \nabla n \\
\tilde{p}_{F\perp} &= \int \frac{m w_\perp^2}{2} \tilde{f}_F \, d\mathbf{w} = -\boldsymbol{\xi}_\perp \cdot \nabla p \\
\tilde{p}_{F\parallel} &= \int m w_\parallel^2 \tilde{f}_F \, d\mathbf{w} = -\boldsymbol{\xi}_\perp \cdot \nabla p
\end{aligned} \tag{A.10}$$

We now derive an energy relation by forming the dot product of eq. (A.1) with $\boldsymbol{\xi}_\perp^*$ and integrating over the plasma volume.

$$\begin{aligned}
\omega^2 K_\perp &= \delta W_\perp + \delta Q_{kk} \\
K_\perp &= \int \rho \left| \boldsymbol{\xi}_\perp \right|^2 d\mathbf{r} \\
\delta W_\perp &= -\int \left[\boldsymbol{\xi}_\perp^* \cdot \left(\tilde{\mathbf{J}} \times \mathbf{B} + \mathbf{J} \times \tilde{\mathbf{B}} \right) - (\nabla \cdot \boldsymbol{\xi}_\perp^*)(\boldsymbol{\xi}_\perp \cdot \nabla p) \right] d\mathbf{r} \\
\delta Q_{kk} &= -\sum_j \int \left[\tilde{p}_{K\perp} \nabla \cdot \boldsymbol{\xi}_\perp^* + (\tilde{p}_{K\perp} - \tilde{p}_{K\parallel})(\boldsymbol{\xi}_\perp^* \cdot \boldsymbol{\kappa}) \right] d\mathbf{r}
\end{aligned} \tag{A.11}$$

where $p(\psi) = p_i(\psi) + p_e(\psi)$ and we have used a simple integration by parts to obtain the terms containing $\nabla \cdot \boldsymbol{\xi}_\perp^*$. The quantity $\delta W_\perp$ represents the ideal MHD potential energy for *incompressible displacements* while δQ_{kk} is the kinetic contribution in which every term contains the trajectory integral $\tilde{s}$. To keep the analysis relatively

concise we focus on internal modes which simplifies the boundary conditions although it is straightforward to generalize the results to include external modes.

The task now is to simplify the expression for δQ_{kk} in order to be able to deduce an MHD comparison theorem. We begin by substituting for the definitions of $\tilde{p}_{K\perp}$ and $\tilde{p}_{K\parallel}$ in δQ_{kk}.

$$\delta Q_{kk} = i\omega \sum_j \int \left[\frac{m w_\perp^2}{2} \nabla \cdot \boldsymbol{\xi}_\perp^* + \left(\frac{m w_\perp^2}{2} - m w_\parallel^2 \right) (\boldsymbol{\xi}_\perp^* \cdot \boldsymbol{\kappa}) \right] \tilde{s} \frac{\partial f}{\partial \varepsilon} d\mathbf{w}\, d\mathbf{r} \tag{A.12}$$

To proceed further we must at this point distinguish between the two different classes of magnetic geometry of interest: (1) either ergodic systems or closed line systems undergoing symmetry breaking perturbations and (2) closed line systems undergoing perturbations that maintain the closed line symmetry. The reason for the separation is that for case (1) the ideal MHD potential energy at marginal stability corresponds to incompressible displacements. This makes it relatively straightforward to deduce a stability comparison theorem since all that is needed is a determination of the sign of δQ_{kk}. For case (2) however, ideal MHD at marginal stability includes a stabilizing contribution from the plasma compressibility. In this case we must work considerably harder to estimate the magnitude as well as the sign of δQ_{kk} to deduce the stability comparison theorem.

- **Case (1) Ergodic systems**

We proceed by adding and subtracting the quantity $q(w_{\|}\tilde{A}_{\|}^{*}-\tilde{\phi}^{*})$ from the integrand in δQ_{kk} in eq. (A.12), recognizing that

$$\begin{aligned}\frac{d\tilde{s}^{*}}{dt} &= i\omega^{*}\tilde{s}^{*}+w_{\|}\mathbf{b}\cdot\nabla\tilde{s}^{*}\\ &= \frac{mw_{\perp}^{2}}{2}\nabla\cdot\boldsymbol{\xi}_{\perp}^{*}+\left(\frac{mw_{\perp}^{2}}{2}-mw_{\|}^{2}\right)(\boldsymbol{\xi}_{\perp}^{*}\cdot\boldsymbol{\kappa})+q(w_{\|}\tilde{A}_{\|}^{*}-\tilde{\phi}^{*})\end{aligned} \tag{A.13}$$

The expression for δQ_{kk} reduces to

$$\delta Q_{kk}=i\omega\sum_{j}\int\left[\frac{d\tilde{s}^{*}}{dt}-q(w_{\|}\tilde{A}_{\|}^{*}-\tilde{\phi}^{*})\right]\tilde{s}\frac{\partial f}{\partial\varepsilon}d\mathbf{w}\,d\mathbf{r} \tag{A.14}$$

The term containing $\tilde{A}_{\|}^{*}$ vanishes because of the definition of the random velocity: $\int\mathbf{w}f\,d\mathbf{w}=0$. To see this, examine the parallel component of this relation and make use of eq. (A.8). The linearized form for each species simplifies to

$$\begin{aligned}0=q\int w_{\|}\tilde{f}\,d\mathbf{w} &= -i\omega\left[q\xi_{\|}\int mw_{\|}^{2}\frac{\partial f}{\partial\varepsilon}d\mathbf{w}+q\int w_{\|}\tilde{s}\frac{\partial f}{\partial\varepsilon}d\mathbf{w}\right]\\ &= -i\omega\left[-qn\xi_{\|}+q\int w_{\|}\tilde{s}\frac{\partial f}{\partial\varepsilon}d\mathbf{w}\right]\end{aligned} \tag{A.15}$$

Invoking charge neutrality then leads to the desired conclusion

$$\sum_{j}q\int w_{\|}\tilde{s}\frac{\partial f}{\partial\varepsilon}d\mathbf{w}=\xi_{\|}e\left(n_{i}-n_{e}\right)=0 \tag{A.16}$$

Equation (A.14) now can be written as

$$\delta Q_{kk} = i\omega \sum_j \int \left(\frac{d\tilde{s}^*}{dt} + q\tilde{\phi}^* \right) \tilde{s} \frac{\partial f}{\partial \varepsilon} d\mathbf{w}\, d\mathbf{r} \tag{A.17}$$

In a similar way we can simplify the term containing $\tilde{\phi}^*$ by making use of the charge neutrality condition. We again make use of eq. (A.8) to calculate the perturbed density for each species.

$$\begin{aligned} \tilde{n} &= -\boldsymbol{\xi}_\perp \cdot \nabla n - \frac{q\tilde{\phi}}{\hat{T}} n - i\omega \int \tilde{s} \frac{\partial f}{\partial \varepsilon} d\mathbf{w} \\ \frac{1}{\hat{T}} &= -\frac{1}{n} \int \frac{\partial f}{\partial \varepsilon} d\mathbf{w} \end{aligned} \tag{A.18}$$

Here $\hat{T}$ has the dimensions of temperature and is indeed equal to the temperature for a Maxwellian distribution function. We now set $q_e \tilde{n}_e + q_i \tilde{n}_i = 0$ which yields the following relation.

$$\tilde{\phi}^* = \frac{i\omega^*}{e^2 n} \frac{\hat{T}_i \hat{T}_e}{\hat{T}_i + \hat{T}_e} \sum_j \int q\tilde{s}^* \frac{\partial f}{\partial \varepsilon} d\mathbf{w} \tag{A.19}$$

To derive the comparison theorem we substitute the expression for $\tilde{\phi}^*$ in terms of the trajectory integrals from eq. (A.19) into eq. (A.17). A short calculation leads to a somewhat complicated expression given by

$$\begin{aligned} \delta Q_{kk} &= \delta Q_1 + \delta Q_2 + \delta Q_3 \\ &= -|\omega|^2 \sum_j \int |\tilde{s}|^2 \frac{\partial f}{\partial \varepsilon} d\mathbf{w}\, d\mathbf{r} \\ &\quad + i\omega \sum_j \int w_\parallel (\mathbf{b} \cdot \nabla \tilde{s}^*) \tilde{s} \frac{\partial f}{\partial \varepsilon} d\mathbf{w}\, d\mathbf{r} \\ &\quad - |\omega|^2 \int \left| \sum_j \int q\tilde{s} \frac{\partial f}{\partial \varepsilon} d\mathbf{w} \right|^2 \frac{\hat{T}_i \hat{T}_e}{e^2 n (\hat{T}_i + \hat{T}_e)} d\mathbf{r} \end{aligned} \tag{A.20}$$

The middle term can be simplified by writing $\tilde{s} = \tilde{s}_r + i\tilde{s}_i$ and expressing the velocity integral explicitly in terms of ε, μ

$$\begin{aligned}\delta Q_2 &= 2\pi i\omega \sum_j \int \nabla \cdot \left[\left(\frac{\tilde{s}_r^2 + \tilde{s}_i^2}{2m^2} \frac{\partial f}{\partial \varepsilon} \right) \mathbf{B} \right] d\varepsilon d\mu \, d\mathbf{r} \\ &+ 2\pi\omega \sum_j \int \left[\tilde{s}_r (\mathbf{b} \cdot \nabla \tilde{s}_i) - \tilde{s}_i (\mathbf{b} \cdot \nabla \tilde{s}_r) \right] \frac{B}{m^2} \frac{\partial f}{\partial \varepsilon} d\varepsilon d\mu \, d\mathbf{r}\end{aligned} \tag{A.21}$$

The first term vanishes by virtue of the divergence theorem when integrating over the plasma volume while the second term is of the form ωR where R is a real quantity. Thus, $\delta Q_2 = \omega R$.

The terms in the sum $\delta Q_1 + \delta Q_3$ can also be simplified by a simple algebraic rearrangement. This leads to a convenient form for δQ_{kk} that can be written as

$$\begin{aligned}\delta Q_{kk} &= \omega R + \delta W_{kk} \\ \delta W_{kk} &= |\omega|^2 \int \frac{d\mathbf{r}}{n} \hat{T}_i \left[\int \frac{\partial f_i}{\partial \varepsilon} d\mathbf{w} \int |\tilde{s}_i|^2 \frac{\partial f_i}{\partial \varepsilon} d\mathbf{w} - \left| \int \tilde{s}_i \frac{\partial f_i}{\partial \varepsilon} d\mathbf{w} \right|^2 \right] \\ &+ |\omega|^2 \int \frac{d\mathbf{r}}{n} \hat{T}_e \left[\int \frac{\partial f_e}{\partial \varepsilon} d\mathbf{w} \int |\tilde{s}_e|^2 \frac{\partial f_e}{\partial \varepsilon} d\mathbf{w} - \left| \int \tilde{s}_e \frac{\partial f_e}{\partial \varepsilon} d\mathbf{w} \right|^2 \right] \\ &+ |\omega|^2 \int \frac{d\mathbf{r}}{n(\hat{T}_i + \hat{T}_e)} \left| \hat{T}_i \int \tilde{s}_i \frac{\partial f_i}{\partial \varepsilon} d\mathbf{w} + \hat{T}_e \int \tilde{s}_e \frac{\partial f_e}{\partial \varepsilon} d\mathbf{w} \right|^2\end{aligned} \tag{A.22}$$

Clearly δW_{kk} is real, and by Schwarz's inequality satisfies $\delta W_{kk} \geq 0$.

The last step in the analysis is to combine the results leading to the following expression for the energy integral.

$$\omega^2 K_\perp = \delta W_\perp + \delta W_{kk} + \omega R \tag{A.23}$$

Observe that $K_\perp$, $\delta W_\perp$, δW_{kk}, and R are all real quantities. We now write $\omega = \omega_r + i\omega_i$ and set the real and imaginary parts of Eq. (A.23) to zero. The imaginary part yields an expression for R.

$$R = 2\omega_r K_\perp \tag{A.24}$$

This is substituted into the real part leading to

$$|\omega|^2 = -\frac{\delta W_\perp + \delta W_{kk}}{K_\perp} \tag{A.25}$$

Equation (A.25) is the desired form of the energy relation used in the main body of the text.

- **Case (2) Closed line systems**

Consider now the case of a closed line configuration undergoing a perturbation that maintains the closed line symmetry. We begin by writing down several coordinate transformations that appear frequently in the analysis. First, we focus on the integration over velocity space converting from $\mathbf{w} \rightarrow \varepsilon, \mu$.

$$\begin{aligned} \int g(\mathbf{r}, w_\perp, w_\parallel) d\mathbf{w} &= 2\pi \int_0^\infty w_\perp \, dw_\perp \int_{-\infty}^\infty dw_\parallel \, g \\ &= \frac{2^{1/2}\pi B}{m^{3/2}} \int_0^\infty d\varepsilon \int_0^{\varepsilon/B} \frac{d\mu}{(\varepsilon - \mu B)^{1/2}} \left(g_+ + g_-\right) \end{aligned} \tag{A.26}$$

where $g_\pm = g(\mathbf{r}, w_\perp, \pm|w_\parallel|)$.

The next transformation involves integration over the combined physical space, velocity space. This can be conveniently carried out by writing the magnetic field in Clebsch coordinates $\mathbf{B} = \nabla\psi \times \nabla\chi$ and choosing the third coordinates as l the arc

length along a magnetic field line. Noting that $d\mathbf{r} = d\psi d\chi dl / B$ we find after a short calculation

$$\begin{aligned}\int g(\mathbf{r}, w_\perp, w_\parallel)\, d\mathbf{r}\, d\mathbf{w} &= \frac{2^{1/2}\pi}{m^{3/2}} \int d\psi\, d\chi d\varepsilon \int_0^L dl \int_0^{\varepsilon/B} \frac{d\mu}{(\varepsilon - \mu B)^{1/2}} (g_+ + g_-) \\ &= \frac{2^{1/2}\pi}{m^{3/2}} \int d\psi\, d\chi d\varepsilon \int_0^{\varepsilon/B_{\min}} d\mu \int_{l_1}^{l_2} \frac{dl}{(\varepsilon - \mu B)^{1/2}} (g_+ + g_-)\end{aligned} \tag{A.27}$$

In the first form $L = L(\psi, \chi)$ is the length of a given magnetic line and it is assumed that $l = 0$ corresponds to the location of the field maximum: $B(l = 0) = B_{\max}$. In the second form we have switched the order of the l and μ integrations. Here $B_{\min}$ is the minimum value of the field and l_1, l_2 are the beginning and end points of the orbit. The values depend on whether the particle is passing or trapped. Specifically, $l_1 = 0$ and $l_2 = L(\psi, \chi)$ for a passing particle characterized by $\varepsilon / \mu > B_{\max}$. For a trapped particle satisfying $B_{\min} < \varepsilon / \mu < B_{\max}$, $l_1(\psi, \chi, \varepsilon, \mu), l_2(\psi, \chi, \varepsilon, \mu)$ correspond to the two turning points of the orbit: $\varepsilon / \mu = B(\psi, \chi, l_1) = B(\psi, \chi, l_2)$.

Lastly, we define two averages that appear in the analysis, one over the field line and the other over the unperturbed orbit.

$$\begin{aligned}\langle g \rangle &= \frac{\int_0^L g \frac{dl}{B}}{\int_0^L \frac{dl}{B}} && \text{field line average} \\ \langle g \rangle_b &= \frac{1}{\tau_b} \int_0^{\tau_b} g\, dt && \text{orbit average}\end{aligned} \tag{A.28}$$

where τ_b is the period of the orbit for passing particles and the half period of the bounce orbit for trapped particles

$$\tau_b = \int_0^{\tau_b} dt = \int_{l_1}^{l_2} \frac{dt}{dl} dl = \left(\frac{m}{2}\right)^{1/2} \int_{l_1}^{l_2} \frac{dl}{(\varepsilon - \mu B)^{1/2}} \tag{A.29}$$

The framework has now been set to obtain a useful bound on δQ_{kk} as defined in eq. (A.12). We make use of eq. (A.16) and write $\delta Q_{kk} = \delta Q_a + \delta Q_b$ where

$$\begin{aligned}
\delta Q_a &= i\omega \sum_j \int d\mathbf{r}\, d\mathbf{w} \frac{\partial f}{\partial \varepsilon} \left[\tilde{I}^* \int_{-\infty}^{t} \tilde{I}\, dt' \right] \\
\delta Q_b &= -i\omega \sum_j \int d\mathbf{r}\, d\mathbf{w} \frac{\partial f}{\partial \varepsilon} \left[\tilde{I}^* \int_{-\infty}^{t} q\tilde{\phi}\, dt' \right] \\
\tilde{I} &= \frac{m w_\perp^2}{2} \nabla \cdot \boldsymbol{\xi}_\perp + m \left(\frac{w_\perp^2}{2} - w_\parallel^2 \right) \left(\boldsymbol{\xi}_\perp \cdot \boldsymbol{\kappa} \right) + q w_\parallel \tilde{A}_\parallel
\end{aligned} \tag{A.30}$$

Next, we make use of the fact that the orbits of all particles (both passing and trapped) in a closed line system are periodic, thus allowing a Fourier decomposition in the trajectory integral. Writing $\tilde{I}(t') = e^{-i\omega t} \hat{I}(t'-t) = e^{-i\omega t} \hat{I}(\tau)$, the periodicity of the particles' motion implies that $\hat{I}(\tau)$ is periodic with a period (or half period for trapped particles) equal to τ_b. The Fourier representation can be written as

$$\begin{aligned}
\tilde{I}(t') &= e^{-i\omega t'} \hat{I}(\tau) = e^{-i\omega t'} \sum_n I_n e^{in\omega_b \tau} \\
I_n &= \frac{1}{\tau_b} \int_0^{\tau_b} \hat{I}(\tau) e^{-in\omega_b \tau}\, d\tau
\end{aligned} \tag{A.31}$$

It then follows that

$$\int_{-\infty}^{t} \tilde{I}(t')\, dt' = i e^{-i\omega t} \sum_n \frac{I_n}{\omega - n\omega_b} \tag{A.32}$$

As the system approaches marginal stability (i.e. $\omega^2 \to 0$) the $n = 0$ term dominates, leading to

$$\int_{-\infty}^{t} \tilde{I}(t')\,dt' \to i\frac{I_0}{\omega} = \left\langle \tilde{I} \right\rangle_b \tag{A.33}$$

A similar argument applies to the integral involving $\tilde{\phi}$. Thus in the limit $\omega^2 \to 0$, the contributions to δQ_{kk} reduce to

$$\begin{aligned} \delta Q_a &= -\sum_j \int d\mathbf{r}\, d\mathbf{w} \frac{\partial f}{\partial \varepsilon} \tilde{I}^* \left\langle \tilde{I} \right\rangle_b \\ \delta Q_b &= \sum_j \int d\mathbf{r}\, d\mathbf{w} \frac{\partial f}{\partial \varepsilon} \tilde{I}^* \left\langle q\tilde{\phi} \right\rangle_b \end{aligned} \tag{A.34}$$

and are finite.

We now focus on δQ_a and obtain a simple lower bound. Utilizing the second form in eq. (A.27) allows us to write

$$\begin{aligned} \delta Q_a &= -\sum_j \frac{2\pi}{m^2} \int d\psi\, d\chi\, d\varepsilon \frac{\partial f}{\partial \varepsilon} G(\psi, \chi, \varepsilon) \\ G &= \int_0^{\varepsilon/B_{\min}} d\mu \left[\tau_b \left(\left| \left\langle \tilde{I}_+ \right\rangle_b \right|^2 + \left| \left\langle \tilde{I}_- \right\rangle_b \right|^2 \right) \right] \end{aligned} \tag{A.35}$$

A simple lower bound follows from an application of Schwarz's inequality.

$$G \geq \frac{1}{\int_0^{\varepsilon/B_{\min}} \tau_b\, d\mu} \left[\left| \int_0^{\varepsilon/B_{\min}} d\mu\, \tau_b \left\langle \tilde{I}_+ \right\rangle_b \right|^2 + \left| \int_0^{\varepsilon/B_{\min}} d\mu\, \tau_b \left\langle \tilde{I}_- \right\rangle_b \right|^2 \right] \tag{A.36}$$

This form is useful because after again reversing the order of integration between μ and l, we can analytically carry out the μ integrations. For example, the denominator integral reduces to

$$\int_0^{\varepsilon/B_{\min}} \tau_b \, d\mu = \left(\frac{m}{2}\right)^{1/2} \int_0^L dl \int_0^{\varepsilon/B} \frac{d\mu}{(\varepsilon - \mu B)^{1/2}}$$
$$= (2m)^{1/2} \varepsilon^{1/2} \int_0^L \frac{dl}{B} \tag{A.37}$$

Similarly, we find

$$\int_0^{\varepsilon/B_{\min}} \tau_b \left\langle \tilde{I}_\pm \right\rangle_b d\mu = \left(\frac{m}{2}\right)^{1/2} \int_0^L dl \int_0^{\varepsilon/B} \frac{\tilde{I}_\pm d\mu}{(\varepsilon - \mu B)^{1/2}}$$
$$= \left(\frac{m}{2}\right)^{1/2} \frac{4}{3} \varepsilon^{3/2} \int_0^L \nabla \cdot \boldsymbol{\xi}_\perp \frac{dl}{B} \pm q\varepsilon \int_0^L \tilde{A}_\parallel \frac{dl}{B} \tag{A.38}$$

These results are substituted back into eqs. (A.35) and (A.36). After an integration by parts the ε integrals can be evaluated analytically in terms of n and p. The end result is the desired estimate of δQ_a given by

$$\delta Q_a \geq \int \frac{5}{3} p \left| \left\langle \nabla \cdot \boldsymbol{\xi}_\perp \right\rangle \right|^2 d\mathbf{r} + \sum_j \int \frac{3n}{4m} \left| \left\langle e\tilde{A}_\parallel \right\rangle \right|^2 d\mathbf{r} \tag{A.39}$$

Observe that the first term on the right hand side is just the ideal MHD δW_C.

The electromagnetic term also appears to be stabilizing although in actual fact its value is equal to zero. This can be seen by utilizing eq. (A.16). We multiply by $\tilde{A}_\parallel^*$ and integrate over the plasma volume which after a short calculation leads to

$$0 = -i\omega \sum_j q \int \tilde{A}_\parallel^* w_\parallel \tilde{s} \frac{\partial f}{\partial \varepsilon} d\mathbf{w}\, d\mathbf{r} = \sum_j \frac{4\pi}{m^2} \int d\psi\, d\chi d\varepsilon \frac{\partial f}{\partial \varepsilon} H$$
$$H = \int_0^{\varepsilon/B_{\min}} \frac{d\mu}{\tau_b} \left| \int_{l_1}^{l_2} e\tilde{A}_\parallel \, dl \right|^2 \tag{A.40}$$

We now add and subtract a term from the function H as follows

$$H = \int_0^{\varepsilon/B_{\min}} \frac{d\mu}{\tau_b} \left| \int_{l_1}^{l_2} e\tilde{A}_\parallel \, dl \right|^2$$
$$= \frac{1}{\int \tau_b \, d\mu} \left\{ \int \tau_b \, d\mu \int \frac{d\mu}{\tau_b} \left| \int e\tilde{A}_\parallel \, dl \right|^2 - \left| \int d\mu \int e\tilde{A}_\parallel \, dl \right|^2 + \left| \int d\mu \int e\tilde{A}_\parallel \, dl \right|^2 \right\} \tag{A.41}$$

In the last term the order of the l and μ integrations is reversed. The term can now be analytically integrated over μ after which the entire expression is substituted into eq. (A.40), yielding

$$\sum_j \int \frac{3n}{4m} \left| \left\langle e\tilde{A}_\parallel \right\rangle \right|^2 d\mathbf{r} = \sum_j \frac{4\pi}{m^2} \int d\psi \, d\chi d\varepsilon \frac{\partial f}{\partial \varepsilon} J$$
$$J = \frac{1}{\int \tau_b \, d\mu} \left\{ \int \tau_b \, d\mu \int \frac{d\mu}{\tau_b} \left| \int e\tilde{A}_\parallel \, dl \right|^2 - \left| \int d\mu \int e\tilde{A}_\parallel \, dl \right|^2 \right\} \tag{A.42}$$

Since $J \geq 0$ by Schwarz's inequality it follows that for $\partial f / \partial \varepsilon < 0$

$$\sum_j \int \frac{3n}{4m} \left| \left\langle e\tilde{A}_\parallel \right\rangle \right|^2 d\mathbf{r} \leq 0 \tag{A.43}$$

which is a contradiction that can only be resolved if $\left\langle e\tilde{A}_\parallel \right\rangle = 0$. Thus, the overall conclusion from eq. (A.39) is that

$$\delta Q_a \geq \int \frac{5}{3} p \left| \left\langle \nabla \cdot \boldsymbol{\xi}_\perp \right\rangle \right|^2 d\mathbf{r} = \delta W_C \tag{A.44}$$

The last step in the analysis is to evaluate δQ_b in the limit $\omega^2 \to 0$ and show that it is positive. Following the procedure used to simplify δQ_a we rewrite δQ_b as follows.

$$\delta Q_b = \sum_j \int \frac{\partial f}{\partial \varepsilon} \left\langle q\tilde{\phi} \right\rangle_b \left\langle \tilde{I}_+^* + \tilde{I}_-^* \right\rangle_b d\mathbf{w} \, d\mathbf{r} \tag{A.45}$$

This expression can be simplified by using the charge neutrality relation. A short calculation yields

$$\begin{aligned} e^2\tilde{\phi}\sum_j \int \frac{\partial f}{\partial \varepsilon} d\mathbf{w} &= i\omega \sum_j \int q \frac{\partial f}{\partial \varepsilon} \tilde{s}\, d\mathbf{w} \\ &= e^2 \sum_j \int \frac{\partial f}{\partial \varepsilon} \left\langle \tilde{\phi} \right\rangle_b d\mathbf{w} - \sum_j \int q \frac{\partial f}{\partial \varepsilon} \left\langle \tilde{I}_+ + \tilde{I}_- \right\rangle_b d\mathbf{w} \end{aligned} \tag{A.46}$$

Next, we take the complex conjugate of eq. (A.46), multiply the result by $\tilde{\phi}$ and integrate over the plasma volume. A straightforward calculation then leads to

$$\begin{aligned} e^2 \sum_j \int\int \frac{\partial f}{\partial \varepsilon} \left[\left\langle \left| \tilde{\phi} \right|^2 \right\rangle_b - \left| \left\langle \tilde{\phi} \right\rangle_b \right|^2 \right] d\mathbf{w}\, d\mathbf{r} &= -\sum_j \int \frac{\partial f}{\partial \varepsilon} \left\langle q\tilde{\phi} \right\rangle_b \left\langle \tilde{I}_+^* + \tilde{I}_-^* \right\rangle_b d\mathbf{w}\, d\mathbf{r} \\ &= -\delta Q_b \end{aligned} \tag{A.47}$$

From Schwarz's inequality it follows that

$$\delta Q_b = -e^2 \sum_j \int\int \frac{\partial f}{\partial \varepsilon} \left[\left\langle \left| \tilde{\phi} \right|^2 \right\rangle_b - \left| \left\langle \tilde{\phi} \right\rangle_b \right|^2 \right] d\mathbf{w}\, d\mathbf{r} \geq 0 \tag{A.48}$$

We can now combine these results to obtain a quantitative bound on δW_{KK} in the limit $\omega^2 \to 0$. Since $\delta W_{kk} = \delta Q_{kk}$ in this limit, we can write

$$\begin{aligned} \delta W_{KK} &= \delta W_\perp + \delta W_{kk} \\ &\geq \delta W_\perp + \delta W_C + \delta Q_b \geq \delta W_{MHD} \end{aligned} \tag{A.49}$$

Equation (A.49) shows that ideal MHD stability implies kinetic MHD stability in closed line systems.

Appendix B

Kinetic MHD Ions, Fluid Electrons Energy Relation

The derivation of the hybrid kinetic-fluid model energy relation is very similar to that presented in Appendix A for the fully kinetic MHD model. Thus it is only necessary to highlight the changes in the important relations. The starting point is the energy relation equivalent to eq. (A.11)

$$\begin{aligned}
\omega^2 K_\perp &= \delta W_\perp + \delta Q_{kf} = \delta W_\perp + \delta Q_i \\
K_\perp &= \int \rho \left|\boldsymbol{\xi}_\perp\right|^2 d\mathbf{r} \\
\delta W_\perp &= -\int \left[\boldsymbol{\xi}_\perp^* \cdot \left(\tilde{\mathbf{J}} \times \mathbf{B} + \mathbf{J} \times \tilde{\mathbf{B}}\right) - (\nabla \cdot \boldsymbol{\xi}_\perp^*)(\boldsymbol{\xi}_\perp \cdot \nabla p)\right] d\mathbf{r} \\
\delta Q_i &= -\int \left[\tilde{p}_{iK\perp} \nabla \cdot \boldsymbol{\xi}_\perp^* + (\tilde{p}_{iK\perp} - \tilde{p}_{iK\parallel})(\boldsymbol{\xi}_\perp^* \cdot \boldsymbol{\kappa})\right] d\mathbf{r}
\end{aligned} \tag{B.1}$$

Here, $p(\psi) = p_e(\psi) + p_i(\psi)$ and the perturbed ion distribution function needed to calculate the ion density and pressure tensor, equivalent to eq. (A.8), is given by

$$\begin{aligned}
\tilde{f}_i\left(\mathbf{r}, \varepsilon, \mu, t\right) &= \tilde{f}_F + \tilde{f}_K \\
\tilde{f}_F &= -\boldsymbol{\xi}_\perp \cdot \nabla f_i + \frac{1}{n}(\tilde{p}_e + \boldsymbol{\xi}_\perp \cdot \nabla p_e) - i\omega m w_\parallel \xi_\parallel \frac{\partial f_i}{\partial \varepsilon} \\
\tilde{f}_K &= -i\omega \tilde{s}_i \frac{\partial f_i}{\partial \varepsilon} \\
\tilde{s}_i &= \int_{-\infty}^{t} \left[m_i \frac{w_\perp^2}{2} \nabla \cdot \boldsymbol{\xi}_\perp + m_i \left(\frac{w_\perp^2}{2} - w_\parallel^2 \right) \boldsymbol{\xi}_\perp \cdot \boldsymbol{\kappa} - \frac{1}{n}(\tilde{p}_e + \boldsymbol{\xi}_\perp \cdot \nabla p_e) \right] dt'
\end{aligned} \tag{B.2}$$

The quantities $\tilde{p}_{iK\perp}$, $\tilde{p}_{iK\|}$ are the kinetic contributions to the ion pressure tensor (proportional to the trajectory integral $\tilde{s}$).

$$\begin{aligned} \tilde{p}_{iK\perp} &= \int \frac{mw_\perp^2}{2} \tilde{f}_K d\mathbf{w} \\ \tilde{p}_{iK\|} &= \int mw_\| ^2 \tilde{f}_K d\mathbf{w} \end{aligned} \tag{B.3}$$

The equations for the perturbed electron pressure have already been derived in Section 3.5 in the main text, and take the form given in eq. (3.78). Since $\tilde{p}_e + \boldsymbol{\xi}_\perp \cdot \nabla p_e$ has a different form for ergodic and closed line systems we treat each case separately when deriving the stability comparison theorems.

- **Case (1) Ergodic systems**

The treatment here closely follows that presented in Appendix A. The critical relations that are modified by the different treatment of electrons are eqs. (A.14) and (A.18). For the hybrid model eq. (A.14) becomes

$$\delta Q_i = i\omega \int \tilde{s}_i \frac{d\tilde{s}_i^*}{dt} \frac{\partial f_i}{\partial \varepsilon} d\mathbf{w}\, d\mathbf{r} - i\omega \int \left(T_e \nabla \cdot \boldsymbol{\xi}^* \right) \tilde{s}_i \frac{\partial f_i}{\partial \varepsilon} d\mathbf{w}\, d\mathbf{r} \tag{B.4}$$

while eq. (A.18) can be written as

$$i\omega \int \tilde{s}_i \frac{\partial f_i}{\partial \varepsilon} d\mathbf{w} = \frac{T_e + \hat{T}_i}{\hat{T}_i} n \nabla \cdot \boldsymbol{\xi} \tag{B.5}$$

We use eq. (B.5) to eliminate $\nabla \cdot \boldsymbol{\xi}$ in eq. (B.4). Then, following the analysis for the fully kinetic MHD model we obtain the desired energy relation for the hybrid model.

$$\left|\omega\right|^2 = -\frac{\delta W_\perp + \delta W_{kf}}{K_\perp} \tag{B.6}$$

where

$$\begin{aligned}
\delta W_{kf}(\boldsymbol{\xi}, \boldsymbol{\xi}^*) &= \left|\omega\right|^2 \int \frac{d\mathbf{r}}{n}(U_i + U_h) \\
U_i &= \hat{T}_i \left[\int \frac{\partial f_i}{\partial \varepsilon} d\mathbf{w} \int \frac{\partial f_i}{\partial \varepsilon} \left|\tilde{s}_i\right|^2 d\mathbf{w} - \left| \int \frac{\partial f_i}{\partial \varepsilon} \tilde{s}_i \, d\mathbf{w} \right|^2 \right] \\
U_h &= \frac{1}{\left(\hat{T}_i + T_e\right)} \left| \hat{T}_i \int \frac{\partial f_i}{\partial \varepsilon} \tilde{s}_i d\mathbf{w} \right|^2
\end{aligned} \tag{B.7}$$

These are the expressions used in the main body of the text.

- **Case (2) Closed line systems**

For the case of closed line systems undergoing perturbations that maintain the closed line symmetry the starting point is eq. (B.1), repeated here for convenience.

$$\begin{aligned}
\omega^2 K_\perp &= \delta W_\perp + \delta Q_i \\
\delta Q_i &= -\int \left[\tilde{p}_{iK\perp} \nabla \cdot \boldsymbol{\xi}_\perp^* + (\tilde{p}_{iK\perp} - \tilde{p}_{iK\parallel})(\boldsymbol{\xi}_\perp^* \cdot \boldsymbol{\kappa}) \right] d\mathbf{r} \\
&= i\omega \int d\mathbf{r}\, d\mathbf{w} \frac{\partial f_i}{\partial \varepsilon} \left[m_i \frac{w_\perp^2}{2} \nabla \cdot \boldsymbol{\xi}_\perp^* + m_i \left(\frac{w_\perp^2}{2} - w_\parallel^2 \right) \boldsymbol{\xi}_\perp^* \cdot \boldsymbol{\kappa} \right] \tilde{s}
\end{aligned} \tag{B.8}$$

Our task is to derive an estimate for this quantity that can be compared with the ideal MHD compressibility term δW_C. As in the Kinetic MHD case derived in

Appendix A, this can only be done analytically in the limit $\omega^2 \to 0$. It is helpful to separate δQ_i into two parts:

$$\begin{aligned}
\delta Q_i &= \delta Q_a + \delta Q_b \\
\delta Q_a &= i\omega \int d\mathbf{r}\, d\mathbf{w} \frac{\partial f_i}{\partial \varepsilon} \frac{d\hat{s}^*}{dt} \hat{s} \\
\delta Q_b &= -i\omega \int d\mathbf{r}\, d\mathbf{w} \frac{\partial f_i}{\partial \varepsilon} \frac{d\hat{s}^*}{dt} \int_{-\infty}^{t} \frac{1}{n} \left(\tilde{p}_e + \boldsymbol{\xi}_\perp \cdot \nabla p_e \right) dt' \\
\frac{d\hat{s}^*}{dt} &= m_i \frac{w_\perp^2}{2} \nabla \cdot \boldsymbol{\xi}_\perp^* + m_i \left(\frac{w_\perp^2}{2} - w_\parallel^2 \right) \boldsymbol{\xi}_\perp^* \cdot \boldsymbol{\kappa}
\end{aligned} \tag{B.9}$$

In the limit $\omega^2 \to 0$ the evaluation of δQ_a is identical to that presented for the pure kinetic MHD case in Appendix A. For the present case we find

$$\begin{aligned}
\delta Q_a &= \frac{5}{3} \int p_i \, | \langle \nabla \cdot \boldsymbol{\xi}_\perp \rangle |^2 \, d\mathbf{r} - \frac{2\pi}{m^2} \int d\psi\, d\chi\, d\varepsilon \frac{\partial f_i}{\partial \varepsilon} G \\
G &= \frac{1}{\int \tau_b \, d\mu} \left[\int \tau_b \, d\mu \int \tau_b \left(\left| g_+ \right|^2 + \left| g_- \right|^2 \right) d\mu - \left| \int \tau_b g_+ \, d\mu \right|^2 - \left| \int \tau_b g_- \, d\mu \right|^2 \right] \\
g_\pm &= \left\langle m_i \frac{w_\perp^2}{2} \nabla \cdot \boldsymbol{\xi}_\perp^* + m_i \left(\frac{w_\perp^2}{2} - w_\parallel^2 \right) \boldsymbol{\xi}_\perp^* \cdot \boldsymbol{\kappa} \right\rangle_b \Bigg|_{\pm w_\parallel}
\end{aligned} \tag{B.10}$$

Clearly $G \geq 0$ by virtue of Schwarz's inequality implying that the second integral in δQ_a is positive.

To determine δQ_b we first need to evaluate the charge neutrality condition. A short calculation yields, in the limit $\omega^2 \to 0$,

$$-n \nabla \cdot \boldsymbol{\xi}^* = -\frac{1}{\hat{T}_i} \left(\tilde{p}_e^* + \boldsymbol{\xi}_\perp^* \cdot \nabla p_e \right) - \int \frac{d\mathbf{w}}{n} \frac{\partial f_i}{\partial \varepsilon} \left\langle \tilde{p}_e^* + \boldsymbol{\xi}_\perp^* \cdot \nabla p_e \right\rangle_b + \int d\mathbf{w} \frac{\partial f_i}{\partial \varepsilon} \left\langle \frac{d\hat{s}^*}{dt} \right\rangle_b \tag{B.11}$$

The next step is to multiply this equation by $\left(\tilde{p}_e + \boldsymbol{\xi}_\perp \cdot \nabla p_e\right)/n$ and integrate over the plasma volume. Recognizing that by exchanging the order of integration between the velocity and space integrals δQ_b can be written as

$$\delta Q_b = \int \mathbf{dr} \frac{1}{n} \int \mathbf{dw} f_\varepsilon^i \left\langle \frac{d\hat{s}^*}{dt} \right\rangle_b \left\langle \tilde{p}_e + \boldsymbol{\xi}_\perp \cdot \nabla p_e \right\rangle_b \tag{B.12}$$

in the limit $\omega^2 \to 0$, another short calculation involving some more exchanges of the order of integration between velocity integrals and integrals over space coordinates leads to the desired expression:

$$\begin{aligned} \delta Q_b = {} & \gamma_e \int \mathbf{dr} p_e \left| \left\langle \nabla \cdot \boldsymbol{\xi}_\perp \right\rangle \right|^2 + \int \mathbf{dr} p_e \left(\left| \nabla \cdot \boldsymbol{\xi} \right|^2 - \left| \left\langle \nabla \cdot \boldsymbol{\xi}_\perp \right\rangle \right|^2 \right) \\ & - \int \frac{d\mathbf{r}\, d\mathbf{w}}{n^2} \frac{\partial f_i}{\partial \varepsilon} \left[\left| \tilde{p}_e + \boldsymbol{\xi}_\perp \cdot \nabla p_e \right|^2 - \left| \left\langle \tilde{p}_e + \boldsymbol{\xi}_\perp \cdot \nabla p_e \right\rangle_b \right|^2 \right] \end{aligned} \tag{B.13}$$

Schwarz's inequality implies that the second and third integrals are positive.

Combining the expressions for δQ_a and δQ_b and setting $\gamma_e = 5/3$ leads to the desired result, since $\delta W_{kf} = \delta Q_i$ in the limit $\omega^2 \to 0$:

$$\begin{aligned} \delta W_{kf} = {} & \int \frac{5}{3} \left(p_e + p_i \right) \left| \left\langle \nabla \cdot \boldsymbol{\xi}_\perp \right\rangle \right|^2 d\mathbf{r} \\ & - \int d\psi\, d\chi\, d\varepsilon \frac{\partial f_i}{\partial \varepsilon} G \\ & + \int \mathbf{dr} p_e \left(\left| \nabla \cdot \boldsymbol{\xi} \right|^2 - \left| \left\langle \nabla \cdot \boldsymbol{\xi}_\perp \right\rangle \right|^2 \right) \\ & - \int \frac{d\mathbf{r}\, d\mathbf{w}}{n^2} \frac{\partial f_i}{\partial \varepsilon} \left[\left| \tilde{p}_e + \boldsymbol{\xi}_\perp \cdot \nabla p_e \right|^2 - \left| \left\langle \tilde{p}_e + \boldsymbol{\xi}_\perp \cdot \nabla p_e \right\rangle_b \right|^2 \right] \end{aligned} \tag{B.14}$$

or using the inequality relations

$$\delta W_{kf} \geq \delta W_C \tag{B.15}$$

This is the key result that shows that the hybrid model predicts greater stability than ideal MHD for closed line systems.

Appendix C

Vlasov-Fluid Energy Relation

The derivation of the energy integral for the Vlasov-Fluid (VF) model begins with the linearized form of the force balance relation given by the first equation in eq. (3.144) in Chapter 3 of the main text.

$$\mathbf{J}\times\tilde{\mathbf{B}}+\tilde{\mathbf{J}}\times\mathbf{B}-\nabla\tilde{p}_e-en\tilde{\mathbf{E}}=e\int\left(\mathbf{E}+\mathbf{u}\times\mathbf{B}\right)\tilde{f}_i\,d\mathbf{u} \tag{C.1}$$

Linearized forms of $\tilde{n}$, $\tilde{p}_e$, $\tilde{\mathbf{B}}$, and $\tilde{\mathbf{E}}$ have been given in terms of the electron displacement $\boldsymbol{\xi}$ by eq. (3.149). We also need the perturbed distribution function which satisfies the linearized Vlasov equation. For equilibria characterized by $f_i=f_i(\varepsilon)$ it follows that

$$\tilde{f}_i=-e\frac{\partial f_i}{\partial\varepsilon}\int_{-\infty}^{t}\mathbf{u}\cdot\tilde{\mathbf{E}}\,dt' \tag{C.2}$$

where the trajectory integral is calculated along the exact (i.e. not gyro expanded) orbit, and we have assumed that $\mathrm{Im}(\omega)>0$, so that $\tilde{f}_i\left(t\to-\infty\right)=0$

Using the expression for $\tilde{\mathbf{E}}$ given in eq. (3.149) and the VF equilibrium relations we find after a short calculation that $\tilde{f}_i$ can be rewritten as

$$\tilde{f}_i = \left[\frac{1}{n}\left(\boldsymbol{\xi}_\perp \cdot \nabla p_i - \gamma_e p_e \nabla \cdot \boldsymbol{\xi}\right) + i\omega\tilde{s}\right]\frac{\partial f_i}{\partial \varepsilon} \tag{C.3}$$

with

$$\tilde{s} = \int_{-\infty}^{t}\left[e(\mathbf{E} + \mathbf{u}\times\mathbf{B})\cdot\boldsymbol{\xi}_\perp - (\gamma_e p_e / n)\nabla\cdot\boldsymbol{\xi}\right]dt' \tag{C.4}$$

Substituting (C.3) and the expressions in eq. (3.149) in eq. (C.1), we obtain, after some more algebra, the desired expression for the linearized force balance equation:

$$\mathbf{J}\times\tilde{\mathbf{B}} + \tilde{\mathbf{J}}\times\mathbf{B} + \nabla\left(\boldsymbol{\xi}_\perp\cdot\nabla p\right) - i\omega e n\boldsymbol{\xi}_\perp\times\mathbf{B} - i\omega e\int\frac{\partial f_i}{\partial\varepsilon}\left(\mathbf{E}+\mathbf{u}\times\mathbf{B}\right)\tilde{s}\,d\mathbf{u} \tag{C.5}$$

where $p = p_e + p_i$.

The next step is to form the dot product of eq. (C.5) with $\boldsymbol{\xi}^*$ and then integrate over the plasma volume. The resulting equation is simplified as follows. The first three terms combine to form the incompressible contribution to the ideal MHD potential energy.

$$\int \boldsymbol{\xi}_\perp^*\cdot\left[\mathbf{J}\times\tilde{\mathbf{B}} + \tilde{\mathbf{J}}\times\mathbf{B} + \nabla\left(\boldsymbol{\xi}_\perp\cdot\nabla p\right)\right]d\mathbf{r} = -\delta W_\perp \tag{C.6}$$

The fourth term in eq. (C.5) reduces to

$$-i\omega e n\int\boldsymbol{\xi}^*\cdot\boldsymbol{\xi}_\perp\times\mathbf{B}\,d\mathbf{r} = -i\omega e n\int\boldsymbol{\xi}_\perp^*\times\boldsymbol{\xi}_\perp\cdot\mathbf{B}\,d\mathbf{r} = \omega R_1 \tag{C.7}$$

where R_1 is a real quantity, since $\boldsymbol{\xi}_\perp^*\times\boldsymbol{\xi}_\perp$ is purely imaginary.

The fifth and last term to evaluate involves the trajectory integral. This term can be simplified by noting that

$$\begin{aligned}\frac{d\tilde{s}^*}{dt} &= i\omega^*\tilde{s}^* + \frac{D\tilde{s}^*}{Dt} \\ &= e(\mathbf{E}+\mathbf{u}\times\mathbf{B})\cdot\boldsymbol{\xi}_\perp^* - (\gamma_e p_e / n)\nabla\cdot\boldsymbol{\xi}^*\end{aligned} \tag{C.8}$$

Here,

$$\frac{D}{Dt} \equiv \mathbf{u}\cdot\nabla + \frac{e}{m_i}\left(\mathbf{E}+\mathbf{u}\times\mathbf{B}\right)\cdot\nabla_w \tag{C.9}$$

The fifth term can now be rewritten as

$$\begin{aligned}&-i\omega e\int\frac{\partial f_i}{\partial\varepsilon}\left(\mathbf{E}+\mathbf{u}\times\mathbf{B}\right)\cdot\boldsymbol{\xi}_\perp^*\,\tilde{s}\,d\mathbf{u}\,d\mathbf{r} \\ &\quad = -i\omega\int\frac{\partial f_i}{\partial\varepsilon}\left(i\omega^*\tilde{s}^* + \frac{D\tilde{s}^*}{Dt} + \frac{\gamma_e p_e}{n}\nabla\cdot\boldsymbol{\xi}^*\right)\tilde{s}\,d\mathbf{u}\,d\mathbf{r}\end{aligned} \tag{C.10}$$

The middle contribution simplifies by writing $\tilde{s} = s_r + is_i$.

$$\begin{aligned}-i\omega\int\frac{\partial f_i}{\partial\varepsilon}\frac{D\tilde{s}^*}{Dt}\tilde{s}\,d\mathbf{u}\,d\mathbf{r} &= -i\omega\int\frac{\partial f_i}{\partial\varepsilon}\left[\frac{D}{Dt}\left(\frac{s_r^2+s_i^2}{2}\right) + i\left(s_i\frac{Ds_r}{Dt} - s_r\frac{Ds_i}{Dt}\right)\right]d\mathbf{u}\,d\mathbf{r} \\ &= \omega\int\frac{\partial f_i}{\partial\varepsilon}\left[\left(s_i\frac{Ds_r}{Dt} - s_r\frac{Ds_i}{Dt}\right)\right]d\mathbf{u}\,d\mathbf{r} \\ &= \omega R_2\end{aligned} \tag{C.11}$$

where R_2 is a real quantity and the integral involving $s_r^2 + s_i^2$ vanishes by the use of Gauss's theorem, once over real space and once over velocity space.

Combining these results leads to the following form of the energy integral

$$\delta W_\perp = \left|\omega\right|^2\int\frac{\partial f_i}{\partial\varepsilon}\left|\tilde{s}\right|^2 d\mathbf{u}\,d\mathbf{r} + \omega\left(R_1+R_2\right) - i\omega\int\frac{\partial f_i}{\partial\varepsilon}\left(\frac{\gamma_e p_e}{n}\nabla\cdot\boldsymbol{\xi}^*\right)\tilde{s}\,d\mathbf{u}\,d\mathbf{r} \tag{C.12}$$

The final step in the derivation is to simplify the last term in eq. (C.12), which is accomplished by the use of the charge neutrality condition $n_e = n_i$. A straightforward calculation yields

$$\frac{1}{e}\frac{dp}{d\phi}\nabla\cdot\boldsymbol{\xi} = i\omega\int\frac{\partial f_i}{\partial\varepsilon}\tilde{s}\,d\mathbf{u} \tag{C.13}$$

The expression for $\nabla\cdot\boldsymbol{\xi}$ is substituted into the last term in eq. (C.12). Making use of the relation

$$\int\frac{\partial f_i}{\partial\varepsilon}d\mathbf{u} = \frac{1}{e}\frac{dn}{d\phi} \tag{C.14}$$

leads to the following form of the energy relation.

$$\begin{aligned}\delta W_\perp = {} & \left|\omega\right|^2\int\frac{\partial f_i}{\partial\varepsilon}\left|\tilde{s}\right|^2 d\mathbf{u}\,d\mathbf{r} + \omega\left(R_1 + R_2\right) \\ & -\left|\omega\right|^2\int\frac{\gamma_e p_e}{\gamma_e p_e + \gamma_i p_i}\frac{\left|\int\frac{\partial f_i}{\partial\varepsilon}\tilde{s}\,d\mathbf{u}\right|^2}{\int\frac{\partial f_i}{\partial\varepsilon}d\mathbf{u}}d\mathbf{r}\end{aligned} \tag{C.15}$$

Here, $\gamma_{e,i}(\psi) = d\ln p_{e,i} \,/\, d\ln n$.

We now write $\omega = \omega_r + i\omega_i$. Setting the imaginary part of eq. (C.15) to zero requires that $R_1 + R_2 = 0$. The remaining real part yields the desired VF energy relation

$$\left|\omega\right|^2 = -\frac{\delta W_\perp}{K_{VF}} \tag{C.16}$$

$$\text{where} \qquad K_{VF} = -\int d\mathbf{r} \frac{1}{\int \frac{\partial f_i}{\partial \varepsilon} d\mathbf{u}} \left[\int \frac{\partial f_i}{\partial \varepsilon} d\mathbf{u} \int \frac{\partial f_i}{\partial \varepsilon} \left|\tilde{s}\right|^2 d\mathbf{u} - \left| \int \frac{\partial f_i}{\partial \varepsilon} \tilde{s}\, d\mathbf{u} \right|^2 \right]$$

$$- \int \frac{\gamma_i p_i}{\gamma_e p_e + \gamma_i p_i} \frac{\left| \int \frac{\partial f_i}{\partial \varepsilon} \tilde{s}\, d\mathbf{u} \right|^2}{\int \frac{\partial f_i}{\partial \varepsilon} d\mathbf{u}} d\mathbf{r} \qquad \text{(C.17)}$$

Although complicated, this expression is positive by virtue of Schwarz's inequality when $\partial f_i / \partial \varepsilon < 0$. Equation (C.17) is the one used in the main body of the text.